



2014

A Metrics-based Sustainability Assessment of Cryogenic Machining Using Modeling and Optimization of Process Performance

Tao Lu

University of Kentucky, taolucn@gmail.com

[Click here to let us know how access to this document benefits you.](#)

Recommended Citation

Lu, Tao, "A Metrics-based Sustainability Assessment of Cryogenic Machining Using Modeling and Optimization of Process Performance" (2014). *Theses and Dissertations--Mechanical Engineering*. 47.
https://uknowledge.uky.edu/me_etds/47

This Doctoral Dissertation is brought to you for free and open access by the Mechanical Engineering at UKnowledge. It has been accepted for inclusion in Theses and Dissertations--Mechanical Engineering by an authorized administrator of UKnowledge. For more information, please contact UKnowledge@lsv.uky.edu.

STUDENT AGREEMENT:

I represent that my thesis or dissertation and abstract are my original work. Proper attribution has been given to all outside sources. I understand that I am solely responsible for obtaining any needed copyright permissions. I have obtained needed written permission statement(s) from the owner(s) of each third-party copyrighted matter to be included in my work, allowing electronic distribution (if such use is not permitted by the fair use doctrine) which will be submitted to UKnowledge as Additional File.

I hereby grant to The University of Kentucky and its agents the irrevocable, non-exclusive, and royalty-free license to archive and make accessible my work in whole or in part in all forms of media, now or hereafter known. I agree that the document mentioned above may be made available immediately for worldwide access unless an embargo applies.

I retain all other ownership rights to the copyright of my work. I also retain the right to use in future works (such as articles or books) all or part of my work. I understand that I am free to register the copyright to my work.

REVIEW, APPROVAL AND ACCEPTANCE

The document mentioned above has been reviewed and accepted by the student's advisor, on behalf of the advisory committee, and by the Director of Graduate Studies (DGS), on behalf of the program; we verify that this is the final, approved version of the student's thesis including all changes required by the advisory committee. The undersigned agree to abide by the statements above.

Tao Lu, Student

Dr. I.S. Jawahir, Major Professor

Dr. J. M. McDonough, Director of Graduate Studies

A METRICS-BASED SUSTAINABILITY ASSESSMENT OF
CRYOGENIC MACHINING USING MODELING AND
OPTIMIZATION OF PROCESS PERFORMANCE

DISSERTATION

A dissertation submitted in partial fulfillment of
the requirements for the degree of Doctor of
Philosophy in the College of Engineering at the
University of Kentucky

By

Tao Lu

Director: Dr. I.S. Jawahir, Professor of Mechanical Engineering

Lexington, Kentucky

2014

Copyright © Tao Lu 2014

ABSTRACT OF DISSERTATION

A METRICS-BASED SUSTAINABILITY ASSESSMENT OF CRYOGENIC MACHINING USING MODELING AND OPTIMIZATION OF PROCESS PERFORMANCE

The development of a sustainable manufacturing process requires a comprehensive evaluation method and fundamental understanding of the processes. Coolant application is a critical sustainability concern in the widely used machining process. Cryogenic machining is considered a candidate for sustainable coolant application. However, the lack of comprehensive evaluation methods leaves significant uncertainties about the overall sustainability performance of cryogenic machining. Also, the lack of practical application guidelines based on scientific understanding of the heat transfer mechanism in cryogenic machining limits the process optimization from achieving the most sustainable performance.

In this dissertation, based on a proposed Process Sustainability Index (*ProcSI*) methodology, the sustainability performance of the cryogenic machining process is optimized with application guidelines established by scientific modeling of the heat transfer mechanism in the process. Based on the experimental results, the process optimization is carried out with Genetic Algorithm (GA).

The metrics-based *ProcSI* method considers all three major aspects of sustainable manufacturing, namely economy, environment and society, based on the 6R concept and the total life-cycle aspect. There are sixty five metrics, categorized into six major clusters. Data for all relevant metrics are collected, normalized, weighted, and then aggregated to form the *ProcSI* score, as an overall judgment for the sustainability performance of the process. The *ProcSI* method focuses on the process design as a manufacturer's aspect, hoping to improve the sustainability performance of the manufactured products and the manufacturing system.

A heat transfer analysis of cryogenic machining for a flank-side liquid nitrogen jet delivery is carried out. This is performed by micro-scale high-speed temperature measurement experiments. The experimental results are processed with an innovative inverse heat transfer solution method to calculate the surface heat transfer coefficient at various locations throughout a wide temperature range. Based on the results, the

application guidelines, including suggestions of a minimal, but sufficient, coolant flow rate are established.

Cryogenic machining experiments are carried out, and *ProcSI* evaluation is applied to the experimental scenario. Based on the *ProcSI* evaluation, the optimization process implemented with GA provides optimal machining process parameters for minimum manufacturing cost, minimal energy consumption, or the best sustainability performance.

KEYWORDS: Sustainable Manufacturing, Sustainability Evaluation, Cryogenic Machining, Heat Transfer, Optimization

Tao Lu

October 17th, 2014

**A METRICS-BASED SUSTAINABILITY ASSESSMENT OF
CRYOGENIC MACHINING USING MODELING AND
OPTIMIZATION OF PROCESS PERFORMANCE**

By

Tao Lu

I.S. Jawahir

Director of Dissertation

J. M. McDonough

Director of Graduate Studies

October 30th, 2014

ACKNOWLEDGMENTS

I would like to express my deepest gratitude to my advisor, Professor I.S. Jawahir, for his precious guidance, trustful support and kind help, in both academic endeavor and personal life. His advice and support helped me overcome countless difficulties and finish this dissertation. His passion and commitment to work has become a great example for me. The great learning from him enables me to grow professionally.

I am grateful to Professor F. Badurdeen and Professor O.W. Dillon, Jr., for their support, patience and guidance. I have learnt a lot from them.

I also would like to thank my committee members Professor K. Rouch and Professor T.J. Balk for their guidance. I want to extend my sincere appreciation to Professor M. Chen from the Department of Civil Engineering for serving as an outside examiner.

I want to thank the colleagues and scholars I worked with in our machining research group, Dr. A.D. Jayal, Mr. M. Shuaib, Dr. F. Pusavec, Dr. D. Umbrello, Dr. G. Rotella, Ms. X. Zhang, Dr. Z. Pu, Dr. S. Yang, Dr. Y. Yusuf, Dr. R. Hamade, Dr. J. Li, and Mr. B. Huang.

In addition, I would like to thank Mr. C.M. Arvin and Mrs. H.M. Adkins, for their professional help and friendship. They made my stay at the University of Kentucky enjoyable.

I want to thank my family, for their unconditional love and life-long trust in every way possible. Without their support I would not be able to accomplish my life goals, this dissertation and beyond.

TABLE OF CONTENTS

ACKNOWLEDGMENTS	iii
TABLE OF CONTENTS.....	iv
LIST OF TABLES.....	x
LIST OF FIGURES	xiii
CHAPTER 1 INTRODUCTION.....	1
1.1 Concepts of Sustainable Manufacturing	1
1.2 Scope of Sustainable Manufacturing	2
1.3 Driving Forces for Metrics-based Method for Sustainability Assessment	3
1.4 Sustainable Cutting Fluid Applications for Machining Processes.....	4
1.5 Research Objectives.....	4
1.6 Dissertation Outline	6
CHAPTER 2 LITERATURE REVIEW.....	8
2.1 General Sustainability Assessment Method.....	8
2.1.1 Established sustainability assessment methods	9
2.1.2 Sustainability assessment for chemical processing.....	14
2.2 Sustainability Assessment for Manufacturing Processes.....	15
2.2.1 6R concept	15
2.2.2 Sustainability assessment methods for discrete product manufacturing	18

2.2.3	Fundamental work related to the development of a new Process Sustainability Index (<i>ProcSI</i>) method	23
2.3	Influence of Cutting Fluids on the Sustainability Performance of Machining Processes	27
2.3.1	Economic impact	27
2.3.2	Environmental impact.....	28
2.3.3	Societal impact.....	29
2.3.4	Alternative sustainable cutting fluid solutions.....	30
2.4	Cooling Effect of Cutting Fluid	33
2.4.1	Cooling effect of conventional flood cooling	34
2.4.2	Cooling effect of MQL application.....	34
2.4.3	Cooling effect of cryogenic machining.....	35
CHAPTER 3	PROCESS SUSTAINABILITY INDEX (<i>PROCSI</i>).....	39
3.1	Scope and System Boundaries	39
3.1.1	Scope of the <i>ProcSI</i> methodology	39
3.1.2	System boundaries of the system	40
3.1.3	Relationship with product sustainability.....	44
3.2	<i>ProcSI</i> Structure.....	45
3.2.1	Hierarchical structure.....	45
3.2.2	Normalization, weighting and aggregation.....	49

3.3	<i>ProcSI</i> Metrics	55
3.3.1	Requirements of metrics for sustainability assessment	55
3.3.2	Manufacturing cost	58
3.3.3	Energy consumption	59
3.3.4	Environmental impact	62
3.3.5	Waste management	64
3.3.6	Operator safety	65
3.3.7	Personnel health	66
3.4	Metrics Applications at Various Levels.....	67
3.4.1	Plant level.....	69
3.4.2	Workstation level	70
3.4.3	Operation level.....	72
3.5	Case Study	72
3.5.1	Background scenarios	73
3.5.2	Data collection	78
3.5.3	Process Sustainability Index (<i>ProcSI</i>) evaluation.....	85
3.5.4	Process optimization for sustainability	88
3.5.5	Case study summary	94
3.6	Summary	94

CHAPTER 4	COOLING MECHANISM IN CRYOGENIC MACHINING.....	96
4.1	Cooling Effect Experiment for Cryogenic Machining.....	97
4.1.1	High speed temperature measurement system and signal processing ..	97
4.1.2	Static cooling experiments.....	103
4.2	Boiling Heat Transfer Modeling for Cryogenic Machining	116
4.2.1	Surface heat transfer modelling under cryogenic condition	116
4.2.2	Surface heat transfer coefficient at various locations and driving pressure.....	139
4.3	Summary	153
CHAPTER 5	SUSTAINABILITY PERFORMANCE OF CRYOGENIC MACHINING	156
5.1	Machining Experiments	156
5.1.1	Orthogonal cutting scenario	156
5.1.2	Determine the cutting edge radius	158
5.1.3	Determine cooling effect.....	160
5.2	Process Performance	166
5.2.1	Cutting forces.....	166
5.2.2	Surface roughness	169
5.2.3	Tool-wear	171
5.3	<i>ProcSI</i> Evaluation of Cryogenic Machining Process.....	172

5.3.1	Manufacturing cost	173
5.3.2	Energy consumption	175
5.3.3	Waste management	178
5.3.4	Environmental impact.....	179
5.3.5	<i>ProcSI</i> score results.....	180
5.4	Summary	181
CHAPTER 6 OPTIMIZATION OF CRYOGENIC MACHINING.....		183
6.1	Input Variables and Objective Function	183
6.1.1	Genetic Algorithm (GA) and its input variables.....	183
6.1.2	Empirical modeling of the process	183
6.1.3	<i>ProcSI</i> score as the objective function.....	184
6.2	Optimization Results.....	185
6.2.1	Optimize for minimal manufacturing cost.....	186
6.2.2	Optimize for minimal energy consumption	187
6.2.3	Optimize for highest <i>ProcSI</i> score.....	188
6.3	Summary	191
CHAPTER 7 CONCLUDING REMARKS AND FUTURE WORK.....		192
7.1	Concluding Remarks.....	192
7.1.1	Process Sustainability Index (<i>ProcSI</i>) method	192

7.1.2	Thermal analysis and modeling of heat transfer in cryogenic machining	193
7.1.3	Experimental works and optimization of cryogenic machining	194
7.2	Future Work	196
7.2.1	Process Sustainability Index (<i>ProcSI</i>) method	196
7.2.2	Heat transfer analysis method	197
7.2.3	Research of cryogenic machining	198
APPENDIX A PROCESSING OF THE THERMOCOUPLE SIGNALS		199
APPENDIX B FINITE DIFFERENCE METHOD FOR THE HEAT TRANSFER PROBLEM		205
APPENDIX C SOLVING THE INVERSE HEAT CONDUCTION PROBLEM WITH LEAST SQUARE METHOD		208
APPENDIX D SOLVING THE INVERSE HEAT CONDUCTION PROBLEM WITH OVER-SAMPLING METHOD		211
APPENDIX E DEFINING THE CUTTING EDGE RADIUS OF A CUTTING TOOL		214
APPENDIX F MESHING FOR GLOBAL RESPONSE		220
APPENDIX G OPTIMIZATION WITH GENETIC ALGORITHM		222
REFERENCES		224
VITA		237

LIST OF TABLES

Table 2.1: Comparison of reviewed sustainability assessment methods for discrete product manufacturing.....	23
Table 3.1: <i>ProcSI</i> with its clusters and sub-clusters.	47
Table 3.2: Sample of the individual metrics for environmental impact.	48
Table 3.3: General score assignment	50
Table 3.4: Manufacturing cost cluster with its sub-clusters and individual metrics (Lu et al., 2014a).	59
Table 3.5 Energy consumption cluster with its sub-clusters and individual metrics (Lu et al., 2014a).	61
Table 3.6: Environmental impact cluster with its sub-clusters and individual metrics (Lu et al., 2014a).	63
Table 3.7 Waste management cluster with its sub-clusters and individual metrics (Lu et al., 2014a).	65
Table 3.8 Operator safety cluster with its sub-clusters and individual metrics (Lu et al., 2014a).	66
Table 3.9 Personnel health cluster with its sub-clusters and individual metrics (Lu et al., 2014a).	67
Table 3.10: Machining parameters used in the experiments (Lu et al., 2014b).....	75

Table 3.11: Coolant application parameters used in the experiments (Lu et al., 2014b)	75
Table 3.12: Capital cost tie-up summary (Lu et al., 2014b)	77
Table 3.13: Data summary for manufacturing cost (Lu et al., 2014b)	79
Table 3.14: Data summary for energy consumption (Lu et al., 2014b)	81
Table 3.15: Data summary for waste management (Lu et al., 2014b)	82
Table 3.16: Data summary for environmental impact (Lu et al., 2014b)	84
Table 3.17: Summary of normalized score, highlighted lines indicate best cases with the corresponding coolant application method (Lu et al., 2014b)	86
Table 3.18: Coefficients for each components in the relationship equation for cutting force and tool-wear rate with each of the coolant application methods	91
Table 3.19: Optimal conditions determined by the optimization and the corresponding <i>ProcSI</i> scores (Lu et al., 2014b)	93
Table 4.1: Fluid flow rate at different driving pressures	106
Table 4.2: Estimated flow rate of liquid nitrogen under the source pressure used in the experiments	108
Table 4.3: Thermal property coefficients for <i>AZ31B</i> alloy	121
Table 4.4: Comparison between typical conventional method and current approach for solving IHTP	138
Table 5.1: Machining parameters used in the experiments	157

Table 5.2: Capital cost tie-up summary.	157
Table 5.3: Data summary for manufacturing cost.	173
Table 5.4: Data summary for energy consumption.	176
Table 5.5: Data summary for waste management.	179
Table 5.6: Data summary for environmental impact.	180
Table 5.7: Summary of normalized score and the overall <i>ProcSI</i> score.	181
Table 6.1: Comparison between best experiment scenario and optimization results for the cluster of energy consumption.	188

LIST OF FIGURES

Figure 2.1: Categories of prominent sustainability evaluation methodologies, adapted from Feng et al. (2010).	9
Figure 2.2: Product design for sustainability (Jawahir et al., 2006a).	13
Figure 2.3: The 6R concept for a closed-loop near perpetual material flow (Jawahir et al., 2006a).....	17
Figure 2.4: Example of an input/output chart for a machining process (Lu et al., 2011).	17
Figure 2.5: Six major elements of sustainable manufacturing processes (Wanigarathne et al., 2004).....	24
Figure 2.6: Heat transfer regimes and typical boiling curve for water at atmospheric pressure (Tong and Tang, 1997).	37
Figure 3.1: System boundary of the proposed <i>ProcSI</i> method.	41
Figure 3.2: Integrated accessories and concentrated and external utilities.	42
Figure 3.3: Life-cycle stages of the production consumables and the manufactured product.	43
Figure 3.4: Sustainable manufacturing metrics hierarchy (Badurdeen et al., 2011).	45
Figure 3.5: Hierarchical structure of the <i>ProcSI</i> evaluation method.	45
Figure 3.6: <i>ProcSI</i> evaluation methodology.	49
Figure 3.7: Normalization curve for noise level in working environment.	51

Figure 3.8: Aggregation example for partial elements of the Economy sub index in the sustainability evaluation of a machining process (Lu et al., 2014a).	55
Figure 3.9: Metric aggregation for the total energy consumption (Lu et al., 2011).	69
Figure 3.10: Simplified input/output flows of a machining process (Lu et al., 2012a).	74
Figure 3.11: Process flow chart (Lu et al., 2014b).	74
Figure 3.12: Sustainability scores for the six clusters of process sustainability (Lu et al., 2014b).	87
Figure 3.13: Population plot for optimization of dry machining process (Lu et al., 2014b).	92
Figure 3.14: Population plot for optimization of cryogenic machining process (Lu et al., 2014b).	93
Figure 3.15: Population plot for optimization of MQL machining process (Lu et al., 2014b).	93
Figure 4.1: Signal amplifier circuit schematic (Analog Devices, 2012).	98
Figure 4.2: (a) Schematic of signal amplifier circuit design; (b) PCB layout screen map of the signal amplifier.	99
Figure 4.3: A sample of the system idle signal.	101
Figure 4.4: Flow chart of signal processing.	102
Figure 4.5: Experimental setup of cryogenic machining: (a) photo (tool approaching the workpiece) and (b) schematic diagram (Pu, 2012).	104

Figure 4.6: System schematic of the low pressure liquid nitrogen delivery system.	105
Figure 4.7: Flow rate at different driving pressure in the water experiments.	106
Figure 4.8: Drawings for the specimen: (a) 2D drawing for the dimensions in mm; (b) 3D drawing for the coordinate system and an illustration of the micro- groove locations.	109
Figure 4.9: Micro-grooves on the test surface: (a) micro-groove locations (groove size not to scale, only first 5 grooves shown); (b) micro-groove dimensions.	110
Figure 4.10: Setup procedures: (a) apply insulation film; (b) install thermocouple; (c) install and clamp side blocks; (d) clamp upper block.	112
Figure 4.11: Surface topography of the micro-groove after a thermocouple is placed inside.	113
Figure 4.12: Flow chart of the static cooling experiments.	115
Figure 4.13: Coordinate system in the heat transfer modeling.	117
Figure 4.14: Thermal properties of <i>AZ31B</i> alloy used in the analysis: (a) specific heat capacity; (b) thermal conductivity.	122
Figure 4.15: A sample of measured and calculated temperature curve with Levenberg-Marquardt method, TC on flat workpiece, direct LN flow, driving pressure $P = 68.9\text{kPa}$	127
Figure 4.16: Noise spectrum of system idle output.	131

Figure 4.17: Flow chart for the inverse heat transfer solution by oversampling approach.....	135
Figure 4.18: A sample of calculated surface heat transfer coefficient curve, for the data presented in Figure 4.15.....	136
Figure 4.19: A comparison of the temperature curves measured and modelled at a open location, Groove 4, $P = 51.7\text{kPa}$	140
Figure 4.20: Surface heat transfer coefficient at the open locations (Grooves 4 though 6).....	141
Figure 4.21: The surface heat transfer coefficient curve at the open locations, with a driving pressure $P = 17.2\text{kPa}$	142
Figure 4.22: A calculated surface heat transfer coefficient curve in the time domain, at Groove 1, $P = 68.9\text{kPa}$	144
Figure 4.23: A calculated surface heat transfer coefficient curve in the full tempearture range, at Groove 1, $P = 68.9\text{kPa}$	145
Figure 4.24: A comparison of the temperature curves measured and modelled at a congested location, Groove 1, $P = 68.9\text{kPa}$	147
Figure 4.25: Surface heat transfer coefficient at the congested locations.....	148
Figure 4.26: A temperature curve measured and modelled for the transition location, Groove 3, $P = 51.7\text{kPa}$	149
Figure 4.27: Surface heat transfer coefficient at the transition location.....	149

Figure 4.28: A temperature curve measured and modelled at the separation point, at Groove 0, $P = 34.5\text{kPa}$	151
Figure 4.29: Surface heat transfer coefficient at the separation point, Groove 0. ..	151
Figure 5.1: Result output of the two methods for defining cutting edge radius of a cutting tool (a) circle fitting; (b) local profile curvature calculation. ..	159
Figure 5.2: Global map of calculated surface heat transfer coefficient at 17.2kPa driving pressure.....	160
Figure 5.3: Global map of calculated surface heat transfer coefficient at 34.5kPa driving pressure.....	161
Figure 5.4: Global map of calculated surface heat transfer coefficient at 51.7kPa driving pressure.....	161
Figure 5.5: Global map of calculated surface heat transfer coefficient at 68.9kPa driving pressure.....	162
Figure 5.6: Calculated surface temperature profile for driving pressure $P = 17.2\text{kPa}$	163
Figure 5.7: Calculated surface temperature profile for driving pressure $P = 35.4\text{kPa}$	164
Figure 5.8: Calculated surface temperature profile for driving pressure $P = 51.9\text{kPa}$	164
Figure 5.9: Calculated surface temperature profile for driving pressure $P = 68.9\text{kPa}$	165

Figure 5.10: Measured cutting forces.	167
Figure 5.11: Measured radial forces.	167
Figure 5.12: Measured surface roughness.	170
Figure 5.13: Cost composition at varying cutting conditions.	174
Figure 5.14: Energy composition of the different cutting conditions.	178
Figure 6.1: Optimization for minimal manufacturing cost, in \$.	186
Figure 6.2: Optimization for minimal energy consumption, in kWh.	187
Figure 6.3: Population plot of optimization for highest <i>ProcSI</i> score.	189
Figure 6.4: <i>ProcSI</i> results from best experimental condition and optimal condition obtained through optimization.	190

CHAPTER 1

INTRODUCTION

1.1 Concepts of Sustainable Manufacturing

Sustainable development is defined as the development that “meets the needs of the present without compromising the ability of future generations to meet their own needs” (UNWCED, 1987). Also, sustainable development is the "process of achieving human development ... in an inclusive, connected, equitable, prudent, and secure manner" (Gladwin et al., 1995). Manufacturing contributes to 16.5% of total GDP worldwide, and 12.4% within US according to World Bank data (The World Bank, 2013). Manufacturing has been the major driving force for economic growth, and it has the highest effect on the economic growth in industry (Bureau of Economic Analysis, 2011). To promote sustainable development, manufacturing should become a major focus. The current trend of tough regulations on environmental impact, customer preferences of “green products” and global competition requires the manufacturing industry to develop new strategies for sustainable development. The development and application of the sustainable manufacturing concept is considered as part of the solution.

The commonly referred definition of sustainable manufacturing is that proposed by the U.S. Department of Commerce, which reads as “the creation of manufactured products that use processes that minimize negative environmental impacts, conserve energy and natural resources, are safe for employees, communities, and consumers and are economically sound” (U.S. Department of Commerce, 2009). In addition to this original definition, National Council For Advanced Manufacturing (NACFAM) emphasizes the

need for considering manufacturing of “sustainable” products and the sustainable manufacturing of all products (NACFAM, 2009). Adapting the US Department of Commerce definition and the NACFAM modification, Jawahir et al. (2013) stressed that sustainable manufacturing must demonstrate reduced negative environmental impact, offer improved energy and resource efficiency, generate minimum quantity of wastes, and provide greater operational safety and personal health, while maintaining and/or improving the product and process quality.

Sustainable manufacturing is not defined as a threshold condition or an ultimate scenario, but it calls for the need for continuous improvement in all aspects of sustainability. To improve sustainability performance in manufacturing, it is necessary to understand how to quantitatively evaluate sustainability performance. A quantitative sustainability assessment could be carried out for manufactured products, manufacturing processes or manufacturing systems if relevant metrics are properly identified and evaluation methods are adequately developed (Jayal et al., 2010). While such comprehensive predictive models are yet to be fully developed and implemented, a metrics-based evaluation of the sustainability content of manufacturing processes seems to have gained momentum in recent times.

1.2 Scope of Sustainable Manufacturing

The development of sustainable manufacturing aims at the sustainable benefits to all stakeholders, according to its definition. Thus, economic, environmental and societal impacts must be fully understood and considered in order to achieve sustainable manufacturing. These three aspects are most commonly known as the Triple Bottom Line

(TBL) (Elkington, 1997), with no reference to manufacturing or industrial applications. Though the economic impacts are well-established, there are still challenges in quantitatively evaluating the impacts of environmental and societal aspects. Beyond this, the interrelationship among these three major aspects makes the problem more complex. To cover these difficulties, when evaluating these impacts in discrete product manufacturing, the total life-cycle, including the four life-cycle stages (*Pre-manufacturing, Manufacturing, Use and Post-use*) must be considered. Also, the recently introduced 6R approach (*Reduce, Reuse, Recycle, Recover, Redesign and Remanufacture*), which promotes a multiple-life-cycle concept, needs to be incorporated for completeness (Jawahir et al., 2006a). In addition, sustainability performance assessment needs to be done at a clarified level within the manufacturing organization. Sustainability evaluation at product level, manufacturing process level, enterprise level and system level would require different data and different analysis methods. This research focuses on the sustainability assessment of manufacturing processes.

1.3 Driving Forces for Metrics-based Method for Sustainability Assessment

Since manufacturing processes are numerous and are highly-dependent on the product being manufactured, the identification and definition of the various factors contributing to sustainability is complex. Identifying the sustainability elements and sub-elements of manufacturing processes, as well as the demarcation of the boundaries can be very difficult, and this would require a significant effort to develop and use. It is essential to establish a unified and comprehensive methodology for evaluating the sustainability performance of a manufacturing process and to enable customization for specific manufacturing processes. All important aspects such as TBL, total life-cycle and the 6Rs

need to be covered to assure the comprehensiveness. There have been guidelines, concepts and principles established for the scope of the sustainable manufacturing concept, but a quantitative evaluation methodology and the associated practice optimization methods are still lacking. A metrics-based quantitative sustainability performance evaluation methodology would be a great fit for these needs.

1.4 Sustainable Cutting Fluid Applications for Machining Processes

Machining is one of the major manufacturing processes. In machining processes, the indiscriminate use of cutting fluids is a major sustainability concern. The cutting fluids may also be referred to as cutting oils, cutting compounds, lubricants, coolants or metal-working fluids depending on the specific application. Aside from being one of the major cost contributors to the machining process, the use of such cutting fluid itself has enormous environmental and societal impacts, involving health effects for shop floor personnel. On the other hand, the proper application of cutting fluids has a significant impact on the machining performance. The ever-continued effort in improving cutting fluid applications leads to the development of alternative solutions such as dry machining, machining with minimum quantity of lubrication (MQL) and cryogenic machining. This dissertation chooses the innovative cryogenic machining process as the major focus, and discusses its proper application for achieving the best overall sustainability performances through a scientific modeling and optimization of the machining process.

1.5 Research Objectives

The literature review suggests two major issues in current understanding of sustainable manufacturing processes. The first is that there is a lack of quantitative and

comprehensive method to evaluate the performance of a manufacturing process regarding sustainability concerns. The second is that, the relationship between the sustainable manufacturing concepts and the practice of manufacturing processes needs to be developed. To improve the sustainability performance of a manufacturing process, one needs to clarify how to evaluate sustainability performance, and how to decide the process parameters for the optimal sustainability performance in a scientific way. This research focuses on the cutting fluid applications, especially cryogenic machining, and is aimed at establishing a new methodology to identify the optimal working conditions for cryogenic machining to enable sustainable manufacturing.

The major objectives of this work can be summarized as:

- 1) Developing a metrics-based sustainability performance assessment methodology for discrete product manufacturing processes. Apart from the fundamental requirements of being comprehensive and quantitative, the methodology is aimed at guiding the manufacturing practices, thus it needs to take the ease of shop floor application into consideration.
- 2) Focussing on the machining process, developing a new procedure to link the scientific modeling of the machining process with the sustainability evaluation, and correlating the sustainability performance with the process parameters:
 - a. Focusing on the cutting fluid application in machining processes, and identifying the sustainability metrics influenced by cutting fluid applications, for both conventional flood cooling approach and alternative sustainable coolant application methods.

- b. Focusing on the cryogenic machining process, modeling the related heat transfer process using the principles of mechanics based on experiments and empirical boiling heat transfer model, and from this heat transfer model, establishing the machining process model.
 - c. Establish a new relationship between the process parameters and the process sustainability performance based on the process model.
- 3) Performing optimization with Genetic Algorithm (GA) to identify the optimal conditions for cryogenic machining process.

1.6 Dissertation Outline

In Chapter 2, a literature review is conducted, covering the two major elements of the research: the sustainability assessment method for manufacturing processes, and the effect of cryogenic machining on process sustainability performance.

In Chapter 3, the newly established Process Sustainability Index (*ProcSI*) methodology is described in detail. It starts with setting the scope and system boundary of the methodology. Then, the overall hierarchical structure and data processing procedure are introduced. After that, the complete metric set is presented. At the end, the *ProcSI* applications at different detail levels, namely the plant level, workstation level and operation level, are discussed. A case study on comparing different sustainable coolant applications in a machining process is given to validate the methodology.

In Chapter 4, experimental work on identifying the surface heat transfer coefficient during cryogenic machining is conducted. It involves innovative high speed temperature measurement experiments, on both a static specimen scenario and a dynamic machining

scenario. the results from the experimental work are used to establish heat transfer model in the cryogenic machining scenario. The findings in this chapter establish fundamental application guidelines to the application of cryogenic machining.

In Chapter 5, based on the application guidelines established in Chapter 4, a set of cryogenic machining experiments is carried out. The results from the experiments are fed into the *ProcSI* metrics to evaluate the sustainability performance of cryogenic machining under the experimental conditions.

In Chapter 6, an optimization process involving Genetic Algorithms (GA) is conducted, based on the empirical model of the cryogenic machining process established from the experiments.

In Chapter 7, conclusions from the research work are summarized, and a recommendation for future work is presented.

CHAPTER 2

LITERATURE REVIEW

2.1 General Sustainability Assessment Method

Ness et al. (2007) reviewed some sustainability assessment tools and classified them to sustainability indicators and indices, product-related assessment tools and integrated assessment tools. The authors highlighted the importance of following an integrated approach that incorporates nature, society, temporal aspects and spatial aspects. They concluded that there is a need for both specific assessment tools that are more case- and site-specific, as well as broader assessment tools that can be generalized. They also emphasize the need for standardized assessment tools.

In early studies (Feng and Joung, 2009; Feng et al. 2010), a comprehensive review of prominent metrics and indicators for sustainability assessment in the manufacturing domain. In their review, they classified the different methodologies based on the level of technical detail (from low to high) and the application domain (product, process, facility, corporation, sector, country and world). This work summarized the various methodologies that have been developed by a wide range of entities including corporations (e.g., Ford), international organizations (e.g., OECD), government organizations (e.g., NIST) and standards organizations (e.g., ISO). These different methodologies are presented in Figure 2.1. The *ProcSI* methodology presented later in this work evaluates the sustainability of manufacturing processes at a relatively high detail level.

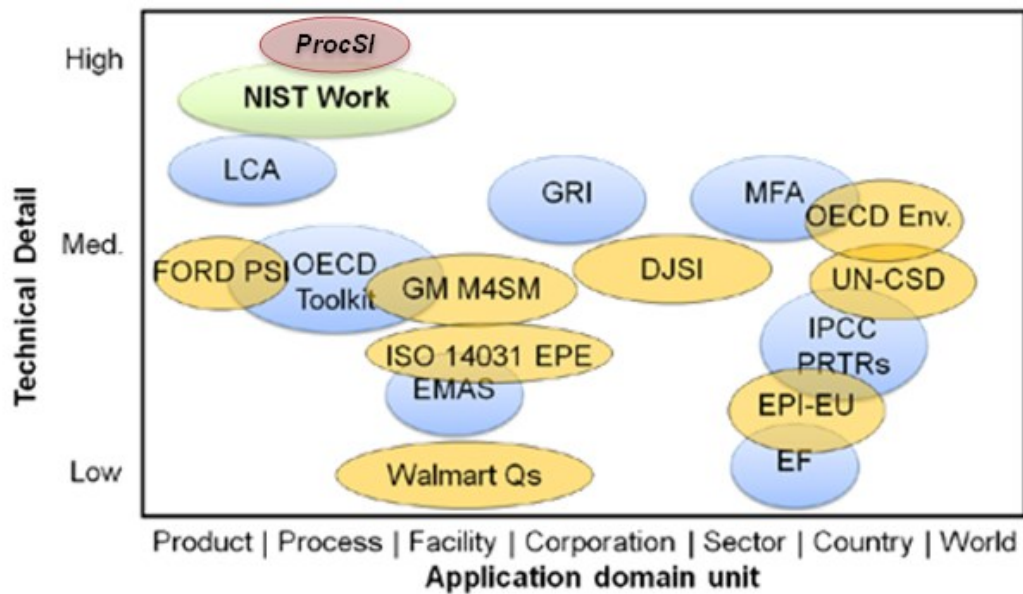


Figure 2.1: Categories of prominent sustainability evaluation methodologies, adapted from Feng et al. (2010).

2.1.1 Established sustainability assessment methods

Organization for Economic Co-operation and Development (OECD)

Extensive work by the Organization for Economic Co-operation and Development (OECD) involves the development of a toolkit to analyze processes and products to identify opportunities for improvement. This toolkit can be used by companies to calculate a set of core indicators that are comparable across companies, processes and products (OECD, 2012).

Product Sustainability Index (PSI) from Ford Europe

In 2006, Ford Europe published a Product Sustainability Index (PSI) method (Schmidt et al., 2006). Their objective was to integrate sustainability into new product development, targeting reduced environmental impact, increased value to the society and improved efficiency and affordability. The PSI consists of eight indicators covering economic,

environmental and societal and health aspects. These indicators focus on sustainability issues influenced by product development, and however, do not include issues related to service of the product, regulatory compliance, product end-of-life (EOL), etc. The subsequent car models designed using the PSI was superior to previous models in all the aspects covered by the indices. However, this method is not applicable to any manufacturing process. Neither does it consider the process-related aspects of manufacturing for evaluating the manufactured products for sustainability.

Product Sustainability Index (PSI)

De Silva (2005) proposed another *PSI* evaluation method, mostly based on consumer electronics. It suggested that the manufacturer should consider the total life-cycle impact of the product when designing a new product (Jawahir, 2006). Six aspects were considered in evaluating a product's sustainability performance, including the environmental impact, societal impact, functionality, resource utilization and economy, manufacturability and recyclability/remanufacturability. The weighting of influential factors was decided by either consumer survey or industrial expert advice. A case study on printer design was presented (De Silva et al., 2009).

Walmart Sustainability Index

Walmart has been working to develop a dedicated, marketability-based environmental product sustainability index (Walmart, 2009a). This was driven by customer demand for information on product sustainability throughout its entire life-cycle. The objective of this effort was to work with suppliers to improve the content of sustainability, and to provide relevant information on product sustainability to customers. Walmart has developed the index for six product categories, and plans to expand the index to develop scorecards for

up to 100 categories (Walmart, 2013). In addition, the company developed a method by using a set of 15 questions to assess a supplier's sustainability performance in four areas: energy and climate, material efficiency, natural resources and people and community (Walmart, 2009 b).

Sustainable Manufacturing Indicator Repository Established by NIST

The National Institute of Standards and Technology (NIST) has recently developed the Sustainable Manufacturing Indicator Repository (NIST, 2011). The purpose was to provide small and medium-sized enterprises (SMEs) in the manufacturing sector with an application and educational tool for sustainable manufacturing. The identified indicators were based on an extensive review of publicly available sustainability indicator sets. The repository has a three-level hierarchical structure: categories, sub-categories and indicators. There are five categories: environmental stewardship, economic growth, social well-being, technological advancement, technological advancement and performance management. The repository presents 212 metrics, all measured at the level of particular manufacturing processes.

Eco-indicator 95 and Eco-indicator 99

PRé Consultants introduced the Eco-indicator 95 (Goedkoop, 1995), and later updated it to Eco-indicator 99 (Ministry of Housing, Spatial Planning and the Environment, 2000). Their methodology is based on damage-oriented product LCA. They apply a weighting methodology that aggregates LCA results into easily understandable and user-friendly indicators, in comparison with the time-consuming and costly LCA methodology. Three types of environmental damages are weighted: human health, ecosystem quality, and resources. The aggregation process is done in three phases: (i) inventory phase where

LCA results for resource use, land use and emissions are calculated, (ii) modeling effects and damages (obtained from the LCA results) to resources, ecosystem quality and human health are analyzed, (iii) weighting the three categories where the seriousness of the damages in the three areas is assessed and the indicators are evaluated.

Sustainability Metrics for Green Sustainable Manufacturing

In 2009, General Motors Corp. (GM) introduced sustainability metrics for green sustainable manufacturing (Dreher et al., 2009). The metrics were based on a survey of available literatures and best practices in the different industrial sectors. They introduced 33 metrics in 6 major areas: environmental impact, energy consumption, personal health, occupational safety, manufacturing costs and waste management. A reference sustainability assessment metric set was established with targets of improving the sustainability of production operations, educating the workforce and setting standards for third party or industry-wide practices.

ISO 14031: Environmental Performance Evaluation

The International Organization for Standardization (ISO) published ISO 14031:1999 Environmental management – Environmental performance evaluation – Guidelines (ISO, 1999; ISO, 2009) for measuring, analyzing, reporting and communicating organizational environmental performance. The ISO 14031 is not a certification standard, but rather a management tool that allows corporations to select environmental performance indicators, track and report these indicators, review performance evaluation and identify opportunities for improving environmental performance. The standard identifies 151 environmental indicators, and it is applied globally in different sectors including manufacturing, health services, transportation and utility services (Putnam, 2002).

Product Sustainability Index (ProdSI)

A comprehensive sustainability performance evaluation method is developed for manufactured product (Zhang et al., 2012a; Shuaib et al., 2014). It is based on the elements and sub-elements of product design for sustainability, as shown in Figure 2.2.

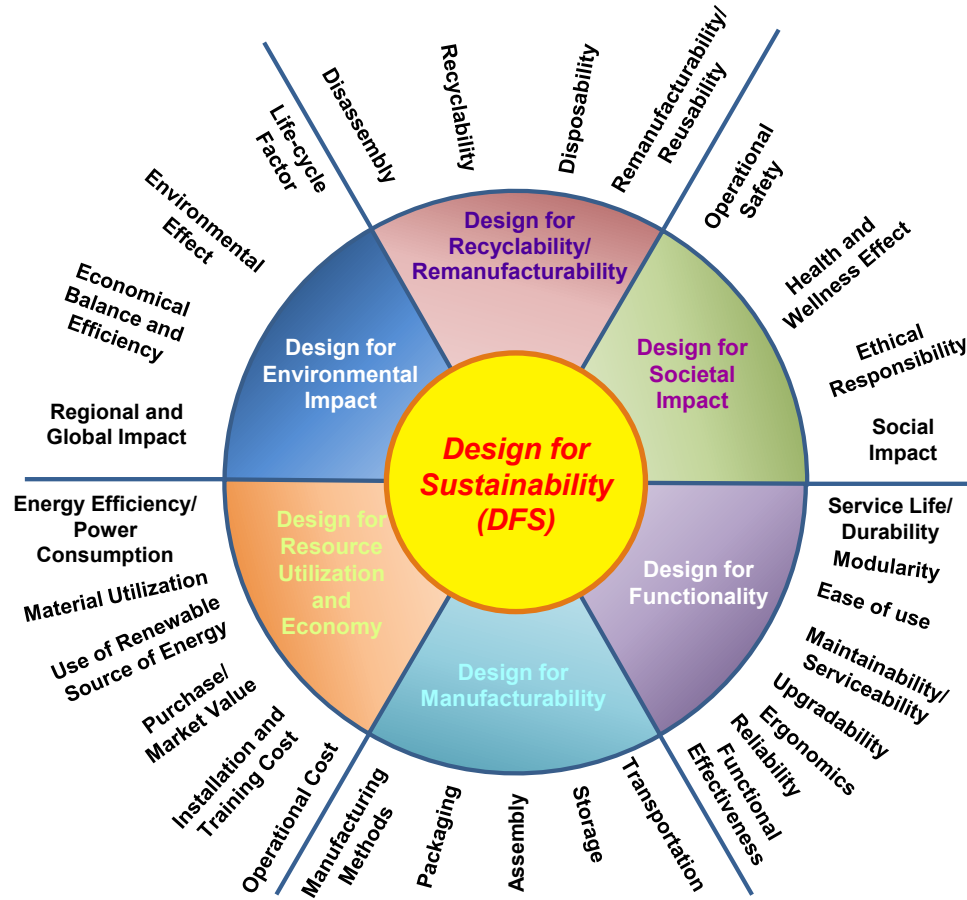


Figure 2.2: Product design for sustainability (Jawahir et al., 2006a).

The *ProdSI* method is a metrics-based method, which is similar in the structure and data processing as the Process Sustainability Index (*ProcSI*) method proposed in this work. It has ninety five metrics categorized into thirteen clusters. The collected data need to be normalized, weighted and aggregated to calculate the overall ProdSI score as the

sustainability performance indication of a manufactured product. During the process, the total life-cycle impact of the product with 6R regards is considered.

2.1.2 Sustainability assessment for chemical processing

A brief review on sustainability assessment of chemical manufacturing processes is presented here although the focus of this PhD research work is on discrete manufacturing processes. In fact, chemical processes and discrete product manufacturing have similarity in some sustainability aspects.

Sikdar (2003) made a general introduction to the sustainability metrics system. It was suggested that all the three aspects of the TBL should be considered for a comprehensive evaluation. However, he suggested that indicator sets which cover only one or two of the three aspects can also be included as part of the hierarchical metrics system. Four types of sustainability systems are considered, namely, global level, geographically-bounded area level, business level and technology level.

Subsequently, Martins et al. (2007) presented a sustainability evaluation method for a chemical production process. The scope was to evaluate the relative sustainability performance of the process to manufacturing a chemical with alternative chemical routines. The major metrics chosen were energy intensity, material intensity, potential chemical risk and potential environmental impact.

Metrics for chemical and other environmental impacts were also identified by Bare et al. (2006). The assessment tool, which is named Tool for the Reduction and Assessment of Chemical and Environmental Impacts (TRACI), is based on LCA and focuses on environmental impact. A normalization database was proposed to serve as a reference for

benchmarking within industries. By using the TRACI framework, metrics-based sustainability assessment of polymer production process was carried out (Tabone et al., 2010).

Six processes to produce dimethyl carbonate (DMC) are assessed for their sustainability performances, considering profit, toxicity and environmental impact (Monteiro et al., 2009a, 2009b). Lange (2009) presented a similar approach, which considers resource consumption, waste emission, hazards and costs. Naidu et al. (2008) assessed three kinds of nanoparticle manufacturing processes based on sustainability metrics. The metrics are categorized into either industrial engineering metrics or green chemistry metrics, along with some additional metrics. In general, all three aspects of TBL are involved. The sustainability performance of a polygeneration process was evaluated by considering economic impact, safety and environmental impact from both emissions and exergy consumption (Gangadharan, 2012).

Sikdar (2009) also presented a methodology to aggregate the measurements for a metric system to generate a representative index. The idea is to set up a benchmark measurement for each metric, and then assign weighting factors for the metrics.

2.2 Sustainability Assessment for Manufacturing Processes

2.2.1 6R concept

When considering the material flow for a sustainable product life-cycle, the '3Rs', which form the basis for green manufacturing, i.e., *Reduce*, *Reuse* and *Recycle*, have often been considered as the reference. An expanded and more comprehensive depiction for sustainable manufacturing has been proposed by Jawahir et al. (2006a) by including three

additional 'Rs', namely *Recover*, *Redesign*, and *Remanufacture*, as shown in a closed-loop material flow system in Figure 2.3. *Recover* is the activity of collecting end-of-life products for subsequent post-use activities. It can be applied to disassembly of specific components from a product at the end of its life-cycle. *Recover* also refers to products that can be sorted and processed to further reduce virgin material usage. *Redesign* of the product in view of simplifying future post-use processes is another important element that incorporates environmental considerations at the design stage of both products and processes. It also offers an opportunity for redesigning the next generation products using recovered materials and residues. *Remanufacture* involves the manufacturing processes utilizing recovered and reconditioned materials and components. It can be used to restore old products to like new condition, and offer similar or even better performance to that of the original products, thus saving natural resources, energy, and cost and reducing the waste generation (Steinhilper, 1993). The benefits of 6Rs compared to 3Rs can be summarized as cost savings, multiple life-cycle applicability, and improved material usage (Joshi et al., 2006). The near-perpetual material flow connects all the 6Rs starting at the pre-manufacturing stage until the post use stage, thus allowing the ecosystem to utilize an optimal level of raw materials and energy, and at the end, producing minimal wastes and emissions, as shown in Figure 2.3.

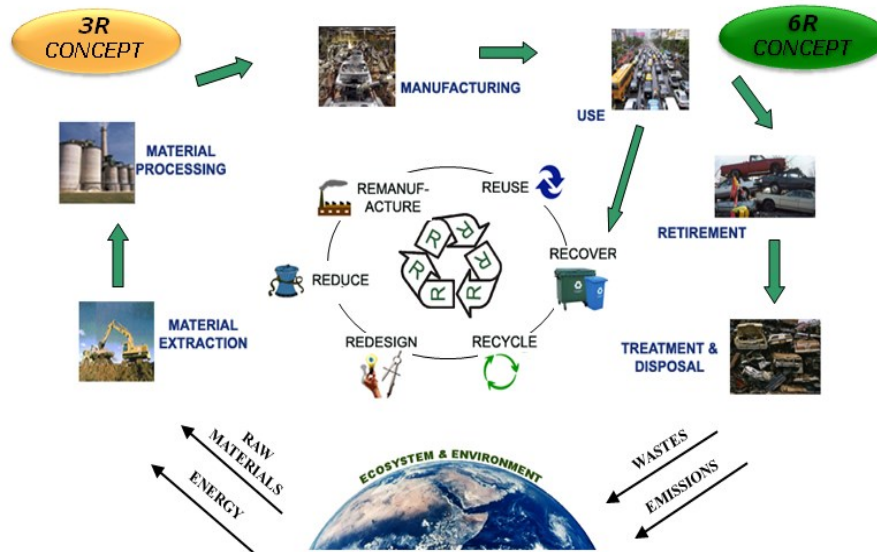


Figure 2.3: The 6R concept for a closed-loop near perpetual material flow (Jawahir et al., 2006a).

Thus, this approach allows moving from the cradle-to-grave concept, which involves only single life-cycle, to multiple life-cycles for a product in a closed-loop material flow (Jawahir et al., 2006a).

When evaluating a manufacturing process with respect to sustainability, each input and output needs to consider the total life-cycle approach, such as that described by Lu et al. (2011) for machining shown in Figure 2.4.

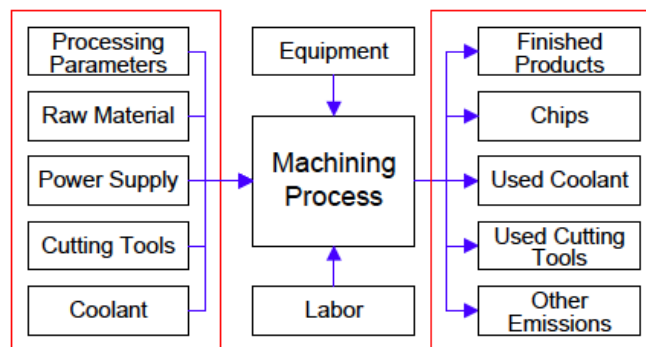


Figure 2.4: Example of an input/output chart for a machining process (Lu et al., 2011).

2.2.2 Sustainability assessment methods for discrete product manufacturing

Ameta et al. (2009) performed a carbon weight analysis for a drilling process. While focusing on the GHG emission, the process was analyzed at the operation level. Case studies based on experimental data was presented. The scope was to allocate the carbon weight generation and to serve as a criterion for the process redesign.

By using LCA, a Life cycle iNdeX (LInX) is proposed (Khan et al., 2004) for product and process design and decision making. The index is generated through a four-level system, involving sub-indices for environment and resources, cost and technology. 11 parameters for environment and resources, 3 parameters for cost, 7 parameters for technology are considered in this study. All three aspects of the Triple Bottom Line (TBL) (Elkington, 1997) are considered in those parameters.

Sustainability assessment of power generation was presented by Diniz Da Costa and Pagan (2006). Environmental impacts of atmospheric acidification, carcinogenic effects, photochemical smog and eutrophication are considered.

A set of core indicators of sustainable production was proposed by Veleva and Ellenbecker (2001). The Lowell Center for Sustainable Production (LCSP) indicator framework composes of five levels, from compliance to effectiveness till supply chain and system performance. The proposed core indicators combine measurements regarding energy and material use, natural environment, economic performance, community development and social justice, workers and products.

Five elements for the sustainable product and sustainable manufacturing processes are proposed by Sarkar et al. (2011). These are environmental stewardship, economic growth, social well-being, technological advancement and performance management.

Kong et al. (2011) presented a software-based energy consumption analysis for a machining process subject to different tool paths. This reveals the preliminary integration of scientific models with the sustainability evaluation.

An LCA of the forklift painting process was carried out by Kim et al. (2010). The LCA analysis considers the consumption of raw material, ancillary material and utility supplies. Overall the environmental impact is estimated by the eco-toxicity of the chemicals used.

LCA type assessment of micro-milling process is carried out with a focus on energy consumptions by Liow (2009). The conventional CNC facility and micro-milling facility are compared, taking into account the consumption of utilities, such as compressed air and metal-working-fluid.

Technology, energy and material are considered as the three major factors in the work by Yuan et al. (2012). A case study on an Atomic Layer Deposition process is carried out, and material and energy efficiency, GHG emission and material toxicity are the metrics involved.

Gutowski et al. (2009) discussed the energy/exergy consumption for manufacturing processes from a thermodynamic point of view. A series of manufacturing processes are compared in terms of energy consumption versus material processing rate.

Gutowski et al. (2006), in their earlier work, also applied the concept of exergy to estimate electricity requirements for a wide range of manufacturing processes. They

presented a simple conceptual model which combined electricity requirement for getting the machine to the ready position (which is constant) and for material processing (which is proportional to processing rate).

Pfefferkorn et al. (2009) proposed a metric for defining the energy efficiency of thermally assisted machining. The metric aims to determine how much thermal energy is required to achieve the needed temperature during the process and on the cost involved. The total thermal energy spent to preheat the workpiece is compared with the theoretical minimum required heat necessary to remove material. Four sets of data is considered: thermally-assisted turning of silicon nitride and partially stabilized zirconia, and micro-end milling of *6061-T6* aluminum and *AISI1018* steel.

Dahmus and Gutowski (2004) presented an environmental impact analysis of machining processes under different manufacturing organization forms, considering the energy consumption of various components of the machine tool and the cutting fluid consumption. In another work, the energy streams inside a machine tool is analyzed to correlate with different process parameters (Ikra et al., 2005).

Dahmus and Gutowski (2007) presented an information model for assessment and modeling of material separation processes that take place in the material recycling processes. Gutowski et al. (2007) also attempted to characterize the material and energy transformations that take place in manufacturing processes. All the energy data is considered by a thermodynamic analysis of the energy required for material use in manufacturing, the energy consumed in manufacturing process itself and the efficiency of material and energy transformations during these processes. The trend of how material and energy are used in a variety of manufacturing processes was presented.

Saloni et al. (2005) presented the characterization of abrasive machining in wood processing. The variables affecting the material removal rate, surface quality and power consumption are considered. A statistical analysis of the considered variables is presented and their interactions are shown.

Floating particles from cutting fluid is considered as a major working environment concern in machining processes. Bell et al. (1999) introduced an analytical model to predict coolant emission due to machining process.

Thorne et al. (1996) proposed an environmental assessment of a machining plant. The focus is on aerosols, bioaerosols and airborne endotoxins generated by the use of metalworking fluids. The study demonstrates that the airborne level of endotoxin in automotive machining plants may exceed the thresholds for respiratory health effect suggesting a more careful monitoring of the inhalation exposure of workers.

Environmental benign manufacturing or green manufacturing are discussed by many researchers. Kondo (1997) presented some environmental concerns in machining processes, including reduction of energy and reduction of cutting fluid. Choi et al. (1997) categorized the material flow of different manufacturing processes into three groups, namely, mass reducing process, mass conserving process and joining process. This provides possibilities to account the physical flows of the process to determine its sustainability performance. In their work, waste, energy consumption and waste water emission are considered.

The environmental burden due to the application of coolant in machining processes is discussed (Sutherland et al., 2000; Weinert et al., 2004). The mist generation due to coolant application and material deformation is analyzed to identify the contribution from

different factors including cutting speed, flow rate, enclosure and distance. The comparison between conventional flood cooling and dry machining is presented.

In 2002, Panel for International Assessment of Environmentally Benign Manufacturing Technologies was founded. A global review on corporate efforts on environmental concerns and research in manufacturing was presented, comparing the general trends in Europe, Japan and USA (Allen et al., 2002; Gutowski et al., 2005).

More recently, the integration of modeling for process design in pursuit of sustainable manufacturing is addressed as an important approach (Jawahir and Dillon, 2007; Jayal et al., 2010). Scientific modeling provides the opportunity to quantify the results of a design, and furthermore support design optimization.

Table 2.1 summarizes the above reviewed work in terms of the levels of detail involved, TBL considerations and total life-cycle considerations.

Table 2.1: Comparison of reviewed sustainability assessment methods for discrete product manufacturing.

Authors	Year	Level	TBL	Total Life cycle
Ameta et al.	2009	Operation	×	×
Khan et al.	2004	System	√	×
Diniz Da Costa and Pagan	2006	Process	×	×
Veleva and Ellenbecker	2001	System	√	√
Sarkar et al.	2011	System	×	×
Kong et al.	2011	Operation	×	×
Liow	2009	Process	×	×
Yuan et al.	2012	Process	√	×
Gutowski et al.	2009	Process	×	×
Sutherland et al.	2000	Operation	×	×
Weinert et al.	2004	Operation	×	×
Pfefferkorn et al.	2009	Operation	×	×
Granados et al.	2009	Operation	√	×
Wanigarathne et al.	2004	Process	√	√
Jawahir and Dillon	2007	Operation	√	√
Jayal et al.	2010	Operation	√	√
√ = concept considered; × = concept not considered				

2.2.3 Fundamental work related to the development of a new Process

Sustainability Index (*ProcSI*) method

Developing sustainable processes to meet different levels of sustainability requirements is one of the most important considerations to enhance manufacturing sustainability. Implementing sustainability in manufacturing processes requires careful planning and execution. Evaluation of the impact of manufacturing processes must consider all three aspects of sustainability: economy, environment and society. The manufacturing

processes are expected to minimize negative impact on the environment such as reducing the energy consumption, protecting air quality, consuming other resources such as water, reducing the waste generated etc. Manufacturing processes are numerous and are highly-dependent on the product being manufactured. Thus, the identification and definition of the various factors contributing to sustainability are complex, and identifying the sustainability elements and sub-elements of manufacturing processes, as well as the demarcation of the boundaries, may require significant efforts. For these reasons, it is essential to establish a unified methodology for evaluating the degree of sustainability of a given manufacturing process.

The first step towards developing a scientific assessment method is to identify the elements of manufacturing processes that contribute to sustainability. Wanigarathne et al. (2004) introduced six elements of sustainable manufacturing processes, shown in Figure 2.5.

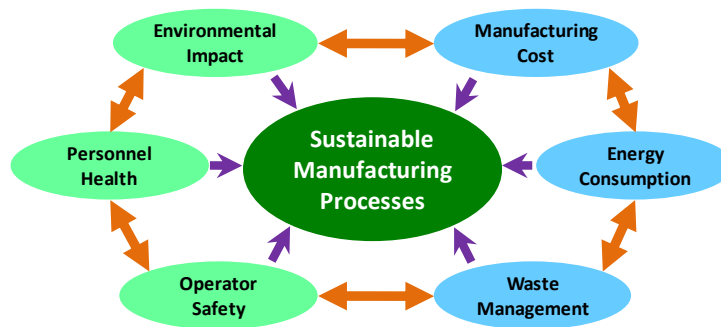


Figure 2.5: Six major elements of sustainable manufacturing processes (Wanigarathne et al., 2004).

Manufacturing cost should be considered to ensure the economic soundness and technological validity. In the content of manufacturing process sustainability assessment, the scope is limited to only the cost involved during the production activities. Thus, direct

and indirect costs from capital-related, environment-related and society-related factors must be considered.

Energy consumption is important, due to the global impact of energy production and consumption. In manufacturing processes, not only the energy consumption of the manufacturing operation/process, but also the energy consumed by machine tool accessories, including coolant pumps, auxiliary equipment, production supporting facilities, in-plant transportation, etc., should all be considered.

Waste management considers the generation and post-treatment of all wastes produced during and after the production activities. A simple target of zero wastes and no emissions may be the ideal case, but is hardly achievable with the current level of technologies. Therefore, the best utilization of the materials to achieve a closed-loop material flow with minimal wastes and emissions must be considered in the manufacturing process sustainability assessment.

Environmental impact accounts for major factors influencing the environment, including resources consumption (i.e., various foot-prints), emissions and waste disposal. Different manufacturing processes would have significantly different behaviors related to this element. Thus, analysis and comparison would be feasible only among similar processes unless a universal benchmarking method is established.

Personnel health deals with the immediate and long-term impacts of the manufacturing processes on the shop floor and supervisory personnel's' health due to the prevalent working environment. It involves not only the compliance with the regulations and standards from governmental agencies or third-party regulatory organizations such as

EPA, OSHA and NIOSH, but also the established personnel's health records and historic data.

Similarly, the element of *safety* concerns the impact of the processes on the operational safety and the conditions enforced.

Quantitative modeling and analysis of all six elements and then, integrating them to make the necessary decisions through an optimization process, require a considerable effort and case studies for validation with real practices. Three of the six elements, manufacturing cost, energy consumption and waste management, can be modeled with analytical techniques due to their deterministic nature. Modeling of the other three elements, the environmental impact, personnel health and operator safety, due to their non-deterministic nature, requires the use of non-deterministic techniques such as fuzzy logic.

Wanigarathne et al. (2004) initiated the development of a sustainability assessment methodology for machining processes by considering the six major elements of sustainable manufacturing processes. Later, this work was extended by Granados et al. (2009) by using a hybrid model to evaluate the machining process sustainability for optimized machining performance, considering both the deterministic and the non-deterministic elements.

Their work shows such sustainability evaluation can be integrated with science-based modeling and optimization methods in order to achieve sustainable manufacturing. These initial studies considered dry machining and near-dry (MQL-based) machining processes as viable alternatives to flood-cooled machining methods. However, these studies were restricted to the limited data available, and a small number of qualitative measurements was considered. Thus, the outcome from these efforts had only limited applications, and a

much more comprehensive and expanded measurement set would be needed. Furthermore, the normalization of the measured data and the score aggregation need to be systematic. In general, this early work serves as a good foundation for quantitative understanding of the complexity of the process sustainability modeling tasks. There is a need for a more comprehensive analysis of sustainability elements through a systematic metrics-based approach.

2.3 Influence of Cutting Fluids on the Sustainability Performance of Machining Processes

In machining, the indiscriminate use of cutting fluids (CFs) or metal working fluids (MWFs) has mixed impacts on the machining process. One of the major purposes of applying cutting fluids during a machining process is for cooling the cutting tool and the workpiece. This will help with tool-life performances and workpiece quality. Another effect of applying CFs is lubrication of the cutting process. Other contributions of the CF application include chip removal and corrosion resistance of the workpiece and machine tool (Rotella et al., 2011).

Conventional cutting fluids, including the major types of mineral oil-based or synthetic/semi synthetic water-based fluids, have various sustainability issues. Categorized according to the triple bottom line of sustainability, some of the major sustainability impacts are reviewed here.

2.3.1 Economic impact

When discussing the economic impact of the CF applications, the scope should not be limited to the purchase price, but should also include the cost involved in coolant system

purchase, maintenance and treatment of used CF. These costs, when combined, could take up to 16% of the total machining cost (Byrne and Scholta, 1993). As a comparison, tool cost is typically only 4% (Adler et al., 2006). Among the total cost involved, the maintenance and treatment cost could be up to four times of the purchase price. This is caused by the fact that many CFs are not bio-degradable and contain hazardous content, thus, they must be contained well, and this would require expensive treatments after disposal (Hong and Zhao, 1999; Bierma and Waterstraat, 2004).

2.3.2 Environmental impact

It is easy to understand that the pre-manufacturing and manufacturing of the cutting fluids involve raw consumption of natural resources including fossil fuels. More importantly, the use and post-use environmental impact of CF applications could not be underestimated.

It is absolutely essential to implement a proper maintenance of the cutting fluids since they are considered a favorable environment for growth of bacteria and fungi. If bacteria grow in the fluids, the lubricity can be compromised, the risk of corrosion of the workpiece and machine tool increases, as well as the danger for workers on the shop floor increases (Sokovic and Mijanovic, 2001). Thus, the use of chemicals and additives such as biocides is necessary to contain the bacterial growth even if they are unfavorable substances for both workers and the environment. In addition to biocides, there are many other chemicals in the cutting fluids, which are also considered hazardous to the environment and human health (NIOSH, 1998a; NIOSH, 2007).

During machining operations, a part of the cutting fluid is vaporized and atomized due to high pressure and temperature and form cutting fluids mist (Alder et al., 2006). This forms a waste stream of the process and leads to chemical emissions.

2.3.3 Societal impact

The application of conventional flood cooling and the disposal of used coolant are the major health threat to the shop floor operators and workers in manufacturing plants. The most commonly observed illnesses associated with the use of coolant are skin problems due to direct contact, lung disease due to aerosols/mist inhalation, and cancer due to the chemical contact. As a result, NIOSH issued a recommended exposure limit (REL) of 0.4 mg/m³ for thoracic particular mass as a time-weighted average (TWA) (NIOSH, 1998a; NIOSH, 2007).

Direct contact of coolant in its application with machining processes is typically due to touching contaminated surface, handling parts and equipment, splashing fluids and coolant mist settling on the skin. In these cases, a different and protective level of machine enclosure would have a reduced level of exposure, but can hardly eliminate the coolant exposure (Hands et al., 1996). Mist generation in coolant applications is considered as the major contamination source in even a well-maintained shop floor environment, and models are built to establish the relationship between mist generation and machining processes (Sutherland et al., 2000; Yue et al., 2004; Sun et al., 2004; Alder et al., 2006).

2.3.4 Alternative sustainable cutting fluid solutions

Due to the burden of conventional flood cooling applications, as presented above, a great amount of effort has been taken to develop alternative coolant application methods.

With a driving force to solve a part or all of the sustainability problems with conventional flood cooling method, innovative coolant application methods are developed with a potential to become sustainable coolant application techniques. There are two principle functions of coolant in the machining processes: cooling and lubrication (Sokovic and Mijanovic, 2001; Greeley and Rajagopalan, 2004; Alder et al., 2006). These potential sustainable coolant application candidates behave in dramatically different ways to achieve these major functions compared to conventional flood cooling.

Dry machining

The first solution is the dry machining method, which is machining without the application of fluid-form coolant. This is achieved along with a series of development in cutting tools and tooling, including process optimization, tool geometry optimization, tool coating technology and rigid and more powerful machine tool systems (Popke et al., 1999; Graham, 2000; Sreejith and Ngoi, 2000).

However, the lack of both cooling and lubrication can hardly be compensated for all materials. Thus, the application of dry machining is limited, and its potential disadvantages in productivity need to be considered together with its benefits of saving coolant usage.

Machining with Minimum Quantity Lubrication (MQL)

Another solution is the machining with Minimum Quantity Lubrication (MQL). Its core concept is to use a minimum quantity of coolant, and is also addressed as near-dry machining (NDM). The typical solution is to feed an air-oil mixture or called aerosol to the cutting zone (Astakhov, 2008). The process which uses compressed air to create and drive small droplets of coolant is called atomization. It is expected that the small amount of coolant will provide sufficient lubrication to the cutting zone, and the evaporation of the coolant is just enough to take away the heat generated in the machining process from the cutting tool and workpiece (Astakhov, 2008; Marksberry, 2004; Wanigarathne, 2006). However, the cooling capability of the MQL application is limited by its small amount of coolant, which has a limited latent heat capacity to absorb a large amount of heat. Furthermore, the atomization is intentionally creating aerosols, thus it could generate even more health-threatening mist than conventional flood cooling application (Gressel, 2001). However, the full extent of such negative impact from the MQL applications has not yet been adequately studied.

Cryogenic machining

The other innovative coolant solution is the cryogenic machining. It utilizes fluid at extremely low temperature as the coolant. Cryogenic coolant and cryogenic machining are the common terms used, though the qualification of cryogenic condition may differ due to different threshold limit of the term “cryogenic”. In physics, the threshold is usually set as -150°C (123°K), and NIST consider the limit as -180°C (93°K). In this case, liquid nitrogen (LN) is the most commonly used cryogenic coolant, which has a saturation temperature of -196°C (77°K) under atmospheric pressure (10.1kPa) (Matweb,

2013a). And, the other often used low temperature media, carbon dioxide (CO_2) does not have liquid phase below 520kPa. The gas phase will deposits directly to a solid phase at the temperature below $-78.5^\circ C$ ($195^\circ K$) (Matweb, 2013b).

The nitrogen gas is inert and non-poisonous, thus is not considered as a hazardous material. The liquid nitrogen applied will evaporates into the atmosphere without any negative effect and will leave no residues on the workpiece or the machine tool surfaces. Application of liquid nitrogen and nitrogen gas does not require additional protective equipment other than standard ventilation. Combining all these advantages above, cryogenic machining is considered a sustainable process (Hong, 2001).

Aside from the process performance benefits, the cryogenic machining shows a potential to improve product quality by introducing better surface integrity on the machined surface of the workpiece, compared with other forms of coolant application. These beneficial features may include low surface roughness, high surface hardness, white layer elimination, fine grain surface and compressive residual stresses (Kaynak et al., 2014).

However, the high unit-price of liquid nitrogen and its one-time use only limitation, extreme low temperature, and most importantly lack of application guidelines, cast some negative opinions on the use of cryogenic machining with liquid nitrogen.

There are both positive and negative opinions on the dimension accuracy of components made by cryogenic machining, frost bite threat and cost-effectiveness (Hong, 2001; Dhar et al., 2002a; Dhar et al., 2002b; Ye and Schoenung, 2004; Dhar and Kamruzzaman, 2007; Pusavec et al., 2010a; Pusavec et al., 2010b; Yasa et al., 2012). In this regard, it should be emphasized that it is rarely clarified if the cryogenic machining parameters are optimized for a certain target, like minimal cost, best product quality or longest tool-life. Actually,

there are far too many different ways to apply cryogenic fluid at or around the cutting zone for a given application, as summarized by Yildiz and Nalbant (2008).

2.4 Cooling Effect of Cutting Fluid

As a fundamental function of coolant application in machining processes, the cooling capability of a coolant application method need to be specified. In a general form, the heat transfer at the coolant contact surface can be summarized as shown in Equation (2.1) as follows.

$$q = h \cdot (T_{surf} - T_{coolant}) \quad (2.1)$$

where, q is the heat flux, in J/s; h is the surface heat transfer coefficient, in W/(°Cm²); T_{surf} is the surface temperature of the workpiece or cutting tool, in °C; and $T_{coolant}$ is the coolant temperature at the contact zone, in °C.

It is obvious that a higher heat flux, which could be translated as faster cooling, can be achieved by either increasing the temperature difference between the surface and the coolant, or by introducing a higher surface heat transfer coefficient. In the case of the conventional flood cooling and MQL applications, the coolant temperature is usually regarded as the room temperature (25°C) or system controlled temperature (typically 20°C). For cryogenic machining, the liquid nitrogen flow will remain at its saturation temperature (-196°C under 10.1kPa pressure) until the liquid phase is totally vaporized. Thus, cryogenic coolant will provide a larger temperature difference between the coolant and the surfaces of the workpiece and cutting tool than the conventional cooling method and MQL cooling. Their surface heat transfer coefficients, due to their different cooling mechanism, could be dramatically different, too.

2.4.1 Cooling effect of conventional flood cooling

In flood cooling analysis, the heat transfer mechanism is considered as convection heat transfer between coolant and the hot surface. The typical suggested value ranges within 1500-2000 W/(°Cm²) in most software. A value of 9000 W/(°Cm²) was suggested for turning and boring operations based on fluid dynamic analytical solutions (Daniel et al., 1996). Shen et al. (2001) estimated the value of surface heat transfer coefficient to be in the range of 2500-4000 W/(°Cm²). This is based on the solution of inverse heat transfer problem (IHTP) with temperature data recorded by multiple thermocouples embedded in the workpiece. Another approach is to estimate the surface heat transfer coefficient by varying the boundary condition in a FEM model to correlate with experimental data (Childs et al., 1988). These approaches are based on the assumption of thermal stable condition, and are widely used by other researchers, giving comparable results under different flow rates and process setup. The values obtained range from 1000 to 12000 W/(°Cm²) (Daniel et al., 1996; Childs et al., 1988; Zheng et al., 2000).

2.4.2 Cooling effect of MQL application

In heat transfer analysis of MQL application, the heat transfer mechanism is considered as a combination of convection heat transfer between air flow and the hot surface, and boiling/vaporization of coolant droplet.

For the air cooling part, a similar approach is adopted as in Section 2.4.1. The values of surface heat transfer coefficient obtained range from 5 W/(°Cm²) to 80 W/(°Cm²) (Daniel et al., 1996; Zheng et al., 2000).

For the fluid droplet vaporizing part, there is a huge variation among published work (Wanigarathne, 2006). Different scenarios are used in analyzing the problem (Deb and Yao, 1989; Sozbir et al., 2003; Ciofalo et al., 1999; Shiina et al., 2000), generally trying to build a relationship between the surface heat transfer coefficient and the mass flow of the MQL application. The values range from 50 to 400 W/(°Cm²). In the work by Ciofalo et al. (1999), the value could be as high as 3000 W/(°Cm²). This implies that in MQL coolant application, the dominant cooling mechanism might be the vaporization/boiling of the coolant.

2.4.3 Cooling effect of cryogenic machining

Cooling in cryogenic machining

Unlike the other forms of coolant application, cryogenic fluid especially liquid nitrogen is under super-critical status, which means that the fluid tends to absorb heat and vaporize whenever possible.

Cryogenic coolant application is believed to have superior cooling capability compared to conventional flood cooling and MQL application, but sometimes it is just taken as a conventional coolant at a lower temperature (Hong and Zhao, 1999; Hong and Ding, 2001; Dhar and Kamruzzaman, 2007). It is also believed that liquid nitrogen between the cutting tool and cutting zone could provide some lubrication effect (Hong et al., 2001; Hong et al., 2002; Hong, 2006; Courbon et al., 2013). But, there is very limited amount of published work on the heat transfer mechanism in cryogenic machining, especially focusing on the fundamental surface heat flux measurement. The most quoted work is from Ding and Hong (1995). In that particular work, $\varnothing 75\mu\text{m}$ fine thermocouples were

embedded beneath the surface of the cutting tool which is subjected to LN jet. The measured temperature gradient is thus used for the consequent finite element modeling (FEM). Such measurements have many difficulties, such as the extremely large temperature gradient involved, limited response time of thermocouples, interference between multiple thermocouples (Dillon, 1966). In general, it could be summarized that there is a lack of fundamental understanding of the heat transfer mechanism due to the cryogenic coolant application in machining.

Boiling heat transfer in material forming processes

When the surface being cooled has a much higher temperature than the saturation temperature of the coolant, boiling occurs. Boiling could provide much higher heat flux than convection heat transfer. Boiling process is typically categorized in three stages: nucleate boiling, transition boiling and film boiling, which is summarized by the famous Nukiyama Curve (Auracher, 2003), like the one shown in Figure 2.6. In the figure, the temperature difference between the hot surface and the coolant saturation temperature is called overheat temperature (Pitts and Sissom, 2011).

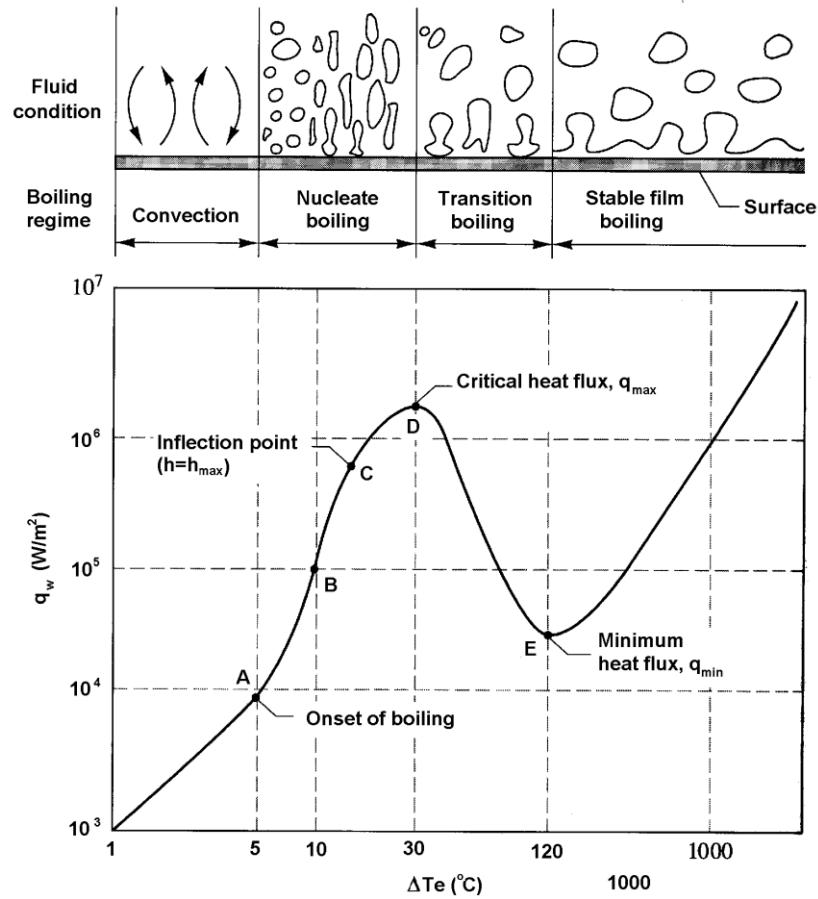


Figure 2.6: Heat transfer regimes and typical boiling curve for water at atmospheric pressure (Tong and Tang, 1997).

However, there is little work correlating the boiling heat transfer with cooling in cryogenic machining. On the other hand, a good amount of researches has been carried out in the area of metal forming process, regarding the boiling heat transfer and jet cooling applications. Surface heat transfer coefficient as high as $2 \times 10^5 \text{ W}/(\text{°Cm}^2)$ was reported for jet cooling on steel strips (Chen et al., 1990). Subsequent work by Chen and Tseng (1992), showed that the control parameters influencing the heat transfer and the background mechanics for the case of controlled cooling of steel rolling can be summarized as:

- The flow rate or jet velocity: effect of flow pattern

- The fluid temperature: the effect of sub-cooling
- The surface temperature: the effect of superheating
- The speed of surface motion

In the case of cryogenic machining, the saturation temperature of the liquid nitrogen can hardly be controlled. Thus, the flow rate/speed, surface temperature and surface speed are considered as the influential factors.

CHAPTER 3

PROCESS SUSTAINABILITY INDEX (*PROCSI*)

3.1 Scope and System Boundaries

It is very important to identify the scope and system boundaries when assessing the sustainability performance of a manufacturing process. In this chapter, we consider the manufacturing of a discrete product. While the proposed methodology could be customized to cover other manufacturing processes, the machining process is used as an example here to illustrate the development of the detailed set of metrics.

3.1.1 Scope of the *ProcSI* methodology

The scope should clarify the overall purpose of the evaluation, and the viewpoint that the evaluation stands for. In our proposed *ProcSI* method, the purpose of the study is to evaluate the sustainability performance of a manufacturing process, and then to identify potential improvement areas to improve sustainability. This requires a detailed methodology that is capable of covering all the important aspects, and highlighting the controllable or manageable features. Furthermore, this new methodology must also offer the scenario to show how certain sustainability impact factors can quantitatively influence the sustainability performance of a manufacturing process. In essence, this new methodology should lead to modeling and planning of a more sustainable manufacturing process. In normal practices, the alternative manufacturing processes, among which the most sustainable one is desired, are typically designed for a specific product or a family of products. Thus, it is reasonable to assume that their effective outputs are same or comparable.

The method can also be used as a benchmark tool for both third party and in-house self-examination. Third party evaluators can also use the method to test the performance of current manufacturing processes used by different manufacturers. The manufacturers can also use the proposed method to compare alternative manufacturing processes to determine the most desired one from a sustainability perspective. Moreover, the capability of integrating predictive models for performance prediction has been considered from the very beginning of the method development. In this case, the method is expected to primarily serve the manufacturers as an engineering tool in developing strategies to improve manufacturing sustainability.

3.1.2 System boundaries of the system

The boundary of the assessment can vary significantly, and should be determined according to the scope of the study. Because the major intent is to help manufacturers improve the process design, the boundary definition must consider the physical flow of the manufacturing process under investigation. Thus, the system boundary is drawn around the manufacturing facility within which the products are manufactured, as shown in Figure 3.1. Enterprise level decision making, supply chain management or national/global industry development, etc., are not the concern here, though the process sustainability would inevitably have an impact on these important sustainability hierarchy levels.

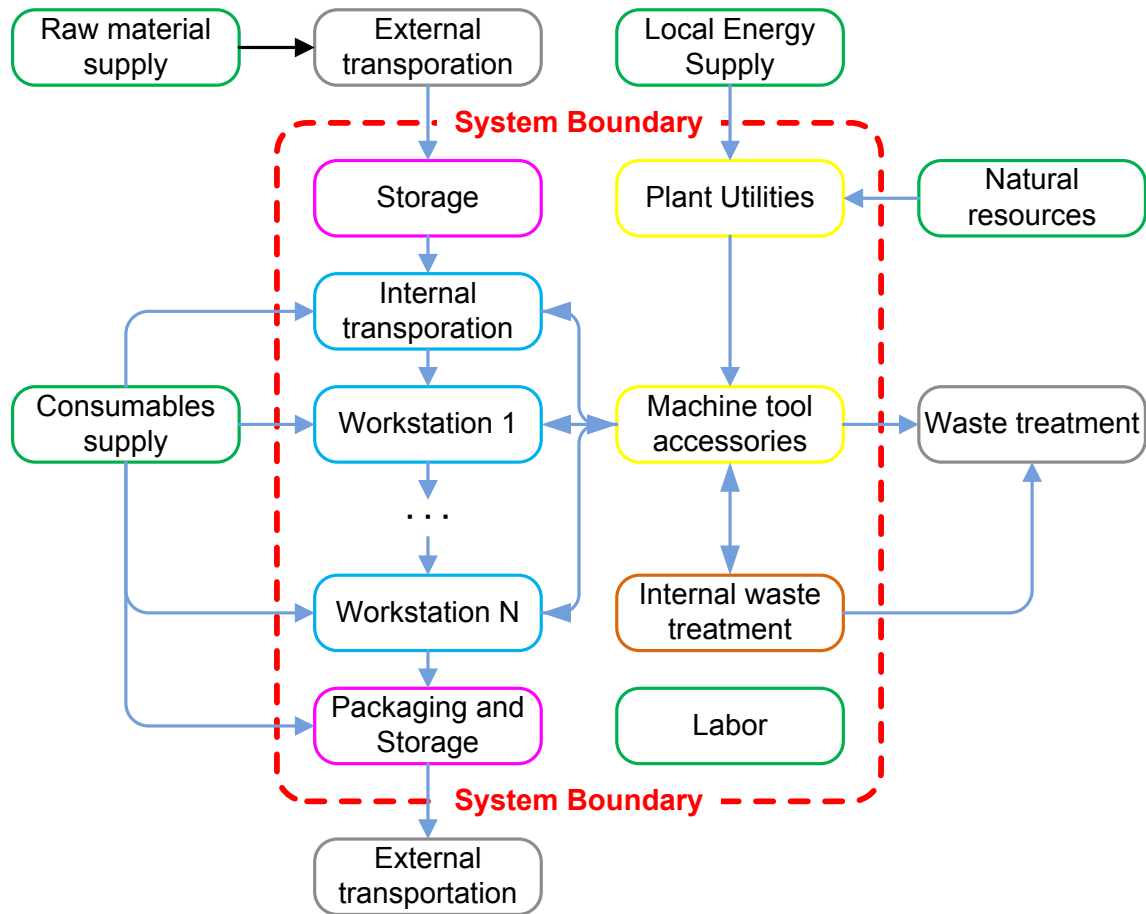


Figure 3.1: System boundary of the proposed *ProcSI* method.

As shown in Figure 3.1, the system will include machine tools which are used to carry out the production activities. CNC machining and turning centers, grinding machines, additive process machines like 3D printers, dedicated work stations, etc., are some of the examples of the production equipment used. The accessories dedicated to a machine tool are considered part of it, such as control or communication units, dedicated coolant supply systems, power management, material handling (including feeding) and chip removal systems. These components of the production equipment are often physically integrated with the machine tool, and can be considered as integrated accessories. From the process point of view, the machine tools are usually considered as long-term capital

investment which is considered in the metric set. As the manufacturing process is the focus, the pre-manufacturing and manufacturing, treatment of the end-of-life machine tools are beyond the scope of analysis here.

The utilities directly serving the machine tools must also be considered. In industrial environment, these include, but are not limited to, in-line transportation, compressed air supply, chilling water supply and fuel supply. It must also be noted that these supporting systems are often centralized, serving many manufacturing processes in the system apart from the one being considered. In such cases, individual process-related consumption rates can be estimated by allocating the total consumption using appropriate criteria. One must distinguish these plant-concentrated utilities within the system boundary from external utilities outside the system boundary. A utility should be considered as part of the system, if it is controlled and managed by the manufacturer, and its statistical data is directly collected by the manufacturer. These ideas are summarized in Figure 3.2.

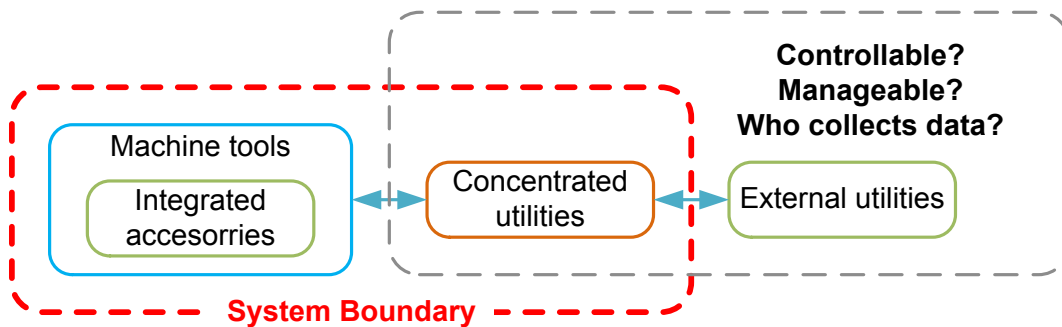


Figure 3.2: Integrated accessories and concentrated and external utilities.

The raw material being processed is another important aspect to be considered, along with the direct consumables including cutting tools and coolant. It should be noted that while the pre-manufacturing of raw materials and consumables is beyond the scope of analysis here, their impacts, when used within the process and corresponding end-of-life

treatment within the plant, need to be considered. The logistic activities related to raw materials, consumables, finished product and wastes outside the plant are also disregarded, as they are typically considered as issues at the level of manufacturing system. Considering the raw materials, cutting tools and coolant, the production activities under investigation here is the use phase of their life-cycle stages. The sustainability assessment of a manufacturing process focuses on the manufacturing phase of the manufactured product, as shown in Figure 3.3.

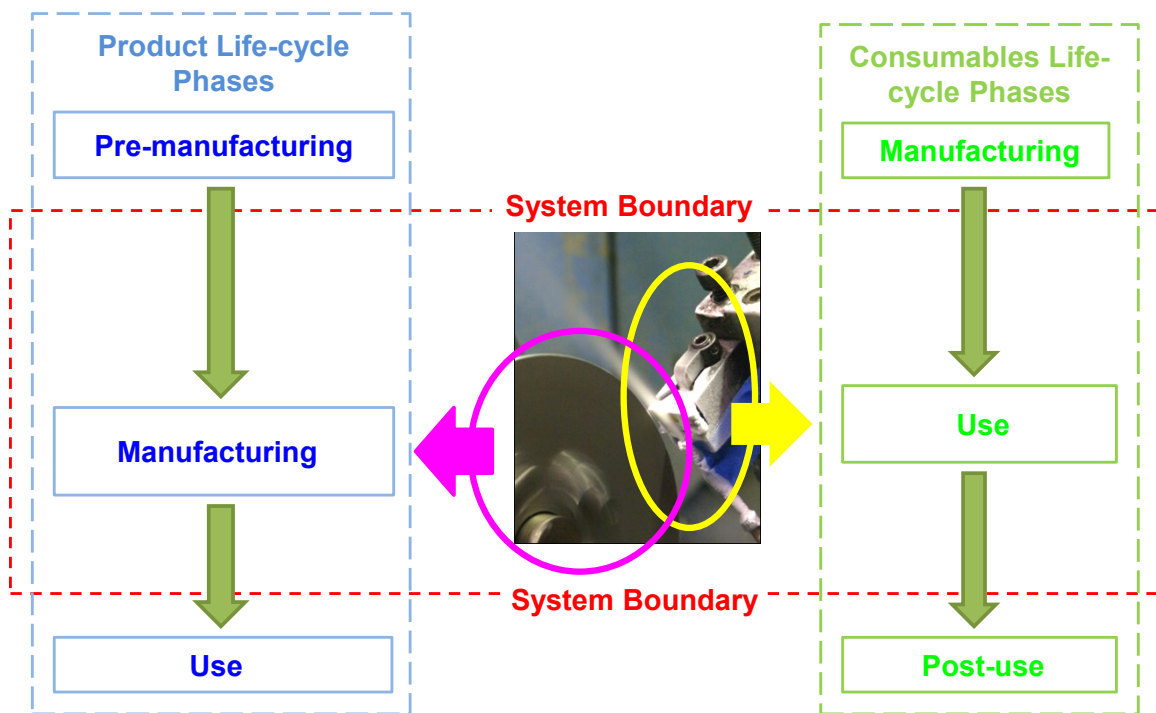


Figure 3.3: Life-cycle stages of the production consumables and the manufactured product.

Both direct and indirect labor involved in operating the manufacturing process are considered for process sustainability assessment. Being a key group of stakeholders of the manufacturing facility, the impact of the manufacturing process on the labor forces, as well as their contribution to the process, must be considered.

Wastes from the process generated in various forms are also considered. These wastes include defective products, non-utilized material, used consumables and other emissions. It should be noted that it is the in-plant management of these wastes is the emphasis, while the exact post-treatment is beyond the scope of manufacturing process sustainability evaluation. Assessing the sustainability performance of a manufacturing process would take the total life-cycle behavior of the consumables into consideration, but, would not include a complete life-cycle analysis. The boundary is set according to several considerations, namely whether the end-of-life treatment is carried out onsite, whether the treatment is integrated with the manufacturing process, and whether the treatment is mandatory according to the abiding standard or enforced regulation. If any of these cases are verified, then the post-treatment of the waste should be included in the system.

3.1.3 Relationship with product sustainability

Manufacturing activity is one of the four life-cycle stages of the manufactured product, so it is natural that many data measured in process sustainability assessment could be used for product sustainability assessment, as shown in Figure 3.4. Due to different scopes of the two assessments, the system boundary needs to be carefully reviewed when accessing the data. The general idea is to make it consistent with the scope, where the major purpose of the process sustainability assessment is to improve the process design.

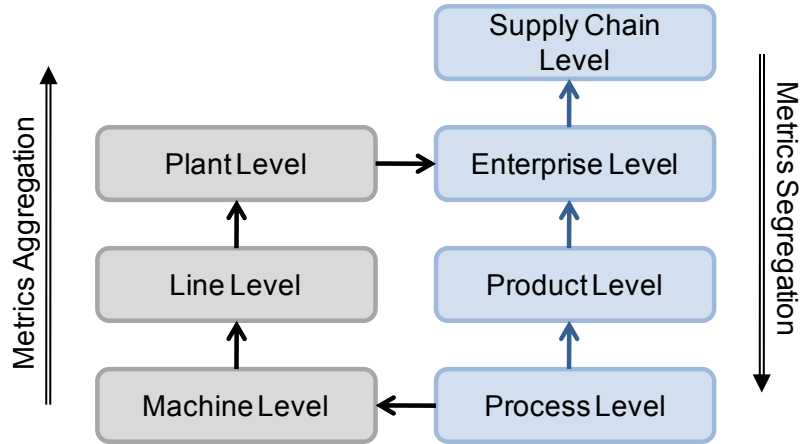


Figure 3.4: Sustainable manufacturing metrics hierarchy (Badurdeen et al., 2011).

3.2 ProcSI Structure

3.2.1 Hierarchical structure

The *ProcSI* is established in a four-level hierarchical structure that segregates the overall process sustainability into process-level quantifiable individual metrics. The top to bottom approach followed ensures that the process sustainability assessment is comprehensive and measurable. The four levels considered are *ProcSI*, *Clusters*, *Sub-clusters* and *Individual metrics* as illustrated in Figure 3.5.

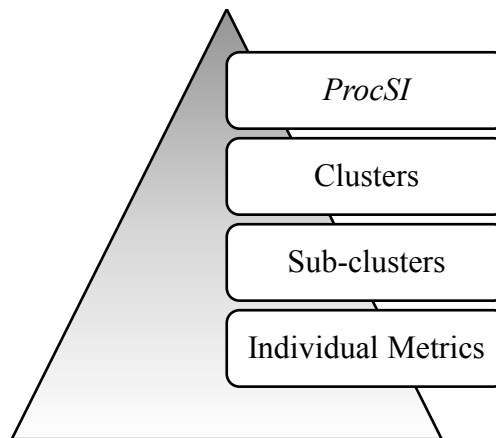


Figure 3.5: Hierarchical structure of the *ProcSI* evaluation method.

The *ProcSI* is a single score on a scale of 0 to 10 that provides the overall sustainability assessment of the manufacturing process. The *ProcSI* is divided into six clusters that represent the six elements of process sustainability originally identified by Wanigarathne et al. (2004): manufacturing cost, energy consumption, environmental impact, waste management, operational safety and personnel health. These six clusters provide a comprehensive representation of the process sustainability that covers the three aspects of the TBL: economy, environment and society.

Since each cluster represents a wide range of impacts that might not be directly related and/or measurable, clusters are divided into sub-clusters which capture the specific areas of impact that each cluster covers. Table 3.1 presents the sub-clusters for process sustainability evaluation of a generic manufacturing process.

Table 3.1: *ProcSI* with its clusters and sub-clusters.

INDEX	CLUSTER	SUB-CLUSTER
<i>ProcSI</i>	Manufacturing Cost	Direct Cost
		Indirect Cost
		Capital Cost
	Energy Consumption	Production
		Transportation
		Facilities
		Production Supply System
		Maintenance
		Efficiency
		Renewable Energy
		Waste Management
	Packaging	
	Used Raw material (Chips)	
	Scrap parts	
	Environmental Impact	Energy
		Water
		Restricted Material
		Disposed Waste
		Noise Pollution
		Heat
	Personal Health	Working environment conditions (Health)
		PLI (Physical load index)
		Absentee rate
Operator Safety	Working environment conditions (Safety)	
	Injury	

The process sustainability sub-clusters are finally divided into individual metrics that measure single and specific aspects of process sustainability. These individual metrics are quantifiable, and because of the hierarchical approach to identifying these metrics, are comprehensive and cover all relevant aspects of process sustainability. A sample of the individual metrics for the environmental impact cluster is presented in Table 3.2.

Table 3.2: Sample of the individual metrics for environmental impact.

INDIVIDUAL METRIC	UNIT	SUB-CLUSTER	CLUSTER
GHG emission from energy consumption of the line	kg/unit	Energy	Environmental Impact
Percentage of renewable energy used	%		
Total water consumption of the line	kg/unit	Water	
Mass of restricted material in disposed cutting tools	g/unit	Restricted material	
Mass of restricted material in used coolant	g/unit		
Mass of restricted material in used packaging	g/unit		
Mass of restricted material in chips going to landfill	g/unit		
Mass of restricted material in scrap parts going to landfill	g/unit		
Mass of non-collected solid waste	kg/unit	Disposed Waste	
Mass of non-collected liquid waste	l/unit		
Mass of non-collected gaseous waste	Kg/unit		
Mass of solid waste going to landfill	Kg/unit		
Mass of liquid waste going to treatment plant	l/unit		
Noise level outside the factory	dB	Noise	
Heat generation	kWh	Heat	

The individual sustainability metrics are defined by carefully examining the inputs and outputs of the manufacturing process and defining formulas to measure each metric. An example for the inputs and outputs of a typical machining process is illustrated in Figure 2.4 (Lu et al., 2011). The individual metrics for this process can be collected onsite, experimentally measured, empirically predicted, or analytically calculated.

The *ProcSI* methodology has a top-down approach for defining the individual metrics for process sustainability. Once these metrics are identified and measured, a bottom-up

approach is applied to aggregate the metrics and to evaluate the *ProcSI*. This is done by normalizing, weighting and aggregation, as illustrated in Figure 3.6. These steps involved in formulating the *ProcSI* methodology are explained in the next Sections.

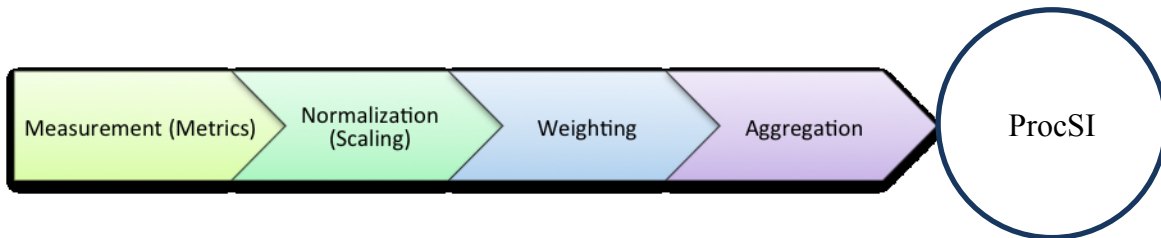


Figure 3.6: *ProcSI* evaluation methodology.

3.2.2 Normalization, weighting and aggregation

Normalization

Since individual process sustainability metrics represent heterogeneous data that might not be directly summed up together, the first step in aggregating the data measured is normalizing. The normalization and weighting processes are usually associated with subjective judgments (Singh et al., 2012). Here, each metric is normalized to a normal scale from 0 to 10, where 0 is the lowest score and 10 is the highest score in terms of sustainability performance. In general, the subjective score assignment trend is given in Table 3.3.

Table 3.3: General score assignment.

Score	Sustainability Status	Potential Reactions
0	Theoretically worst scenario	Eliminate the process with alternatives or immediate fault correction
2	Bad situation	Immediate modification to the process according to established normal practices
4	Meeting minimum requirements	Major improvement in organization and production management
6	Above average status	Production optimization activities and technological enhancement
8	Industrial leading status	Continuous improvement and revolutionary changes
10	Theoretically best scenario	Maintain the practice

Normalization is done by establishing reference points for each individual metric for the manufacturing process being evaluated. Based on these reference points, a normalization curve or formula that converts the measured value of the individual metrics to the normalized scale from 0 to 10 can be generated. It should be noted that the function generated must be monotonic to represent the preference of the measurement. In case there are more than two reference points, a set of Sectional curves or formulas may be adopted.

These reference points can be based on regulations and standards. An example is the noise level in the working environment. In a general case of an operator that works 8-hour shifts, a score of 4 is assigned to the threshold time-weighted-average (TWA) value of 90 dBA defined by OSHA (1997). We set 90 dBA as meeting the minimum requirements as a stricter threshold value of 85 dBA is suggested by NIOSH (1998b). A score of 0 is assigned to the value of 140 dBA, which is the ceiling limit of short time

impulse exposure set by both OSHA (1997) and NIOSH (1998b). A score of 10 is assigned to the noise level of a typical quiet office, 50 dBA, which is considered to be the optimal condition. Accordingly, the normalization curve and formula can be generated as illustrated in Figure 3.7.

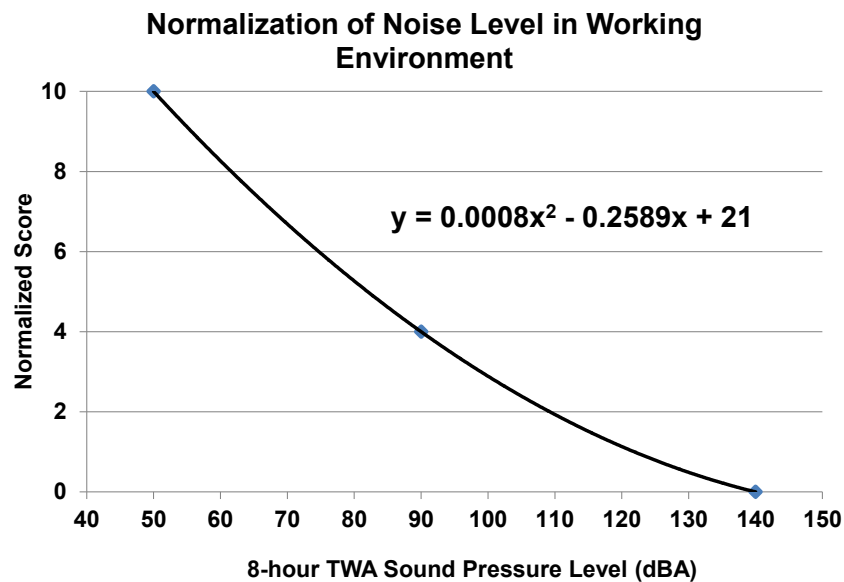


Figure 3.7: Normalization curve for noise level in working environment.

Another technique to set the reference points for a normalization curve is desirability. An example is defective product loss. A simple approach here is to assign a score of 10 to 0% losses and a score of 0 to 100% losses and use a linear line to set the normalization formula. In other cases for the same individual metrics, an intermediate reference point can also be introduced to define the normalization curve and function (e.g., assign a score of 8 to the production target of 2% defective product loss).

In some cases, reference points cannot be defined. In these cases, subjective normalization can be applied either on a continuous or discrete normalization scale. An example is exposure to high electrical voltage. In this case, a three-level scale can be

defined by assigning scores of 0, 5 and 10 to high exposure, medium exposure and low exposure, respectively. The three levels of exposures can be determined by examining the electrical voltage, personal protection, guarding and automated interlocks in the process or equipment. Such a judgment will be highly specific regarding to the particular piece of equipment under investigation.

Weighting

Before the normalized individual metrics can be aggregated, a weight can be assigned to each metric, sub-cluster and cluster. The weighting is done to capture the significance of each individual metric. Metrics that are more significant or that have higher impacts of the overall process sustainability are assigned higher weights, and vice versa. The weighting is user-defined and customizable for each manufacturing process.

Subjective weighting evaluation can be performed by experts assigning the proper weights. In this process, surveys and questionnaires are typically involved engaging customers, industrial peers, experts, manufacturers, and so on. This approach is easy to apply, but might be considered less accurate since subjective individual evaluations are considered.

Other objective analytical weighting techniques can also be applied. One technique is the analytic hierarchy process (AHP). In this technique, problems are decomposed into sub-problems, of which their meaning and importance are analyzed individually and compared to one another. Based on the comparison, the overall weighting factors can be generated. Gupta et al. (2010) presented the AHP application to assign weighting to product sustainability metrics in the product sustainability index (*ProdSI*) methodology. Although objective weighting techniques can provide a more accurate evaluation of

individual weighting, these techniques usually require more information input and analysis; which can be a challenge when considering the size of the comprehensive individual metrics for process sustainability.

Aggregation

After the normalization phase is completed, the metrics, sub-clusters and clusters are ready to be aggregated in order to calculate the *ProcSI* final score.

Generally, data aggregation describes data combined from several measurements. The method aims to replace groups of measurements with summary statistics based on those measurements. The aggregation process is done bottom-up; thus, starting with normalized individual metrics, an index for each sub-cluster can be calculated as in Equation (3.1).

$$SC_n = \sum w_j^m M_j \quad (3.1)$$

where,

- SC_i score for the i^{th} sub-cluster
- w_j^m weighting factor for the j^{th} metric
- M_j score for the j^{th} metric.

Then, each normalized sub-cluster is aggregated into a single score for the individual cluster as reported in Equation (3.2).

$$C_i = \sum_{i=1}^{14} w_i^{sc} SC_i \quad (3.2)$$

Finally, the *ProcSI* is calculated as presented in Equation (3.3).

$$ProcSI = \sum_{i=1}^6 w_i^c C_i \quad (3.3)$$

where,

C_i score for the i^{th} cluster, namely the manufacturing cost, energy consumption, environmental impact, waste management, operator safety and personnel health.

w_i^c weighting factor for the i^{th} cluster.

w_i^{sc} weighting factor for the i^{th} sub-cluster.

For example, Figure 3.8 shows a schematic calculation for the sustainability evaluation of a generic manufacturing process. Machining cost is further divided into four sub clusters namely Direct Cost, Losses, Capital Cost and Indirect cost. Each of those clusters is depicted by a series of individual metrics such as labor cost, scrap ratio, cost of depreciation, etc. The Energy Consumption Cluster is similarly divided into five sub clusters: Production, Maintenance, Transportation, Auxiliary Systems and Renewable Energy. Each of them is defined by a number of measurements in the individual metrics.

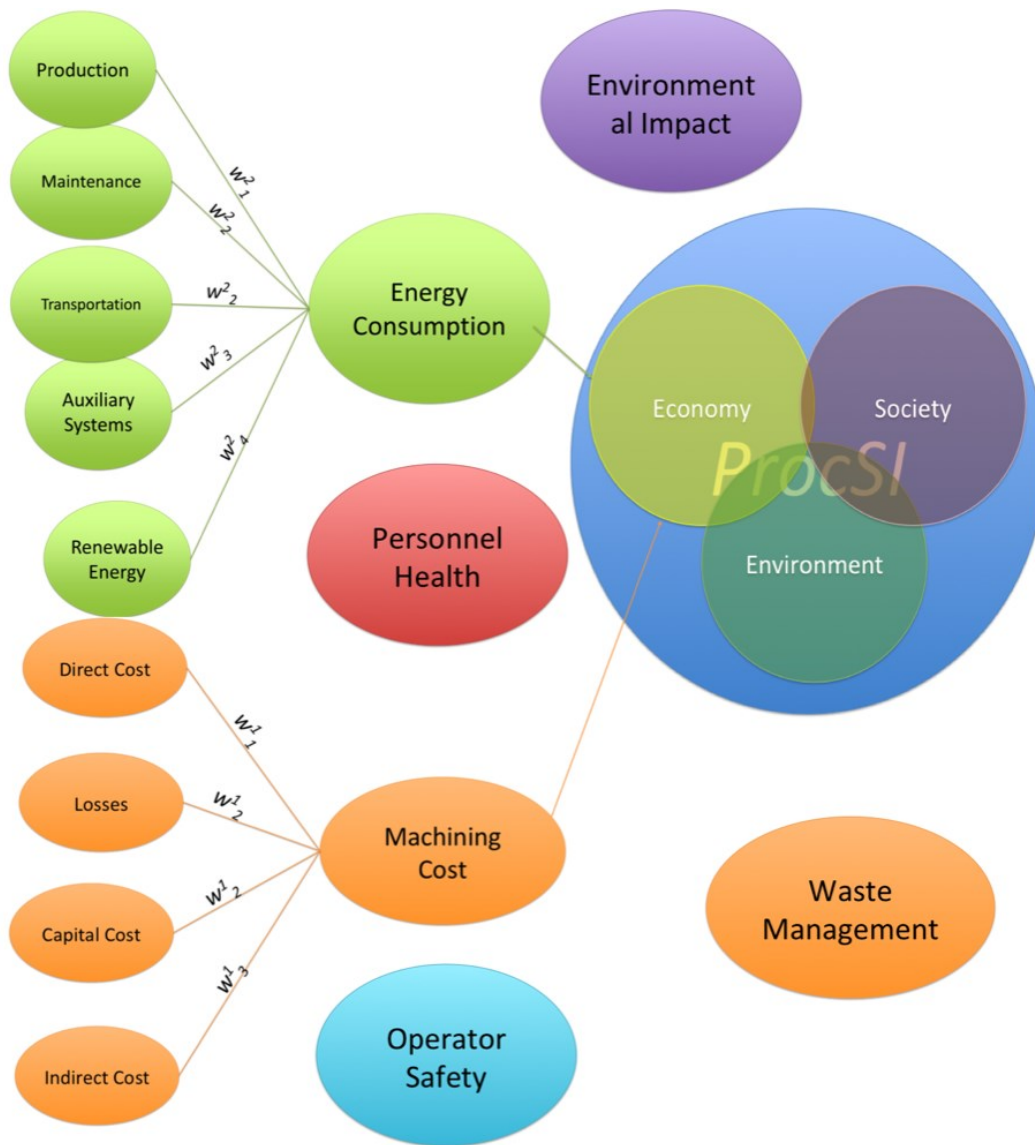


Figure 3.8: Aggregation example for partial elements of the Economy sub index in the sustainability evaluation of a machining process (Lu et al., 2014a).

3.3 ProcSI Metrics

3.3.1 Requirements of metrics for sustainability assessment

Feng et al. (2010) define a performance metric as “a standard means of measuring and tracking an indicator. It can be measured in quantitative or qualitative ways. Measured

result can be an absolute or a relative value, and a normalized or a non-normalized number”.

There has been attempts to develop guidelines to applicable sustainability metrics. Fiskel et al. (1998) in their early work proposed seven questions addressing seven key issues as follows:

1. *Comprehensive*: Does the set of performance indicators address all of the organization’s major aspects and objectives?
2. *Controllable*: Can the organization, group, manager or employee significantly influence the desired results?
3. *Cost-Effective*: Can the necessary data be obtained from existing sources or otherwise easily collected?
4. *Manageable*: Is the set of indicators limited to the minimal number required to meet the other criteria?
5. *Meaningful*: Will individuals throughout the organization and external stakeholders easily understand the indicators?
6. *Robust*: Do the indicators address inputs and processes (leading indicators) and outcomes (lagging indicators)?
7. *Timely*: Can measurement occur with sufficient frequency to enable timely, informed decision-making?

Dreher et al. (2009) in an enterprise sustainability project report also stated five criteria, which a successful metrics system needs to meet:

1. Address the needs of all stakeholders (community, government, and business)
2. Facilitate innovation and growth; continuous improvement must be the

cornerstone

3. Harmonize local, state, national, and international levels of business units and operations
4. Be fully compatible with existing business systems (add value)
5. Measure the right things – what is measured is what gets managed

Feng et al. (2010) also identified seven characteristics of the sustainability performance indicators as follows:

1. *Measurable*: Indicator must be capable of being quantitatively measured in a phenomenon that is of a sustainability concern, e.g., economic benefit, social well-being, environmental friendliness, and technical advancement.
2. *Relevant and Comprehensive*: Indicator must provide useful sustainability information on manufacturing processes. It must fit the purpose of measuring performance and addressing all of the organization's major aspects and objectives.
3. *Understandable and Meaningful*: Indicator should be easy to understand by the community, especially, for those who are not experts.
4. *Manageable*: Indicators are limited to the minimal number required to meet the measurement purpose. At the same time, the organization should be allowed to make the decision on the number and type of indicators to apply (Jackson and Roberts, 2000).
5. *Reliable*: Information provided by indicator should be trustworthy. It can address inputs (leading indicators) and outcomes (lagging indicators) of a process (Sustainable Measures, 2009).
6. *Cost-Effective Data Access*: Indicator has to be based on accessible data. The

information needs to be available or can be gathered when it is necessary from existing sources or otherwise easily collected.

7. *Timely manner*: Measurement takes place with the frequency to enable timely, informative decision-making

According to the criteria mentioned above, a comprehensive set of metrics for manufacturing process sustainability assessment was identified. The identified metrics cover all six elements of sustainable manufacturing: manufacturing cost, energy consumption, waste management, environmental impact, operator safety and personnel health. The following is the description of the metrics in each element.

3.3.2 Manufacturing cost

This cluster covers the costs incurred during the manufacturing the process. The costs are calculated on a \$/unit basis to maintain connectivity with different metrics. This cluster involves three sub-clusters: direct cost, indirect cost, and capital cost. These sub-clusters along with their individual metrics and the measurement methods identified for each sub-cluster are presented in Table 3.4.

Table 3.4: Manufacturing cost cluster with its sub-clusters and individual metrics (Lu et al., 2014a).

Sub-cluster	Individual Metric	Measurement Method
Direct Cost	Labor cost	Total employee payment to machining positions / Total number of product units made
	Operation energy cost	Total cost for energy consumed in machine operation / Total number of product units made
	Consumable related cost	Total cost of consumables / Total number of product units made
	Cutting tool related cost	(Total cost for purchasing new tools + cost for regrinding used tools - cost of recycling used tools) / Total number of product units made
	Packaging related cost	(Total cost for purchasing new packages + used package treatment fee) / Total number of product units made
	Scrap cost	Total cost of scrapped product units / Total number of product units made
	Cost of by-product treatment	Total cost for by-product treatment (which are not covered above) / Total number of product units made
	Training cost	Total training cost / Number of employees
Indirect Cost	Indirect labor cost	Total indirect labor cost / Total number of product units made
	Maintenance cost	Total cost for equipment maintenance / Total number of product units made
	Audit and legal cost	Total cost of audits, legal services and litigation / Total number of product units made
	Cost of PPE and safety investment	Total cost of PPE and equipment / Total number of product units made
Capital Cost	Cost of depreciation	Total depreciation of storage and fixed-facilities / Total number of product units made
	Cost of jigs/fixtures investment	Total cost of jigs and fixtures / Total number of product units made

3.3.3 Energy consumption

This cluster covers the energy consumed by the manufacturing process. This includes the energy consumed during the various manufacturing activities, e.g., machine tool

operation, product transportation, facilities operation and maintenance. It also covers energy efficiency and renewable energy use. The sub-clusters identified for this cluster are: production, transportation, facilities, production supply system, maintenance, efficiency and renewable energy. These sub-clusters along with their individual metrics and the measurement methods are presented in Table 3.5.

Table 3.5 Energy consumption cluster with its sub-clusters and individual metrics (Lu et al., 2014a).

Sub-cluster	Individual Metric	Measurement Method
Production	In-line electricity consumption	Total electricity consumption of all units and equipment in the line / Total number of product units made
	In-line fossil fuel consumption	Total fossil fuel consumption of all units and equipment in the line / Total number of product units made
Transportation	Transportation electricity consumption	Total energy consumption of all transportation equipment in the beginning or end of the line / Total number of product units made
	Transportation fossil fuel consumption	Total fossil fuel consumption of all transportation equipment in the beginning or end of the line / Total number of product units made
Facilities	Electricity consumption on maintaining facility environment	Total energy consumption of all environmental maintenance units and equipment / Total number of product units made
	Fossil fuel consumption on maintaining facility environment	Total energy consumption of all environmental maintenance units and equipment / Total number of product units made
Production Supply System	Electricity consumption of concentrated supply system	Total energy consumption of all supply systems equipment / Total number of product units made
	Fossil fuel consumption of concentrated supply system	Total fossil fuel consumption of all supply systems equipment / Total number of product units made
Maintenance	Electricity consumption on maintenance	Total electricity consumption for maintenance operations / Total number of product units made
	Fossil fuel consumption on maintenance	Total fossil fuel consumption for maintenance operations / Total number of product units made
Efficiency	Energy efficiency	Useful equivalent energy output from the process/ total energy input
Renewable Energy	Percentage of renewable energy used	Total consumption of renewable energy / total energy consumption

3.3.4 Environmental impact

This cluster covers the negative environmental impacts resulting from the manufacturing process. The environmental impact considers the manufacturing facilities in addition to the overall eco-system. The sub-clusters are categorized to various types of environmental impacts: energy, water, restricted material, disposed waste, noise pollution and heat. These sub-clusters along with their individual metrics and the measurement methods are presented in Table 3.6.

Table 3.6: Environmental impact cluster with its sub-clusters and individual metrics (Lu et al., 2014a).

Sub-cluster	Individual Metric	Measurement Method
Energy	GHG emission from energy consumption of the line	Total energy consumption / Total number of product units made
	Percentage of renewable energy used	Total renewable energy used / Total energy consumption
Water	Total water consumption of the line	Total water consumption / Total number of product units made
Restricted Material	Mass of restricted materials in disposed consumables	Mass of restricted materials in disposed consumables/ Total number of product units made
	Mass of restricted material in disposed packaging	Mass of restricted material in used packaging/ Total number of product units made
	Mass of restricted material in disposed raw materials	Mass of restricted materials in raw material going to landfill / Total number of product units made
	Mass of restricted material in scrap parts going to landfill	Mass of restricted material in scrap parts going to landfill / Total number of product units made
Disposed Waste	Mass of non-collected solid wastes	Total mass of non-collected wastes / Total number of product units made
	Mass of non-collected liquid wastes	Total mass of non-collected liquid wastes / Total number of product units made
	Mass of non-collected gaseous wastes	Total mass of non-collected gaseous wastes / Total number of product units made
	Mass of solid wastes going to landfill	Total mass of solid wastes going to landfill/ Total number of product units made
	Mass of liquid waste disposed	Total mass of liquid wastes going to landfill/ Total number of product units made
Noise Pollution	Noise level outside the plant	Noise level measured outside the plant
Heat	Heat generation	Heat generated by the manufacturing line / Total number of product units made

3.3.5 Waste management

This cluster covers all types of wastes produced during the manufacturing operations. It also incorporates waste management operations and the 6R application for waste reduction. The sub-clusters are categorized according to the type of wastes: consumables, packaging, raw material wastes and scrapped parts. These sub-clusters along with their individual metrics and the measurement methods are presented in Table 3.7.

Table 3.7 Waste management cluster with its sub-clusters and individual metrics (Lu et al., 2014a).

Sub-cluster	Individual Metric	Measurement Method
Consumables	Ratio of consumables recovered	Mass of recovered consumables / Total number of product units made
	Ratio of consumables reused	Mass of reused consumables / Total number of product units made
	Ratio of consumables recycled	Mass of recycled consumables / Total number of product units made
	Mass of disposed used consumables	Mass of used consumables going to landfill / Total number of product units made
Packaging	Ratio of used packaging recovered	Mass of recovered packaging / Total number of product units made
	Ratio of used packaging reused	Mass of reused packaging / Total number of product units made
	Ratio of used packaging recycled	Mass of recycled packaging / Total number of product units made
	Mass of disposed used packaging	Mass of used packaging going to the landfill / Total number of product units made
Used Raw Material (Chips)	Ratio of used raw material recovered	Mass of used raw material recovered/ Total number of product units made
	Ratio of used raw material reused	Mass of used raw material reused/ Total number of product units made
	Ratio of used raw material recycled	Mass of used raw material recycled/ Total number of product units made
	Mass of disposed used raw material	Mass of used raw material going to landfill / Total number of product units made
Scrap Parts	Ratio of scrap parts recovered	Mass of scrap part recovered/ Total number products made
	Ratio of scrap parts remanufactured	Mass of remanufactured scrap part / Total number products made
	Ratio of scrap parts recycled	Mass of recycled scrap part / Total number products made
	Mass of disposed scrap parts	Mass of scrap part going to the landfill / Total number products made

3.3.6 Operator safety

This cluster covers operator safety risks, working conditions and incident occurrence.

The two sub-clusters involved are: working environment conditions and injuries. These

sub-clusters along with their individual metrics and the measurement methods are presented in Table 3.8.

Table 3.8 Operator safety cluster with its sub-clusters and individual metrics (Lu et al., 2014a).

Sub-cluster	Individual Metric	Measurement Method
Working Environment Conditions (Safety)	Exposure to corrosive/toxic chemicals	Number of points with corrosive or toxic chemicals / Total number of employees (break down to chemical list)
	Exposure to high temperature surfaces	Total number of high temperature points exposed to the operator / Total number of employees
	Exposure to high speed components and splashes	Total number of points with high speed components exposed to the operator / Total number of employees
	Exposure to high voltage electricity	Total number of points with high voltage electricity exposed to the operator / Total number of employees
	Other threatening exposure	Total other exposed points with hazardous effects (splash, sparks, high energy laser, etc.) / Total number of employees
Injuries	Injury rate	Total injuries / Total number of product units made

3.3.7 Personnel health

This cluster focuses on the operator health. It examines factors that can impact health, e.g., hazardous materials concentration, ergonomics, etc., and it tracks the health-related incidents. The sub-clusters involved are: working environment conditions (health), Physical Load Index (PLI) and absentee rate. These sub-clusters, along with their individual metrics and the measurement methods are presented in Table 3.9.

Table 3.9 Personnel health cluster with its sub-clusters and individual metrics (Lu et al., 2014a).

Sub-cluster	Individual Metric	Measurement Method
Working Environment Conditions (Health)	Chemical concentration	Chemical concentration in the working environment (break down to the chemical list)
	Mist/dust level	Micro-particle concentration in the working environment
	Noise exposure	Noise level in the working environment
	Temperature	Temperature level in the working environment
	Other hazardous exposure	Hazardous exposure level in the working environment
PLI	Physical load index	Measured physical load index (Hollman et al., 1999)
Absentee rate	Health-related absenteeism rate	Health-related absenteeism rate

3.4 Metrics Applications at Various Levels

Even with a comprehensive set of metrics, it is still not easy to identify how the data is collected within the system boundary, and how the input parameters interact to lead to the measured results.

Apart from the lack of appropriate data, the difficulty would be that the organization of the process under investigation can vary significantly from one to another. The manufacturing process for a certain product can be a long list of processes in different forms. It is not only the differences in the complexity, and the number of input parameters that make it difficult, but also the organization of the process. When the process involves multiple machine tools, shared equipment and utilities, redundant machines, etc., the system boundary would be confusing. Indeed, the term

“manufacturing process” has become a combination of activities, consists of sub-processes which could be studied alone. When the data from all those machines are collected then aggregated, the details of how the input parameters and dynamics of the sub-processes affect the overall performance have been lost.

In such case, the proposed methodology should consider not only what content the metrics set should involve, but also how it should be applied conforming to practical situations. Considering the common manufacturing organizations, it seems reasonable to apply the methodology at various levels of the organization, clarifying the boundary of data collection activities and the aggregation process. The structure of the manufacturing organization that the *ProcSI* method considered is generalized in three levels: the operation level, the workstation level, and the plant level. In practice, the organization of a set of manufacturing processes for a product can be far more complex than three levels. But, it would involve too many specific details and could hardly represent the general behavior of the processes. Indeed, the three levels proposed here do not necessarily mean to correspond to the exact organization of the manufacturing process on each level, but to emphasize the level of details and scope of data collection activities involved at each of the levels. An example of the metrics hierarchy structure is shown in the Figure 3.9.

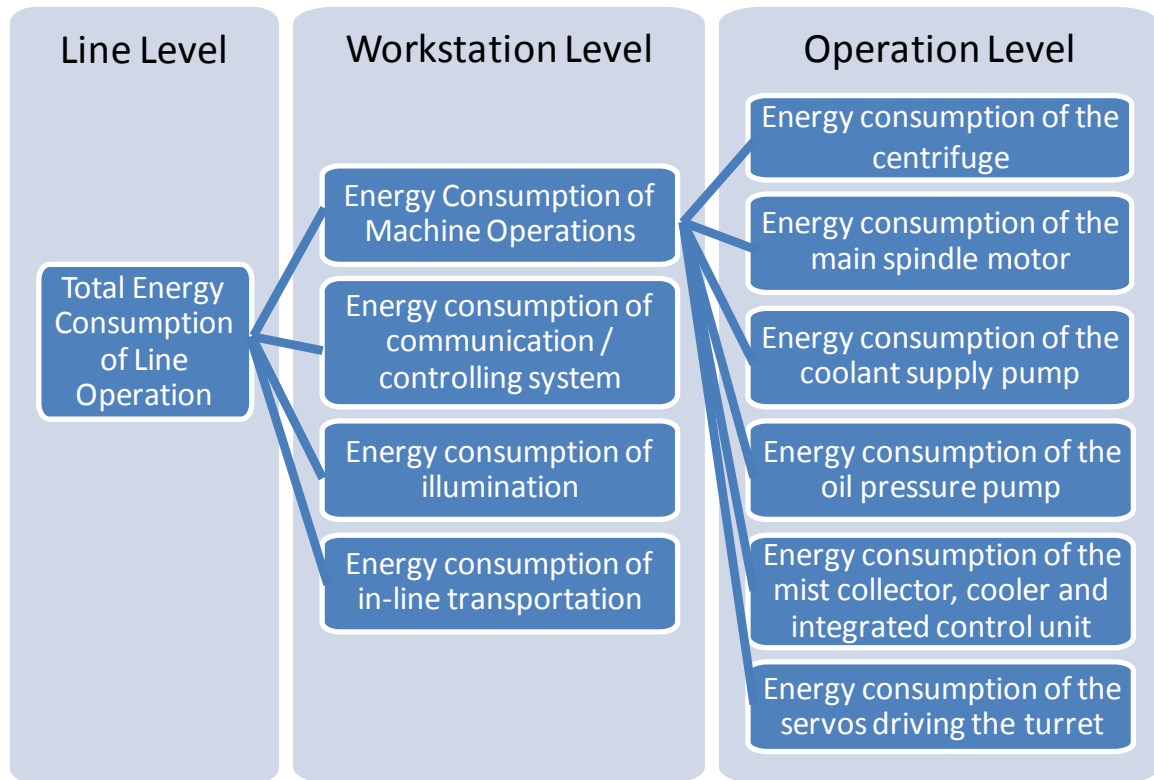


Figure 3.9: Metric aggregation for the total energy consumption (Lu et al., 2011).

3.4.1 Plant level

The plant level is the top level of the assessment, where the whole set of manufacturing processes under investigation will be considered altogether. All things within the system boundary will be studied, but the measurements will not be allocated unless specified by the metrics. The term “plant” here does not necessarily mean the physical building where the machine tools stay or where the manufacturing processes take place. First, it implies that the level of detail considered should be under the enterprise level which is commonly discussed. Typically, the detail of management system, external logistics and other enterprise level considerations will not be involved. Second, it covers not only the machine tools directly related to the manufacturing processes, but also the supporting facilities, the labor forces and the working environment.

Data on the plant level can be gathered by the management team from each department of the plant. Plant level assessment is often the preferred level of detail that companies feel like to deal with, according to the experiences during the recent case-studies with our partners in a NIST-sponsored project (ISM, 2013). There are several practical reasons for this. At first, the data is usually readily available. Normal manufacturing management would have been collecting many of the data requested by the metrics, thus less additional data collection effort is needed. Second, even data collection or data mining need to be carried out, there are typically less people involved, and the departments involved have been cooperating on the high level for a long time. The last thing is that, the metrics would give a general picture describing the sustainability performance of the plant, which is usually what the management team cares about. They deal with fewer details of the manufacturing process, and are usually familiar with the overall reporting mechanism running in the plant for years.

As mentioned above, the details of the manufacturing process are not described by the plant level data, but only the general input and output. The mechanics of the manufacturing process is hardly considered. At the plant level, though the *ProcSI* assessment may identify some under-performed factors, it would be difficult for people to locate the exact problem without further investigation. It would not reveal the control parameters contributing to the problems, either. As a result, additional problem-solving efforts are needed.

3.4.2 Workstation level

The workstation level considers more details about the manufacturing process than the plant level. In general cases, it considers the working conditions of the individual

machine tools and accessories involved in the process. The overall performance of each individual unit, either a machine tool or an accessory, is accounted for.

Sustainability assessment at the workstation level usually will be more specific on the process layout in the manufacturing facility. And, by accounting for each of the functional units, production-related consumption, non-production related or indirectly related consumption, can be distinguished. The efficiency or the effectiveness of the manufacturing process can be estimated.

Furthermore, as each piece of equipment is assessed independently, its performance, and more importantly, its contribution towards the overall performance of the process can be revealed. Assessment on the workstation level would provide an opportunity to improve the overall process design, such as process layout. Selection of machine tools can be supported too, while the impact of each alternative machine tool towards the general behavior is recorded. By considering the different *ProcSI* score they would receive with each set up, decision can be made with more quantitative and comprehensive considerations.

Assessment on the workstation level still does not involve details about the machine tools and the working conditions of all accessories, such as the settings of some specific parameters. There is very limited predictability of a certain process design, which is mostly based on empirical data and suggested machine specifications. It might be detailed enough for preliminary process design, but would hardly give sufficient information for a detailed process optimization.

3.4.3 Operation level

The operation level describes the manufacturing operation in a great detail. Typically, it involves a specific machine tool, with specific accessories supporting the process, carrying out a basic operation under certain control parameters.

An example of such operations can be a CNC lathe doing an outside diameter turning on a cylinder *AISI4040* steel bar with certain type of insert and tool holder, under flood cooling condition at certain cutting speed, feed and depth cut. In this case, the physical properties of the machine tool, the cutting parameters, the material specifications and the environmental conditions are known, which makes it possible to analyze the process with scientific models. The scientific models provide the correlation between control parameters of the manufacturing process and its physical behavior. In this case, the *ProcSI* can predict the sustainability performance of the manufacturing process under the assumptions of the integrated models.

3.5 Case Study

To validate the *ProcSI* methodology, an assessment of a turning process with different coolant applications is carried out. The coolant applications considered here include dry machining, minimum quantity lubrication (MQL) and cryogenic machining. These coolant application methods are considered as alternatives to the conventional flood cooling method, in an effort to reduce the conventional cutting fluid's economic, environmental and societal impacts highlighted in numerous previous works (Byrne and Scholta, 1993; Hong and Zhao, 1999; Sutherland et al., 2000; Yue et al., 2004; Sun et al., 2004).

First, with the enhancement of machine tool and advanced cutting tool technology, people began cutting metal without any coolant, which is the dry machining method. MQL lubrication method composes atomizing and delivering a minimum quantity of lubricants to the cutting zone by a compressed air jet. A more recent and valuable alternative to the use of conventional cutting fluids is cryogenic cooling. It involves injecting liquid nitrogen coolant to the exterior surfaces of the tool and the workpiece to maintain the strength and hardness of the tool.

3.5.1 Background scenarios

The coolant application in a turning process is selected as the major variable under investigation in this study. In practical applications, other parameters, including the cutting speed, feed and depth of cut will change along with the choices of cooling media. In the current case, the best behaving parameters in terms of cutting speed and tool nose radius are found with each one of the three coolant application methods. These three sets of parameters are taken as the optimal scenario under such coolant applications, respectively. However, the specific parameters of coolant application, including its flow-rate, nozzle direction and cooling time, etc., are kept constant. By reviewing each input/output flow, as shown in Figure 3.10, the influencing behavior of the process can be identified.

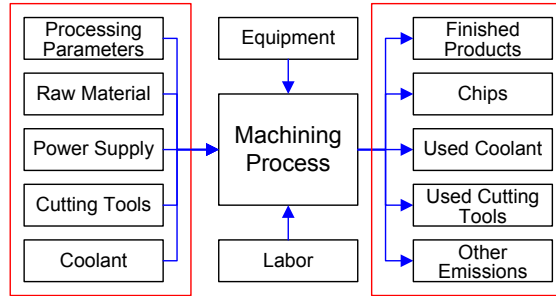


Figure 3.10: Simplified input/output flows of a machining process (Lu et al., 2012a).

The process was set to be a single feature turning process. It is a simple outside diameter bar turning process, making a cylinder which is 120 mm in diameter and 100 mm in length. The operation time with automation is estimated based on industrial practices. Figure 3.11 summarizes the process flow involved in the machining operation and estimated time used. Note that the main spindle will rotate only during the tool idling process and the cutting process. The same applies to the coolant applications and this should be considered in power consumption calculation.

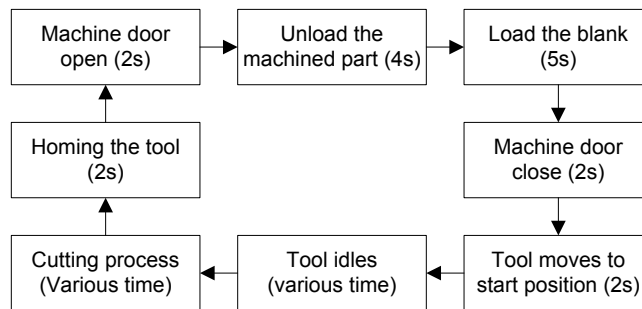


Figure 3.11: Process flow chart (Lu et al., 2014b).

The material used in machining is *AA7075-T651* aluminum alloy. Uncoated carbide tool (Kennametal grade K313) is held on a CTGPL164C tool holder, and the tool was mounted on a Mazak QuickTurn 10 CNC lathe. The insert type is TPG43X series with a nose radius at 0.4 mm, 0.8 mm or 1.2 mm. The cutting speed will be set at 180 m/min,

320 m/min or 720 m/min, with a feed rate of 0.1 mm/rev and a depth of cut at 0.5 mm.

The machining parameters are summarized in Table 3.10.

Table 3.10: Machining parameters used in the experiments (Lu et al., 2014b).

Machining Parameter	Parameter Value	
Insert Grade	K313 uncoated carbide	
Tool Geometry	Nose radius (mm)	0.4, 0.8, 1.2
	Model	TPG43X
	Chip breaker	No
Cutting Geometry	Rake angle	0°
	Lead angle	0°
	Clearance angle	7°
Machining Parameters	Cutting speed (m/min)	180, 320, 720
	Feed (mm/rev)	0.1
	Depth of cut (mm)	0.5

The coolant-related parameters are summarized in Table 3.11.

Table 3.11: Coolant application parameters used in the experiments (Lu et al., 2014b).

Coolant	Flow Rate	Nozzle Direction	Tool Idle Time	Cooling Media
Dry Machining	N/A	N/A	N/A	N/A
MQL Machining	60 ml/hour	Rake	10 second	Unist Coolube 2210
Cryogenic Machining	10 g/s	Flank	5 second	Liquid nitrogen

For the overall assessment, we assumed a batch of 1000 workpieces to be made, while the unit data was taken as the average value of the corresponding experiments. Experimental data on power consumption, surface roughness and tool-wear rate in previous work (Rotella et al., 2012) are used.

Process Input

The different scrap rate will contribute to the raw material consumption. Cutting parameters will have impacts on the power consumption of the process. Other than these,

the changes in the cutting zone temperatures and consequently different material behavior introduced by different coolant application methods are expected to change the measured cutting power consumption too.

Similarly, the tool-life under each condition set will be different. The data of average tool-wear rates from the experiments were used to estimate the total number of tool inserts consumed.

Coolant consumption is naturally influenced by different coolant application methods and the corresponding parameters used. The coolant flow rate is specified in Table 3.11.

To be specific, dry cutting does not utilize any coolant, MQL uses an oil-based coolant, namely Unist Coolube 2210, and cryogenic cutting uses liquid nitrogen as the coolant. The coolant is applied during the tool idling step and the cutting step, and the total consumption is estimated by multiplying the pre-set flow rate and the durations of the two steps.

Process behavior

Due to the different pre-cooling applications during which the tool will remain idle, the process time of the turning operation will be different. This influenced the cost calculation, including the capital tie up and the direct cost. The capital tie up is based on a two year pay-back scenario, assuming two 8-hour shifts pay day, 5 days a week and 50 weeks per year working scenario. The purchasing prices of the equipment involved are estimated and are summarized in Table 3.12, along with estimation of residual value with a 20% annual depreciation rate. On the labor cost part, 4 labor hours per day is assigned to this process based on estimation, with a \$30 per hour flat labor cost.

Table 3.12: Capital cost tie-up summary (Lu et al., 2014b).

Equipment	Purchasing Price	Residual Value	Cost Tie-up
CNC Lathe	\$ 200,000	\$ 128,000	\$ 9.00 / hour
MQL Unit	\$ 1,500	\$ 960	\$ 0.07 / hour
Air Compressor	\$ 500	\$ 320	\$ 0.02 / hour
Liquid Nitrogen Dispenser	\$ 50,000	\$ 32,000	\$ 2.25 / hour

Apart from this, the tool change activity is considered, by setting an average operation time of 2 minutes for each cutting tool replacement. The number of tool changing is estimated based on the tool-wear data measured.

Process output

The quality of finished products for each cooling condition is different. The surface integrity, including surface hardness, surface roughness and surface microstructure, is behaving differently under each condition set (Rotella et al., 2012). In this study, we assume the major quality judgment is made upon the surface roughness R_a . Based on the average surface roughness value we measured, and the assumption that the surface roughness values of all the workpieces made with one machining condition set is subject to normal distribution, we could calculate the scrap rate when setting a assumed quality threshold value of $R_a = 0.6 \mu\text{m}$. The probability of failing is described based on the probability density function of a normal distribution. The probability of failing, which is the scrap rate, is described by Equation (3.4) (Kirk, 2007).

$$f(R_{ax}; R_{at}, \sigma^2) = 1 - \int_{-\infty}^{R_{at}} \frac{1}{\sigma\sqrt{2\pi}} e^{-\frac{(x-R_{ax})^2}{2\sigma^2}} dx \quad (3.4)$$

where, R_{ax} is the average R_a value measured for a condition set; R_{at} is the threshold value of R_a , which is set as $0.6 \mu\text{m}$ constantly; the variance $\sigma = 0.25 \times R_{ax}$ is used for all cases. It can be described in the cumulative distribution form as Equation (3.5) (Kirk, 2007).

$$F(R_{ax}; R_{at}, \sigma^2) = 1 - \frac{1}{2} \left[1 + \operatorname{erf} \left(\frac{R_{at} - R_{ax}}{\sqrt{2\sigma^2}} \right) \right] \quad (3.5)$$

where the function $\operatorname{erf}()$ is the error function. Equation (3.5) is used to calculate the scrap rate.

In practice, MQL may leave a minimum amount of coolant on the chip. And, the liquid nitrogen applied in cryogenic machining will evaporate into the atmosphere and leaves a completely clean chip. As no specific chip collections are applied in the study, we assume all chips will go through same recycling process. The difference in chip-forms cannot be spotted clearly, and therefore, in this study, the chips from different conditions are considered the same. Note that this might not be the case in industrial practice, as clean chips can be easier to recycle, and the manufacturer will gain more economical benefits from selling cleaner chips.

Neither the MQL nor the cryogenic machining will leave any collectable coolant residues. Thus, the consideration of used coolant treatment can be neglected. The amount of used cutting tools will be influenced due to different tool-wear/tool-life behavior. Apart from the mere consumption of coolant for MQL, no other emissions are considered in this study.

3.5.2 Data collection

In this section, the metrics discussed in the previous sections are reviewed to identify those measurements that are changed at each of the condition set.

Manufacturing cost

Only direct cost and capital cost is considered in this cluster. Labor cost, operation energy cost, coolant related cost and cutting tool related cost are considered, along with the

capital cost assigned to the operation time. It should be noted that the cost data is not normalized until cluster level. Thus the normalization is done directly to the measurement of *Total cost*. The measurements are based on data described in Section 3.5.1. The comparison is summarized in Table 3.13.

Table 3.13: Data summary for manufacturing cost (Lu et al., 2014b).

Cutting speed (m/min)	Nose radius (mm)	Lubrication	Scrap loss (\$)	Capital tie up (\$)	Labor cost (\$)	Tool cost (\$)	Cost of coolant (\$)	Cost of energy (\$)	Total cost (\$)
720	0.4	DRY	0	130.34	108.62	387.50	0.00	0.34	626.80
180	1.2	DRY	385.8	392.40	327.00	1400.00	0.00	0.37	2505.57
320	0.8	DRY	321.5	224.81	187.34	187.50	0.00	0.34	921.49
720	0.8	DRY	0	128.24	106.87	300.00	0.00	0.33	535.44
180	0.8	DRY	1028.8	370.47	308.72	337.50	0.00	0.36	2045.84
180	0.4	DRY	3665.1	412.39	343.66	1475.00	0.00	0.38	5896.53
320	0.4	DRY	514.4	230.87	192.39	412.50	0.00	0.35	1350.51
720	1.2	DRY	128.6	132.98	110.82	487.50	0.00	0.33	860.23
320	1.2	DRY	257.2	245.29	204.41	1050.00	0.00	0.35	1757.25
720	0.4	CRYO	0	166.92	111.28	362.50	90.14	0.36	731.21
180	1.2	CRYO	385.8	464.22	309.48	237.50	325.37	0.60	1722.96
320	0.8	CRYO	64.3	289.93	193.29	100.00	187.53	0.43	835.48
720	0.8	CRYO	0	166.92	111.28	87.50	90.14	0.35	456.19
180	0.8	CRYO	643	466.06	310.71	325.00	326.66	0.53	2071.96
180	0.4	CRYO	257.2	463.29	308.86	975.00	324.72	0.52	2329.60
320	0.4	CRYO	128.6	290.22	193.48	275.00	187.72	0.43	1075.45
720	1.2	CRYO	0	166.92	111.28	87.50	90.14	0.37	456.22
320	1.2	CRYO	0	289.64	193.10	312.50	187.34	0.45	983.03
720	0.4	MQL	0	147.50	121.70	425.00	2.35	0.42	696.97
180	1.2	MQL	2057.6	397.81	328.23	250.00	7.95	0.73	3042.32
320	0.8	MQL	1028.8	250.60	206.77	375.00	4.65	0.57	1866.40
720	0.8	MQL	0	147.50	121.70	225.00	2.35	0.40	496.96
180	0.8	MQL	1478.9	394.34	325.36	87.50	7.88	0.70	2294.69
180	0.4	MQL	257.2	387.02	319.32	1050.00	7.73	0.32	2021.59
320	0.4	MQL	128.6	247.15	203.92	187.50	4.59	0.29	772.05
720	1.2	MQL	0	147.50	121.70	87.50	2.35	0.33	359.38
320	1.2	MQL	643	249.12	205.55	237.50	4.63	0.35	1340.15

Energy consumption

The sub-clusters involved will be the production energy consumption and production supply system energy consumption. Among them, the tool spindle power consumption and coolant supply system consumption are considered. Similar to the cost data, the energy consumption data is summed up as the total energy consumption. The normalization is done to the measurement of *Total energy consumption*. The comparison is summarized in Table 3.14.

Table 3.14: Data summary for energy consumption (Lu et al., 2014b).

Cutting speed (m/min)	Nose radius (mm)	Lubrication	Spindle energy consumption (kWh)	Coolant delivery system energy consumption (kWh)	Total energy consumption (kWh)
720	0.4	DRY	6.18	0.00	6.18
180	1.2	DRY	6.70	0.00	6.70
320	0.8	DRY	6.11	0.00	6.11
720	0.8	DRY	6.00	0.00	6.00
180	0.8	DRY	6.50	0.00	6.50
180	0.4	DRY	6.97	0.00	6.97
320	0.4	DRY	6.34	0.00	6.34
720	1.2	DRY	6.05	0.00	6.05
320	1.2	DRY	6.39	0.00	6.39
720	0.4	CRYO	5.55	1.01	6.56
180	1.2	CRYO	7.29	3.65	10.94
320	0.8	CRYO	5.67	2.10	7.77
720	0.8	CRYO	5.30	1.01	6.32
180	0.8	CRYO	6.01	3.67	9.68
180	0.4	CRYO	5.78	3.64	9.43
320	0.4	CRYO	5.66	2.11	7.76
720	1.2	CRYO	5.73	1.01	6.74
320	1.2	CRYO	6.15	2.10	8.25
720	0.4	MQL	5.65	1.98	7.64
180	1.2	MQL	6.59	6.71	13.29
320	0.8	MQL	6.46	3.93	10.39
720	0.8	MQL	5.37	1.98	7.36
180	0.8	MQL	6.10	6.65	12.75
180	0.4	MQL	5.85	6.53	12.38
320	0.4	MQL	5.26	3.87	9.13
720	1.2	MQL	6.06	1.98	8.05
320	1.2	MQL	6.37	3.90	10.27

Waste management

From the point of view of used coolants and chip generation, it was assumed that nothing will be changed due to different coolant applications. The amount of used cutting tools generated, which will be all sent to recycling, is considered. The chip generation is given

a medium score in aggregation. The mass of scrap parts is calculated based on the calculated scrap rate described in Section 3.5.1 and average mass of an un-machined workpiece. The comparison is summarized in Table 3.15.

Table 3.15: Data summary for waste management (Lu et al., 2014b).

Cutting speed (m/min)	Nose radius (mm)	Lubrication	Mass of used cutting tools (kg)	Total mass of scrap parts (kg)	Total mass of chips (kg)
720	0.4	DRY	0.31	0.00	26.43
180	1.2	DRY	1.12	19.07	26.59
320	0.8	DRY	0.15	15.89	26.56
720	0.8	DRY	0.24	0.00	26.43
180	0.8	DRY	0.27	50.85	26.85
180	0.4	DRY	1.18	181.15	27.93
320	0.4	DRY	0.33	25.42	26.64
720	1.2	DRY	0.39	6.36	26.48
320	1.2	DRY	0.84	12.71	26.53
720	0.4	CRYO	0.29	0.00	26.43
180	1.2	CRYO	0.19	19.07	26.59
320	0.8	CRYO	0.08	3.18	26.45
720	0.8	CRYO	0.07	0.00	26.43
180	0.8	CRYO	0.26	31.78	26.69
180	0.4	CRYO	0.78	12.71	26.53
320	0.4	CRYO	0.22	6.36	26.48
720	1.2	CRYO	0.07	0.00	26.43
320	1.2	CRYO	0.25	0.00	26.43
720	0.4	MQL	0.34	0.00	26.43
180	1.2	MQL	0.20	101.70	27.27
320	0.8	MQL	0.30	50.85	26.85
720	0.8	MQL	0.18	0.00	26.43
180	0.8	MQL	0.07	73.09	27.04
180	0.4	MQL	0.84	12.71	26.53
320	0.4	MQL	0.15	6.36	26.48
720	1.2	MQL	0.07	0.00	26.43
320	1.2	MQL	0.19	31.78	26.69

Environmental impact

Differences in energy usage will be considered here, utilizing statistical data about greenhouse gas (GHG) emission for the local power grid (US. EPA, 2012).

MQL will generate restricted material emission, while other cooling methods will not produce such emissions. It should be noted that the evaporated liquid nitrogen is not considered as waste, considering that it does not have any known impact on the environment. The data is summarized in Table 3.16.

Table 3.16: Data summary for environmental impact (Lu et al., 2014b).

Cutting speed (m/min)	Nose radius (mm)	Lubrication	GHG from energy use (kg)	Mass of restricted material emission (kg)
720	0.4	DRY	5.56	0.00
180	1.2	DRY	6.03	0.00
320	0.8	DRY	5.50	0.00
720	0.8	DRY	5.40	0.00
180	0.8	DRY	5.85	0.00
180	0.4	DRY	6.28	0.00
320	0.4	DRY	5.70	0.00
720	1.2	DRY	5.44	0.00
320	1.2	DRY	5.75	0.00
720	0.4	CRYO	5.90	0.00
180	1.2	CRYO	9.85	0.00
320	0.8	CRYO	7.00	0.00
720	0.8	CRYO	5.68	0.00
180	0.8	CRYO	8.71	0.00
180	0.4	CRYO	8.48	0.00
320	0.4	CRYO	6.99	0.00
720	1.2	CRYO	6.07	0.00
320	1.2	CRYO	7.42	0.00
720	0.4	MQL	6.87	0.55
180	1.2	MQL	11.96	1.87
320	0.8	MQL	9.35	1.09
720	0.8	MQL	6.62	0.55
180	0.8	MQL	11.47	1.85
180	0.4	MQL	11.14	1.82
320	0.4	MQL	8.22	1.08
720	1.2	MQL	7.24	0.55
320	1.2	MQL	9.25	1.09

Operator safety

None of the three coolant application methods will have any obvious safety threat. For In the case of cryogenic machining, when a moderate to small flow rate is applied, the threat of frostbite is minor.

Personnel health

Mist level in the working environment will be influenced due to the use of MQL coolant application, and that is the only metric influenced in this cluster. An overall score of 7 is given to all MQL conditions about this cluster to represent the preference of mist-free operating environment.

3.5.3 Process Sustainability Index (*ProcSI*) evaluation

The data comparison shown in Table 3.13 to Table 3.16 clearly shows the difference among the three coolant applications, except for the lack of measurements in the clusters of operator safety and personnel health.

Normalization

The data is normalized by internal comparison, as described in previous work (Lu et al., 2012b). On a 0 to 10 scale, the worst case is given a score of 4, and the best case is given a score of 8. Then, a linear normalization is applied to the data between these two extremes, as shown in Equation (3.6).

$$S = 4 \times \left[1 + \frac{(M - M_{min})}{(M_{max} - M_{min})} \right] \quad 3.6$$

where, S is the score for the medium measurement of a particular metric. M_{max} is the highest physical measurement, M_{min} is the lowest physical measurement, and M is the medium measurement.

When the theoretical best or worst case is achieved, a score of 0 or 10 can be given, according to the desirability of that particular measurement. The normalized scores for the six *ProcSI* clusters are summarized in Table 3.17.

Table 3.17: Summary of normalized score, highlighted lines indicate best cases with the corresponding coolant application method (Lu et al., 2014b).

Cutting speed (m/min)	Nose radius (mm)	Lubrication	Cost Score	Energy Score	Waste Score	Environmental Score	Operator Safety	Personnel Health	<i>ProcSI</i>
720	0.4	DRY	7.81	7.90	7.71	8.95	10	10	8.73
180	1.2	DRY	6.45	7.61	6.46	8.81	10	10	8.22
320	0.8	DRY	7.59	7.94	7.67	8.97	10	10	8.70
720	0.8	DRY	7.87	8.00	7.80	9.00	10	10	8.78
180	0.8	DRY	6.78	7.73	7.01	8.86	10	10	8.40
180	0.4	DRY	4.00	7.47	4.00	8.73	10	10	7.37
320	0.4	DRY	7.28	7.81	7.31	8.91	10	10	8.55
720	1.2	DRY	7.64	7.97	7.52	8.99	10	10	8.69
320	1.2	DRY	6.99	7.79	6.89	8.89	10	10	8.43
720	0.4	CRYO	7.73	7.69	7.74	8.85	10	10	8.67
180	1.2	CRYO	7.02	5.29	7.58	7.65	10	10	7.92
320	0.8	CRYO	7.66	7.03	7.94	8.51	10	10	8.52
720	0.8	CRYO	7.93	7.83	8.00	8.91	10	10	8.78
180	0.8	CRYO	6.76	5.98	7.30	7.99	10	10	8.01
180	0.4	CRYO	6.58	6.12	6.96	8.06	10	10	7.95
320	0.4	CRYO	7.48	7.03	7.73	8.52	10	10	8.46
720	1.2	CRYO	7.93	7.59	8.00	8.80	10	10	8.72
320	1.2	CRYO	7.55	6.77	7.78	8.38	10	10	8.41
720	0.4	MQL	7.76	7.10	7.68	7.66	10	7	7.87
180	1.2	MQL	6.06	4.00	6.35	4.00	10	7	6.23
320	0.8	MQL	6.91	5.59	6.98	6.04	10	7	7.09
720	0.8	MQL	7.90	7.26	7.87	7.74	10	7	7.96
180	0.8	MQL	6.60	4.30	6.92	4.18	10	7	6.50
180	0.4	MQL	6.80	4.50	6.89	4.33	10	7	6.59
320	0.4	MQL	7.70	6.28	7.81	6.41	10	7	7.53
720	1.2	MQL	8.00	6.88	8.00	7.55	10	7	7.91
320	1.2	MQL	7.29	5.66	7.39	6.08	10	7	7.24

High-lighting shows the working conditions with highest *ProcSI* score among all the working conditions with a same coolant application method.

For all three coolant applications, the highest cutting speed shows as optimal, due to the significant saving in operation time and corresponding better performances in various

aspects including less cost associated with operating time and less coolant assumption due to short duration of application.

Aggregation

Different weighting methods are also discussed (Zhang et al., 2012a). In the current study, equal weights are applied in every step of aggregation. The overall *ProcSI* score is calculated by averaging the scores for the six clusters of process sustainability. The aggregated scores for the best case with each of the three coolant application methods are summarized in Figure 3.12.

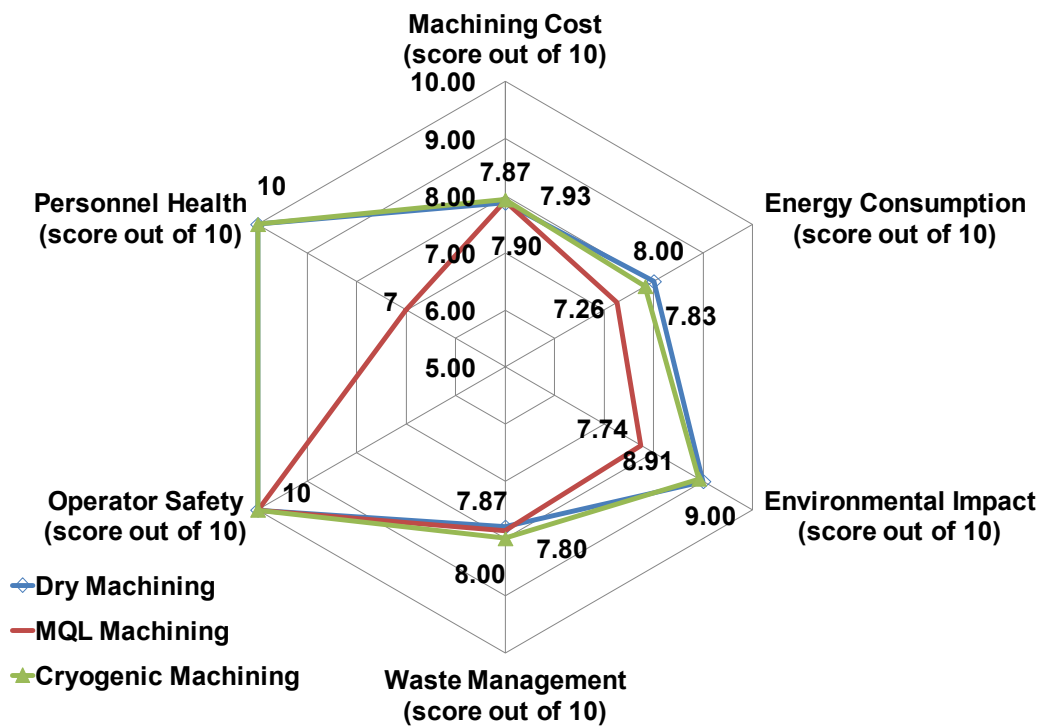


Figure 3.12: Sustainability scores for the six clusters of process sustainability (Lu et al., 2014b).

Discussion

Although there is quite a burden of capital investment and coolant cost, cryogenic machining performs well with good tool-life and corresponding savings on cutting tools. MQL machining has a small increase in capital investment and coolant cost compared to dry machining and overcomes the effect by better tool-life. It should be noted that due to the expensive coolant cost, cryogenic machining will be beneficial in cost only when higher cutting speed is used and thus the total consumption is small.

The air compressor used in the MQL machining consumes significant amount of energy, and it contributes to the relatively poor energy behavior of the MQL machining. A similar situation also happens in cryogenic machining, to a less extent. It should be noted that the savings on spindle power are often over-whelmed by the increase in energy consumption of accessories.

Energy consumption leads to the GHG emission accounted in the cluster of environmental impact. The only restricted material involved is the MQL coolant. As a result, the MQL machining shows the lowest score here.

There are little differences in the performance of waste management for all three coolant applications, due to small differences in the used tool category. The clusters of operator safety and personnel health have been discussed in Section 3.5.2.

3.5.4 Process optimization for sustainability

Optimization with genetic algorithm is applied to find the optimal cutting parameters based on the experimental data. Unlike conventional process optimization for best economic performances or optimal production capability, the objective here is to

optimize the process for best sustainability performance, which is indicated by higher *ProcSI* score.

Objective function

The proposed objective function is defined as Equation (3.7).

$$F(V, n) = \frac{1}{6}(C_{MC} + C_{En} + C_{Env} + C_{Wa} + C_{PH} + C_{OS}) = \frac{1}{6} \left[C_{MC} + C_{En} + \frac{1}{2}(M_{CO_2} + M_{RME}) + \frac{1}{3}(M_{UCT} + M_{SP} + M_{Ch}) + C_{PH} + C_{OS} \right] \quad (3.7)$$

While the $F(V, n)$ is the objective function with the cutting speed, V , and the nose radius, n , as the input variables. C_{Ec} , C_{En} , C_{Env} , C_{Wa} , C_{PH} and C_{OS} are the scores for the clusters of manufacturing cost, energy consumption, environmental impact, waste management, personnel health and operator safety. The methods to generate these scores are stated in Section 3.5.3. To be specific, the score for the cluster of environmental impact is calculated by averaging the metric level scores for the metrics of CO_2 emission, M_{CO_2} and restricted material emission, M_{RME} . The score for the cluster of waste management is generated by taking the average of the scores for the metrics of mass of used cutting tools, M_{UCT} , mass of scrap parts, M_{SP} , and mass of chips generated, M_{Ch} . Aggregation of scores is carried out with equal weighting.

Empirical model integration

The relationship between the input variables and the behavior of the process are defined by empirical models built upon experimental data (Rotella et al., 2012). The input parameters involved here are the cutting speed, V in m/min, and nose radius of the cutting tool, n in mm. Directly related process behavior parameters include the surface roughness, R_a in μm , cutting power, P in kW, and tool wear rate, $TWear$ in $\mu\text{m/s}$. The empirical

models are second order polynomial functions built using non-linear least square method. These process behavior parameters are used to calculate other process behavior parameters, and ultimately some of the metric measurements. Other process behavior and metric measurements are calculated as stated in Sections 3.5.1 and 3.5.2.

For example, under dry machining, the relationship between the surface roughness and the input variables are defined by Equation (3.8).

$$R_a = 0.6148 - 4.607 \times 10^{-4} \times V - 0.3677 \times n + 2.434 \times 10^{-4} \times V \times n + 1.036 \times 10^{-7} \times V^2 + 0.1614 \times n^2 \quad (3.8)$$

When MQL is applied, the relationship is defined by a different set of coefficients in the equation, as shown in Equation (3.9).

$$R_a = 0.2980 - 0.1195 \times 10^{-3} \times V - 0.2747 \times n + 0.1135 \times 10^{-3} \times V \times n + 1.808 \times 10^{-7} \times V^2 - 0.1563 \times n^2 \quad (3.9)$$

And, for cryogenic machining conditions, the relationship between the process control variables and the value of R_a is shown in Equation (3.10).

$$R_a = 0.4749 - 0.5862 \times 10^{-3} \times V - 0.01641 \times n + 0.1633 \times 10^{-3} \times V \times n + 2.729 \times 10^{-7} \times V^2 - 0.0250 \times n^2 \quad (3.10)$$

Similar equations are applied to the cutting force and tool-wear rate, and the corresponding coefficients are summarized in Table 3.18.

Table 3.18: Coefficients for each components in the relationship equation for cutting force and tool-wear rate with each of the coolant application methods.

	Coefficients for Cryogenic Machining		Coefficients for Machining with MQL		Coefficients for Dry Machining	
	Cutting force (N)	Tool-wear rate ($\mu\text{m/s}$)	Cutting force (N)	Tool-wear rate ($\mu\text{m/s}$)	Cutting force (N)	Tool-wear rate ($\mu\text{m/s}$)
1	66.35	0.1807	50.76	-0.03044	72.83	0.2717
V	-0.03971	4.538×10^{-4}	-7.937×10^{-5}	8.970×10^{-4}	-0.03285	7.727×10^{-4}
n	-16.94	-0.5513	9.247	-0.1398	-16.80	-1.026
$V \times n$	-0.02463	-1.998×10^{-4}	-6.755×10^{-3}	-3.019×10^{-4}	-5.058×10^{-3}	-1.126×10^{-5}
V^2	5.045×10^{-5}	-1.914×10^{-7}	-1.034×10^{-6}	-5.262×10^{-7}	3.155×10^{-5}	-6.250×10^{-7}
n^2	22.24	0.3332	0.9583	0.09146	11.79	0.6891

Optimization with genetic algorithm

The determination of the optimal conditions can be taken as a constrained optimization problem, which can be summarized as follows.

$$\text{Minimize} \quad F(V_i, n_i) = \frac{1}{6}(C_{MC} + C_{En} + C_{Env} + C_{Wa} + C_{PH} + C_{OS})$$

$$\text{With respect to} \quad V_i, n_i (i = 1 \dots N)$$

$$\text{Subject to} \quad V_{min} \leq V_i \leq V_{max}$$

$$n_{min} \leq n_i \leq n_{max} \quad (3.11)$$

The V_{min} and V_{max} are the lowest and highest cutting speed allowed respectively. And n_{min} and n_{max} are the smallest and largest nose radius of cutting tools allowed. To ensure that the empirical models remain valid within the variable region, these parameters are set as the extreme conditions used in the experiments, which are summarized in Equation (3.12).

$$V_{min} = 180 \text{ m/min}; V_{max} = 720 \text{ m/min}; n_{min} = 0.4 \text{ mm}; n_{max} = 1.2 \text{ mm} \quad (3.12)$$

The optimization is carried out with genetic algorithm (GA). GA is a common evolutionary algorithm (EA) which generates solutions in order to optimize a problem. GA is given its name due to the techniques involved which were inspired by natural evolution. Such techniques include inheritance, mutation, selection and crossover (Koza, 1992).

The results of the optimal solutions for each of the three coolant application methods are summarized in the following population plots, namely Figure 3.13, Figure 3.14 and Figure 3.15. The pink dash-dot lines indicate the constrained parameter ranges, and the blue diamond marks indicate the optimal conditions determined under each of the coolant application methods. The colored curves form the function response map.

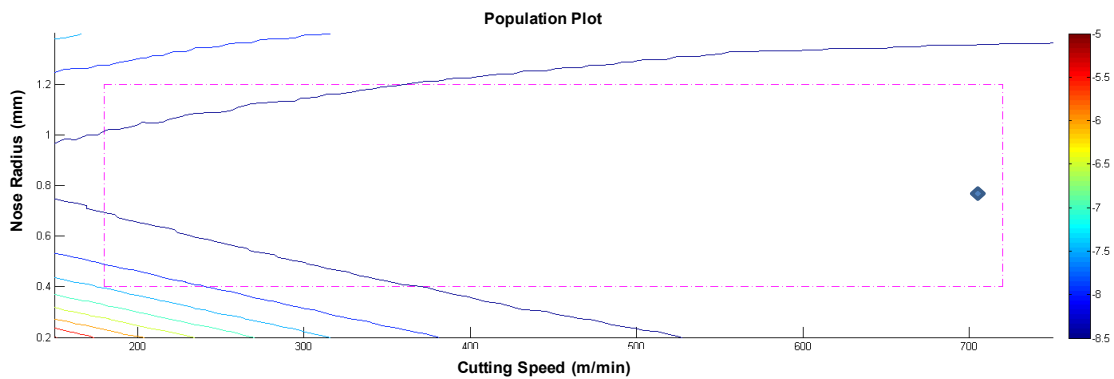


Figure 3.13: Population plot for optimization of dry machining process (Lu et al., 2014b).

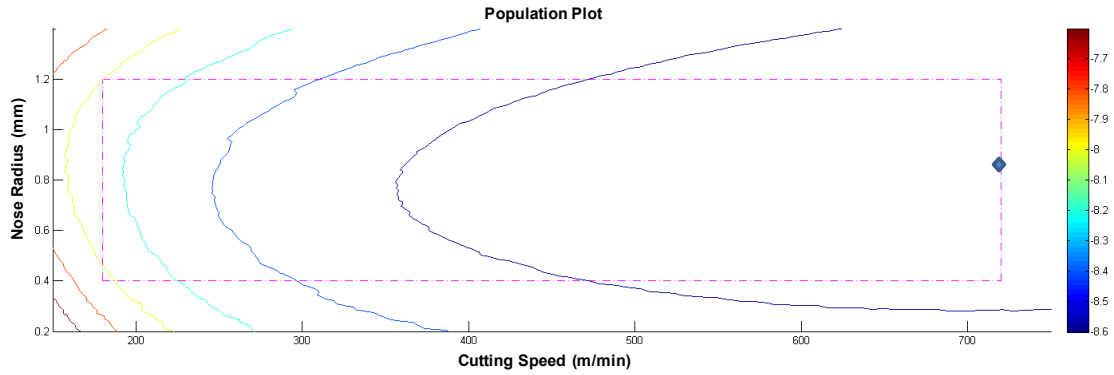


Figure 3.14: Population plot for optimization of cryogenic machining process (Lu et al., 2014b).

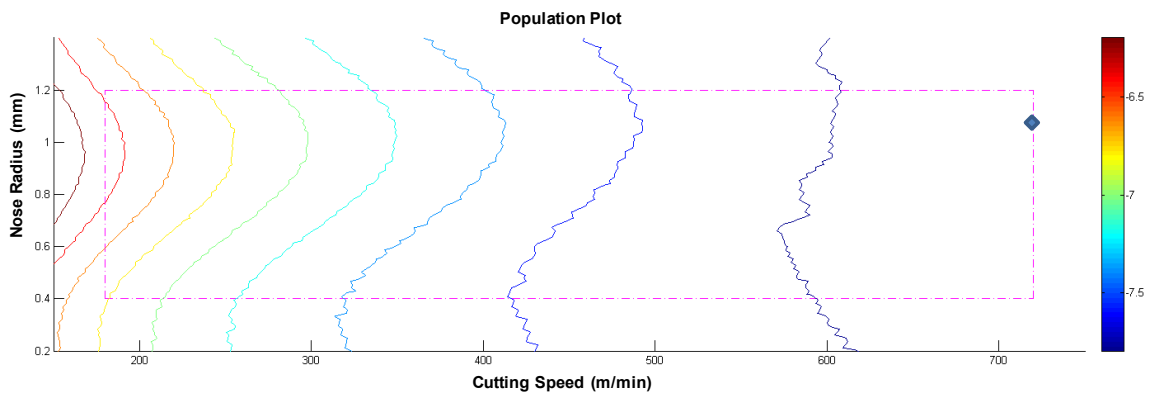


Figure 3.15: Population plot for optimization of MQL machining process (Lu et al., 2014b).

The optimized results and the related *ProcSI* performances are summarized in Table 3.19.

It should be noted that, due to the limited accuracy of the empirical models, the data may be not exactly the same with the experimental results.

Table 3.19: Optimal conditions determined by the optimization and the corresponding *ProcSI* scores (Lu et al., 2014b).

Coolant Application	Cutting Speed (m/min)	Nose Radius (mm)	Cost Score	Energy Score	Waste Score	Environmental Score	Operator Safety	Personnel Health	<i>ProcSI</i>
Dry	705	0.76	7.99	8.04	7.86	9.02	10	10	8.82
Cryogenic	720	0.86	7.98	7.83	7.98	8.92	10	10	8.78
MQL	720	1.08	8.03	6.98	7.97	7.61	10	7	7.22

It can be seen that the optimal situation may achieve better scores compared to the results from the experimental work, both on single clusters and globally.

3.5.5 Case study summary

Application of the *ProcSI* methodology involves data collection for the metrics, normalization and weighting, and the summarization of results. With detailed metrics proposed, the application of the metrics and inter-relationship at operation level, workstation level and plant level are discussed. An operation level assessment of a turning process is given. The scenario settings, system analysis, data collection, index generation and comparison are presented. The optimal cutting conditions for each of the three coolant application methods are decided based on the *ProcSI* score, and the comparison among the three best cases with dry machining, cryogenic machining and MQL machining are given. The application of the *ProcSI* method is shown in this section. According to the suggestions given by the optimization, the best performance is achieved applying dry machining at a cutting speed of 705m/min and using a nose radius of 0.76mm.

3.6 Summary

The Process Sustainability Index (*ProcSI*) is developed as a comprehensive and quantitative sustainability performance assessment methodology for universal discrete product manufacturing processes, and machining is taken as an example. The *ProcSI* methodology is described from top to bottom, from the general scope and system boundary to the overall structure, then the metric set and their applications at various levels. The major elements may be summarized as follows:

- The scope and system boundary is defined from the aspect of the manufacturers. The major purpose of this methodology is to help manufacturers to decide the optimal manufacturing processes and the corresponding process parameters. Thus, the system boundary is set around the physical boundary of the manufacturing facility under concern.
- The data flow of the *ProcSI* methodology is organized in a four-level hierarchical structure. The index is segregated into clusters, then sub-clusters and finally individual metrics. The measurements come from bottom to top, going through the procedure of normalization, weighting and aggregation.
- The whole metric set is developed according to previously established requirements. Organized in six clusters, the metrics' measurement methods are presented.
- Focusing on the organization within a manufacturing facility, the application of the *ProcSI* methodology at the operation level, workstation level and plant level is discussed.

CHAPTER 4

COOLING MECHANISM IN CRYOGENIC MACHINING

A comprehensive process sustainability performance assessment is presented in Section 3.5. However, the assessment and optimization are based on empirical modelling from the experimental data. The models established do not represent the actual physical mechanism of the process. On the other hand, the models, sustainability assessment and corresponding optimization are all very much limited by the selection of experimental variables. Especially in the case of comparing different coolant applications, the coolant is applied based on previous experiences. The interactions among the coolant, the workpiece and cutting tools are not yet clarified. Thus, the validity of the sustainability assessment and optimization is limited by many non-proven assumptions, and this has a high degree of uncertainty.

Concerning cryogenic machining, there were no scientific application guidelines established. This is the driving force for establishing a relationship between the influential factors and the coolant performance. To be specific, the performance mentioned here is mainly cooling, while the lubricating effect will also be discussed, in totality.

Most effort in this chapter is to determine the surface heat transfer coefficient in Equation (2.1) about surface heat flux, surface temperature difference and surface heat transfer coefficient. The coolant temperature for liquid nitrogen is constant under normal open atmosphere condition, and the temperature difference between the coolant (liquid nitrogen) and the workpiece surface is decided by the workpiece surface temperature.

And the surface heat flux, along with material thermal properties, decides the temperature change of the workpiece, including its surface. Thus it is possible to establish a relationship between the surface temperature and surface heat transfer coefficient by tracking the temperature profile of the workpiece in a transient heat transfer process. And this approach is dramatically different from getting isolated data points in experiments under thermal steady-state conditions.

4.1 Cooling Effect Experiment for Cryogenic Machining

4.1.1 High speed temperature measurement system and signal processing

The proposed solution for temperature measurement of a rapid changing thermal field is to use an ultra-thin thermocouple, coupled with a high bandwidth signal amplifier and a high speed data acquisition system. The captured voltage data will be mapped to the standard thermocouple table (NIST, 2012) to give the corresponding temperature reading, which is expected to compensate for the error from the non-linear behavior of thermocouples. The thermocouples used in the experiments are Omega® CHCO-001 E-type thermocouples (TCs), with a wire diameter of 25 μ m. The bead diameters are measured to be around 50 μ m. E-type thermocouple is selected due to its wide temperature range, high sensitivity, lower response to magnetic field and relatively low thermal conductivity (Burns and Scroger, 1989). The thermocouple used is verified for use at a wide temperature range between -200°C to 900°C, although extended temperature range can be reached according to the calibration table.

The signal amplifier is based on Analog Devices® AD8421BRZ instrumentation amplifier, which gives a 3dB bandwidth of 2MHz at the gain of 100. Reference design

given in the product datasheet is used, as shown in Figure 4.1. The signal amplifier has a $\pm 7V$ power supply unit built with the LM317/317 bipolar regulated power supply unit, sourced by two lithium batteries for long battery life and good voltage stability.

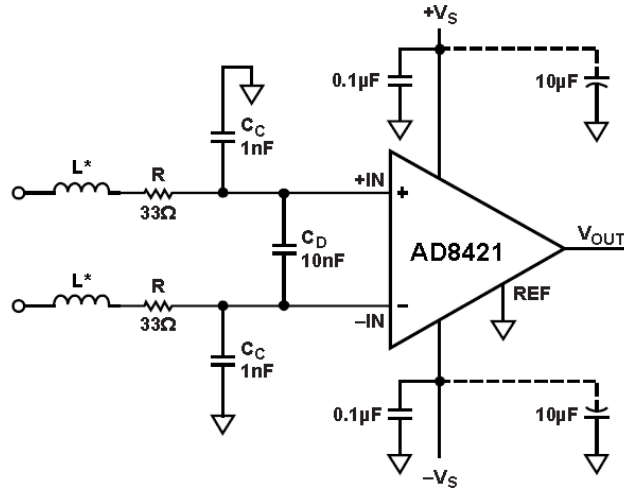
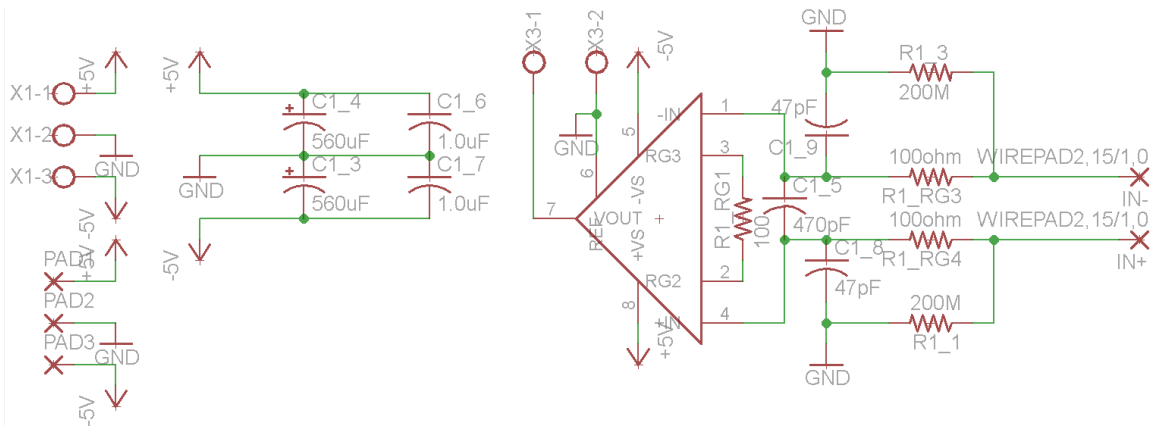
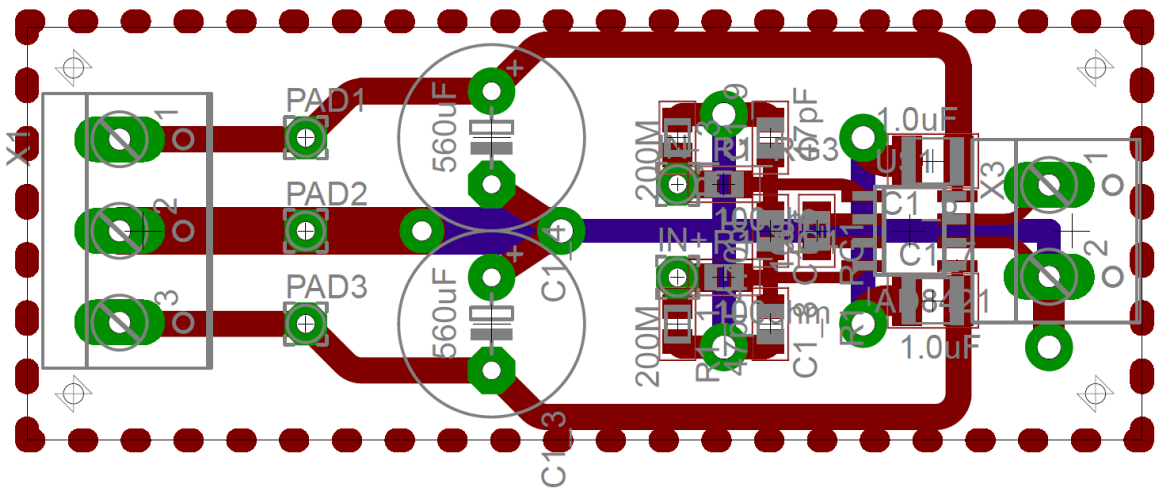


Figure 4.1: Signal amplifier circuit schematic (Analog Devices, 2012).

It should be noted that the electrical routing of the system is critical to its performance. Along with proper circuit routing, surface mounting devices (SMD) are used for the signal amplifier to achieve desirable performance. Shielded twisted-pair cables are used between each of the two devices of the system. The circuit schematic and the two-layer PCB layout are shown in Figure 4.2.



(a)



(b)

Figure 4.2: (a) Schematic of signal amplifier circuit design; (b) PCB layout screen map of the signal amplifier.

The data acquisition unit used is National Instruments® NI USB-6366 USB-interfaced simultaneous data acquisition (DAQ) system, which provides a maximum sampling rate of 2MHz per channel. Matlab® codes are generated for data collection and processing.

The DAQ system has a rated resolution of 0.16mV at the selected scanning range of $\pm 5V$.

The power supply ripple noise is too low to be measured by the DAQ unit, as it is overwhelmed by the native noise of the DAQ unit.

The components for the passive electromagnetic interference (EMI) filter are altered to permit a differential-mode -3dB cutting frequency $f_{diff} = 1.61\text{MHz}$ and common-mode -3dB cutting frequency $f_{comm_neg} = f_{comm_pos} = 33.86\text{MHz}$, which is given by Equations (4.1) to (4.3), as follows (Analog Devices, 2012):

$$f_{diff} = \frac{1}{2\pi(R_{R1_RG3} + R_{R1_RG4}) \left(C_{C1_5} + \frac{C_{C1_8} \times C_{C1_9}}{C_{C1_8} + C_{C1_9}} \right)} \quad (4.1)$$

$$f_{comm_neg} = \frac{1}{2\pi R_{R1_RG3} C_{C1_9}} \quad (4.2)$$

$$f_{comm_pos} = \frac{1}{2\pi R_{R1_RG4} C_{C1_8}} \quad (4.3)$$

Symbols in the equations above refer to the notations in the circuit schematics in Figure 4.2.

The loaded noise recorded by the DAQ unit is 20mV peak-to-peak, which corresponds to the worst case uncertainty of $\pm 2.94^\circ\text{C}$. When filter is not applied, root mean square noise amplitude is 0.60mV, which corresponds to $\pm 0.10^\circ\text{C}$ when tested under room temperature and $\pm 0.22^\circ\text{C}$ near -190°C . A sample of the system idle output is shown in Figure 4.3. The accuracy of the system is calculated as $\pm 3.34^\circ\text{C}$ in the worst case, and the residual sum of square (RSS) error is $\pm 1.90^\circ\text{C}$ (Lepkowski, 2004). Most of the error comes from the uncertainty of thermocouple, which is labelled by the manufacturer as $\pm 1.5\%$ of measured value or $\pm 1.5^\circ\text{C}$, whichever is greater.

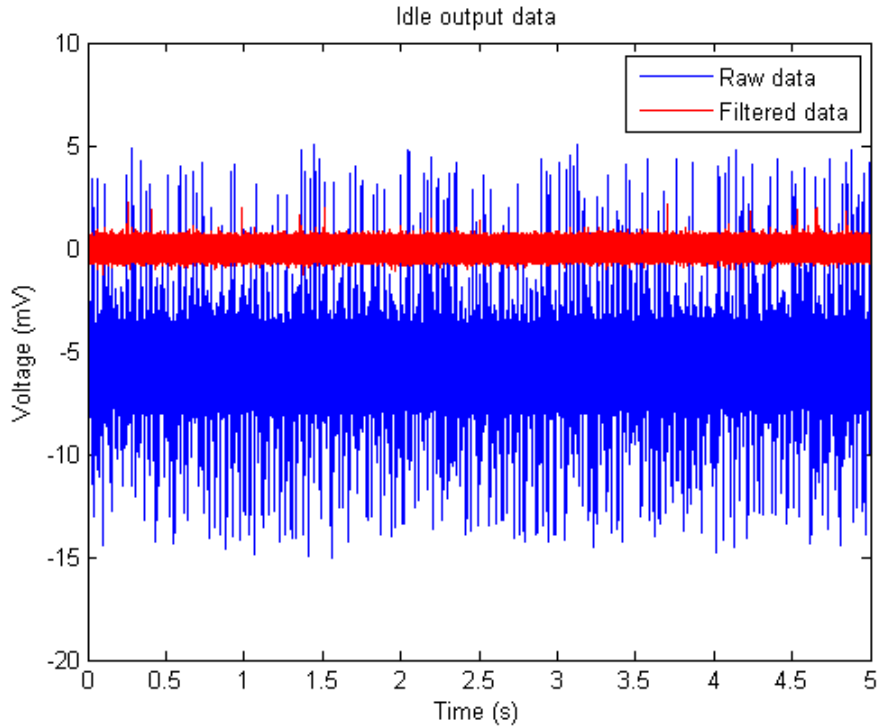


Figure 4.3: A sample of the system idle signal.

Due to the small diameter, the thermocouple shows significant resistance, which is measured to be 870Ω for $25\mu\text{m}$ diameter thermocouple with 30cm leads. To overcome the significant signal drifting introduced by the resistance, an amplifier chip with low offset voltage and small input bias current is needed, along with unusually large current return resistors ($200\text{M}\Omega$ used). This is one of the critical reasons why the AD8421BRZ amplifier chip is chosen in this application, instead of the lower noise model AD8429 in the same product family. And, the commonly seen thermocouple breakage detection design is abandoned to reduce signal drifting. Furthermore, when setting the EMI filter parameters, it must assure that the bandwidth is not limited due to the resistance of the thermocouple.

The flow chart of signal processing is presented in Figure 4.4.

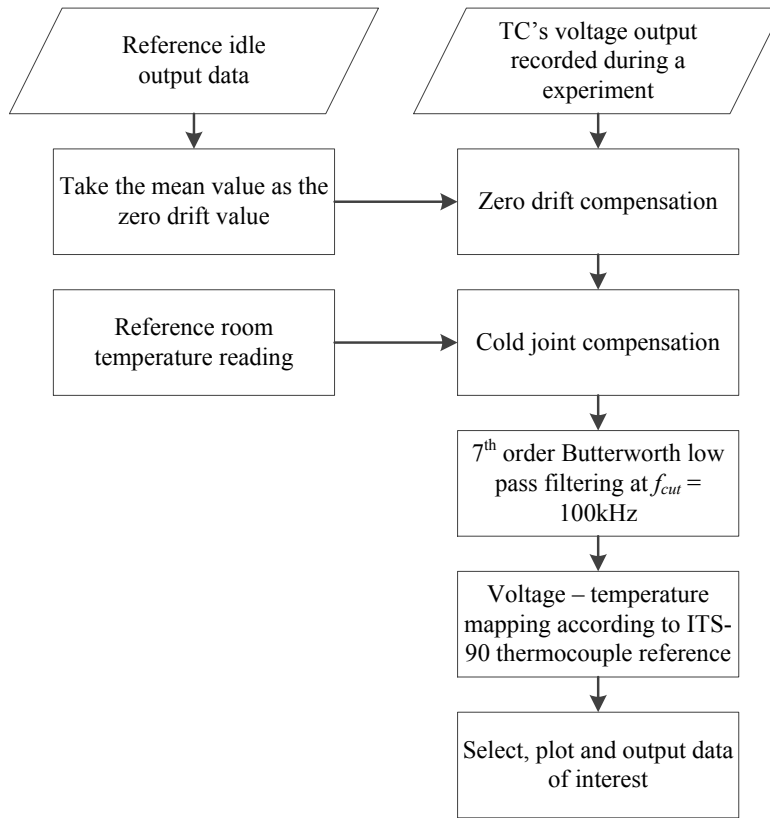


Figure 4.4: Flow chart of signal processing.

The detailed Matlab® code for signal processing can be found in APPENDIX A.

A sampling rate of 2MHz is used throughout the study. The system is tested by taping the thermocouple to a plastic strip under direct liquid nitrogen (LN) flow, and the thermocouple junction is exposed. The maximum recorded temperature gradient is 60°C/ms. This corresponds to a system bandwidth of approximately 153Hz, and is limited by the capability of the thermocouple and the surface heat transfer coefficient. It is used as a reference for future discussion about system capability and signal processing.

The system is very sensitive to radio frequency interference (RFI), due to the antenna-like structure of the bare-wire thermocouple. The major radio frequency noise sources in the lab are Wi-Fi signal, cell-phone signals and electromagnetic radiation from power

machine tools, and the most effective radio frequency is typically well above the bandwidth of the DAQ system. The observed effect is higher amplitude of noise in the higher end of the system bandwidth. It is supposed to be caused by aliasing effect while the high frequency noise sources are recorded at the system's low sample rate (Foley et al., 1995). The maximum sample rate of 2MHz is used as it provides the largest possible headroom for noise filtering. More importantly it allows the largest value of oversampling factor for the oversampling process discussed in Section 4.2.1.

4.1.2 Static cooling experiments

The purpose of the static cooling experiments is to provide fundamental understanding of the heat transfer phenomena in the flank side liquid nitrogen application in cryogenic machining. To be specific, the heat transfer model generated should be able to provide proper boundary conditions for cryogenic machining models, and help to understand the major factors influencing the cooling effect in cryogenic machining.

In the case of machining, the heat sources are complex. The workpiece is often subject to motion, which prohibits the attachments of measurement devices. Thus, it is proposed to build the heat transfer model with static cooling experiments. Then, the model is validated with machining experiments.

Scenarios

The orthogonal cutting scenario is the foundation here, as shown in Figure 4.5.

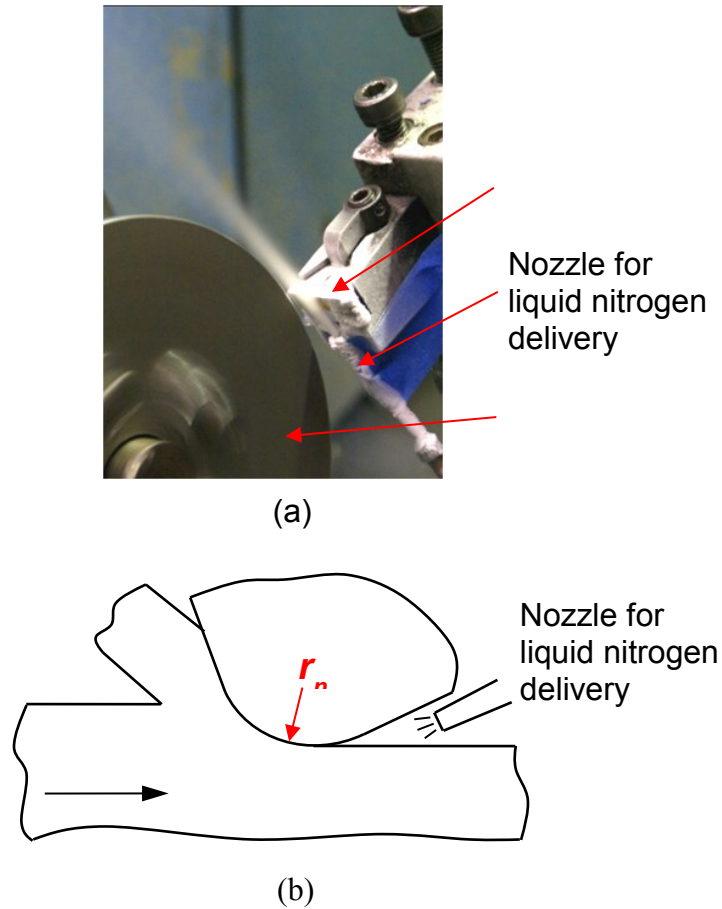


Figure 4.5: Experimental setup of cryogenic machining: (a) photo (tool approaching the workpiece) and (b) schematic diagram (Pu, 2012).

From the thermal aspect, the model discusses the thermal dissipation on the machined surface of the workpiece when liquid nitrogen is applied into the opening between the flank side of the cutting tool and the machining surface.

Coolant delivery system

A customized coolant delivery system is developed. It is designed as a low pressure delivery system with controllable driving pressure. The system schematics is shown in Figure 4.6.

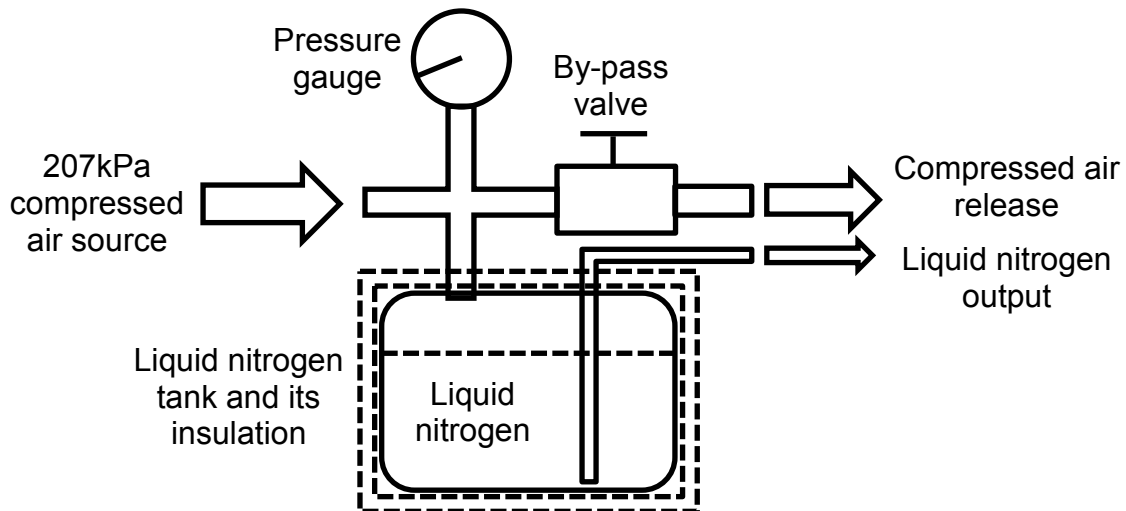


Figure 4.6: System schematic of the low pressure liquid nitrogen delivery system.

The driving pressure is controlled by the by-pass valve. A small amplitude of pressure can be steadily applied by switching the valve from wide open towards close, and the pressure drop through the narrowing valve seat would cast a small pressure to the liquid nitrogen tank. Only a small amount of compressed air, which is equal to the volumetric flow rate of liquid nitrogen output, will be injected into the liquid nitrogen tank to minimize liquid nitrogen loss due to external heating.

The relationship between the driving pressure and flow rate is calibrated with water pumping experiments. The results are shown in Table 4.1.

Table 4.1: Fluid flow rate at different driving pressures.

Pressure (kPa)	Fluid	Volumetric Flow Rate ($10^{-6} \text{ m}^3/\text{s}$)	Flow Speed (m/s)	Reynolds Number (Re)
17.2	Water	26.9	3.39	1.21×10^4
34.5	Water	33.7	4.26	1.52×10^4
51.7	Water	39.0	4.92	1.76×10^4
68.9	Water	44.5	5.62	2.00×10^4
86.2	Water	50.6	6.39	2.28×10^4
96.5	Water	53.3	6.73	2.40×10^4
110.3	Water	57.8	7.30	2.61×10^4
124.1	Water	61.5	7.77	2.77×10^4

The Reynolds Number is given as $Re = \rho \bar{u} d / \mu$, where ρ is the density of fluid; \bar{u} is the mean velocity of fluid in m/s; d is the hydraulic diameter of the pipe, in m; μ is the dynamic viscosity of the fluid, in Pa·s. For all water based experiments, the resulting Reynolds numbers Re are greater than 6000, thus, the flow inside the pipe should be considered as turbulent flow (Streeter, 1962). The relationship between the pressure and the volumetric flow rate is shown in Figure 4.7.

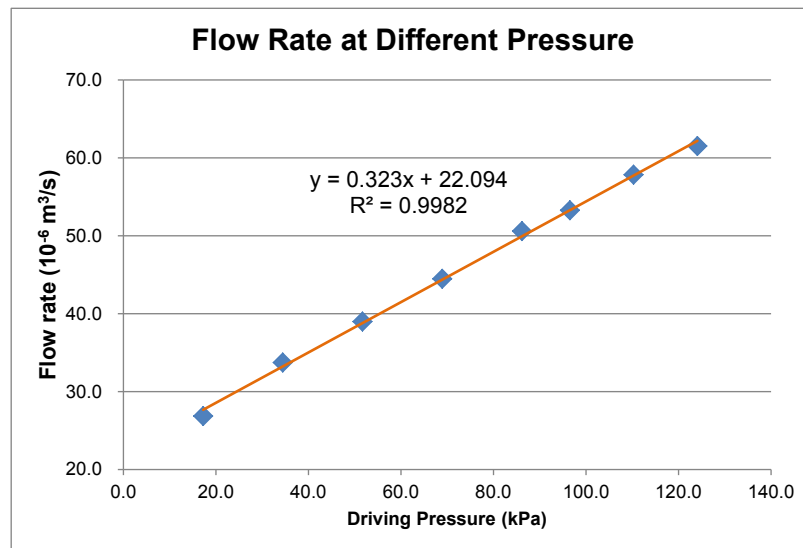


Figure 4.7: Flow rate at different driving pressure in the water experiments.

In a simple form, the Hagen-Poiseuille relation is shown in Equation (4.4), which describes the flow rate in a pipe based on the pipe size, the fluid properties and the pressure drop (Sutera and Skalak, 1993). It is derived from the Navier-Stokes equations, meaning it is a momentum balance, and presents a linear relationship between pressure drop, viscosity of the fluid and the volumetric flow rate.

$$P - \rho g \Delta h = \frac{128 \mu L Q}{\pi d^4} \quad (4.4)$$

where P is the driving pressure, in Pa; ρ is the density of fluid, in kg/m^3 ; g is the specific gravity, in m^2/s ; Δh is the equivalent head loss of the flow due to height difference and tube joints, in m; f is ; L is the length of the tubing, in m; d is the diameter of the tubing, in m; \bar{u} is the average flow speed in the tube, in m/s; and Q is the volumetric flow rate, in m^3/s .

However, the Hagen-Poiseuille relation is based on laminar flow condition. The calculated Reynolds Numbers in Table 4.1 for different conditions show the flow is turbulent. The Darcy-Weisbach equation is often used in this case, and one of its form concerning pressure drop and mean flow speed is give in Equation (4.5) (De Nevers, 2004).

$$P - \rho g \Delta h = \rho g \cdot \frac{f_D L}{d} \cdot \frac{\bar{u}^2}{2g} \quad (4.5)$$

where, f_D is the Darcy Friction Factor, a dimensionless coefficient of laminar or turbulent flow; \bar{u} is the mean velocity of the flow, in m/s.

The friction factor f_D is not a constant, and depends on the parameters of the pipe and the velocity of the fluid flow, and is often obtained from published charts, which are often referred to as Moody diagrams. For turbulent flow and a smooth pipe, a simple

relationship is given by the Blasius correlation, which is valid for straight tubes and $Re \leq 10^5$, as shown in Equation (4.6) (Trinh, 2010):

$$f = 0.079Re^{-0.25} = 0.079 \times \left(\frac{\rho \bar{u} d}{\mu} \right)^{-0.25} \quad (4.6)$$

Then, the flow rate of liquid nitrogen at different source pressure can be estimated based on the viscosity and density difference between water and liquid nitrogen, as summarized in Table 4.2.

Table 4.2: Estimated flow rate of liquid nitrogen under the source pressure used in the experiments.

Pressure (kPa)	Fluid	Mass Flow Rate (g/s)	Flow Speed (m/s)	Reynolds number (Re)
17.2	LN	28.6	4.48	7.27×10^4
34.5	LN	35.9	5.62	9.12×10^4
51.7	LN	41.6	6.50	1.05×10^5
68.9	LN	47.4	7.41	1.20×10^5
$\mu_{water} = 8.903 \times 10^{-4} \text{ Pa}\cdot\text{s}, \rho_{water} = 1000 \text{ kg/m}^3; \mu_{LN} = 1.58 \times 10^{-4} \text{ Pa}\cdot\text{s}, \rho_{LN} = 808 \text{ kg/m}^3$				

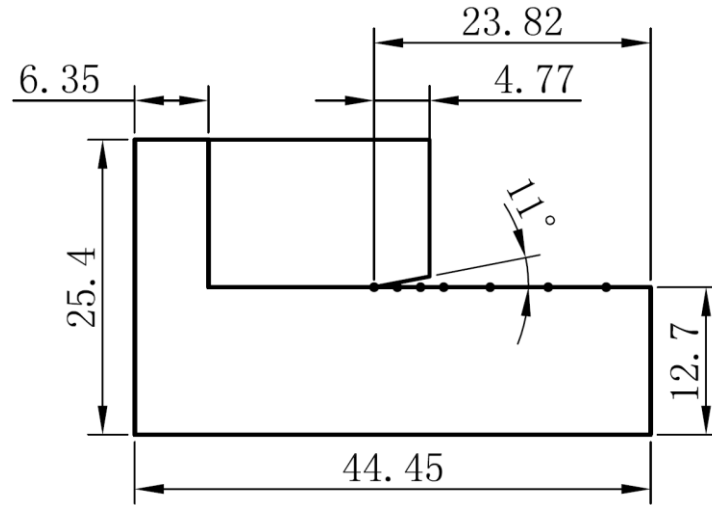
It should be emphasized that, the flow rate of liquid nitrogen listed above is an estimation based on empirical and analytical relationships, while some of the values of Re calculated are slightly larger than the expected range used for the Blasius correlation. The purpose of the above data is to provide references for comparison. The exact volumetric flow is difficult to measure due to the constant boiling of the liquid nitrogen pool and the ice formation due to moisture condensation around the LN tank.

It can be seen that due to the low viscosity, the flow rate of liquid nitrogen tends to be higher than the flow rate of water at the same source pressure. Higher flow speed and lower viscosity lead to a tendency to develop turbulent flow. Some literature (Chen and Tseng, 1992) recommends laminar flow for its good wettability on the hot surface. But, it

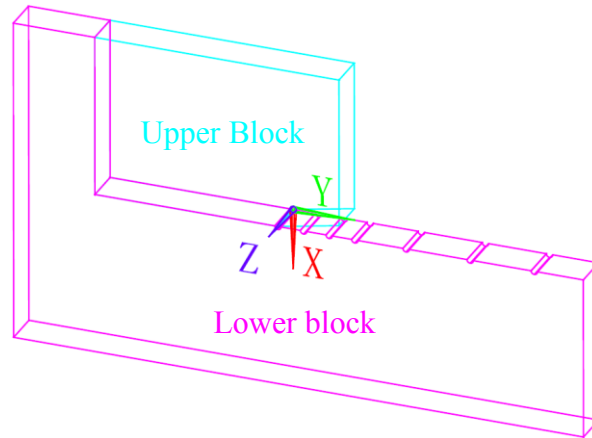
could be concluded that in the case of cryogenic machining, laminar flow condition is very difficult to achieve even with a very low pressure system.

Specimen

The 2D and 3D drawings of the specimen are shown in Figure 4.8.



(a)

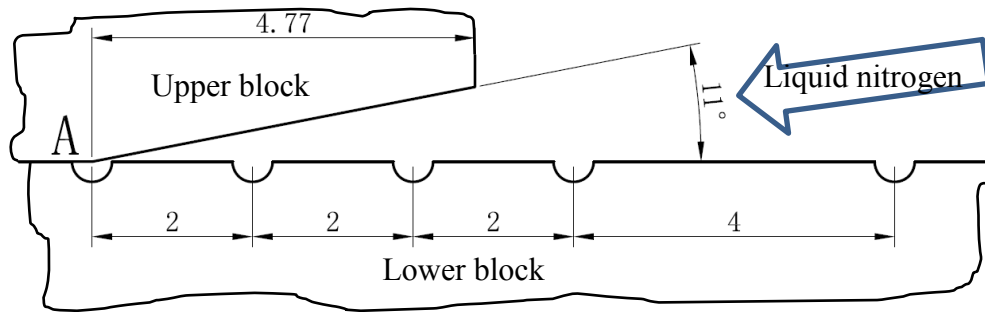


(b)

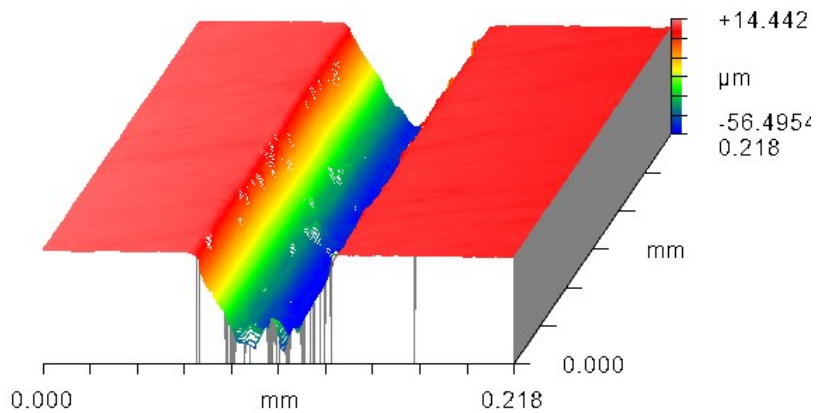
Figure 4.8: Drawings for the specimen: (a) 2D drawing for the dimensions in mm; (b) 3D drawing for the coordinate system and an illustration of the micro-groove locations.

The specimen is made from 3mm thick *AZ31B* sheet. The upper block and the test surface on the lower block forms a 11° opening, while the upper surface of the opening is to simulate the flank surface of a 4.77mm thick insert, and the test surface on the lower block is to simulate the machined surface on the workpiece. The test surface is milled and then, polished to a smooth surface with $R_a = 0.3\mu\text{m}$, a similar roughness to the machined surface.

There are seven micro-machined grooves on the test surface, numbered groove 0 through 6. The details of the micro grooves on the test surface are illustrated in Figure 4.9.



(a)



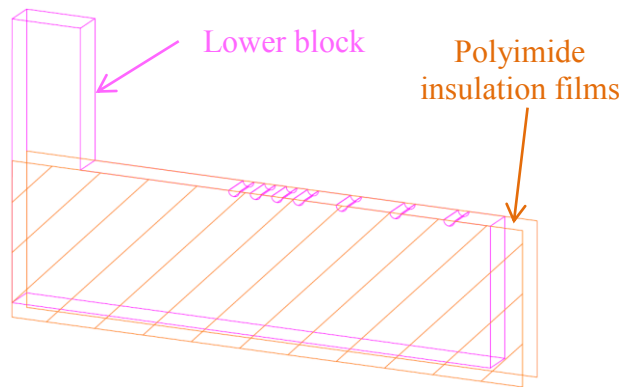
(b)

Figure 4.9: Micro-grooves on the test surface: (a) micro-groove locations (groove size not to scale, only first 5 grooves shown); (b) micro-groove dimensions.

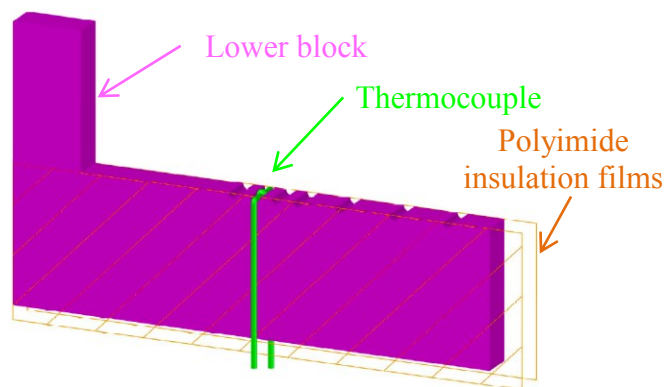
Point *A* indicates the separation point of cutting tool and machined surface on the workpiece. The seven micro-grooves, named Groove 0 through 6, are located at a distance of 0, 2, 4, 6, 10, 15 and 20mm away from the point *A*. The micro-grooves are trapezoid shaped. They have opening width around 80-100 μm and bottom width around 20-30 μm . The depths of the grooves range from 35 μm to 40 μm .

Setup

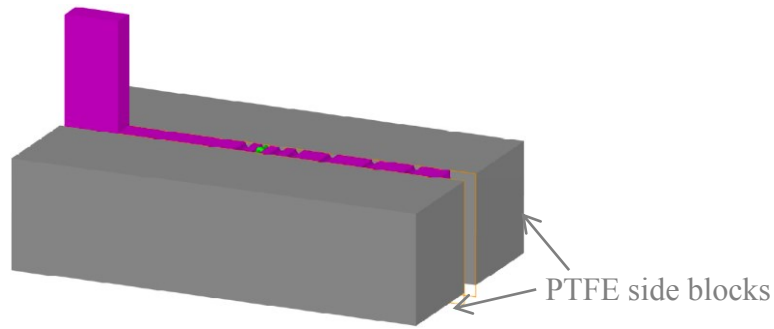
The steps by step procedure followed is summarized in Figure 4.10.



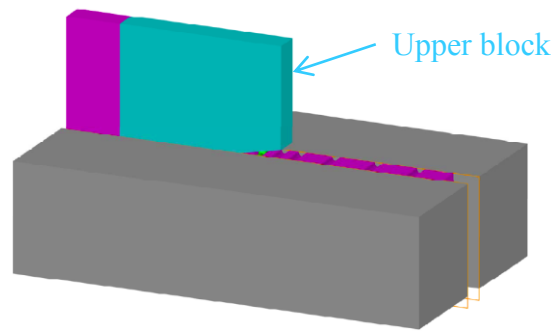
(a)



(b)



(c)



(d)

Figure 4.10: Setup procedures: (a) apply insulation film; (b) install thermocouple; (c) install and clamp side blocks; (d) clamp upper block.

The first step is to attach a thin layer of insulation plastic film on the side surface of the lower block, to provide proper electrical insulation between the side surface of the lower block and the thermocouple wires. The plastic film used is $25\mu\text{m}$ ($\pm 5\mu\text{m}$) thick polyimide film in raw amber color and it bears a temperature rating from -268°C to 400°C . The film is attached to the lower block by two drops of hot melt adhesive at the front and back of the lower block, which are placed far away from the test region.

Then, a thermal conductive grease is applied to the groove. A thermocouple is laid flat in one of the micro-grooves, and the joint of the thermocouple is kept approximately at the middle position in the groove in z direction. The two poles of the thermocouple are

placed outside the insulation film. After that, the thermocouple is tensioned downwards (positive x direction) with an elastic low density polyethylene (LDPE) strip which holds the rest of thermocouple. Excess thermal conductive grease is then wiped out. This will keep the thermocouple at the bottom of the grooves, and its bead extends within a few microns above the test surface, as proven by surface microscopic measurement shown in Figure 4.11.

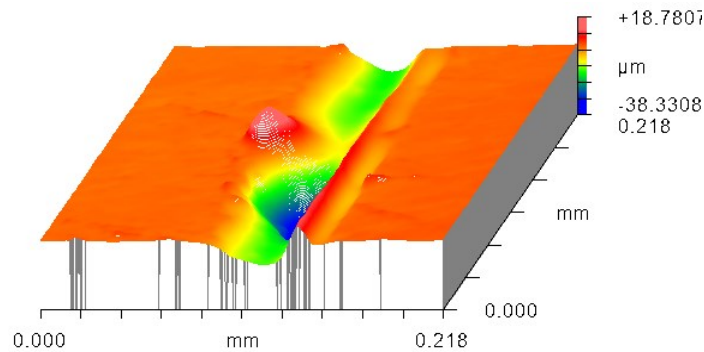


Figure 4.11: Surface topography of the micro-groove after a thermocouple is placed inside.

The third step is to clamp two plastic blocks to the side of the lower block. They are used as thermal insulation in the z direction and they also block the side flow of the coolant. The block has a square cross Section of 12.7mm by 12.7mm (± 1.2 mm), and is made of PTFE (Teflon®) plastic which has a temperature rating from -212°C to 260°C . The top surface of the block and the test surface of the lower block are aligned by precision parallels. A bench vise clamps the whole setup by holding the two plastic blocks by the side, in z direction.

The last step is to clamp the upper block to the lower block by a mini c-clamp, applying clamping force in x direction.

Coolant flow from the delivery system described in the previous section is applied into the opening, simulating the cooling scenario of flank-side cooled orthogonal machining. Temperature change at a very close distance to the surface is recorded by the thermocouple and adjacent measurement system.

Procedure

After the specimen is correctly setup, the static cooling experiment is ready to run. The procedure of the experiments is described in Figure 4.12.

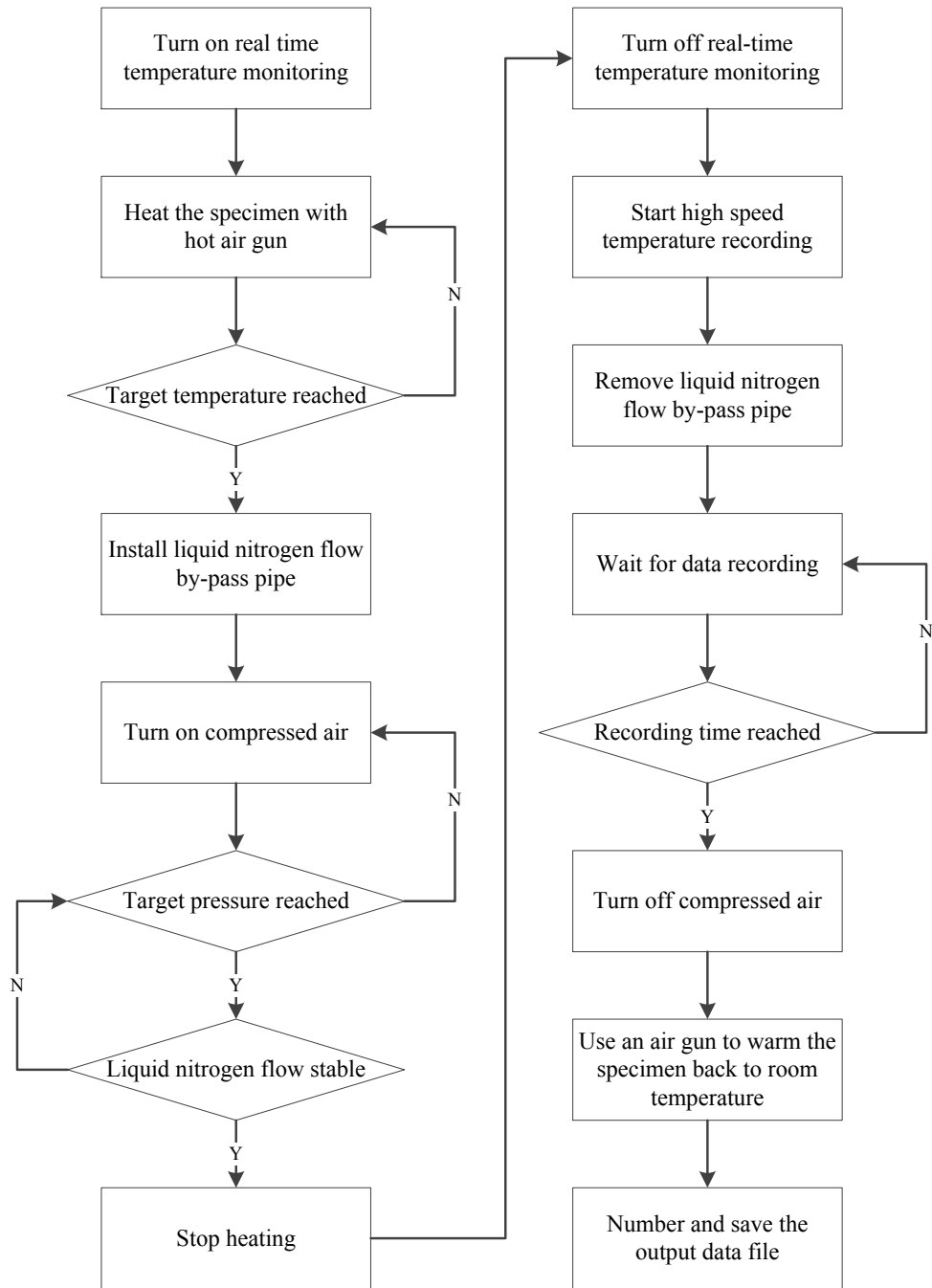


Figure 4.12: Flow chart of the static cooling experiments.

The output file contains recorded thermocouple voltage readings. Temperature data can be obtained by going through the signal processing described in Section 4.1.1. The resulting temperature curve describes the temperature change of the specimen surface, but, further modelling effort is needed for analysis.

4.2 Boiling Heat Transfer Modeling for Cryogenic Machining

4.2.1 Surface heat transfer modelling under cryogenic condition

Building the transient heat transfer problem

In both the static experiments and the machining experiments, the test piece does not necessarily achieve thermal steady-state. Especially for the cooling effect investigation, it is a transient heat transfer problem.

The general heat transfer governing equation is given by Equation (4.7):

$$\frac{D}{Dt} \int (\rho e + \frac{1}{2} \rho v^2) dV = - \int q \cdot n dA + \int t_{(n)} \cdot v dA + \int \rho g \cdot v dV + \int \phi dV \quad (4.7)$$

where, t is time; ρ is the density of the material; e is the internal energy density; v is the speed; V is the volume; q is the heat flux on the surface; n is the normal direction; A is the surface area; g is the standard gravity; and ϕ is internal heat generation rate. The right four terms of Equation (4.7) represent the surface heat transfer, surface work, body work and internal heat source, respectively.

For our problem of the cooling of the workpiece during cryogenic machining, after the workpiece surface exits the contact zone with the cutting tool and remains exposed to liquid nitrogen flow, there is no surface work and body work. There may be internal heat source due to material phase change, grain boundary activity, and/or grain refinement/growth. We ignore the internal heat source due to their relatively small contribution to the general heat transfer behavior in the cooling zone.

Thus, the governing Equation (4.7) can be simplified and written in Gaussian polar coordinates as follows:

$$\frac{\partial}{\partial x} \left(k \frac{\partial T}{\partial x} \right) + \frac{\partial}{\partial y} \left(k \frac{\partial T}{\partial y} \right) + \frac{\partial}{\partial z} \left(k \frac{\partial T}{\partial z} \right) + q^m = \rho C_p \frac{\partial T}{\partial t} \quad (4.8)$$

where, x, y, z are the three spatial coordinates of the Cartesian coordinate system; k is the heat conductivity of the material; t is time; T is the temperature distribution function $T(x, y, z, t)$; q^m is the heat generation rate per unit volume; ρ is the density of the test material; and C_p is the specific heat capacity of the test material. The coordinate system is shown in Figure 4.13.

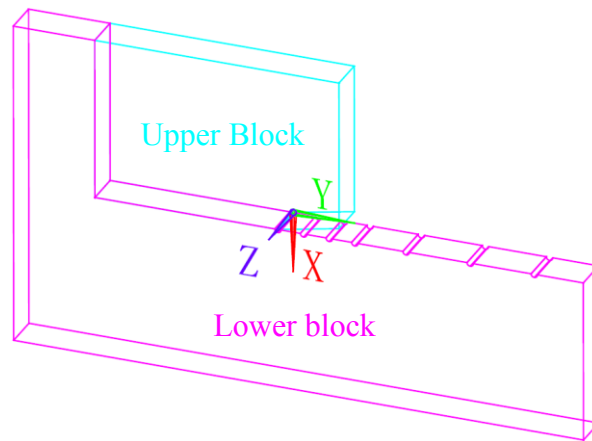


Figure 4.13: Coordinate system in the heat transfer modeling.

The static test and machining experiments assume two-dimensional heat plane condition, which implies that the differences of tested behavior in the z -direction are small enough to be ignored. To be specific for the heat transfer problem illustrated in Section 4.1.2, the cooling on the side-wall of the specimen is to be questioned most. Liquid nitrogen has a very low viscosity and the size of the nozzle is carefully selected to limit the flow on the top surface, the liquid nitrogen tends to flow away from the specimen along the surface direction (in the z - y plane) instead of sticking to the side wall of the specimen. There is no observable liquid nitrogen flow on the side-walls. There is still surface heat transfer between the side walls and the ambient air. Considering the significant difference

between the boiling heat flux on the test surface and the convective heat transfer on the side-wall, it is safe to assume the difference in the z direction due to side-wall heat transfer is small. This can be confirmed by comparing surface heat transfer coefficient of natural convection heat transfer and the calculated boiling heat transfer coefficients.

The surface heat transfer coefficient has a non-uniform distribution in the y direction. This is due to the different local flow condition at different y locations. But, it is experimentally difficult to measure temperature at multiple locations in the current setup.

The difficulty is attributed to the following:

- 1) Due to the fast response requirements, the thermocouple used is bare wire type which has no insulation on it. Thermocouples may form a false joint with the workpiece. Thus, multiple thermocouples may interfere with each other.
- 2) It is difficult to synchronize the measurements, when either done simultaneously or individually. When measurements of various points are involved, the exact time of contact with liquid nitrogen is also difficult to identify. Thus the time domain is not synchronized and the measurement may not be valid.

Therefore, it is proposed to model the heat transfer by multiple one-dimensional heat transfer problems. Each of the one-dimensional heat transfer model represents the local heat transfer coefficient at the location of measurement. The heat transfer coefficient in the y direction is assumed as independent, and the overall distribution is simply the joint of multiple local heat transfer coefficient at various locations in the y direction. This needs the measurements less influenced by the heat transfer in y direction and most sensitive to the heat transfer in x direction. This is one of the reasons that the thermocouples are located extremely close to the surface.

Based on the discussion above, the Equation (4.8) is further simplified as

$$\frac{\partial}{\partial x} \left(k \frac{\partial T}{\partial x} \right) + q^m = \rho C_p \frac{\partial T}{\partial t} \quad (4.9)$$

When assuming that:

- 1) the material has a homogeneous heat conductivity throughout the space, thus k is a constant and does not change at different locations or at different temperatures; and
- 2) the internal heat source due to material change is ignored, thus $q^m = 0$.

Equation (4.9) can be further modified as:

$$\frac{\partial^2 T}{\partial x^2} = \frac{1}{\alpha} \cdot \frac{\partial T}{\partial t} \text{ at } y = y_i, i = 0, 1, 3, \dots, 6 \quad (4.10)$$

where, α is thermal diffusivity, defined by $\alpha = k/(\rho \cdot C_p)$; the y_i indicates the i th location of measurements. And, the boundary conditions in the current case are:

$$-k \frac{\partial T}{\partial x} = h \cdot (T - T_{LN}) \text{ at } x = 0 \quad (4.11)$$

$$-k \frac{\partial T}{\partial x} = h_{air} \cdot (T - T_{air}) \text{ at } x = L \quad (4.12)$$

$$T = T_{air} = 24^\circ\text{C} \text{ at } t = 0, \text{ in } 0 \leq x \leq L \quad (4.13)$$

where, k is the heat conductivity of the material, in $\text{W}/(^\circ\text{C}\cdot\text{m})$; x is the distance from the test surface, in m; t is the time from the initial liquid nitrogen contact, in s; T is the temperature distribution function $T(x, t)$; ρ is the density of the test material, in kg/m^3 ; C_p is the specific heat capacity of the test material, in $\text{J}/(^\circ\text{C}\cdot\text{kg})$; L is the height of the specimen, in m; h is the surface heat transfer coefficient on the test side, in $\text{W}/(^\circ\text{C}\cdot\text{m}^2)$; T_{LN} is the saturation temperature of liquid nitrogen, in $^\circ\text{C}$; h_{air} is the surface heat transfer

coefficient on the free-side, which is exposed to air, in $W/(^{\circ}C \cdot m^2)$; and T_{air} is the temperature of the air, in $^{\circ}C$.

Finite difference method

A commonly used tool to numerically solve transient heat conduction problem is Finite Difference Modeling (FDM). It is typically used for direct heat conduction problem, and is chosen as the tool for its simplicity, solution stability and relatively fast calculation speed.

FDM is based on space and time meshes. The mesh in space is formed by a series of points, equally separated by a constant space Δx . Thus, the one-dimensional space is meshed into a series of points $x_i, i = 0, 1, 2, \dots, N$. Points x_0 and x_N are the boundary nodes, located at $x = 0$ and $x = L$, respectively. And, the other nodes are interior nodes. Similarly, mesh in time is formed by a series of instants of time, equally separated by a constant time period Δt . They are noted as $t_j, j = 0, 1, 2, \dots, M$, where t_0 represents the initial time instant of the system, and t_M notes the end of the time period under consideration. Based upon the notations above, the overall temperature distribution is given by $T(x_i, t_j) = T_{i,j}$.

The basic idea of FDM is to replace the derivatives in the mathematical formulation of the problem by suitable approximation on a finite different mesh (Ozisik, 1993). There are typically two ways of approximation, the explicit scheme and implicit scheme, and they are briefly introduced in APPENDIX B. As the computation speed is taken as the priority here, and a large ram space is available, the implicit scheme is used.

The assumption of homogeneous material may not fit well with the fact, as the specimen temperature varies along an enormous range and its thermal conductivity and specific heat capacity are subject to temperature changes. The thermal properties are suggested to be modeled by 7th order logarithm summation equation by NIST’s material cryogenic property database (Marquardt et al., 2000). To be specific, the property x is given by:

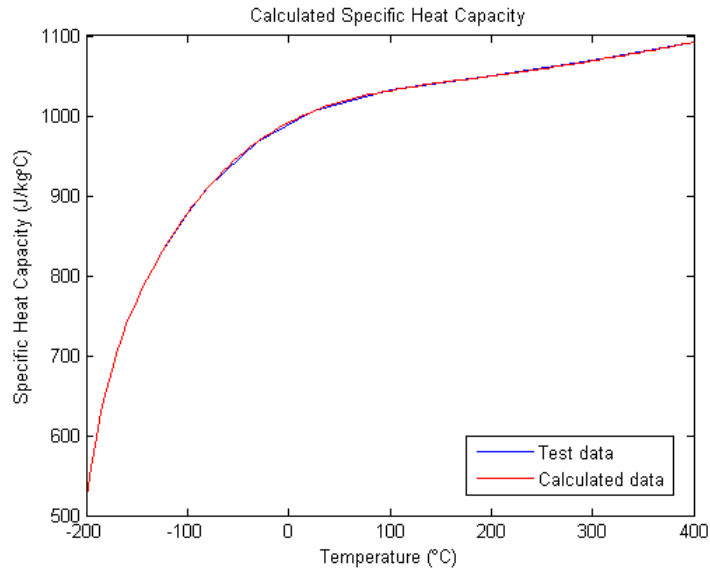
$$\log(x) = \sum_{i=0}^n a_i \cdot (\log T)^i \quad (4.14)$$

where T is the temperature in °K; a_i are the coefficients to be determined by experimental data. By using non-linear least square fitting to the test data (Lee et al., 2013), the following coefficients can be calculated for the thermal conductivity and specific heat capacity, as summarized in Table 4.3.

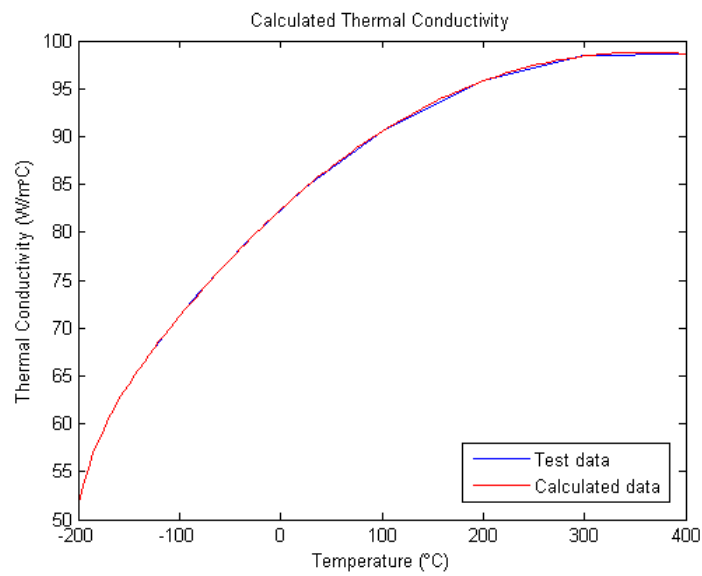
Table 4.3: Thermal property coefficients for *AZ31B* alloy.

Coefficients	Thermal Conductivity k (in W/m°C)	Specific Heat Capacity C_p (in J/kg°C)
a_0	-194.5263	-1.349480
a_1	475.4458	-382.5377
a_2	-481.3477	962.9201
a_3	261.1623	-997.7259
a_4	-80.44582	548.5754
a_5	13.50081	-168.9559
a_6	-1.013267	27.63922
a_7	0.01141235	-1.876087

Seven significant digits are used universally here. NIST’s literature (Marquardt et al., 2000) recommended using five to seven significant digits. The thermal properties of *AZ31B* alloy are interpolated and extrapolated to a slightly wider range (-200°C to 400°C) using the coefficients above. The curves are shown in Figure 4.14.



(a)



(b)

Figure 4.14: Thermal properties of *AZ31B* alloy used in the analysis: (a) specific heat capacity; (b) thermal conductivity.

In the thermal analysis, the thermal properties are considered as local thermal properties at each node. Thus, when considering Equations (4.8) and (4.9), the derivations of

thermal properties are ignored. But, the values of thermal properties of a node at current temperature are used for the calculation of the temperature of next step for this node. As both the grid size and the time step are small, the spatial and time gradient of temperature field are small, thus, such approximation would have only minor effect on the model accuracy. On the positive side, the computation power requirements are relatively low with this approximation method.

The impact of grid size on model accuracy is also tested. Grid sizes of half, one-fourth and one-eighth of the original size of 27 μ m are tested. Within the recording accuracy, which is two digits after decimal points for the surface heat transfer coefficient h in W/($^{\circ}$ C m²), there are no differences among the results from models with difference grid sizes. This can be concluded as due to the small grid size and time step, which lead to sufficiently small errors from derivation estimation in both space and time domain. On the other hand, reducing grid size has a significant impact on the computation power required for the calculation. Thus, the grid size is kept as original for all other calculation and discussion.

Inverse heat transfer problem (IHTP)

The transient heat transfer question here is an inverse problem which is given by:

$$k \frac{\partial^2 T}{\partial x^2} = \rho C_p \frac{\partial T}{\partial t} \text{ at } 0 < x < L, \text{ for } 0 < t < t_f \quad (4.15)$$

$$-k \frac{\partial T}{\partial x} = h \cdot (T - T_{LN}) = ? \text{ at } x = 0 \quad (4.16)$$

$$-k \frac{\partial T}{\partial x} = h_{air} \cdot (T - T_{air}) \text{ at } x = L \quad (4.17)$$

$$T = T_{air} = 24^{\circ}\text{C} \text{ at } t = 0, \text{ in } 0 \leq x \leq L \quad (4.18)$$

$$T(x_1, t_j) \equiv Y_j \text{ for } t = t_j, j = 1, 2, 3, \dots, N \quad (4.19)$$

where, k is the thermal conductivity of the material, in $\text{W}/(^{\circ}\text{C}\cdot\text{m})$; x is the distance from the test surface, in m ; t is the time from the initial liquid nitrogen contact, in s ; T is the temperature distribution function $T(x, t)$; ρ is the density of the test material, in kg/m^3 ; C_p is the specific heat capacity of the test material, in $\text{J}/(^{\circ}\text{C}\cdot\text{kg})$; L is the height of the specimen, in m ; h is the surface heat transfer coefficient on the test side, in $\text{W}/(^{\circ}\text{C}\cdot\text{m}^2)$; T_{LN} is the saturation temperature of liquid nitrogen, in $^{\circ}\text{C}$; h_{air} is the surface heat transfer coefficient on the free side, which is exposed to air, in $\text{W}/(^{\circ}\text{C}\cdot\text{m}^2)$; T_{air} is the temperature of the air, in $^{\circ}\text{C}$; x_l is the location of the test point, in m ; t_j is the time when measurements are taken, in s ; Y_j is the measured temperature of point x_l at time t_j , in $^{\circ}\text{C}$; and N is the total number of measurements taken.

The inverse method can be stated as a method, which utilizes the measured data Y_j ($j = 1, 2, 3, \dots, M$) to estimate the M surface heat transfer coefficient components, $h(t_j) = h_j$ ($j = 1, 2, 3, \dots, M$). The problem is mathematically ill-posed in the sense that its existence, uniqueness, and/or stability are not ensured, and a successful solution of the inverse problem generally involves the transformation of the inverse problem into a well-posed approximate solution (Ozisik and Orlande, 2000). In most methods, the solutions of inverse heat transfer problems are obtained in the least square sense.

To illustrate the sensitivity of IHTP to small changes in the measured input data, an example is given about a one-dimensional quasi-stationary temperature field in a semi-infinite solid subject by periodically varying heat flux at the boundary surface. The maximum amplitude at any location is given as (Ozisik, 1989; Ozisik, 1993; Ozisik and Orlande, 2000):

$$[T(x, t)]_{max} = \frac{q_0}{k} \sqrt{\frac{\alpha}{\omega}} \cdot \exp\left(-x \sqrt{\frac{\omega}{2\alpha}}\right) \quad (4.20)$$

where, q_0 is maximum amplitude of oscillations for the varying heat flux; ω is the frequency of oscillations in angular velocity form, given by $\omega = 2\pi \cdot f$, and f is the frequency. This indicates that if the surface heat flux is to be determined by utilizing the measured temperature at an interior points, any measurement error will be magnified exponentially with the distance x and the square root of the fluctuating frequency ω of the heat flux. This is another reason that we want to put the sensor location as close to the test surface as possible. Also, the error will be magnified linearly with the amplitude of oscillations.

Some of the standard assumptions of the random error ϵ_i in temperature measurement for inverse heat transfer problems are (Ozisik and Orlande, 2000):

- 1) The errors are additive.
- 2) The temperature errors, ϵ_i , have a zero mean.
- 3) The errors have constant variance.
- 4) Two measurement errors, ϵ_i and ϵ_j , where $i \neq j$, are uncorrelated if the covariance of the two errors are zero.
- 5) The measurement errors have a normal distribution.
- 6) The statistical parameters such as the standard deviation, σ , are known.
- 7) The measurement time t_i and measurement location x_j , the dimensions of the specimen and the thermal properties are all accurately known.

Least square method

The least square method for solving IHTP is to transfer the mathematically ill-posed problem into a well-posed problem, by minimizing the least squares norm rather than make it necessarily zero (Ozisik, 1993). Then the problem becomes an optimization problem, where great varieties of algorithms could be used. Among them, the Levenberg-Marquardt algorithm is one of the most commonly used methods.

The Levenberg-Marquardt method is a parameter estimation method, which determines the optimal parameters in a pre-defined target function in the sense least square fitting. In the study here, fifth to ninth order polynomial functions, power functions, exponential function and simple combinations of the above-listed functions are used as target functions. A brief introduction to the Levenberg-Marquardt iteration method and an example of solving the IHTP with least square method is given in APPENDIX C.

Apart from the Levenberg-Marquardt method, reflective trust region method and genetic algorithm are used for similar parameter estimations. However, these methods did not give exceptional results compared to the Levenberg-Marquardt method.

There are two major difficulties in applying least square method in the current case. The first one is that, the least square method could give a rough approximation to the temperature curve of the experiments, but the error is very significant. This is due to the fact the heat transfer phenomenon in the current case is not stable, and it could involve different and multiple cooling mechanisms. As a result, the actual surface heat transfer coefficient curve would be sectional and highly non-linear. Such non-linearity dramatically reduces the accuracy of curve fitting and increases the calculation required

for a fitting. A sample of the temperature curve measured compared with calculated curve by Levenberg-Marquardt method is shown in Figure 4.15.

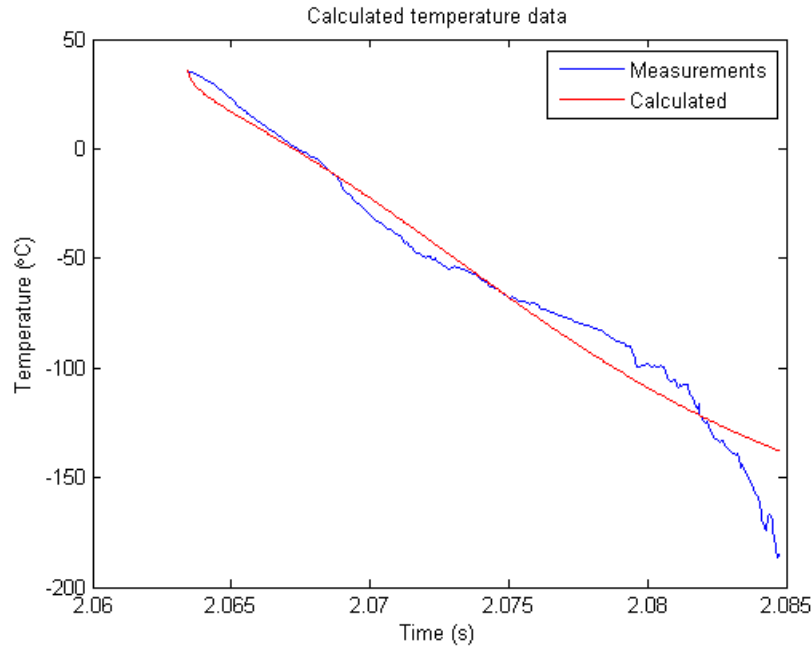


Figure 4.15: A sample of measured and calculated temperature curve with Levenberg-Marquardt method, TC on flat workpiece, direct LN flow, driving pressure $P = 68.9\text{kPa}$.

The calculation speed is another issue here. It typically takes two hours to complete a set of experiment data by least square method. Also, for the same reason mentioned above that a proper fitting condition is difficult to meet here, it is also caused by the extremely high sampling rate involved in this study, and the algorithm needs to be carried out on an exceptionally large data set.

Facing these two difficulties here, an algorithm based on function estimation could dramatically reduce the amount of data and improve the processing speed is required. To be specific, the proposed algorithm does not require pre-defined function form, and should reduce the processing power required by effectively reducing the amount of data

without limiting the system high bandwidth/fast response. This leads to the following oversampling method.

Oversampling method for noise suppression

Apart from the least square methods commonly used, additional consideration about the instability of solutions for inverse heat transfer problems leads the analysis of errors in the temperature measurements and corresponding calculation.

Now, consider the measurements are presented in an additive error form, that is,

$$H_i = M_i + \epsilon_i = (T_i + E_i) + \epsilon_i \quad (4.21)$$

where, at time $t = t_i$, M_i indicates the true response of the temperature measurement system, which is composed by the true temperature T_i and time-constant error E_i ; and ϵ_i is the random error.

In physical sense, the time constant error in the current system may be caused by inaccurate composition of the thermocouple, inaccurate gain of the amplifier circuits, thermal and electrical induced signal drifting, etc. The time-constant error is based on a reasonable assumption that the errors from the above mentioned sources are non-periodic, and is small compared to the nominal signal, and is either constant or monotone. The random error may be caused by the EMI noise, thermal noise of the measurement circuits, power supply ripple, etc. Hereby it is assumed that, the time-constant error E_i consists of a portion, which is proportional to the true temperature, and a constant error, as described in Equation (4.22).

$$T_i + E_i = (1 + e)T_i + e_c \quad (4.22)$$

where, e is a constant ratio between the varying time-constant error and true temperature; and e_c is the constant error.

Revisit the Equation (4.20), the random measurements error is what got magnified by the solution and creates the instability of results. Then, by following the Equation (4.2) to suppress the magnified error, possible solutions are listed as follows:

- 1) Reducing the distance, x : Placing the sensor location as close as possible to the temperature calculation location. This will reduce the error exponentially.
- 2) Reducing the amplitude of oscillations, ϵ : Refining the measurement system and developing signal post-processing techniques to reduce noise. This will reduce the error linearly.

In practice, the location where the thermocouple has been placed would be the closest possible location to the surface. Thus, the distance x has been fixed, and it should be treated as a constant in the current problem.

The amplitude of error is usually considered as a constant if the measurements are taken only once at an instant. As stated in the assumptions that the random error follows a normal distribution, and have a zero mean. Thus, if increasing the number of a repetitive measurements from N times to $N \times M$ times, according to the Bienaymé formula for standard error of means, the standard errors of the two measurement sets are:

$$SE_N = \sqrt{M} \cdot SE_{N \cdot M} \quad (4.23)$$

The factor M is named oversampling factor here. In electrical sense, if more repetitive measurements are taken by M times, the overall power of error will be reduced by M times, which corresponding to a reduced voltage error of square root of M times. This is

the fundamental concept of oversampling for noise reduction in signal processing. Additional benefits provided by oversampling include high initial system bandwidth for anti-aliasing/noise filtering and higher system resolution. The prior is discussed in Section 4.1.1. The latter is of less importance here, as the resolution of the DAQ unit is well beyond being sufficient for the purpose of study here and the system resolution is limited by the accuracy and stability of the thermocouple, thus its effects are ignored.

Providing the opportunity to apply oversampling process is the reason why an extraordinarily high sampling rate of 2MHz is used. In practice, the following cumulative moving average processing is carried out to the measured temperature data:

$$Y'_j = \frac{1}{M} \sum_{i=j \times M+1}^{i \times (M+1)} Y_i \quad (4.24)$$

$$t'_j = \frac{1}{M} \sum_{i=j \times M+1}^{i \times (M+1)} t_i \quad (4.25)$$

$$i = 1, 2, 3, \dots, N; j = 0, 2, 3, \dots, N/M-1 \text{ (rounded)}$$

This is very similar to applying moving average filtering. It does not only complete the oversampling/down-sampling processing for noise reduction, but also limits the frequency of signals by a factor of M , which equals a low pass filtering effect. It does not change the true temperature and time-constant error in Equation (4.22).

By applying Fast Fourier Transform (FFT) to a section of idle data after zero drift compensation, we have the random noise spectrum of the system as shown in Figure 4.16. Disregarding the few spikes, the system idle noise can be assumed as an ideal white noise, which has a uniform power density throughout its spectrum. Another reason is that, the white noise assumption makes the following discussion more general and applicable to other problems.

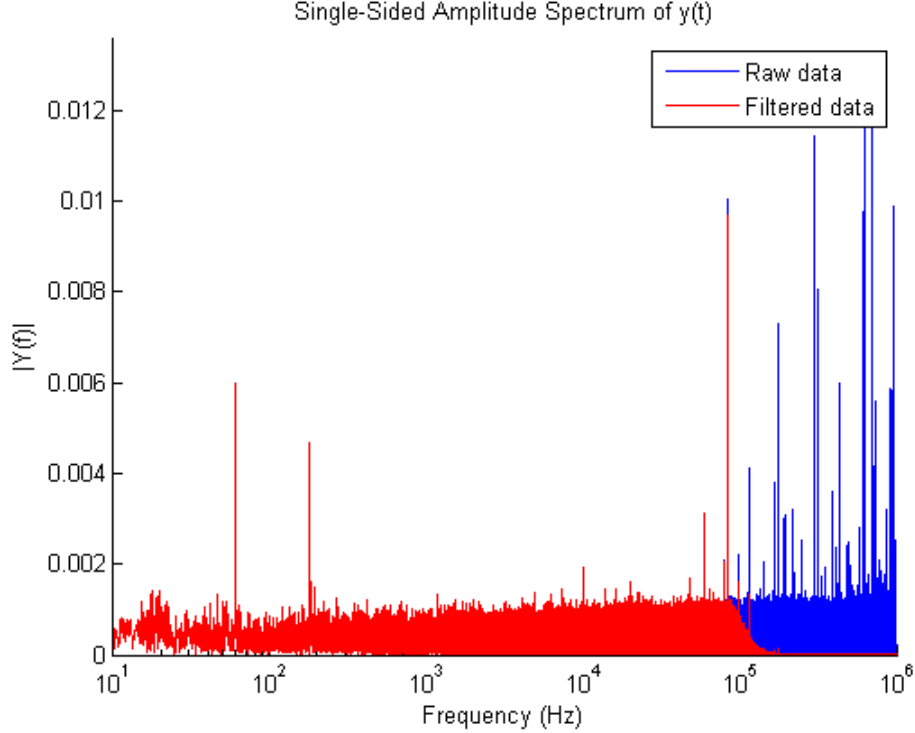


Figure 4.16: Noise spectrum of system idle output.

Considering the down-sampling process at a factor of M described in Equations (4.24) and (4.25), effective noise amplitude is enlarged more at higher frequency, and is given by Equation (4.26) (Mancini, 2013):

$$NV'_{rms} = \sqrt{\int_1^{\frac{BW}{M}} \frac{(N_0)^2}{M} df} = \frac{N_0}{\sqrt{M}} \cdot \sqrt{\left(\frac{BW}{M} - 1\right)} \approx \frac{N_0 \cdot \sqrt{BW}}{M} = \frac{NV_{rms}}{M} \quad (4.26)$$

where, NV'_{rms} is the effective noise amplitude considering the low pass filtering effect, in μV ; BW is the system bandwidth in Hz; N_0 is the noise density, in $\mu\text{V}/(\text{Hz})^{1/2}$; and f is the frequency in Hz. The Equation (4.26) above presents the damping effect of calculation stability for ideal white noise of a given noise density N_0 , when a down-sampling process at a factor of M is applied. Note that original measurement set is unchanged when $M = 1$. However, the approximation in Equation (4.26) is valid only when $BW/M \gg 1$, which indicates that the fundamental idea of this method is only valid when a large bandwidth is

provided by a very high sampling rate, and the oversampling factor is relatively small compare to the bandwidth. Given that the system bandwidth is 1MHz at the 2MHz sampling rate, the oversampling factor M should not be larger than 10^5 in any case to maintain the noise damping capability of the method.

In general, compared to a normal fast sampling with a low pass filter, oversampling method has a benefit of lowering the effective random error at a factor of M at the cost of M times more sampling effort at a same bandwidth.

Down-sampling also increases the temperature differences between each step. The average temperature difference per step is increased by a factor of M , although the temperature differences between each two consecutive steps are not assured. It can be concluded that the average signal to noise ratio (SNR) is thus improved by a factor of M^2 .

The maximum original average temperature difference between steps is approximately $T_{step} = 0.005^\circ\text{C}/\text{step}$. The amplitude of the idle random noise, NV_{rms} , is calculated as 0.60 mVrms at the gain of 100 times. And, the system bandwidth, BW , is 1MHz under the sampling rate of 2MHz. Thus, the noise density, N_0 , under the white noise assumption is thus given by:

$$N_0 = \frac{NV_{rms}}{Gain \cdot \sqrt{BW}} = 6.0 \times 10^{-3} \mu\text{V}/\sqrt{\text{Hz}} \quad (4.27)$$

Based on the 0.20mV RMS noise amplitude, the original signal which has gone through the Butterworth low pass filtering has a random error with peak to peak amplitude of 1.32 mV (99.9% trust region). This corresponds to a maximum temperature fluctuation of $T_{noise} = 0.49^\circ\text{C}$ around -190°C temperature range, where the thermocouple has a low

sensitivity around $27\mu\text{V}/^\circ\text{C}$. Thus, it is within expectation that original data sets ($M = 1$) show significant instability with the algorithm, as the solutions' uniqueness is not assured. To have stable results, we would expect the temperature difference between steps must be much larger than the temperature fluctuation caused by noise, which is $T_{step} \gg T_{noise}$. If assuming a requirement of $T_{step} \geq n \cdot T_{noise}$, it can be easily calculated, and the value of M needed be larger than 54 for $n = 10$ for the current system. Actual minimum value of factor M may be different due to local variance of T_{step} . In practice, stable results can be achieved with $M \geq 50$, and $M \geq 100$ is used in the signal processing. At this time, the effective sampling rate is 20 kHz, which is far more than is sufficient to record the temperature changes we have as stated. The high speed temperature measurement system can accept a maximum value of $M = 1307$ without sacrificing the bandwidth and time resolution, assuming ten times the system bandwidth is needed for sufficient time resolution. In the cases of slower cooling, as stated above, the SNR is improved by a factor of M^2 , and the system bandwidth is only reduced by a factor of M . Thus it is always desirable to increase the value of M to fulfil the requirement of $T_{step} \gg T_{noise}$, before the signal's Nyquist sampling rate is reached. In general, as long as the system is capable of capturing the fastest temperature change after the over-sampling process, it will always be valid for slower temperature change with the same amplitude of noise.

It can be concluded that the method is valid for a large temperature gradient problem only when the distance between surface and sensor location x is sufficiently small and the measurement system is sufficiently fast and accurate. If a larger x is involved, error will be magnified according to Equation (4.20). If the measurement system is not fast enough, the bandwidth of the system will be insufficient after the cumulative moving average

processing. If the static noise of the measurement system is significant, it would require even more intense noise canceling process, which is sometimes not practical.

A linear search algorithm is carried out, based on the finite difference method with an implicit scheme to find the surface heat transfer coefficient at each time instant t'_j . The flow chart for this procedure is shown in Figure 4.17. The details of the algorithm can be found in APPENDIX C. It should be noted that the algorithm is corresponding the surface heat transfer coefficient h_j with the surface temperature $T_{0,j}$, and the thermocouple (TC) measured temperature is $T_{1,j}$, at each time instant.

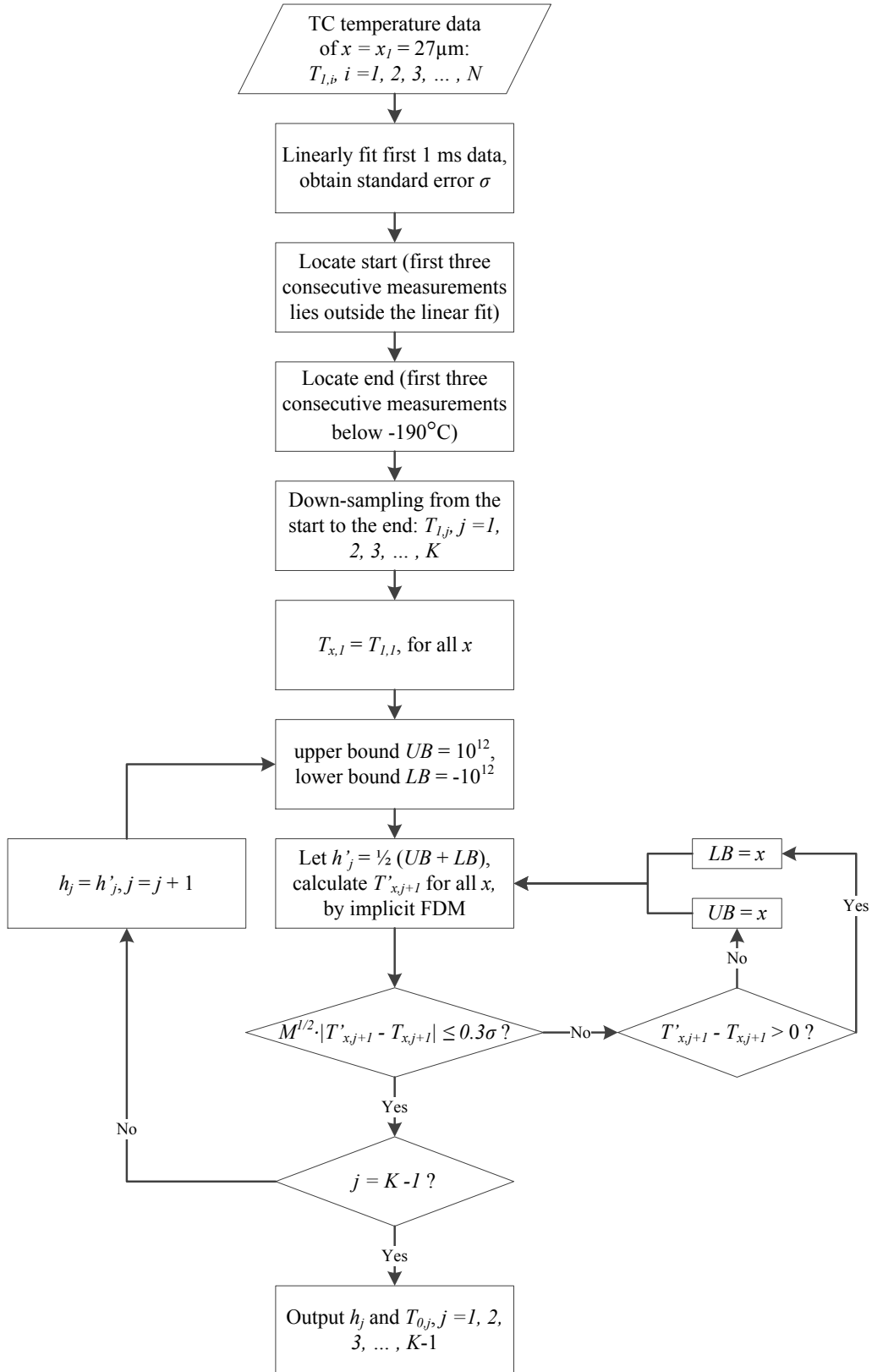


Figure 4.17: Flow chart for the inverse heat transfer solution by oversampling approach.

The surface heat transfer coefficient is thus numerically solved according to the measurements of temperature, as shown in Figure 4.18.

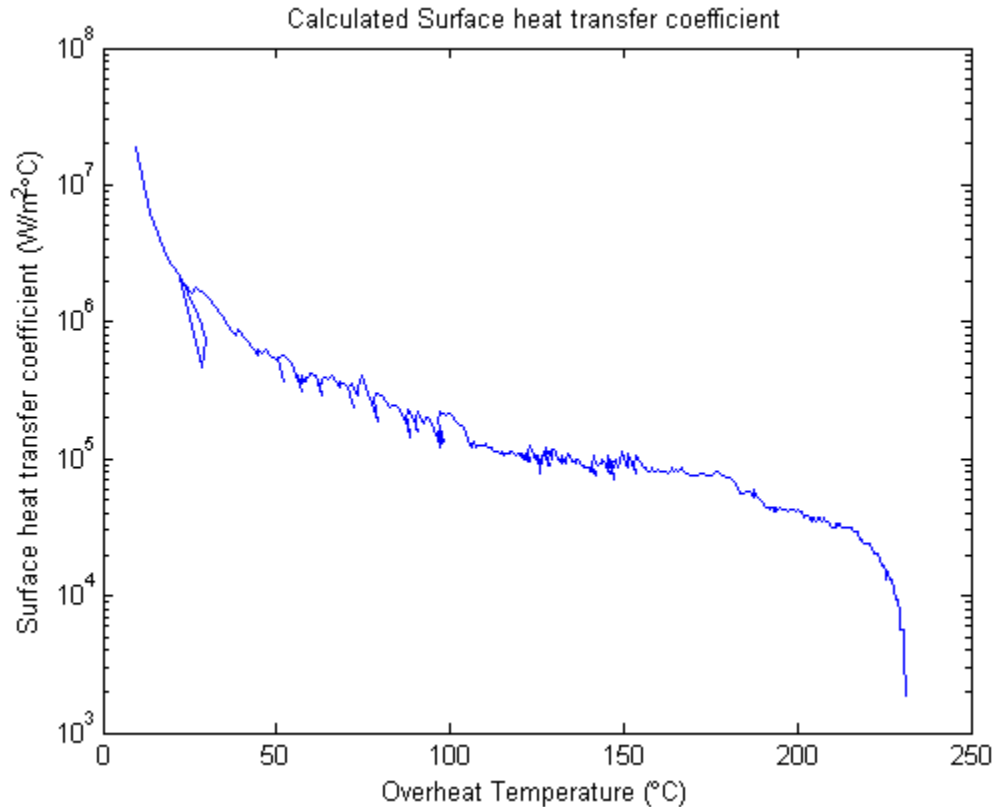


Figure 4.18: A sample of calculated surface heat transfer coefficient curve, for the data presented in Figure 4.15.

Calibrate natural convection heat transfer coefficient

The value for natural convection surface heat transfer coefficient is typically $h_{air} = 5$ to $20\text{W/m}^2\text{°C}$. In the current practice, there is no way to guarantee static air condition. Thus, the natural convection heat transfer coefficient needs to be calibrated.

This is done by experiment, where the test specimen is heated up then cooled by natural convection with air. Then, by applying the IHTP solving methods above assuming that the top and bottom surface has a same heat transfer coefficient, the average values of four

repeated tests are determined as $h_{air} = 32\text{W}/(\text{°Cm}^2)$. The value is higher than the commonly used value, and varies from $h_{air} = 25\text{W}/(\text{°Cm}^2)$ to $h_{air} = 43\text{W}/(\text{°Cm}^2)$ among the three trials. The coolant introduces air flows around the specimen, so it would be reasonable to use either the average value or the higher value as the references for the other IHTP problems. When the surface heat transfer coefficient on the coolant exposure side is high, the natural convection heat transfer coefficient has a relatively minor influence on the results. On the other hand, when the surface heat transfer coefficient on the test side is comparable to that of natural convection cooling, having a reasonable estimation of the natural convection surface heat transfer coefficient would help to improve the accuracy of the heat transfer model.

Summary of heat transfer modelling with over-sampling method

The over-sampling method proposed is in general a signal processing method. Combined with the high speed low noise temperature measurement system developed, it is a different modelling approach for inverse heat transfer problems compared with conventional methods. Table 4.4 summarizes the comparison between the typical conventional method used for solving IHTP and the current approach.

Table 4.4: Comparison between typical conventional method and current approach for solving IHTP.

	Typical conventional method	High speed measurement with over-sampling approach
Fundamental assumption	Noise is too large to solve the problem directly; need to estimate	Actively reduce noise until the problem can be solved directly
Measurement noise	Generally not important	Need to have low noise measurement to start with
Measurement speed	Prefer low but sufficient sampling rate	Prefer highest possible sampling for more headroom of processing
Solving algorithm	Complex optimization algorithm, often slow	Simple and fast

Typical conventional methods utilize estimation algorithm to solve the problem with high noise in the temperature measurement and a noise amplification effect in IHTP. The approach proposed here focuses on eliminating random noise in the experimental front end and signal processing, and it enables the use of simple solving method which otherwise would not be capable of solving IHTP. The simple algorithm is built upon the cost of precision experimental front-end and large amount of data recorded. On the other hand, the low noise data from the over-sampling process can be processed by other IHTP solution methods, although the benefit of low noise might not be taken into effect.

Also, just like other function estimation methods, the remaining noise in the data will reflect onto the surface heat transfer coefficient curves established. It should be noted that the over-sampling approach inherently combines filtering and noise suppression. Thus, when applying the over-sampling method, it can be subjective to decide if a higher over-sampling factor M should be used for a smoother curve or a lower M should be used to represent the transient behavior of the curve. On the other hand, building a smooth

analytical function based on a noisy curve is beyond the purpose of study here. Nevertheless, it could be easier to deal with a small set of surface heat transfer data generated by the proposed approach, knowing that the most troublesome noise amplification effect in IHTP has been dealt with, rather than a large set of raw temperature data not even processed with IHTP solution.

The most obvious limitation of the current approach is its dependence on low noise data. For a smooth process in preliminary tests, it is not a problem. But, when the stability of the liquid nitrogen flow is not guaranteed, the approach here would only be able to extract the smooth region of the temperature curve measured, and the resulting surface heat transfer coefficient calculation is limited to a smaller temperature range.

4.2.2 Surface heat transfer coefficient at various locations and driving pressure

With the modeling method proposed in Section 4.2.1, the results from the static cooling experiments described in Section 4.1.2 can be processed. The surface heat transfer coefficients of various locations on the specimen surface, which are stated in Section 4.1.2, can be calculated to present the heat transfer mechanism of the liquid nitrogen flow on the machine surface in cryogenic machining.

There is a good repeatability between several (typically, three to four times) trials under each condition. Thus, without specific note, the following results presented in this section are the single representing cases for each condition.

According to the location of the thermocouple, four different patterns are identified in general. To be specific, Groove 0 mentioned in Section 4.1.2 and Figure 4.9, is called the separation point. Grooves 1 and 2, where the thermocouple lies in the congested space

between upper block and lower block, are called the congested locations. Groove 3, where the groove is just at the opening of the conical space between the upper block and lower block, is called the transition location. Grooves 4 through 6, where the thermocouple sits on top of the lower block with an open exposure to the incoming liquid nitrogen flow, are called open locations.

Open locations

Grooves 4 though 6 lie on top of the open surface of the lower block, as described in Section 4.1.2 and Figure 4.9. In the case of machining, they are on the workpiece machined surface with open exposure to the liquid nitrogen flow. The typical temperature curve measured and modeled is shown in Figure 4.19.

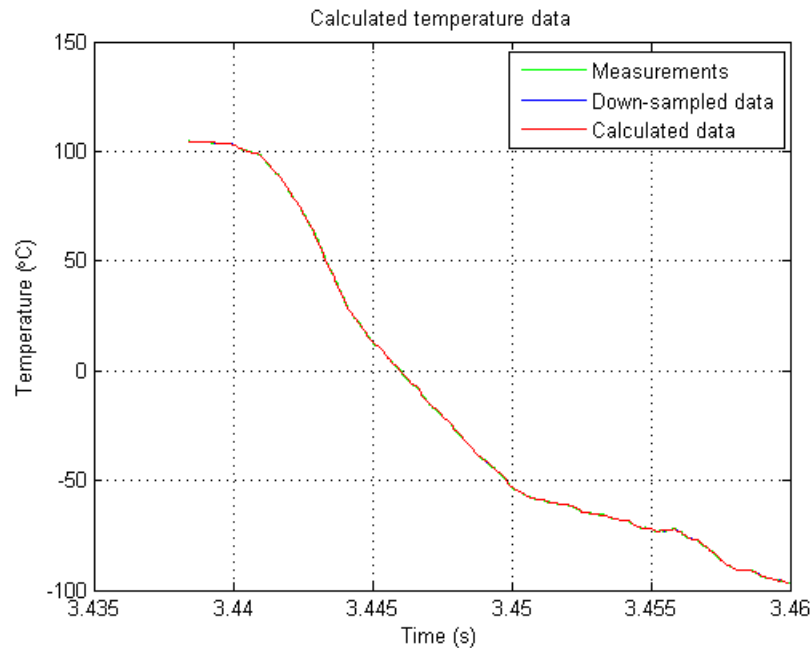


Figure 4.19: A comparison of the temperature curves measured and modelled at a open location, Groove 4, $P = 51.7\text{kPa}$.

It can be seen that the down-sampled data and calculated data follow the original measurement so well that they overlap with each other in the figure.

For the different driving pressure P , the calculated surface heat transfer coefficient is summarized in Figure 4.20.

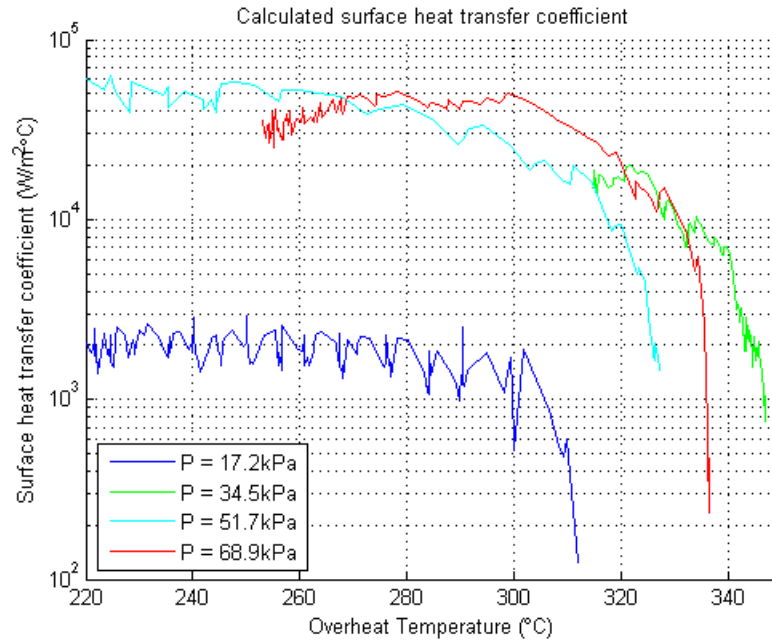


Figure 4.20: Surface heat transfer coefficient at the open locations (Grooves 4 though 6).

An obvious outlier is identified as the case of drive pressure, $P = 17.2 \text{ kPa}$, for the situation with the lowest flow rate. To confirm this, the condition with $P = 17.2 \text{ kPa}$ has been repeated for seven times, and they showed same results. The result of this condition is shown in Figure 4.21.

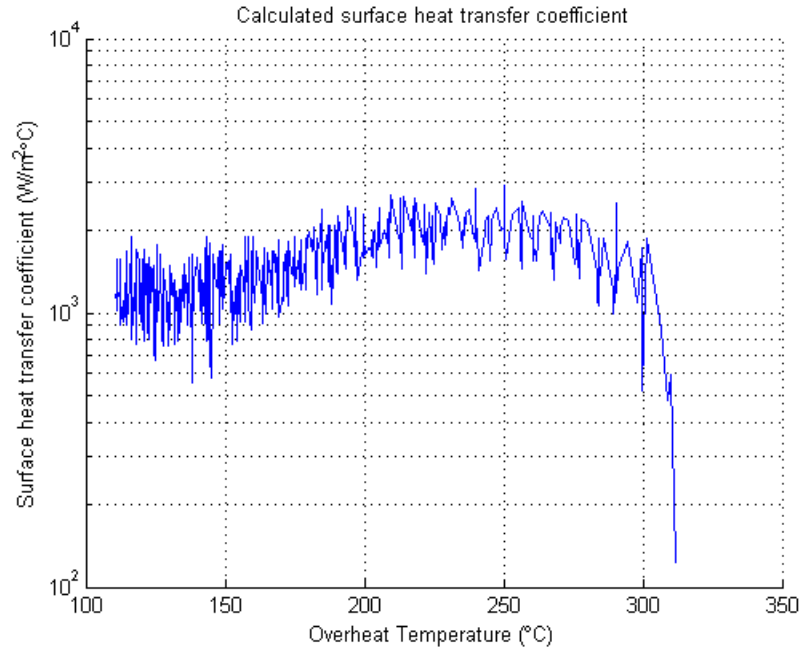


Figure 4.21: The surface heat transfer coefficient curve at the open locations, with a driving pressure $P = 17.2\text{kPa}$.

Throughout the whole temperature range, the surface heat transfer coefficient remains almost constant. The value of $10^3\text{W}/(\text{°Cm}^2)$ to $2 \times 10^3\text{W}/(\text{°Cm}^2)$ is comparable to that of forced convection heat transfer. This is the proof that there were no, or only very limited level of boiling heat transfer occurs in this case.

The liquid nitrogen flow after entering the delivery pipeline will evaporate in gaseous form. Though the shortest possible tubing has been used, it could not prevent the flow from being a two phase flow. Room temperature air heats the tubing surface with a natural convection heat transfer. Thus, the amount of heat absorbed by the tubing and the liquid nitrogen flow inside is generally a constant value over time. Thus, with a liquid nitrogen supply at a higher flow rate, a constant volume of the LN flow will be evaporated, and thus a less portion of gaseous form will be delivered. It could be understood that due to the small flow rate at the driving pressure $P = 17.2\text{kPa}$, there is a

very limited amount of liquid phase nitrogen existing in the flow. This results in a comparatively very low surface transfer coefficient in this case.

The cooling behavior with higher driving pressure at the open locations is dramatically different from that of a convective cooling. The most concerned overheating temperature range would be 220°C to 320°C, corresponding to the overheat temperature value at room temperature and work zone temperature of *AZ31B* machining (Pu, 2012), respectively. The surface heat transfer coefficients go beyond $5 \times 10^4 \text{ W}/(\text{°Cm}^2)$, and that is more than one order of magnitude higher than typical convection cooling. But, the differences between the three cases with a driving pressure above 34.7kPa are not too obvious, considering the instability of the process and the amplitude of noise in the curve. Further increasing the flow rate does not increase the heat transfer coefficient once the driving pressure of 34.7kPa is reached and boiling heat transfer takes place.

Most importantly, it should be emphasized that the surface heat transfer coefficient is not a single constant value for boiling heat transfer. In the high overheat temperature region, the boiling mechanism will always be film boiling, and the surface heat transfer coefficient would not be very high. This does not mean the surface heat transfer coefficient can be as low as $10^3 \text{ W}/(\text{°Cm}^2)$. The low values shown in most experiments are initial contact of the flow on the surface, while the flow front is only nitrogen vapor and cooled air, and there was no boiling heat transfer. The situation can be seen from the time domain curve shown in Figure 4.22.

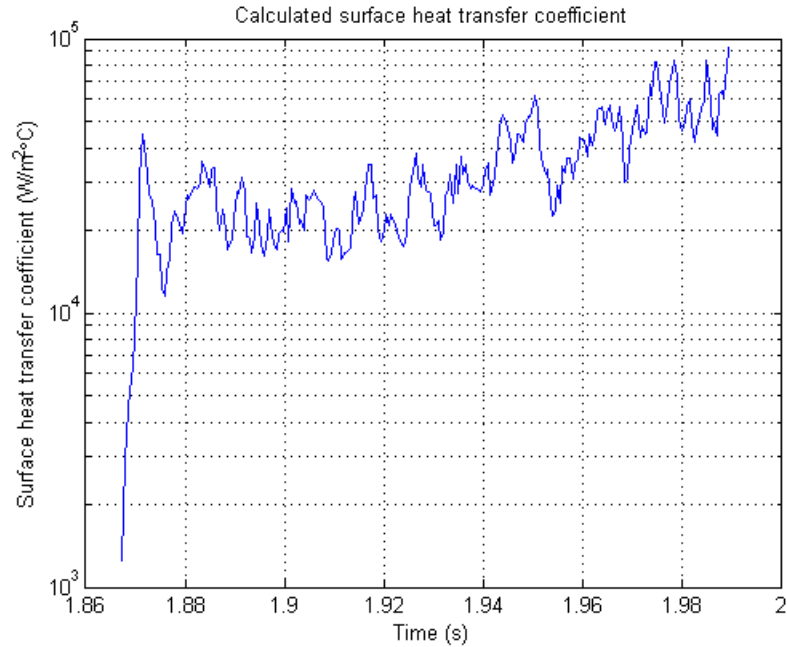


Figure 4.22: A calculated surface heat transfer coefficient curve in the time domain, at Groove 1, $P = 68.9\text{kPa}$.

It can be seen that it takes a very short time until the value of surface heat transfer coefficient to reach $10^4\text{W}/(\text{°Cm}^2)$. Thus, it would be reasonable to consider that during the most concerned temperature range for the machining of *AZ31B* magnesium alloy, the effective value of surface heat transfer coefficient at the congested region lies in the range between $10^4\text{W}/(\text{°Cm}^2)$ to $3 \times 10^4\text{W}/(\text{°Cm}^2)$.

Also, the general trend is that the value of surface heat transfer coefficient will be generally lower at a higher overheat temperature, and higher at a lower overheat temperature. This can be seen in a full temperature range surface heat transfer coefficient curve shown in Figure 4.23.

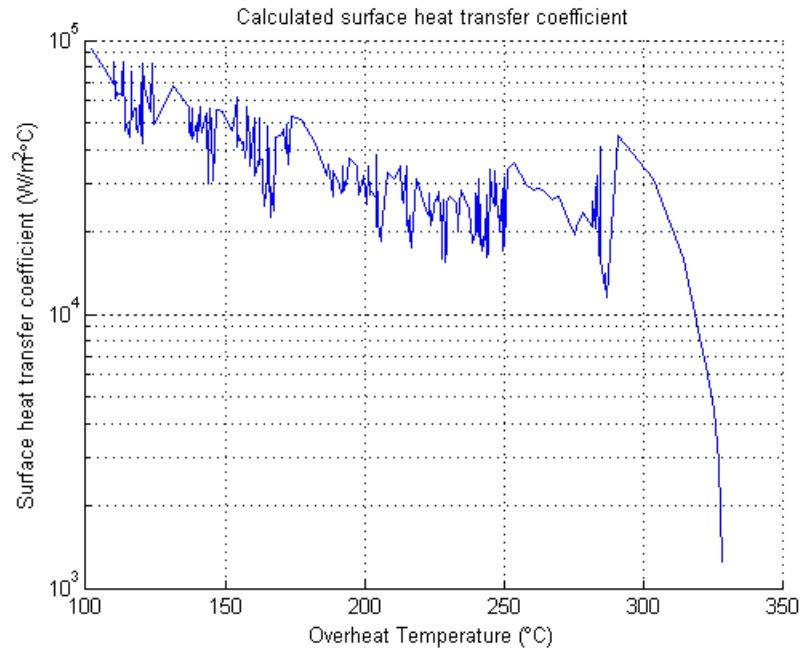


Figure 4.23: A calculated surface heat transfer coefficient curve in the full temperature range, at Groove 1, $P = 68.9\text{kPa}$.

The value of the calculated surface heat transfer coefficient begins to rise further from $3 \times 10^4 \text{W}/(\text{°Cm}^2)$ to $10^5 \text{W}/(\text{°Cm}^2)$ around the overheat temperature of 150°C . This is most likely due to the transition from film boiling heat transfer to transition boiling heat transfer. While the vapor film is no longer continuous, unstable bubbles enable the direct contact between coolant flow and the surface of the specimen. However, due to the unstable nature of transition boiling, the transition threshold of overheat temperature and corresponding value of the surface heat transfer coefficient are found to be inconsistent among experiments.

On the other hand, the value of surface heat transfer coefficient could reach or even go beyond the value of $10^5 \text{W}/(\text{°Cm}^2)$, while the overheat temperature is low and the cooling mechanism goes deeper into the transition boiling region. This reveals the potential of a better flow control to encourage transition boiling heat transfer, which could further

improve the heat flux to a great extent. Potential solutions would be either laminar flow jet or a much higher flow rate for vapor boundary penetration (Chen and Tseng, 1992), which is not available in the current case. Unfortunately, with the current experimental setup, the transition boiling could happen only at a very low temperature, which does not help cool the high temperature workpiece in a machining process.

There were no critical surface heat transfer coefficient or critical heat flux identified, and the overheat temperature range considered never goes below 20°C. Therefore, nucleate boiling heat transfer is not in the range of consideration.

Congested locations

Grooves 1 and 2 lie inside the conical opening formed by the upper block and the lower block, as described in Section 4.1.2 and Figure 4.9. In the case of machining, they are inside the congested region between the tool flank surface and the workpiece machined surface. The typical measured temperature curve is shown in Figure 4.24.

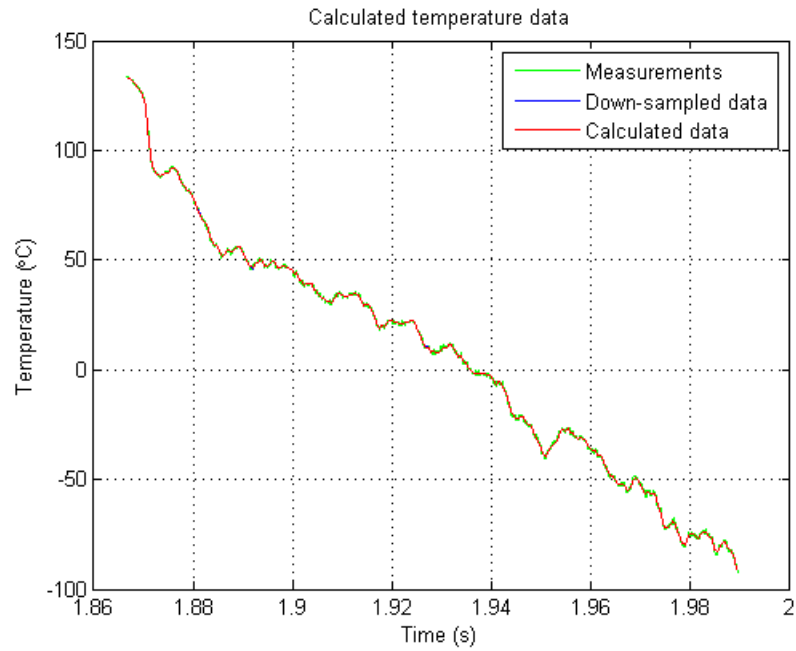


Figure 4.24: A comparison of the temperature curves measured and modelled at a congested location, Groove 1, $P = 68.9\text{kPa}$.

For the different driving pressure, the calculated surface heat transfer coefficient is summarized in Figure 4.25.

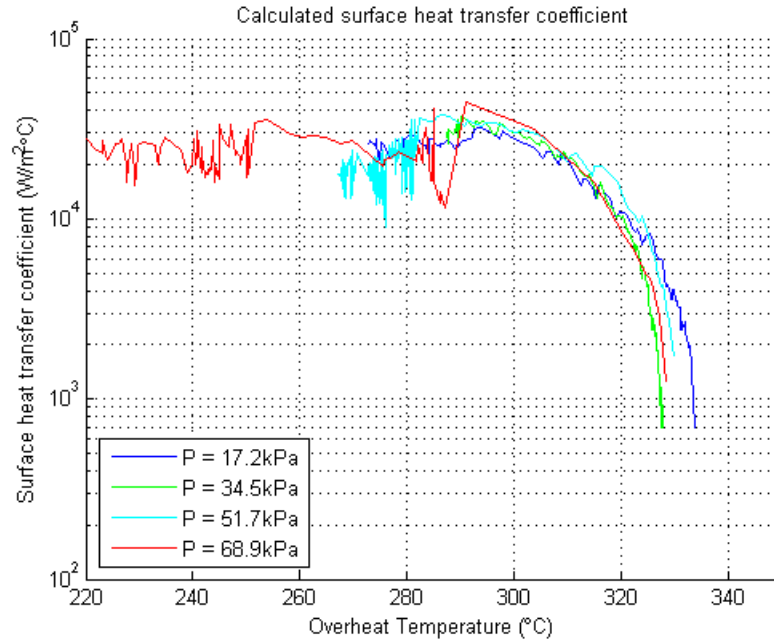


Figure 4.25: Surface heat transfer coefficient at the congested locations.

There is no clear difference among the values of surface heat transfer coefficient for different flow rates. Compared with the cases for open locations, it could be summarized that due to the congested geometry of the cone region formed by the upper block and lower block, the limited amount of liquid phase nitrogen in even the lowest flow rate situation is able to activate boiling heat transfer. Once the boiling heat transfer is activated, there is no obvious improvement by further increasing the flow rate, as seen in Figure 4.20 and Figure 4.25.

Transition point

Groove 3, as described in Section 4.1.2 and Figure 4.9, is the groove just at the opening of the conical space between the upper block and lower block. It is named as a transition point due to its transition pattern of surface heat transfer coefficient. The typical temperature curve measured modeled is shown in Figure 4.26.

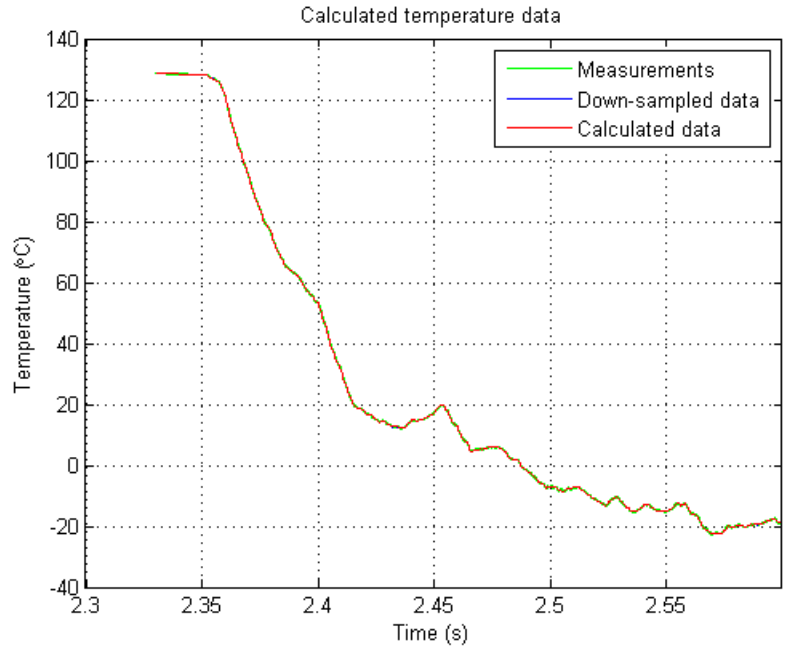


Figure 4.26: A temperature curve measured and modelled for the transition location, Groove 3, $P = 51.7\text{kPa}$.

For different driving pressures, the calculated surface heat transfer coefficient is summarized in Figure 4.27.

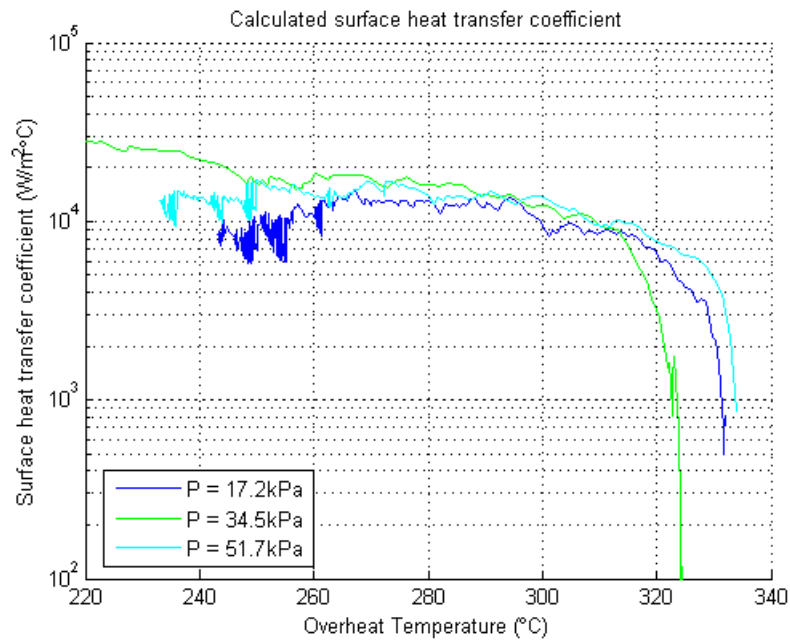


Figure 4.27: Surface heat transfer coefficient at the transition location.

At the transition location, the surface heat transfer coefficient of the condition with a driving pressure of 17.2kPa shows a similar pattern as the boiling heat transfer. However, the value is generally half to two thirds of those with higher flow rates. This indicates that transition from the cases of open locations to the cases of congested locations, giving the current location lies between the two groups.

The surface heat transfer coefficient obtained at the transition point is constantly lower than other locations at the same driving pressure. This may be caused by the irregular flow pattern near the cone opening, and needs further study.

Again, further increasing the flow rate does not increase the value of the surface heat transfer coefficient at Groove 3.

Separation point

The first location is Groove 0, as described in Section 4.1.2 and Figure 4.9. It is where the upper block and lower block separate from each other. In the case of machining, it is the separation point of the insert flank surface and the machined surface on the workpiece. The typical measured and modeled temperature curve is presented in Figure 4.28.

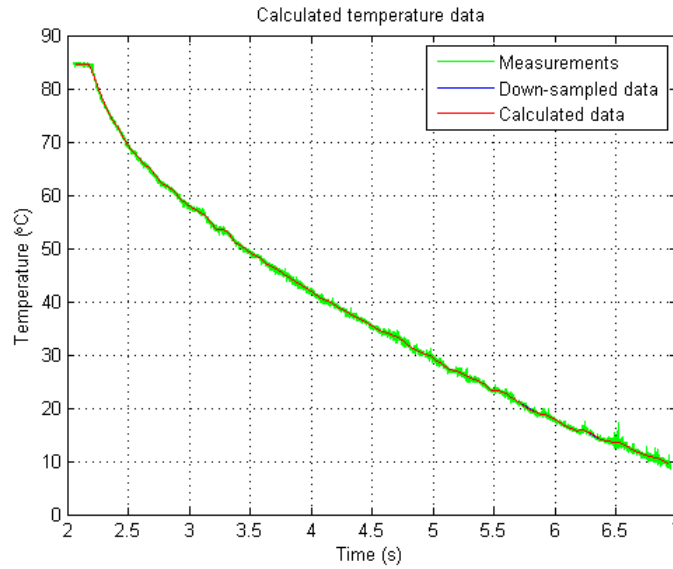


Figure 4.28: A temperature curve measured and modelled at the separation point, at Groove 0, $P = 34.5\text{kPa}$.

For different driving pressures, the surface heat transfer coefficient curves calculated from the experimental data are summarized in Figure 4.29.

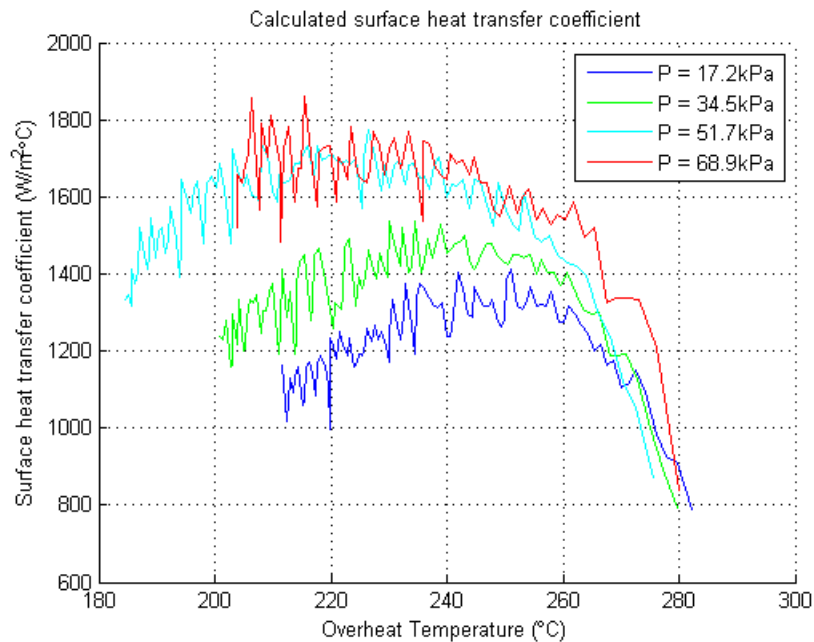


Figure 4.29: Surface heat transfer coefficient at the separation point, Groove 0.

The temperature drop at the separation point is slow compared to the other locations. The calculated values of the surface heat transfer coefficient, h , have a generally linear relationship with the driving pressure. The values lie in the range of 1000 to 1700 W/(°Cm²). This is comparable to the values of h by applying air blast and normal flood cooling. It is a proof that there were no boiling heat transfer at the separation point. In other words, there is no liquid phase nitrogen reaches the specimen surface at this location.

It has been found that in the cases of boiling, bubble entrapment tends to happen at the bottom of a cone shaped opening (Bankoff, 1958; Griffith and Wallis, 1960; Hsu, 1962). It is summarized that in the case of boiling, a small angle of opening would lead to bubble entrapment which is difficult to remove. Thus, the surrounding liquid would not be able to reach the tip of the conical region.

In the current case, although liquid nitrogen has a low viscosity thus, a better wettability, the angle of opening between the upper and lower block is small, and the system is using a relatively low pressure/low flow speed. As a result, the liquid nitrogen flow is not able to penetrate into the tip of the cone opening.

This explains the trend we see in this case. Instead of boiling heat transfer, at the separation point, the dominant heat transfer mechanism is convection heat transfer from vaporized liquid nitrogen flow. In the case of simple forced convection heat transfer, the surface heat transfer coefficient is proportional to the coolant flow speed.

A further discussion point on this is the lubricating effect of liquid nitrogen in the case of machining. Although fundamental studies prove that liquid nitrogen has a lubricating effect for mechanical friction (Hong, 2006; Hong et al., 2001; Hong et al., 2002; Jun,

2005), the existence of liquid nitrogen at the tool-workpiece joint is questionable. In such studies, the liquid nitrogen is applied either as a coolant pool or a flow stream towards non-heated joint. Considering that in machining processes, the workpiece surface is hot after separation from the tool flank surface, a pool cooling scenario or a steady-state cooling scenario may have difficulties proving the lubricating effect of liquid nitrogen in machining.

It is considered not important to identifying the size of the bubble by adding further test locations between Groove 0 and Groove 1. As Groove 1, which is only 2mm away from the separation point, has been proven to have boiling heat transfer, we could assume the entrapped bubble reaches 1mm. Further effort will not change this value more than 1mm, either towards the tip of the cone, or towards the opening. This is negligible comparing to the total size of 20mm for the cooling region.

4.3 Summary

In this section, a comprehensive approach is presented to determine the heat transfer mechanism of cryogenic machining with a flank side liquid nitrogen delivery. This helps to understand the cooling rate and its contributing factors for cryogenic machining.

The proposed method is based on a high speed temperature measurement system and over-sampling process. It deals with inverse heat transfer problem of a transient heat transfer process by reducing the random noise to a very low level, when the problem can be solved directly. The solution of IHTP is based on implicit finite difference method and a simple linear search algorithm.

For the experimental part, a set of static cooling experiments are carried out. The major variables under consideration are driving pressure/flow rate and location on the specimen surface.

By applying the proposed heat transfer modeling approach to the results of the experiments, a series of heat transfer coefficient curves are established. Boiling heat transfer pattern can be recognized and distinguished from convection heat transfer. Also, the change from film boiling to transition boiling can be identified. It is found that with the lowest liquid nitrogen flow rate, it is marginal to achieve boiling heat transfer. However, further increasing the flow rate within the range tested has no obvious benefit in improving the heat transfer speed.

From these findings shown above, the following guidelines could be established for applying cryogenic machining:

- 1) The surface heat transfer coefficient should not be taken as a constant value for boiling heat transfer
- 2) When boiling heat transfer is achieved, the value of surface heat transfer coefficient is much higher than that of convection heat transfer.
- 3) With boiling heat transfer, in the concerned temperature range of cryogenic machining, the value of surface heat transfer coefficient is lower at high temperature, and higher at low temperature, due to the effect of film boiling.
- 4) It would be beneficial, in terms of increasing the value of surface heat transfer coefficient, if transition boiling could be achieved. Nucleate boiling is difficult to achieve. Vapor film penetration is a critical issue in this regard.

- 5) The fundamental idea is to supply sufficient amount of liquid phase nitrogen to achieve boiling heat transfer.
- 6) Further increase in liquid nitrogen flow rate, within the test range, does not help increase the cooling capability of the cryogenic coolant, when boiling heat transfer has been achieved.

CHAPTER 5

SUSTAINABILITY PERFORMANCE OF CRYOGENIC MACHINING

5.1 Machining Experiments

5.1.1 Orthogonal cutting scenario

A set of experiments, similar to the scenarios set in Section 3.5 is designed, for an orthogonal cutting process. The experimental setup is similar to that in Pu's work (2012) and is shown in Figure 4.5. However, the major variables under consideration are cutting speed and coolant flow rate.

The material used in machining is hard rolled *AZ31B* magnesium alloy sheet. Uncoated carbide tool insert, type TNMG432, Kennametal tool grade K420, is held on a MTFNL2525M22 tool holder, and the tool was mounted on a Haas TL2 CNC lathe. The cutting speed range was from 50m/min to 500m/min, at a constant feed rate of 0.2 mm/rev. The machining parameters are summarized in Table 5.1.

Table 5.1: Machining parameters used in the experiments.

Machining Parameter	Parameter Value	
Process Info	Process type	Orthogonal
	Starting diameter	130mm
	End diameter	80mm
Insert Grade	K420 uncoated carbide	
Tool Geometry	Edge radius (μm)	42.8 \pm 2.8
	Model	TNMG432
	Chip breaker	Yes
Cutting Geometry	Rake angle	-5°
	Clearance angle	5°
Machining Parameters	Cutting speed (m/min)	50, 100, 250, 500
	Feed (mm/rev)	0.2
Coolant Condition	Driving pressure (kPa)	17.2, 34.5, 51.7, 68.9

The same low pressure liquid nitrogen delivery system, discussed previously is used, and the coolant-related parameters are discussed in Section 4.1.2 and is summarized in Table 4.2. The coolant coverage length on the machined surface of the workpiece is estimated as 20mm in all cases.

Other process behavior is set as similar to that described in Section 3.5.1. The capital cost tie-up is based on 20% annual depreciation rate, as summarized in Table 5.2.

Table 5.2: Capital cost tie-up summary.

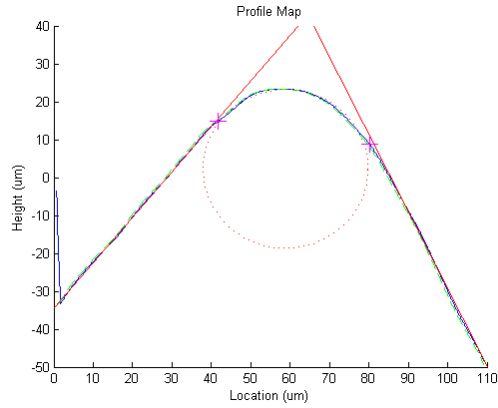
Equipment	Purchase Price	Residual Value	Cost Tie-up
CNC Lathe	\$ 35,000	\$ 22,400	\$ 3.15 / hour
Air Compressor	\$ 500	\$ 320	\$ 0.02 / hour
Liquid Nitrogen Dispenser	\$ 500	\$ 320	\$ 0.02 / hour

5.1.2 Determine the cutting edge radius

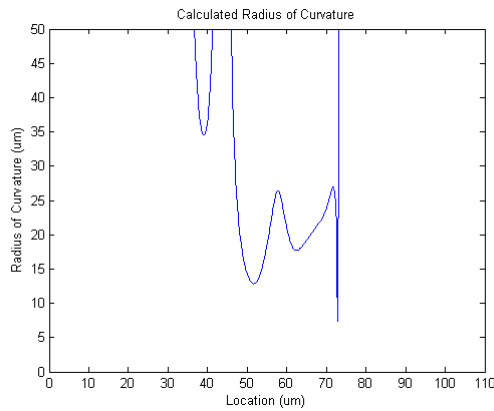
Special attention is given to the edge radius of the cutting tools used in the machining experiments. Determining the roundness/sharpness of a cutting tool with a single parameter is not easy. The cross section of a cutting edge is usually considered as circular, thus the parameter “cutting edge radius” is typically used. There is detailed discussion about defining cutting edge geometries elsewhere (Wyen et al., 2012).

The major challenges of defining the edge radius of a cutting tool lie on two problems. The first is how to determine the curved section of a cutting edge cross section. The second is how to obtain the curvature information of the curved section. Based on some reviews of previous literatures, two customized approaches are considered to calculate the cutting edge radius. The methods are based on profile lines of the cutting edge cross section, captured by a white light interferometer (Zygo® NewView™ 7300).

The first method is based on out-lying points’ recognition and circular fitting of scattered points. The second method is based on local radius of curvature calculation. It is assumed this method can deal with local oscillation better as the radius is graphically presented. An illustration of the two methods for a same cutting edge is shown in Figure 5.1.



(a)



(b)

Figure 5.1: Result output of the two methods for defining cutting edge radius of a cutting tool (a) circle fitting; (b) local profile curvature calculation.

The detailed algorithm can be found in APPENDIX E.

The measurements are done on three independent cutting edges at five locations on each edge. The results suggest that the average cutting edge radius of $42.8 \pm 2.8 \mu\text{m}$. This should be considered as a medium sharpness tool. Compared to the uncut chip thickness (feed rate) of $200 \mu\text{m}$, it could be concluded that the ploughing effect will be limited, and the parameters are valid for a smooth cutting process. And the uncut chip thickness is kept constant, assuming its effect on temperature is minor compared to the cutting speed.

5.1.3 Determine cooling effect

To model the cooling effect of flank-side liquid nitrogen flow on the machined surface, the surface heat transfer coefficient at any location within the coolant coverage and at any given temperature need to be determined. Then, FDM model can be used to determine the temperature profile as a function of the depth beneath the machined surface. The temperature profile when a given surface point exits the coolant coverage is considered the indication to judge the cooling capability.

Global map of the surface heat transfer coefficient

The global response map of the surface heat transfer coefficient is obtained by using a mesh technique based the results discussed in Section 4.2.2. The detail of the meshing algorithm can be found in APPENDIX F.

The results of the meshed global maps are shown in Figure 5.2 to Figure 5.5.

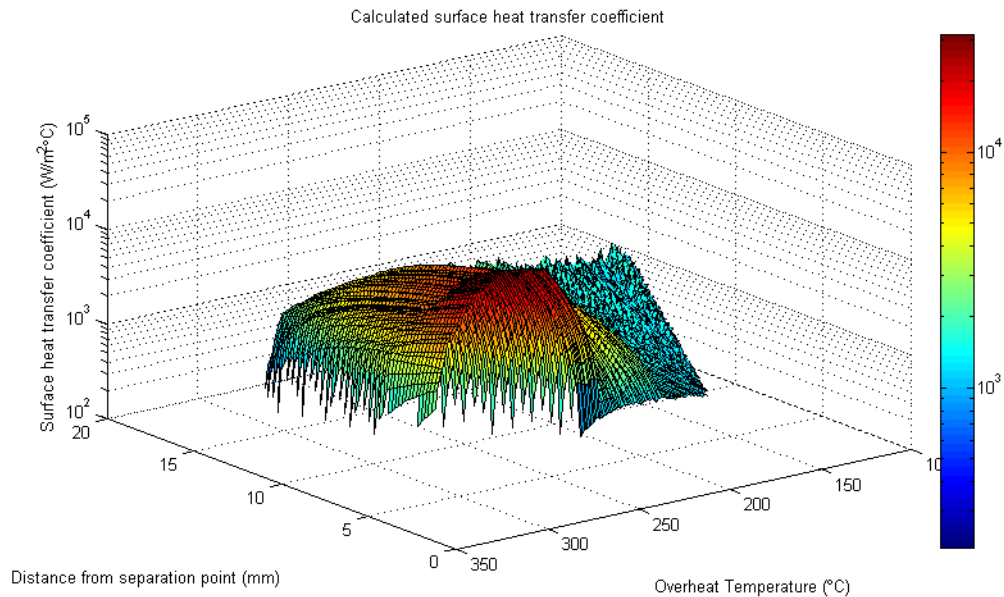


Figure 5.2: Global map of calculated surface heat transfer coefficient at 17.2kPa driving pressure.

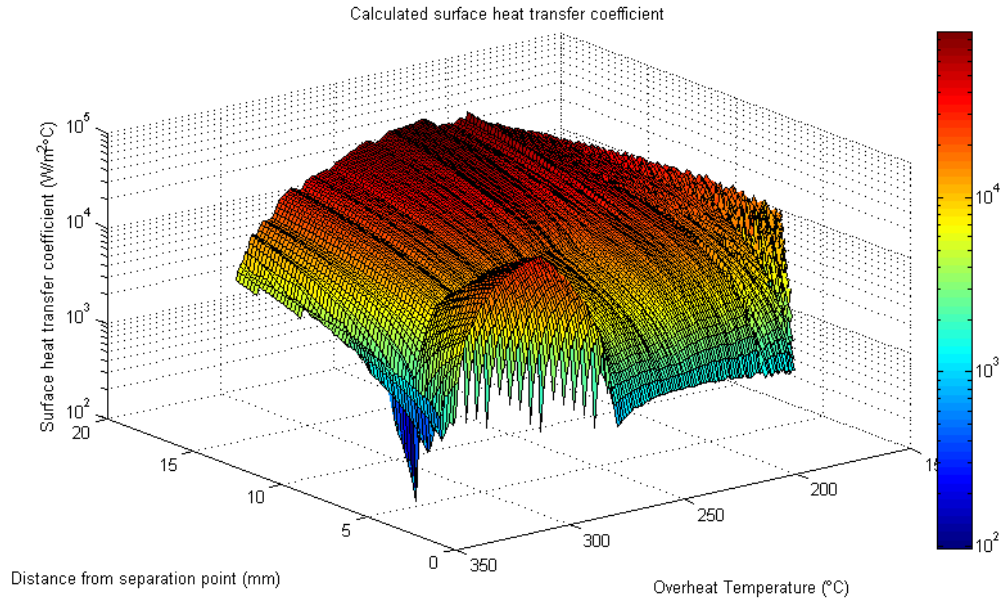


Figure 5.3: Global map of calculated surface heat transfer coefficient at 34.5kPa driving pressure.

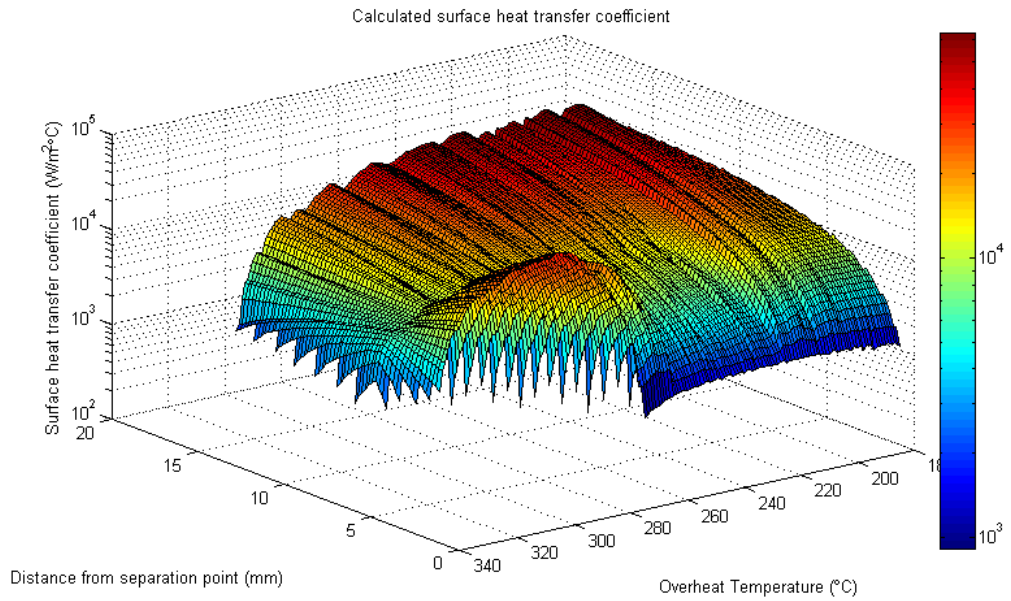


Figure 5.4: Global map of calculated surface heat transfer coefficient at 51.7kPa driving pressure.

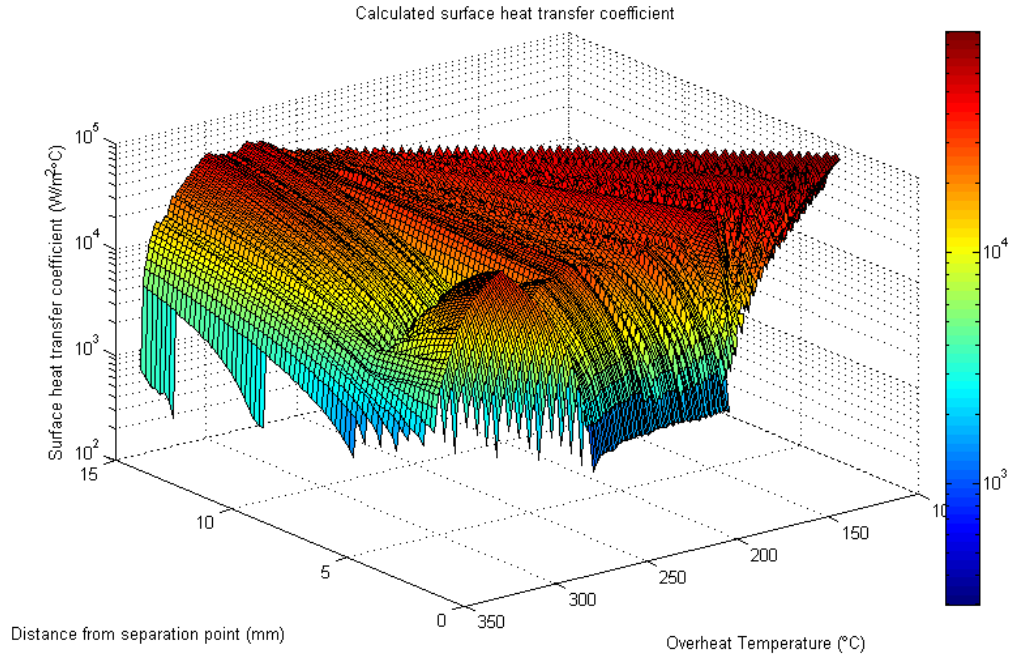


Figure 5.5: Global map of calculated surface heat transfer coefficient at 68.9kPa driving pressure.

The curves describes the surface heat transfer coefficient at various locations and temperature. At the separation point, where the distance is zero, the surface heat transfer coefficient is very small. It rapidly increases with the distance, as in the congested region, boiling is activated. Due to the irregular flow pattern at the transition point, the surface heat transfer coefficient decreases. When it goes into the open locations, the heat transfer coefficient rises again for all cases except the case when the smallest flow rate is applied. For the small flow rate condition, the surface heat transfer coefficient will continue decreasing till the end of the coolant covered region. The mechanism are discussed in detail in Section 4.2.2.

Cooling effect modeling

It is assumed that the whole specimen temperature is 61°C when leaving the separation point, according to the cutting temperature data in literature (Pu, 2012). It was assumed that a uniform temperature in the whole specimen in the current case, and it will give relatively more conservative results than normal machining cases, where only the top layer is heated. Transient heat transfer modeling with implicit FDM schemes is used. The algorithm is mostly the same as that explained in APPENDIX B.

The calculated near surface temperature curves are shown in Figure 5.6 to Figure 5.9, for different driving pressure.

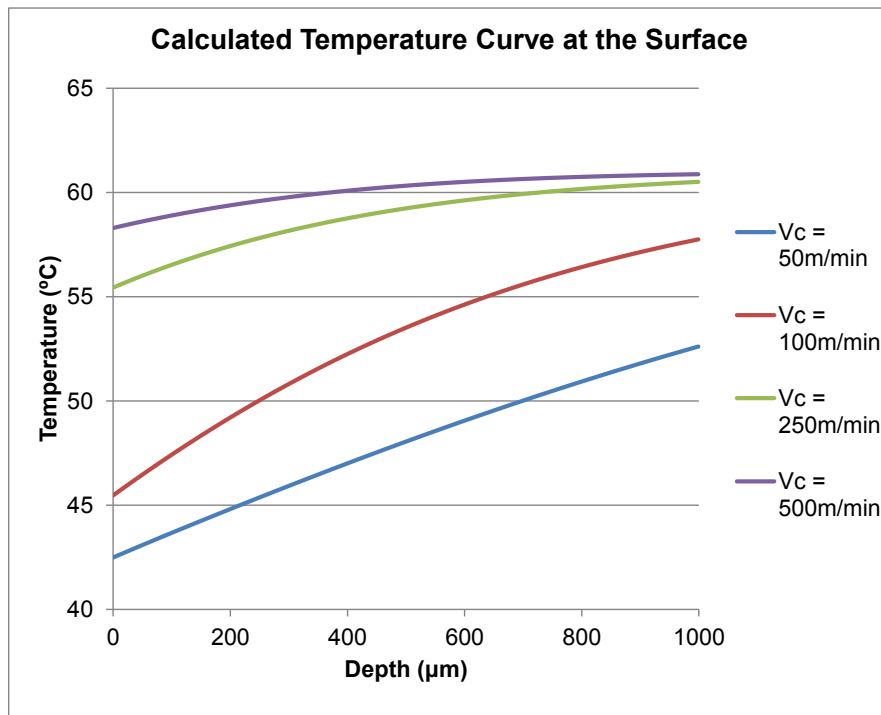


Figure 5.6: Calculated surface temperature profile for driving pressure $P = 17.2\text{kPa}$.

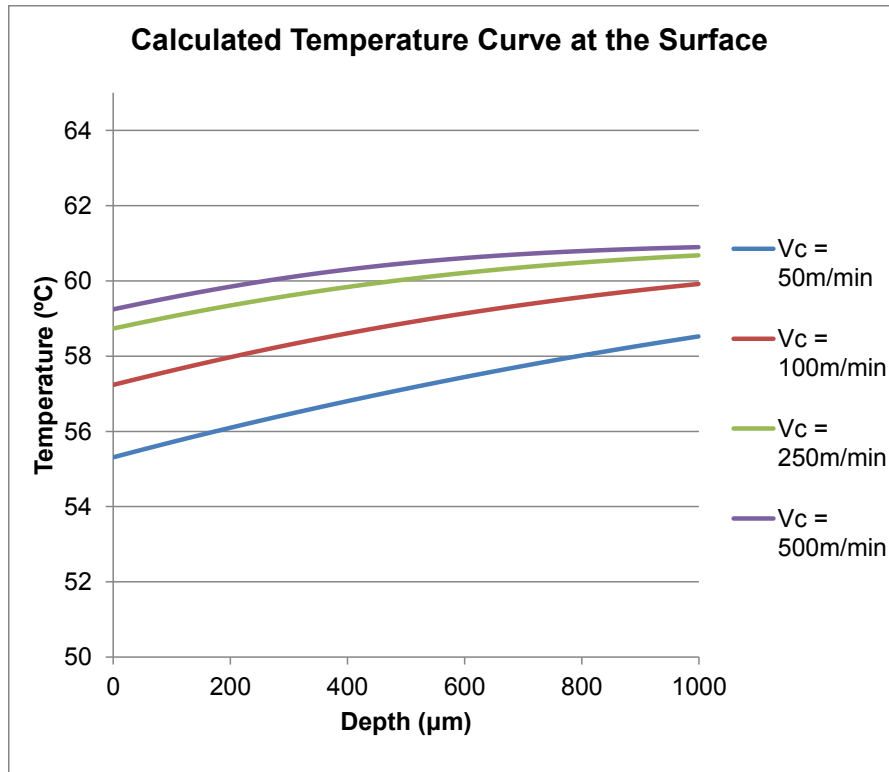


Figure 5.7: Calculated surface temperature profile for driving pressure $P = 35.4\text{kPa}$.

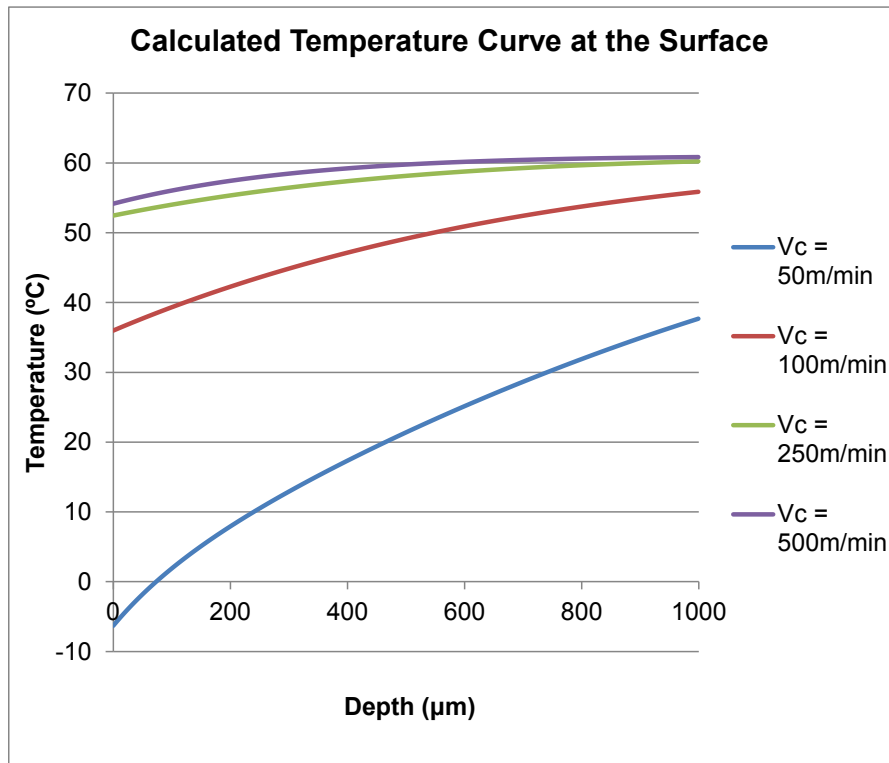


Figure 5.8: Calculated surface temperature profile for driving pressure $P = 51.9\text{kPa}$.

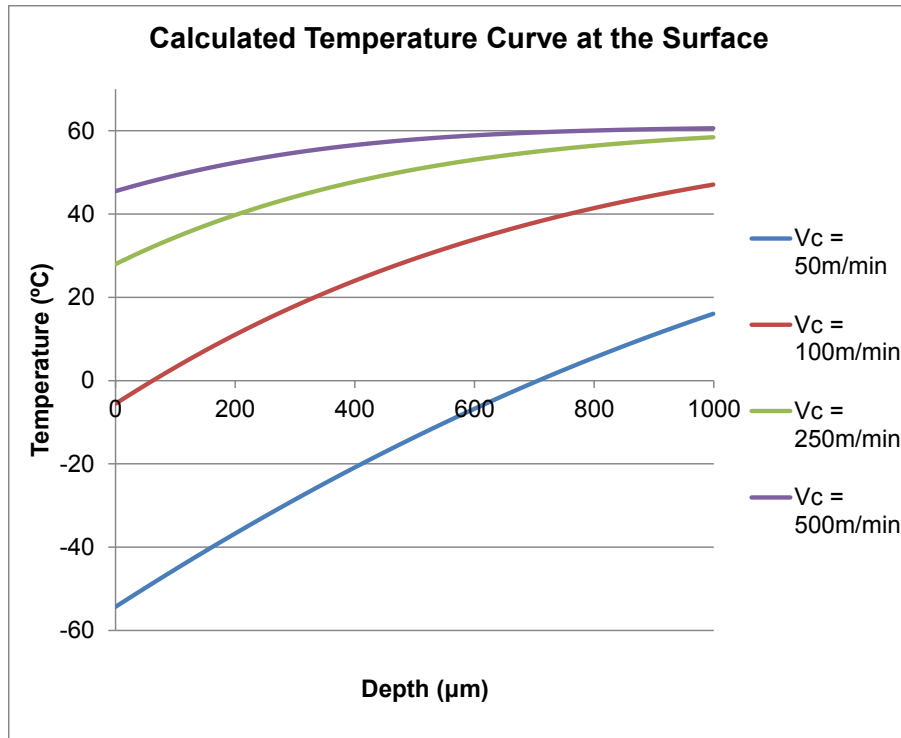


Figure 5.9: Calculated surface temperature profile for driving pressure $P = 68.9\text{kPa}$.

The accuracy of the surface heat transfer coefficient values is significantly influenced by the meshing process, thus the temperature profile calculated could have a significant margin of error. The purpose of this study is to illustrate the impact of cutting speed on the cooling capability of flank-side liquid nitrogen jet.

In the calculations reported above, the coolant coverage length is kept constant. When the cutting speed is increased, the duration of coolant exposure for a given point on the machined surface is proportionally reduced. It is obvious that due to the much shorter exposure time, the cooling effect of liquid nitrogen flow is significantly reduced at higher cutting speed. Combined with the guidelines obtained in Section 4.3, it can be seen that the coolant exposure time is another major influencing factors for the cooling effect of flank-side liquid nitrogen along with the surface heat transfer coefficient.

These points should be combined with the guidelines obtained in Section 4.3. Increasing the coolant coverage area on the machined surface in the cutting speed direction would have a significant impact on the cooling effect in cryogenic machining, while increasing coolant flow rate might only have a minor effect.

5.2 Process Performance

Cutting forces, surface roughness and tool-wear are measured during the experiments.

Chatter is observed during the cutting process at the cutting speed of 50m/min and 100m/min. This influences the cutting force components and the surface roughness measured.

5.2.1 Cutting forces

The dynamometer used has a natural frequency of 500Hz. Thus, as suggested by the manufacturer of the dynamometer, all data acquired by the dynamometer should go through a low pass filter, with a cutting frequency of at most 1000Hz.

Zero drift compensation is applied at first. Then, the cutting force data have gone through a moving average filtering with a window size of 0.01s. After that, a two second period of stable cutting region is picked out for consideration. The mean value of the data in that time range is considered as the value of the cutting forces, while the standard deviation can be calculated for the corresponding data set.

The measured cutting force values are summarized in Figure 5.10 for a range of coolant delivery driving pressure.

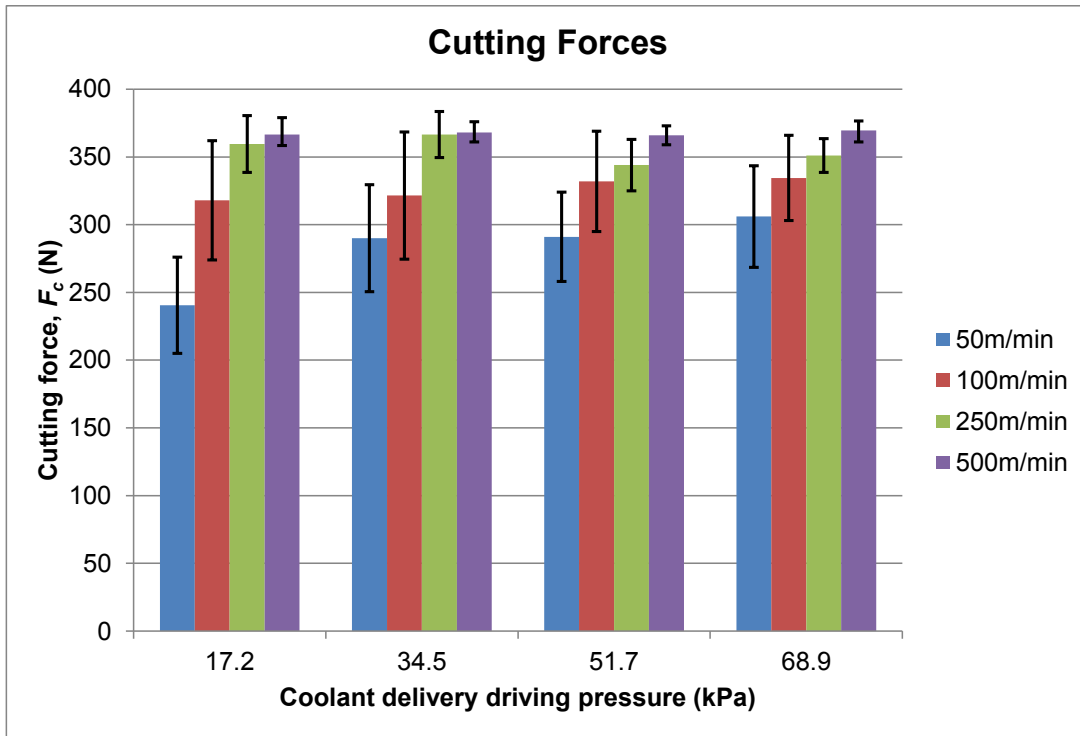


Figure 5.10: Measured cutting forces.

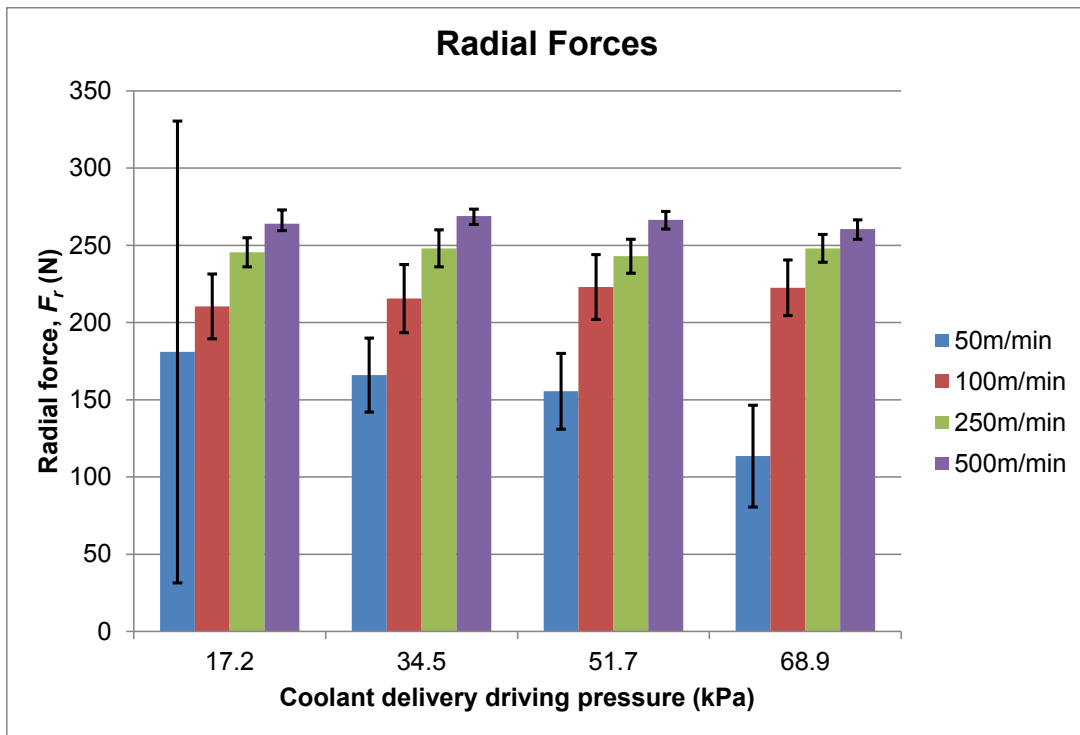


Figure 5.11: Measured radial forces.

It should be noted that the error bar shown here follow the three-sigma rule, which corresponds to 99.73% trust region. However, it is also used to conclude the amplitude of vibration.

The findings in Section 4.2.2 suggest that the flow rate of coolant has a minor effect on the machining performance. This is in general the case here, as most cases do not show any dramatically different behavior at different flow rates.

However, it should be noted that the cooling of workpiece is not only decided by the coolant parameters, but also the duration of time it is exposed to the coolant. At a higher cutting speed with proportionally higher spindle speed, the workpiece exposure time will be proportionally shorter, thus the coolant would have even less effect on the process behavior.

On the other hand, when more cooling effect is expected, the correct solution is to increase the coolant exposure time. This can be achieved by either reducing the cutting speed or increasing the coolant coverage area. As stated in Section 4.2.2, increasing flow rate would not help unless boiling heat transfer has not been triggered due to low flow rate.

To be specific, at the lowest cutting speed of 50m/min, the lowest coolant flow rate at the driving pressure of 17.2kPa has less temperature hardening effect compared to the cases with higher flow rate, as indicated in Section 4.2.2. Thus the cutting force is lower than those cases at higher flow rates. The difference among the cases of sufficient coolant flow is not obvious.

When the cutting speed is increased beyond 100m/min, the shortened coolant exposure time would thus reduce the effect of different coolant behavior. Combined with the findings in Section 4.2.2, this explains the similar cutting forces at higher flow rates and higher cutting speeds.

On the other hand, the influence of cutting speed to the cutting force behavior is within expectation. The cutting forces increase till smooth material shearing is achieved, and further increasing the cutting speed does not significantly increase the cutting force.

Chattering behavior is obvious with the measurement error indication for the cases with low cutting speed of 50m/min and 100m/min. At low cutting speed, chattering is observed and the corresponding vibration casts major variation in the cutting force signal recorded. And, the chattering behavior vanishes at higher cutting speed, and the process turns into stable cutting. Though not observed in the experiments or on the workpiece surface with naked eyes, the force data indicates that there is still a certain amount of vibration at the cutting speed of 250m/min. The cryogenic coolant application does not show an obvious influence on the vibration behavior in this case due to reduced coolant exposure time.

5.2.2 Surface roughness

The measured surface roughness values are summarized in Figure 5.12. The surface roughness measurement is carried out on a white light interferometer (Zygo® NewView™ 7300). Three locations on each sample are used, and five sampling profile lines are considered at each location. Error bars indicate the extreme scenarios.

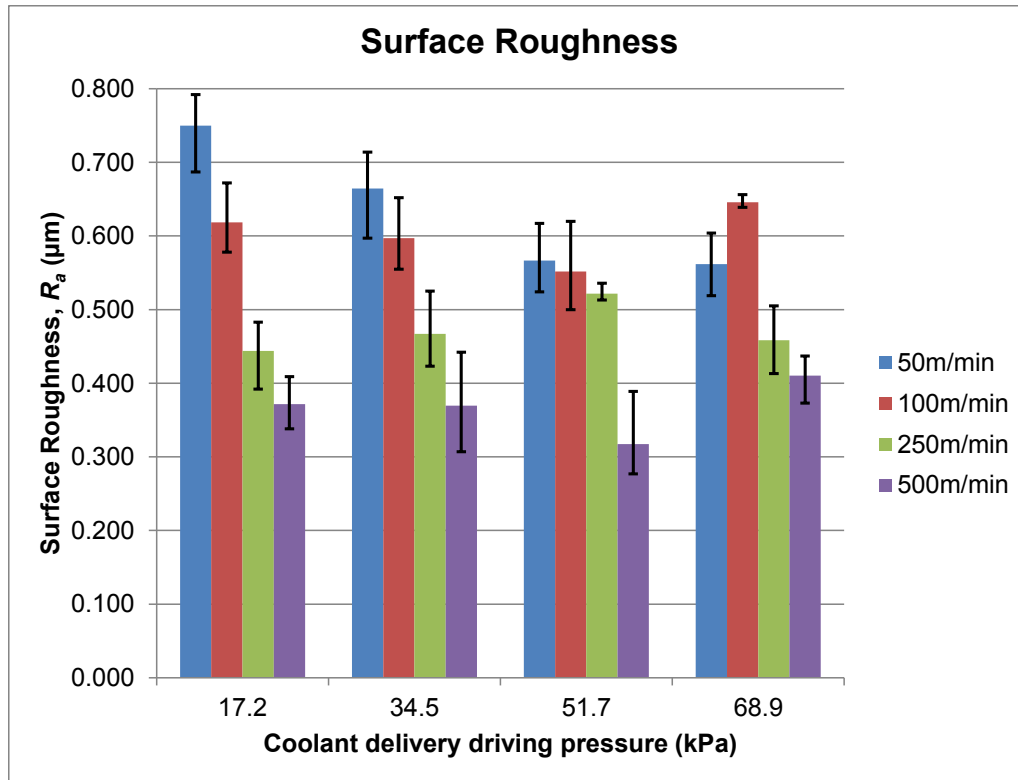


Figure 5.12: Measured surface roughness.

As mentioned in the previous section about cutting forces, chattering happens at the low cutting speeds of 50m/min and 100m/min. This can also be revealed by the high roughness values measured for these cases.

Again, the influence of flow rate for machining with a cutting speed higher than 100m/min is not obvious, due to both the minor difference on cooling performance at different cooling rate, and also the reduced coolant exposure time.

The interesting finding is the reducing trend in surface roughness value at the low cutting speed of 50m/min when increasing the coolant flow rate. In this case, the saturation happens at the driving pressure of 51.7kPa. It should be noticed that the high surface roughness values at this cutting speed are caused by chattering and vibration, which depend both on material properties, system stiffness and the native frequency of the

structure. Instead of stabilizing the material deformation directly, the cooling effect may increase the elastic modulus of the workpiece and the cutting tool, which enhances the rigidity of the system and changes the native frequency. As a result, the vibrating force caused by unstable material deformation remains the same, where segregated chips are always produced at low cutting speeds, a more rigid mechanical structure due to the better cooling helps improving the surface quality of the product. The higher saturation point at 51.7kPa instead of 34.5kPa shown during the thermal analysis in Section 4.2.2 could be understood as a wider splashing of liquid nitrogen flow towards the surrounding part of the workpiece and the cutting tool, which is not considered in the thermal analysis. However, it should be emphasized that the benefit from the higher flow rate stops at the driving pressure of 51.7kPa, and it is only valid at low cutting speeds.

On the other hand, when the cutting speed increases, the cooling effect is reduced due to the reduced coolant exposure time. Thus, the conditions of cutting speed $V_c = 100\text{m/min}$ could not see the benefit of surface quality improvement along with increased coolant flow rate, compared to the cases of $V_c = 50\text{m/min}$.

5.2.3 Tool-wear

Due to the low strength of the material used in these machining experiments, and the relatively short experiment duration, the tool-wear pattern is difficult to identify on the used tool. The method proposed here is to compare the cutting edge radius before and after the cutting process.

Cutting edge radius measurements are carried out on both new and used cutting tools. The three trials give measured worn edge radius values of $44.4\pm 3.0\mu\text{m}$, $46.2\pm 6.0\mu\text{m}$ and $47.4\pm 6.4\mu\text{m}$, respectively. Compared to the measured edge radius value of fresh edges,

which is $42.8 \pm 2.8 \mu\text{m}$, the edge radius increment is overwhelmed by the measurement errors. No valid tool-wear pattern can be extracted from the results, and the tool-wear effect is therefore not considered in this study.

It should be noted that it is a major limitation in this sustainability assessment study of cryogenic machining, as one of its major process performance advantages is established.

5.3 *ProcSI* Evaluation of Cryogenic Machining Process

The procedure of applying *ProcSI* evaluation on an existing machining process has been demonstrated in Section 3.5. Collected data in the current experiments and corresponding analysis are presented here.

As there were no difference in operator safety and personnel health issues identified, the score of the two clusters will be simply set as the full score of 10.

Same approach to estimate scrap rate is used as described in Section 3.5.1. Quality threshold is set as $R_a = 0.75 \mu\text{m}$, with an assigned variance of $\sigma = 0.15$. Unit price of the workpiece is estimated as \$14 per piece according the market value of the material.

There are three cases showing exceptionally high scrap rate, which may influence the effect of normalization. That is because they consume so many resources to fix the scrap parts that the differences of other parameters would have very marginal impact on the results after normalization. In practice, such situation should not be considered as a stable process. Thus, when deciding the best and worst cases in the normalization, these cases are not considered. But their measurement are still normalized in the same way, and if their calculated score is lower than two, a score of two out of ten is given to indicate the inappropriate process parameters.

5.3.1 Manufacturing cost

Similar approach is made as that of Section 3.5.2, with the exception that the tool cost is ignored in this case. However, different flow rates of liquid nitrogen are considered, as described in Section 4.1.2. The data is summarized in Table 5.3. The three worst cases are highlighted with red and the best case is highlighted with green.

Table 5.3: Data summary for manufacturing cost.

Test Number	Cutting speed (m/min)	Driving Pressure (kPa)	Scrap loss (\$)	Capital tie-up (\$)	Labor cost (\$)	Coolant cost (\$)	Energy cost (\$)	Total Cost (\$)	Cost Score
1	50	17.2	7000	95.01	223.38	289.60	1.82	7609.81	2.00
2	50	34.5	2730	75.69	177.96	289.59	1.52	3274.76	2.00
3	50	51.7	224	64.35	151.30	284.70	1.30	725.65	6.01
4	50	68.9	182	64.16	150.85	323.87	1.31	722.20	6.02
5	100	17.2	1092	44.65	104.97	113.51	1.00	1341.98	4.00
6	100	34.5	616	43.24	101.66	138.11	0.97	899.98	5.44
7	100	51.7	112	41.75	98.15	154.19	0.95	407.04	7.05
8	100	68.9	1974	47.26	111.10	199.14	1.08	2332.58	2.00
9	250	17.2	0	28.26	66.45	52.79	0.75	148.25	7.89
10	250	34.5	0	28.26	66.45	66.26	0.75	161.73	7.85
11	250	51.7	28	28.32	66.58	76.77	0.73	200.40	7.72
12	250	68.9	0	28.26	66.45	87.42	0.74	182.87	7.78
13	500	17.2	0	23.88	56.14	35.25	0.68	115.95	8.00
14	500	34.5	0	23.88	56.14	44.25	0.68	124.95	7.97
15	500	51.7	0	23.88	56.14	51.17	0.68	131.86	7.95
16	500	68.9	0	23.88	56.14	58.38	0.68	139.08	7.92

For the cases at low cutting speeds, the poor product quality induced by chattering is the major cost contributor. The high scrap rate behavior leads to further prolonged cutting time, which results in a poor overall manufacturing cost performance.

The processes at higher cutting speeds benefit from both good product quality and the reduced cutting time involved. The reduced cutting time leads to a minimal amount of

liquid nitrogen consumption, which is critical in reducing cost. However, as can be seen in the situation with higher cutting speed, the impact of coolant cost is not significant, even when the potential benefits of better tool-life is not considered here.

The cost composition is summarized in Figure 5.13. Note that the test numbers 1, 5, 9 and 13 are done at a driving pressure of 17.2kPa. The test numbers 2, 6, 10 and 14 are done at a driving pressure of 34.5kPa. The test numbers 3, 7, 11 and 15 are done at a driving pressure of 51.7kPa. The test numbers 4, 8, 12 and 16 are done at a driving pressure of 68.9kPa.

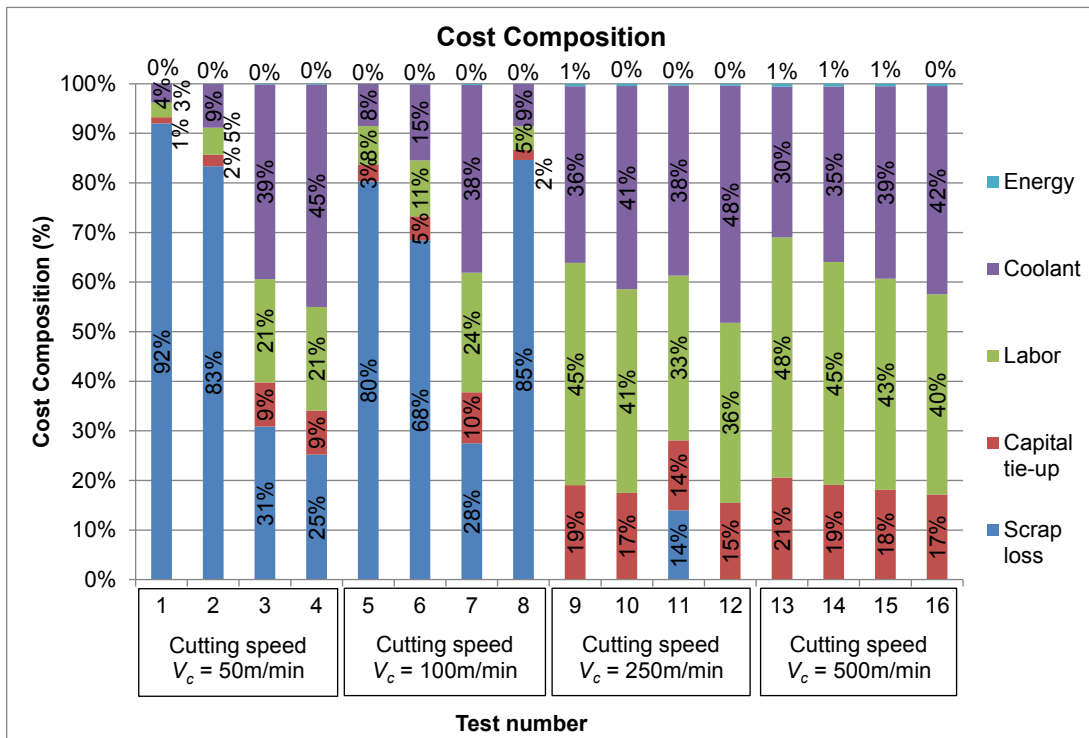


Figure 5.13: Cost composition at varying cutting conditions.

From the cost composition point of view, at lower cutting speeds of 50m/min and 100m/min, the major contributor is the scrap loss. Even under these situations, the long

cutting time requires a significant period of coolant application, which results in a significant amount of coolant consumption and the corresponding high coolant cost.

For the conditions of higher speed, where product quality is no longer a problem here, the coolant cost and labor cost take the major part of the overall cost. It should be noted that it is based on a much reduced total cost. As a certain amount of coolant is wasted during the idling process, the different coolant flow rates have a limited impact on the total consumption of coolant. Thus, the difference of cost at different flow rates is noticeable but relatively not minor.

In all these conditions, the energy cost is a minor part compared to other categories.

5.3.2 Energy consumption

Compared to the approach shown in Section 3.5.2, the power consumption for coolant delivery system is better addressed by counting the flow rate and output pressure of the compressed air source. The data is summarized in Table 5.4. The three worst cases are highlighted with red and the best case is highlighted with green.

Table 5.4: Data summary for energy consumption.

Test Number	Cutting speed (m/min)	Driving Pressure (kPa)	Idle energy (kWh)	Cutting energy (kWh)	Coolant delivery system energy (kWh)	Total energy consumption (kWh)	Energy Score
1	50	17.2	5.96	5.51	11.31	22.77	2.00
2	50	34.5	4.75	5.29	9.01	19.05	2.66
3	50	51.7	4.03	4.52	7.66	16.21	4.09
4	50	68.9	4.02	4.73	7.64	16.39	4.00
5	100	17.2	2.80	5.23	4.43	12.46	5.98
6	100	34.5	2.71	5.13	4.30	12.13	6.15
7	100	51.7	2.62	5.11	4.15	11.88	6.28
8	100	68.9	2.96	5.83	4.70	13.49	5.47
9	250	17.2	1.77	5.49	2.06	9.32	7.57
10	250	34.5	1.77	5.60	2.06	9.43	7.51
11	250	51.7	1.78	5.26	2.07	9.10	7.68
12	250	68.9	1.77	5.36	2.06	9.19	7.63
13	500	17.2	1.50	5.60	1.38	8.47	8.00
14	500	34.5	1.50	5.62	1.38	8.49	7.98
15	500	51.7	1.50	5.59	1.38	8.46	8.00
16	500	68.9	1.50	5.64	1.38	8.52	7.97

The case shown in Section 3.5.2 utilizes a liquid nitrogen delivery system which is self-pressurized. The current system uses an external compressed air source to deliver the liquid nitrogen. This could introduce more energy consumption compared to the previous case, but in fact it saves the consumption of liquid nitrogen used as a power source. However, in the previous study the raw consumption of liquid nitrogen was not comprehensively addressed to include those used for pressurizing the tank.

It should be noted that due the design of the liquid nitrogen system, even if the liquid nitrogen is delivered at different flow rates, most of the compressed air is release from the by-pass valve. Thus, the energy consumption rate of the delivery system remains constant

at different liquid nitrogen driving pressure. Thus, it is a design flaw of the delivery system that most of the energy consumption is wasted.

The energy consumed on actual cutting is lower at lower cutting speeds, even when considering the extra amount of workpieces processed due to higher scrap rate. This is caused by the lower cutting force in these cases. However, the saving of cutting energy at low cutting speed is overwhelmed by the idle power and energy consumption on coolant delivery system. The energy consumption of these two energy streams rely on the total amount of time consumed for all the work and coolant application time, respectively. As a result of the much longer cutting time consumed at low cutting speed, the low cutting speed conditions save energy at the cutting process, but lose more on idling and coolant delivery system. From the other point of view, cutting at higher cutting speeds consumes more in cutting energy itself to save energy consumed in other categories.

The energy compositions for all the conditions are summarized in Figure 5.14.

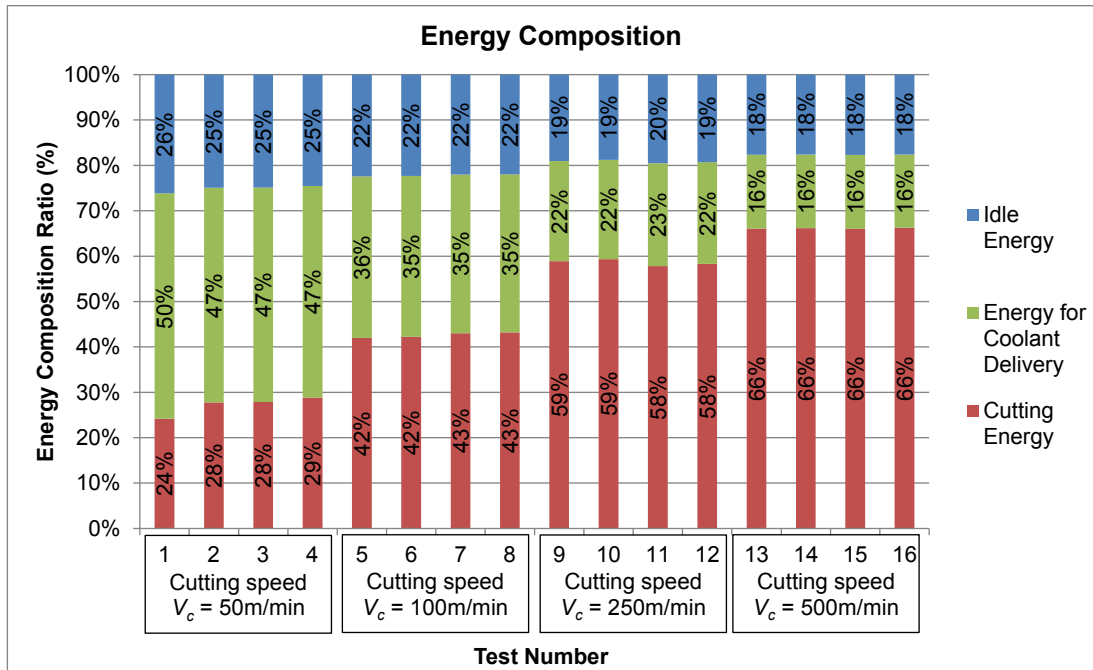


Figure 5.14: Energy composition of the different cutting conditions.

From the energy composition point of view, it is evident that the cutting energy takes higher ratio at higher cutting speeds. The trend is more caused by the reduction of energy consumption in other categories, rather than the increase of cutting energy itself. From this point of view, cutting at higher cutting speeds could be considered as energy efficient for both total energy consumption, and also the effective ratio of energy consumed.

5.3.3 Waste management

The two most common waste streams are the scrap parts and chips produced. The data is summarized in Table 5.5. The three worst cases are highlighted with red and the best cases are highlighted with green.

Table 5.5: Data summary for waste management.

Cutting speed (m/min)	Driving Pressure (kPa)	Total mass of scrap parts (kg)	Total mass of chips (kg)	Waste Score
50	17.2	30.03	65.68	2.00
50	34.5	11.71	52.33	2.00
50	51.7	0.96	44.49	7.17
50	68.9	0.78	44.36	7.32
100	17.2	4.62	47.16	4.00
100	34.5	2.64	45.72	5.71
100	51.7	0.48	44.14	7.58
100	68.9	8.47	49.96	2.00
250	17.2	0.00	43.79	8.00
250	34.5	0.00	43.79	8.00
250	51.7	0.12	43.88	7.90
250	68.9	0.00	43.79	8.00
500	17.2	0.00	43.79	8.00
500	34.5	0.00	43.79	8.00
500	51.7	0.00	43.79	8.00
500	68.9	0.00	43.79	8.00

Due to the waste streams considered here, all conditions that have no scrap parts made will lead to the optimal score given.

On the other hand, it could be seen that there are very few waste streams in the case of cryogenic machining. No residue from the coolant application is one of the major advantages of cryogenic machining.

5.3.4 Environmental impact

The only environmental impact factor that could be addressed here is the CO_2 emission due to the energy consumption. A score of 10 is given to the sub-cluster of Restricted Material. The data is summarized in Table 5.6. The worst case is highlighted with red and the best cases are highlighted with green.

Table 5.6: Data summary for environmental impact.

Cutting speed (m/min)	Driving Pressure (kPa)	CO ₂ (kg)	Environmental Score
50	17.2	20.50	5.39
50	34.5	17.14	6.33
50	51.7	14.59	7.05
50	68.9	14.75	7.00
100	17.2	11.21	7.99
100	34.5	10.92	8.07
100	51.7	10.69	8.14
100	68.9	12.14	7.73
250	17.2	8.39	8.78
250	34.5	8.49	8.76
250	51.7	8.19	8.84
250	68.9	8.27	8.82
500	17.2	7.62	9.00
500	34.5	7.64	8.99
500	51.7	7.62	9.00
500	68.9	7.66	8.99

As only the indirect CO₂ emission due to energy consumption is taken into calculation, the results are directly related to the total energy consumption of the process. Again, it could be seen that cryogenic machining has very limited environmental burden in its application. No restricted material usage or extra waste streams is involved in its application.

5.3.5 ProcSI score results

The scores of the four clusters taken into calculation for different conditions of the process are summarized in Table 5.7. Note that a score of 10 is given to the cluster of personnel health and operator safety, respectively as justified previously. The overall ProcSI score is however calculated by taking the average of all the six clusters.

Table 5.7: Summary of normalized score and the overall *ProcSI* score.

Cutting speed (m/min)	Driving Pressure (kPa)	Cost Score	Energy Score	Waste Score	Environmental Score	<i>ProcSI</i>
50	17.2	2.00	2.00	2.00	5.39	5.232
50	34.5	2.00	2.66	2.00	6.33	5.499
50	51.7	6.01	4.09	7.17	7.05	7.387
50	68.9	6.02	4.00	7.32	7.00	7.391
100	17.2	4.00	5.98	4.00	7.99	6.996
100	34.5	5.44	6.15	5.71	8.07	7.563
100	51.7	7.05	6.28	7.58	8.14	8.175
100	68.9	2.00	5.47	2.00	7.73	6.200
250	17.2	7.89	7.57	8.00	8.78	8.707
250	34.5	7.85	7.51	8.00	8.76	8.686
250	51.7	7.72	7.68	7.90	8.84	8.689
250	68.9	7.78	7.63	8.00	8.82	8.705
500	17.2	8.00	8.00	8.00	9.00	8.832
500	34.5	7.97	7.98	8.00	8.99	8.825
500	51.7	7.95	8.00	8.00	9.00	8.825
500	68.9	7.92	7.97	8.00	8.99	8.814

The best case among all the conditions is the one at the highest cutting speed and lowest liquid nitrogen flow rate. Cutting speed has the most obvious influence on the overall process sustainability performance. In general, all the cases with different flow rates at higher cutting speeds of 250m/min and 500m/min are not much different from each other.

5.4 Summary

A comprehensive process sustainability evaluation based on the Process Sustainability Index (*ProcSI*) method is carried out. The manufacturing cost composition and energy consumption composition are discussed. In general, the conditions where high cutting speed is used give the best overall sustainability performance, due to their excellent performance in product quality and short processing time. Although the influence of

coolant flow rate is not major in this case, a small flow rate is favored against a higher flow rate.

This could be understood, as stated in the Section 4.2 and Section 4.3, that once a sufficient, but small amount of liquid nitrogen is applied, it will give the same cooling performance as higher flow rate. Thus, to achieve a truly sustainable condition, the cryogenic machining should be applied in a similar way as the machining with MQL. When more cooling capacity is needed, the solution is to enlarge the coolant coverage area to increase the coolant exposure time instead of increasing coolant flow rate. Determining the minimal, but sufficient amount of coolant flow rate is a key issue in cryogenic machining applications.

CHAPTER 6

OPTIMIZATION OF CRYOGENIC MACHINING

6.1 Input Variables and Objective Function

A similar approach to that shown in Section 3.5 is applied in this chapter for optimizing the cryogenic machining process. Apart from the objective of getting the highest possible *ProcSI* score, as described in Equation (3.4), the optimization for minimum manufacturing cost and for minimum energy consumption are also presented.

6.1.1 Genetic Algorithm (GA) and its input variables

Genetic algorithm (GA) is a search heuristic that mimics the natural evolution. It starts with a set of data scattered around the parameter range and test out the result response to the parameter changes, by applying mutation, crossover, inheritance, selection, etc. The best set of parameters is determined by a certain number of “generations” of test runs, where local optimal conditions are avoided. The detail of the application of Genetic Algorithm can be found in APPENDIX G.

The input variables are the cutting speed and the driving pressure of the coolant delivery system, as discussed in the experimental work in Section 5.1.1.

6.1.2 Empirical modeling of the process

The relationship between the input variables and the behavior of the process are defined by empirical models built upon experimental data, similar to the approach presented in Section 3.5.4. The input parameters involved here are the cutting speed, V in m/min, and

driving pressure, P in kPa. The actual mass flow rate in g/s is calculated as stated in Section 4.1.2.

Directly related process behavior parameters include the surface roughness, R_a in μm , cutting force, F in N.

The empirical models are 3rd order polynomial functions built using non-linear least square method. These process behavior parameters are used to calculate other process behavior parameters, and ultimately some of the metric measurements. Other process behavior and metric measurements are calculated as stated in Section 5.3.

Surface roughness

The empirical model established for surface roughness is shown in Equation (6.1).

$$R_a = 0.78442 - 1.8688 \times 10^{-3} \times V + 3.9466 \times 10^{-3} \times P - 7.6778 \times 10^{-7} \times V^2 + 3.8533 \times 10^{-5} \times V \times P - 2.8078 \times 10^{-4} \times P^2 + 4.9000 \times 10^{-9} \times V^3 - 5.3021 \times 10^{-8} \times V^2 \times P - 3.0976 \times 10^{-8} \times V \times P^2 + 2.5608 \times 10^{-6} \times P^3 \quad (6.1)$$

The corresponding coefficient of determination R^2 value of the fitting is 0.9264.

Cutting force

The empirical model established for cutting force is shown in Equation (6.2).

$$F = 65.911 + 2.3239 \times V + 7.7495 \times P - 7.1159 \times 10^{-3} \times V^2 - 1.6503 \times 10^{-2} \times V \times P - 0.13870 \times P^2 + 6.9944 \times 10^{-6} \times V^3 + 1.8897 \times 10^{-5} \times V^2 \times P + 4.5970 \times 10^{-5} \times V \times P^2 + 9.3928 \times 10^{-4} \times P^3 \quad (6.2)$$

The corresponding R^2 value of the fitting is 0.9784.

6.1.3 ProcSI score as the objective function

The determination of the optimal conditions can be taken as a constrained optimization problem. The case to optimize for the highest *ProcSI* score can be summarized as follows.

Maximize $ProcSI(V_i, P_i) = \frac{1}{6}(C_{MC} + C_{En} + C_{Env} + C_{Wa} + C_{PH} + C_{OS})$

with respect to $V_i, P_i (i = 1 \dots N)$

subject to

$$V_{min} \leq V_i \leq V_{max}$$

$$P_{min} \leq P_i \leq P_{max} \quad (6.3)$$

The objective function is defined as Equation (6.4).

$$ProcSI(V, Q) = \frac{1}{6}(C_{MC} + C_{En} + C_{Env} + C_{Wa} + C_{PH} + C_{OS}) = \frac{1}{6} \left[C_{MC} + C_{En} + \frac{1}{2}(M_{CO_2} + M_{RME}) + \frac{1}{2}(M_{SP} + M_{Ch}) + C_{PH} + C_{OS} \right] \quad (6.4)$$

While the $F(V, n)$ is the objective function with the cutting speed, V , and the driving pressure, P , as the input variables. C_{Ec} , C_{En} , C_{Env} , C_{Wa} , C_{PH} and C_{OS} are the scores for the clusters of manufacturing cost, energy consumption, environmental impact, waste management, personnel health and operator safety. The methods to generate these scores are shown in Section 5.3. To be specific, the score for the cluster of environmental impact is calculated by averaging the metric level scores for the metrics of CO_2 emission, M_{CO_2} and restricted material emission, M_{RME} . The score for the cluster of waste management is generated by taking the average of the scores for the mass of scrap parts, M_{SP} , and the mass of chips generated, M_{Ch} . Aggregation of scores is carried out with equal weighting applied to each of the cluster.

6.2 Optimization Results

6.2.1 Optimize for minimal manufacturing cost

The target function in this case is set as the minimal manufacturing cost. The result of the population plot is shown in Figure 6.1. The pink dash-dot line indicates the constrained parameter ranges.

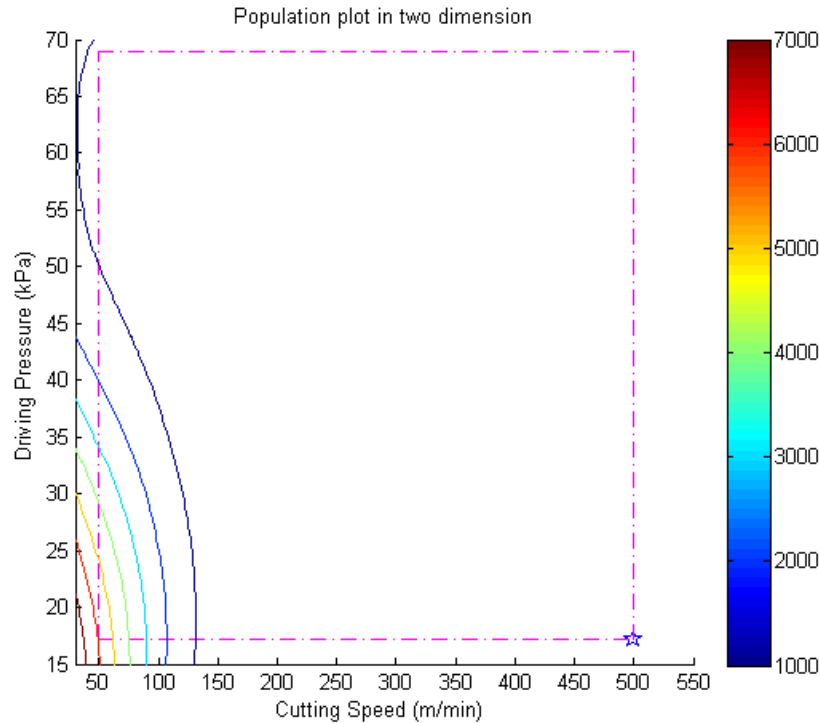


Figure 6.1: Optimization for minimal manufacturing cost, in \$.

The optimal condition determined is at the highest cutting speed, $V_c = 500$ m/min, and the lowest driving pressure, $P = 17.2$ kPa. The best-performing condition in the cluster of cost determined in experiments and the optimal condition identified here are the same conditions, cutting speed, $V_c = 500$ m/min, and the driving pressure, $P = 17.2$ kPa. This conditions is on the edge of valid parameter ranges, thus it suggests potential for further improvement by extending the parameter range.

6.2.2 Optimize for minimal energy consumption

The target function in this case is set as the minimal energy consumption. The result of the population plot is shown in Figure 6.2. The pink dash-dot line indicates the constrained parameter ranges.

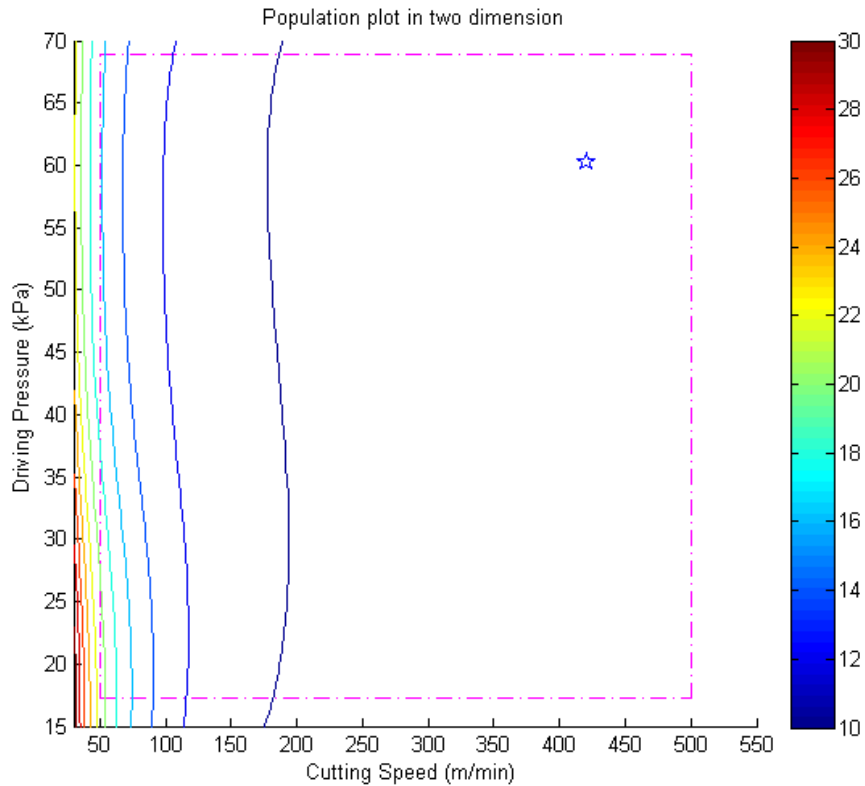


Figure 6.2: Optimization for minimal energy consumption, in kWh.

The optimal condition determined is cutting speed, $V_c = 420$ m/min, and the driving pressure, $P = 60.3$ kPa. The function response curve reveals that the difference at different coolant driving pressures is marginal.

A comparison is given for the best performing experimental condition in the cluster of energy consumption, and the optimal parameters suggested by the GA. The comparison is summarized in Table 6.1.

Table 6.1: Comparison between best experiment scenario and optimization results for the cluster of energy consumption.

Source	Cutting speed (m/min)	Driving Pressure (kPa)	Idle energy (kWh)	Cutting energy (kWh)	Coolant delivery system energy (kWh)	Total energy consumption (kWh)	Energy Score
Experiments	500	51.7	1.50	5.59	1.38	8.46	8.00
GA	420	60.3	1.55	4.99	1.51	8.05	8.21

The optimal condition determined by optimization with GA is superior in energy consumption than the best condition obtained from the experiments. That is due to the reduction in cutting energy by setting the cutting parameters to a more conservative value. Although the overall machining time is increased, the total energy consumption is reduced. Fundamentally, this is caused by the increased cutting forces at higher cutting speed, as mentioned in Section 5.2.1. Limited by the range of experimental parameters, the potential limit of cutting force is not revealed. The comprehensive benefits of high speed machining might not have been involved here (Drossel et al., 2012).

6.2.3 Optimize for highest *ProcSI* score

The target function in this case is set as the lowest energy consumption. The result of the population plot is shown in Figure 6.3. The pink dash-dot line indicates the constrained parameter ranges.

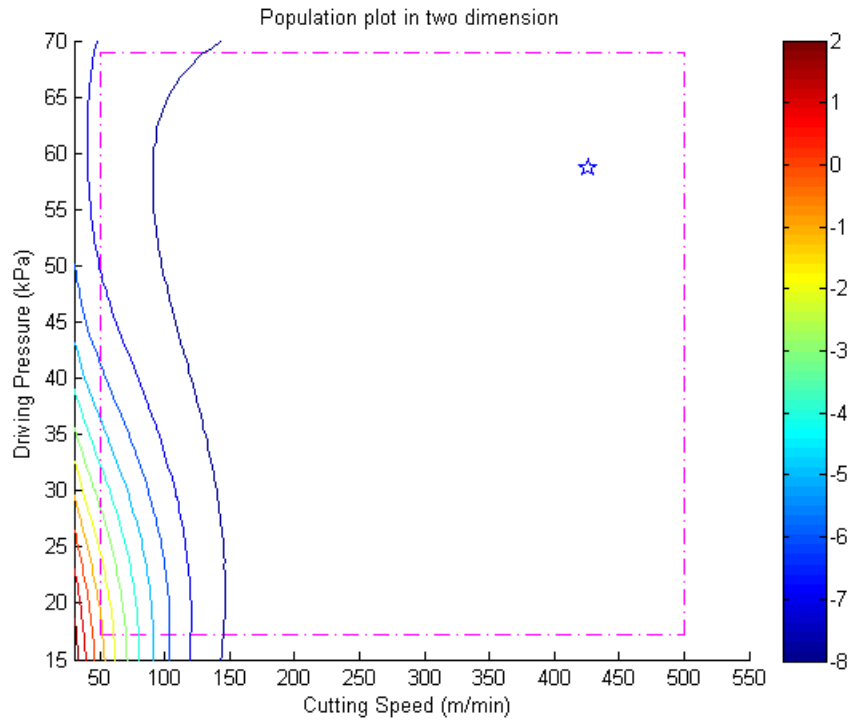


Figure 6.3: Population plot of optimization for highest *ProcSI* score.

The optimal condition determined is cutting speed, $V_c = 426$ m/min, and the driving pressure, $P = 58.6$ kPa.

A comparison is given for the best performing experimental condition in the overall sustainability performance, and the optimal parameters obtained from the use of the GA, is summarized in Figure 6.4.

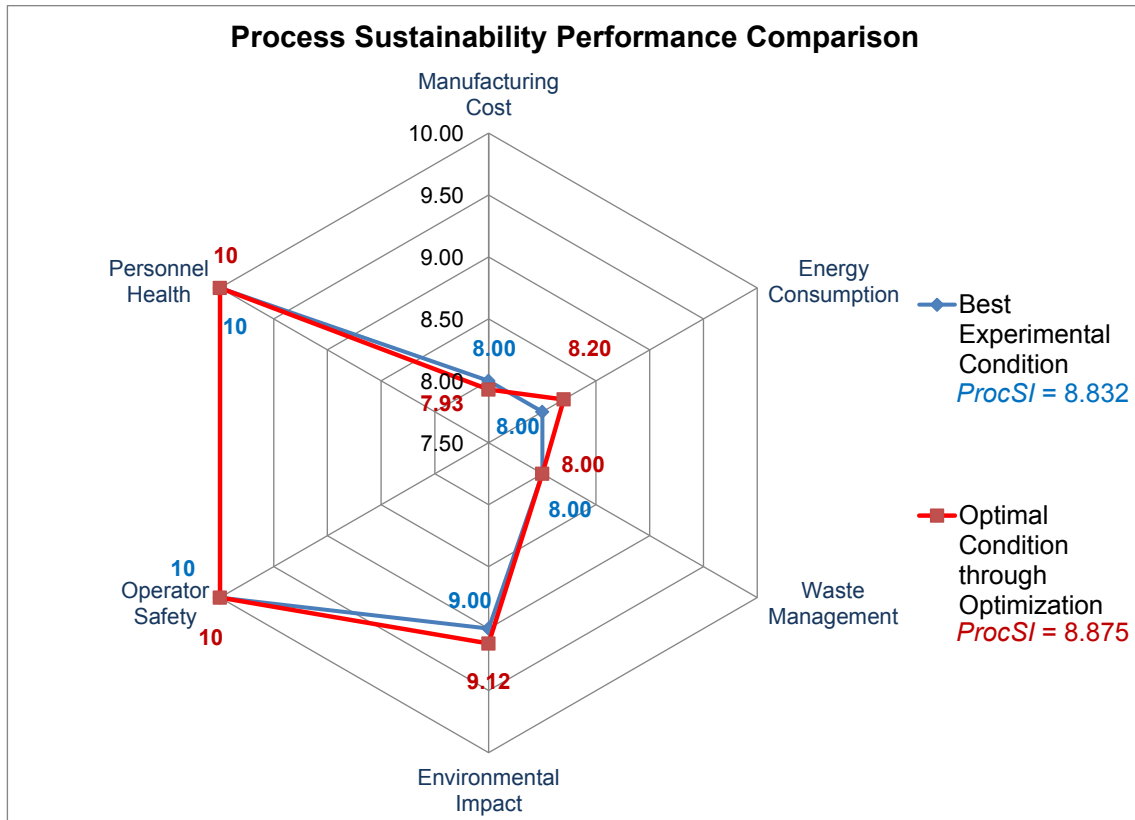


Figure 6.4: *ProcSI* results from best experimental condition and optimal condition obtained through optimization.

While the best condition in the experimental scenario shows better performance in cost, the optimal condition determined by optimization with GA is superior in energy consumption.

Compared to the other two optimization cases in Sections 6.2.1 and 6.2.2, the optimization results here are a compromise between the two. As the increment of cost benefits is minor at the higher cutting speeds tested, the saving of energy shows more enhancements to the overall sustainability performance of the process.

6.3 Summary

An optimization method based on Genetic Algorithm (GA) is carried out for cryogenic machining process. Along with the often discussed optimization for minimal cost and minimal energy consumption, an optimization for the best process sustainability performance presented in this chapter. In this particular case, the effect of coolant rate on the process performance is found to be marginal. Thus, the results are much more sensitive to the cutting speed rather than the coolant flow rate. According to the data in the orthogonal cutting experiments on *AZ31B* magnesium alloy, a moderate cutting speed is preferred due to its balance between productivity and cutting energy consumed.

CHAPTER 7

CONCLUDING REMARKS AND FUTURE WORK

7.1 Concluding Remarks

In this research work, based on the recently established Process Sustainability Index (*ProcSI*) methodology, the sustainability performance of the cryogenic machining process is experimentally studied, modeled and optimized with application guidelines established by analytical modeling of the heat transfer mechanism in the cryogenic machining process. Based on the experimental results, the optimization carried out with genetic algorithm (GA) provides the optimal process conditions for minimum cost, minimal energy consumption, or most importantly the best sustainability performance.

7.1.1 Process Sustainability Index (*ProcSI*) method

The first major contribution of this research is the development of a comprehensive sustainability performance evaluation method for manufacturing processes. The major findings include:

- A comprehensive process sustainability evaluation method needs to consider the TBL of sustainable manufacturing, and include 6R and total life-cycle concepts.
- The scope of the sustainability evaluation of manufacturing processes is discussed. Focusing on improving process design for manufacturers, the proposed *ProcSI* method has a system boundary around the manufacturing plant.
- A metrics-based process sustainability evaluation method is developed, including sixty five metrics categorized into six sustainability clusters, namely, manufacturing

cost, energy consumption, waste management, environmental impact, personnel health, operator safety.

- The sustainability evaluation of manufacturing processes with the *ProcSI* method can be applied at different detail levels for different area of interest. Three levels are identified, namely plant level, workstation level and operation level.

7.1.2 Thermal analysis and modeling of heat transfer in cryogenic machining

Another major contribution of this research is the heat transfer analysis of cryogenic machining with flank-side liquid nitrogen jet delivery. Many of the findings could also be applied to other conditions of cryogenic machining. The major findings include:

- A precision, low noise, high speed temperature measurement system is developed for the micro-scale temperature measurement of high thermal gradient thermal field.
- The innovative over-sampling based signal processing provides exceptional noise suppression capability with little computational power requirement.
- New solution approach to inverse heat transfer problem (IHTP) developed in this work is based on low noise, high speed temperature measurement and over-sampling process. This method proves the potential of solving the stability problem of IHTP with simple and fast algorithms by enhancing the measurement system and signal processing. This method is used to calculate the surface heat transfer coefficient during flank-side liquid nitrogen jet delivery.
- The calculated local surface heat transfer coefficient suggests that liquid nitrogen flow can not penetrate into the separation point in the conical opening formed by tool flank and machined workpiece. In other words, liquid nitrogen can hardly go inside the tool-workpiece contact region to provide any lubrication or cooling.

- Boiling heat transfer is the dominant heat transfer mechanism in cryogenic machining. It induces a high surface heat transfer coefficient as high as $10^5 \text{ W}/(\text{°Cm}^2)$. Due to the overheat temperature range and surface motion, the heat transfer starts as film boiling and may transfer into transition boiling. This decides the surface heat transfer coefficient to be lower at high surface temperature and higher at low surface heat transfer.
- The liquid flow rate has a minor effect on the surface heat transfer coefficient. When a sufficient amount of liquid phase nitrogen is provided to the machined surface to maintain boiling heat transfer, further increasing liquid nitrogen flow rate will not increase the heat transfer coefficient.
- The boiling mechanism shows a similar pattern at various distances from the separation point on the machined surface. However, the congested zone between the tool flank and the machined surface on the workpiece does show the concentration effect of liquid nitrogen. On the other hand, a high flow rate is required to maintain boiling heat transfer at the open region.

7.1.3 Experimental works and optimization of cryogenic machining

The experimental work in cryogenic machining, and the corresponding optimization effort contribute to establishing application guidelines for cryogenic machining. The major findings include:

- Coolant exposure time is a critical contributing factor towards the cooling capability in cryogenic machining. The cooling effect will be reduced with shorter coolant exposure time due to higher cutting speed. As the surface heat transfer coefficient

might be difficult to increase by increasing the flow rate, the corresponding solution would be increasing the coolant coverage area.

- Cooling effect in cryogenic machining may have other effects than cooling the tool and workpiece. In this case, a higher system stiffness is found with cryogenic machining due the cooling of the surrounding environment, when there is a vibration potential in the system.
- The process sustainability performance could vary significantly with different process parameters. When process parameters are not correctly set and optimized, the potentially sustainable cryogenic machining could give unsatisfactory results.
- The best sustainability performance of cryogenic machining is achieved by a compromise among the preferences of its contributing factors. The combination of high speed machining and low liquid nitrogen flow rate gives the maximum economic benefits. On the other hand, the most energy efficient case would be achieved at a moderate cutting speed and high flow rate. As a result, the process parameters providing best *ProcSI* score lie in-between the two. This provides an engineering decision making opportunity by making compromises among all factors. Sustainable manufacturing process is not achieved by a single technique, but a combination of numerous different aspects, which is the basis for the the core thinking of sustainable manufacturing.

7.2 Future Work

7.2.1 Process Sustainability Index (*ProcSI*) method

The newly developed *ProcSI* method has only a moderate level consideration of personnel health and operator safety aspects. Further study is needed in improving the metric setup, data processing and normalization in these two clusters.

Normalization, weighting and aggregation approaches used in this research are the common methods. Comprehensive research on these important aspects such as the sensitivity analysis could help to improve the data assessment of the metrics' measurement.

Different normalization and weighting approaches could be provided for different application scenarios, and to satisfy the different interests and needs from different stakeholders.

The development of the *ProcSI* method is based on material removal processes. Thus, its application in other categories of manufacturing processes would provide valuable input in guiding the customization of the process for a wider range of applications.

Product from a manufacturing process is expected to meet the pre-decided quality requirements, and further improvement in product quality by optimizing the process is not taken into account. The purpose of such a scenario is to adapt to current manufacturing scenarios. But in this case, the correlation between sustainability performance of a manufacturing process and its product is not well considered. Further work is expected to comprehensively develop interactive sustainability performance evaluation for both product and process.

7.2.2 Heat transfer analysis method

The low noise, high speed temperature measurement system developed is very sensitive to radio frequency interference, due to its sensor structure and system sensitivity. It would further help enhancing the experiment setup by applying cleaner environment with low noise radio radiation background, and better measurement system design.

The liquid nitrogen flow rate from the present delivery system is somewhat limited. This creates a major limitation on the experimental results obtained. It also suggests that a well-designed stable and efficient liquid nitrogen delivery system is mandatory for a truly sustainable cryogenic machining process.

The over-sampling method provides exceptional low noise temperature data which otherwise was not available. Conventional IHTP solution would not take use of this advantage. The solution method used in this study is relatively crude and simple. A more comprehensive algorithm could be developed for a better robustness which could adapt to local errors.

Similar approaches could be extended to other cases of cryogenic machining, such as liquid nitrogen jet on the rake surface, or combination of various coolant delivery methods. However, it could anticipate that the complex geometry, flow pattern and subjects in motion would create a range of difficulties in the study. The currently proposed method is based on static surface temperature measurement. It would be a great benefit if similar micro scale high speed temperature measurement could be achieved on moving subjects.

7.2.3 Research of cryogenic machining

When liquid nitrogen is applied from the rake side, the study of prevalent more complex interactions among workpiece, chip, cutting tool and the coolant would have a huge research potential. Given the fact that liquid nitrogen would cool down a thin layer of material surface during a very short period of exposure, the impact of process parameters could be different from that seen in conventional machining. For example, different ratios between the depth of cut or feed rate and the depth of the cooled layer could lead to dramatically different deformation process due to different material temperature, properties, and thus, different stress, strain, strain-rate and temperature distributions around the cutting zone. The problem could share some similarities to the study of machining on pre-machined surface.

While the coolant is what makes cryogenic machining different from other forms of machining process, the study on coolant parameters in cryogenic machining could be extended. The jet design, flow pattern and location of cooling along with workpiece pre-heating/pre-cooling, could establish appropriate guidelines for cryogenic machining applications.

Concerning the particular machining process in this study, it could be extended to high speed machining study. Magnesium alloy is suitable for high speed machining, however, the current experimental parameters have not revealed the potential benefits of high speed machining. Also, tool-wear and surface integrity patterns could be further studied.

Regarding the modeling of cryogenic machining process, the findings in the thermal analysis could help the process modelling effort such as finite element model (FEM) with the accurate input for the boundary conditions.

APPENDIX A

PROCESSING OF THE THERMOCOUPLE SIGNALS

The Matlab® code is based on the signal process presented in Section 4.1.1 and summarized in Figure 4.4. Programming environment is Matlab® 2014a (8.3.0.532).

The code can be used for K-type and E-type thermocouples by changing the value of a variable.

Signal zero drift is based on a pre-recorded idle data set. The parameters for cold joint compensation and signal filtering can be customized.

The signal voltage to temperature convention is based on ITS-90 standard for thermocouples (NIST, 2012). Logical indexing of large data matrix is used for best processing speed, while the equivalent conventional logic loop code is given as a reference. The algorithm covers the whole temperature ranges of K-type and E-type thermocouples. For K-type thermocouple, the temperature range is -200°C to 1372°C. During the range of -200°C to 0°C, the error range is -0.02°C to 0.04°C; during the range of 0°C to 500°C, the error range is -0.05°C to 0.04°C; during the range of 500°C to 1372°C, the error range is -0.05 °C to 0.06°C. For E-type thermocouple, the temperature range is -200°C to 1000°C. During the range of -200°C to 0°C, the error range is -0.01°C to 0.03°C; during the range of 0°C to 1000°C, the error range is -0.02°C to 0.02°C.

```
close all;
clear;
clc;
TC_type=2;           %T/C type, 1 for type K, any other number for
type E
disp('Starting...select zero-drift file>>');
[filename0, pathname0]=uigetfile({'*.*', 'all files (*.*)'}, 'Pick the
zero-drift file');
```

```

tic;
disp('Reading initialization data>>');
File0=fullfile(pathname0,filename0); %get
the zero-drift file
voltage0=importdata(File0,'\t',5); %read
the data
dimi=size(voltage0.data);
zd=mean(voltage0.data(round(dimi(1)*0.1):dimi(1),:)); %zero
drift calculation
disp('Initialization completed>>');
toc;
disp('Select data file>>');
[filename1,pathname1]=uigetfile({'*.*','all files (*.*)'},'Pick the
input file');
tic;
disp('Reading data file>>');
File1=fullfile(pathname1,filename1); %get
the input file
voltage=importdata(File1,'\t',5); %read
the data
toc;
tic;
if(TC_type==1)
    disp_str=['Thermocouple type K'];
else
    disp_str=['Thermocouple type E'];
end;
disp(disp_str);
disp('Pre-processing>>');
dimi=size(voltage.data);
dimi(2)=dimi(2)+1;
resistor=100;
%for AD8429BRZ instrumentation amplifier, the gain G=6000/Rg+1, while
Rg is
%the resistor value of the gain setting resistor
%for AD8421BRZ instrumentation amplifier, the gain G=9900/Rg+1, while
Rg is
%the resistor value of the gain setting resistor
gain=9900/resistor+1; %number of times for the amplifier gain
%gain=1;
%rt=input('Input room temperature in C, default is 20 C>>\n'); %room
temperature
if isempty(rt)
    rt=25;
end;
sr=textscan(char(voltage.textdata(2,1)),'%f'); %get sample rate number
from file
sample_rate=cell2mat(sr(1,1));
ori(:,1)=(0:1/sample_rate:(dimi(1)-1)/sample_rate);
ori(:,2:dimi(2))=voltage.data(:);
figure; %plot original voltage data
plot(ori(:,1),ori(:,2:dimi(2)),'blue');
for i=2:dimi(2) %zero-drift compensation
    ori(:,i)=ori(:,i)-zd(:,i-1);
end;
%%% Butterworth filtering %%%
f_cut = 100e3; % Cut-off frequency (Hz)

```

```

forder = 7;          % Filter order
[bc,ac] = butter(forder,2*f_cut/sample_rate,'low'); % [0:pi] maps to
[0:1] here
for i=2:dimi(2)
    ori(:,i)=filter(bc,ac,ori(:,i));          %Filtering
end;
disp_str=['Butterworth low-pass filtering order = ',num2str(forder)];
disp(disp_str);
disp_str=['Butterworth low-pass filtering cutting frequency = ',
num2str(f_cut/1000),'kHz'];
disp(disp_str);
%%% Butterworth filtering %%%
%%% Moving average filtering %%%
% ac=1;
% t=0.010e-3;
% f_window=sample_rate*t;
% bc=ones(f_window,1)/f_window;          %averaging over t ms
% for i=2:dimi(2)
%     ori(:,i)=filter(bc,ac,ori(:,i));          %Filtering
% end;
% disp_str=['Moving average filtering every ',num2str(t*1000),'ms
(Window size = ',num2str(f_window),' samples)'];
% disp(disp_str);
%%% Moving average filtering %%%
tv=[0,0.039,0.079,0.119,0.158,0.198,0.238,0.277,0.317,0.357,0.397,0.437
,0.477,0.517,0.557,0.597,0.637,0.677,0.718,0.758,0.798,0.838,0.879,0.91
9,0.96,1,1.041,1.081,1.122,1.163,1.203,1.244,1.285,1.326,1.366,1.407,1.
448,1.489,1.53,1.571,1.612];
%thermocouple voltage in mV, from 0C to 40C
cjc=tv(rt+1)*gain;          %cold junction compensation
ori(:,2:dimi(2))=ori(:,2:dimi(2))+cjc;
hold on;
plot (ori(:,1),ori(:,2:dimi(2)),'red');          %plot processed voltage data
grid on;
xlabel('Time (s)');
ylabel('Voltage (mV)');
title('Voltage data');
legend('Raw data','Processed data');
ori(:,i:dimi(2))=ori(:,i:dimi(2))/gain;          %Original T/C voltage
toc;
%%% Frequency analysis %%%
%figure;
%ini_noise=ori(0.1*sample_rate+1:0.8*sample_rate,2:dimi(2));
%ini_noise=ori(:,2:dimi(2));
%length_noise=length(ini_noise);
%plot(0.2:1/sample_rate:0.2+(length_noise-1)/sample_rate,ini_noise);
%NFFT=2^nextpow2(length_noise);
%noise_fr=fft(ini_noise,NFFT)/length_noise;
%f=sample_rate/2*linspace(0,1,NFFT/2+1);
%Plot single-sided amplitude spectrum.
%figure;
%plot(f,2*abs(noise_fr(1:NFFT/2+1)));
%axis([10, 1e6, 0, Inf]);
%set(gca,'XScale','log');
%title('Single-Sided Amplitude Spectrum of y(t)');
%xlabel('Frequency (Hz)');
%ylabel('|Y(f)|');

```

```

%%% Frequency analysis %%%
tic;
disp('Converting voltage to temperature>>');
te=zeros(dimi(1),dimi(2));
te=zeros(dimi(1),dimi(2));
te(:,1)=ori(:,1);
jud=ori(:,2:dimi(2));
if(TC_type==1)
%%% Type-K Thermocouple %%%
    inv_coeff_low=[0,25.173462,-1.1662878,-1.0833638,-0.8977354,-
0.37342377,-0.086632643,-0.010450598,-0.00051920577];
    inv_coeff_low=inv_coeff_low(9:-1:1);    %low temperature (-200C to
0C) inverse coefficient
    inv_coeff_mid=[0,25.08355,0.07860106,-0.2503131,0.0831527,-
0.01228034,0.0009804036,-4.41303E-05,1.057734E-06,-1.052755E-08];
    inv_coeff_mid=inv_coeff_mid(10:-1:1);    %mid temperature (0C to
500C) inverse coefficient
    inv_coeff_hig=[-131.8058,48.30222,-1.646031,0.05464731,-
0.0009650715,8.802193E-06,-3.11081E-08];
    inv_coeff_hig=inv_coeff_hig(7:-1:1);    %high temperature (500C to
1372C) inverse coefficient
    jud=ori(:,2:dimi(2));
    jud(jud<=54.886)=0;
    jud(jud>54.886)=1372;
    te(:,2:dimi(2))=te(:,2:dimi(2))+jud;    %data filling for very
high (>1372C) temperature range
    jud=ori(:,2:dimi(2));
    jud(jud>=-5.891)=0;
    jud(jud<-5.891)=-200;
    te(:,2:dimi(2))=te(:,2:dimi(2))+jud;    %data filling for very
low (<-200C) temperature range
    jud=ori(:,2:dimi(2));
    jud(jud<=0 | jud>=20.644)=0;
    jud(jud>0 & jud<20.644)=polyval(inv_coeff_mid,jud(jud>0 &
jud<20.644));
    te(:,2:dimi(2))=te(:,2:dimi(2))+jud;    %temperature
calculation for mid temperature range (0C to 500C)
    jud=ori(:,2:dimi(2));
    jud(jud>=0 | jud<-5.891)=0;
    jud(jud<0 & jud>=-5.891)=polyval(inv_coeff_low,jud(jud<0 & jud>=-
5.891));
    te(:,2:dimi(2))=te(:,2:dimi(2))+jud;    %temperature
calculation for low temperature range (-200C to 0C)
    jud=ori(:,2:dimi(2));
    jud(jud<20.644 | jud>54.886)=0;
    jud(jud>=20.644 &
jud<=54.886)=polyval(inv_coeff_hig,jud(jud>=20.644 & jud<=54.886));
    te(:,2:dimi(2))=te(:,2:dimi(2))+jud;    %temperature
calculation for high temperature range (500C to 1372C)
    % for j=2:dimi(2)
    %     for i=1:dimi(1)
    %         jud=ori(i,j);    %actual
thermocouple output voltage
    %         if (jud>=0 && jud<20.644)    %temperature
calculation for mid temperature range (0C to 500C)
    %             te(i,j)=polyval(inv_coeff_mid,jud);
    %         else

```



```

%           if (jud<0 && jud>=-5.891)           %temperature
calculation for low temperature range (-200C to 0C)
%           te(i,j)=polyval(inv_coeff_low,jud);
%           else
%           if (jud>=20.644 && jud<=54.886) %temperature
calculation for high temperature range (500C to 1372C)
%           te(i,j)=polyval(inv_coeff_hig,jud);
%           else
%           if (jud>54.886)           %data filling for
very high (>1372C) temperature range
%           te(i,j)=1372;
%           else
%           if (jud<=-5.891)           %data filling for
very low (<-200C) temperature range
%           te(i,j)=-200;
%           %te(i,j)=polyval(inv_coeff_low,jud);
%           end;
%           end;
%           end;
%           end;
%           end;
%           end
% end;
%%% Type-K Thermocouple %%%
else
    %%% Type-E Thermocouple %%%
    inv_coeff_low=[0,1.6977288e1,-4.3514970e-1,-1.5859697e-1,-
9.2502871e-2,-2.6084314e-2,-4.1360199e-3,-3.4034030e-4,-1.1564890e-5];
    inv_coeff_low=inv_coeff_low(9:-1:1); %low temperature (-200C to
0C) inverse coefficient
    inv_coeff_hig=[0,1.7057035e1,-2.3301759e-1,6.5435585e-3,-
7.3562749e-5,-1.7896001e-6,8.4036165e-8,-1.3735879e-9,1.0629823e-11,-
3.2447087e-14];
    inv_coeff_hig=inv_coeff_hig(10:-1:1); %high temperature (0C to
1000C) inverse coefficient
    jud=ori(:,2:dimi(2));
    jud(jud<=76.373)=0;
    jud(jud>76.373)=1000;
    te(:,2:dimi(2))=te(:,2:dimi(2))+jud; %data filling for very
high (>1000C) temperature range
    jud=ori(:,2:dimi(2));
    jud(jud>=-8.825)=0;
    jud(jud<-8.825)=-200;
    te(:,2:dimi(2))=te(:,2:dimi(2))+jud; %data filling for very
low (<-200C) temperature range
    jud=ori(:,2:dimi(2));
    jud(jud>=0 | jud<-8.825)=0;
    jud(jud<0 & jud>=-8.825)=polyval(inv_coeff_low,jud(jud<0 & jud>=-
8.825));
    te(:,2:dimi(2))=te(:,2:dimi(2))+jud; %temperature
calculation for low temperature range (-200C to 0C)
    jud=ori(:,2:dimi(2));
    jud(jud<0 | jud>76.373)=0;
    jud(jud>=0 & jud<=76.373)=polyval(inv_coeff_hig,jud(jud>=0 &
jud<=76.373));
    te(:,2:dimi(2))=te(:,2:dimi(2))+jud; %temperature
calculation for high temperature range (0C to 1000C)

```

```

    %% Type-E Thermocouple %%
end;
toc;
tic;
disp('Output>>');
figure;
plot (te(:,1),te(:,2:dimi(2)));    %plot temperature result
hold on;
grid on;
line ([0,dimi(1)/sample_rate],[-196,-
196], 'color','red');    %theoretical LN temperature @1 atm
%line ([0,dimi(1)/sample_rate],[-182,-182], 'color','green'); %typical
experimentally measured LN temperature
xlabel('Time (s)');
ylabel('Temperature (\circC)');
title('Calculated temperature data');
toc;
disp('Select target time period>>');
i=input('Press Enter to continue, anything else to end>>');
if isempty(i)
    while isempty(i)
        begin=input('Input starting time>>');
        begin=round(begin*sample_rate)+1;
        ending=input('Input ending time>>');
        ending=round(ending*sample_rate)+1;
        figure;
        plot(te(begin:ending,1),te(begin:ending,2:dimi(2)));
        i=input('Press Enter to continue, anything else to end>>');
        if isempty(i)
            close Figure 3;
        end;
    end;
else
    begin=1;
    ending=dimi(1);
end;
tic;
te2=te(begin:ending,:);
fn1=textscan(filename1,'%s%s','Delimiter','.');
filename2=strcat(char(fn1{1,1}),'_C.txt');
File2=fullfile(pathname1,filename2);    %generate the output file,file
name is 'INPUT FILE NAME_temperature in C.txt'
output_file=fopen(File2,'w');    %output to file
fprintf(output_file,'Time (s)\tTemperature (C)\r\n');
fprintf(output_file,'%3.7f\t%4.3f\r\n',te2');
fclose(output_file);
toc;
disp('Completed>>');

```

APPENDIX B

FINITE DIFFERENCE METHOD FOR THE HEAT TRANSFER PROBLEM

The follow introduction of the explicit scheme and implicit scheme can be found in many literatures (Ozisik, 1993; Incropera and DeWitt, 2000). The general approach is briefly introduced here. In the explicit scheme, using forward difference in time to represent the time rate of temperature change, for the right hand side of Equation (4.10) at nodal location (x_i, t_j) , we have:

$$\frac{1}{\alpha} \cdot \frac{\partial T}{\partial t} \approx \frac{1}{\alpha} \cdot \frac{T(x_i, t_{j+1}) - T(x_i, t_j)}{\Delta t} = \frac{1}{\alpha} \cdot \frac{T_{i,j+1} - T_{i,j}}{\Delta t} \text{ at } x = x_i \quad (\text{B.1})$$

For the left hand side of Equation (4.10), by using central difference approximation on the same location (x_i, t_j) , we have:

$$\frac{\partial T^2}{\partial x^2} \approx \frac{T(x_{i+1}, t_j) - 2 \cdot T(x_i, t_j) + T(x_{i-1}, t_j)}{\Delta x^2} = \frac{T_{i+1,j} - T_{i,j} + T_{i-1,j}}{\Delta x^2} \text{ at } t = t_j \quad (\text{B.2})$$

By substitution of the Equations (B.1) and (B.2) above into Equation (4.10) and rearrange it, an explicit formula can be given to calculate $T_{i,j+1}$:

$$T_{i,j+1} = T_{i,j} + Fo \cdot (T_{i+1,j} - 2 \cdot T_{i,j} + T_{i-1,j}) \quad (\text{B.3})$$

here, the Fourier number Fo is defined as $Fo = \alpha \cdot \Delta t / \Delta x^2$.

In the implicit scheme, for the left hand side of Equation (4.10), by using central difference approximation on the same location (x_i, t_{j+1}) , we have:

$$\frac{\partial T^2}{\partial x^2} \approx \frac{T(x_{i+1}, t_{j+1}) - 2 \cdot T(x_i, t_{j+1}) + T(x_{i-1}, t_{j+1})}{\Delta x^2} = \frac{T_{i+1,j+1} - 2 \cdot T_{i,j+1} + T_{i-1,j+1}}{\Delta x^2} \quad (\text{B.4})$$

Combining Equation (B.1) and (B.4) and rearranging, we have:

$$-Fo \cdot T_{i-1,j+1} + (2 \cdot Fo + 1) \cdot T_{i,j+1} - Fo \cdot T_{i+1,j+1} = T_{i,j} \quad (\text{B.5})$$

For the boundary nodes, the approximation is different. Without deduction, it is given here as:

$$T_{0,j+1} = 2 \cdot Fo \cdot T_{1,j} + (1 - 2 \cdot Fo - 2 \cdot Fo \cdot Bi) \cdot T_{0,j} + 2 \cdot Fo \cdot Bi \cdot T_{coolant} \quad (\text{B.6})$$

And the Biot number Bi is given in finite difference form as $Bi = h \cdot \Delta x / k$.

Thus a system of linear equations about $T_{i,j}$ and $T_{i,j+1}$ is established. Then, the $T_{i,j+1}$ for all i can be calculated by setting a coefficient matrix A (about Fo and Bi) and a value vector Tb (about $T_{i,j}$, $T_{coolant}$, Fo and Bi) such that $A T_{i,j+1} = Tb$, then can solve the equation system at once.

The two following sub-routines are Finite Difference Method algorithm to calculate the temperature distribution of one dimensional specimen, considering the surface heat transfer on top and bottom surfaces. They calculate the temperature distribution of the next time step, given the temperature distribution of current temperature step.

Note that the *sumlog* function is a customized sub-routine to help calculate the material thermal properties, as described in Section 4.2.1. It equals Equation (4.14) in computation sense.

```
function y=FDM_Step_NonConstant (h1)
global step T n dx dt size_effect x_SHC x_TC Tln2 Tair;
% k=96.0; %thermal conductivity, in W/(m*C)
% Cp=1.00e3; %heat capacity, in J/(kg*C)
rou=1.77e3; %density, in kg/m^3
%h1=1e6; %surface heat transfer coefficient, test side,
in W/(C*m^2)
h2=32; %surface heat transfer coefficient, air side,
in W/(C*m^2)
%Tln2=-196; %liquid nitrogen temperature
%Tair=25; %air temperature
% alpha=k/(rou*Cp); %alpha number
% Fo=alpha*dt/(dx^2); %Fourier number
% Bil=h1*dx/k; %Biot number on test side
```

```

% Bi2=h2*dx/k;           %Biot number on air side
%%%%%%%%%%%%%%%%%%%%%%%%%%%%%%%%%%%%%%%%%%%%%%%%%%%%%%%%%%%%%%%%%%%%%%%%
%%% setting coefficient matrix %%%
%%%%%%%%%%%%%%%%%%%%%%%%%%%%%%%%%%%%%%%%%%%%%%%%%%%%%%%%%%%%%%%%%%%%%%%%
A=zeros(n,n);
Tb=zeros(n,1);
for i=1:1:n-2

alpha=sumlog(x_TC,T(i+1,step)+273)/(rou*sumlog(x_SHC,T(i+1,step)+273));
Fo=alpha*dt/(dx^2);
A(i,i:i+2)=[-Fo, 1+2*Fo, -Fo];
end;
alpha=sumlog(x_TC,T(1,step)+273)/(rou*sumlog(x_SHC,T(1,step)+273));
Fo=alpha*dt/(dx^2);
Bi1=h1*dx/sumlog(x_TC,T(1,step)+273);           %Biot number on test side
A(n-1,1)=1+2*Fo+2*Fo*Bi1;
A(n-1,2)=-2*Fo;
Tb(n-1,1)=2*Fo*Bi1*Tln2+T(1,step);
alpha=sumlog(x_TC,T(n,step)+273)/(rou*sumlog(x_SHC,T(n,step)+273));
Fo=alpha*dt/(dx^2);
Bi2=h2*dx/sumlog(x_TC,T(n,step)+273)           %Biot number on air side
A(n,n)=1+2*Fo+2*Fo*Bi2;
A(n,n-1)=-2*Fo;
Tb(n,1)=2*Fo*Bi2*Tair+T(n,step);
%%%%%%%%%%%%%%%%%%%%%%%%%%%%%%%%%%%%%%%%%%%%%%%%%%%%%%%%%%%%%%%%%%%%%%%%
%%% setting coefficient matrix %%%
%%%%%%%%%%%%%%%%%%%%%%%%%%%%%%%%%%%%%%%%%%%%%%%%%%%%%%%%%%%%%%%%%%%%%%%%
Tb(1:n-2,1)=T(2:n-1,step); %value vector
T(:,step+1)=mldivide(A,Tb);
y=T(size_effect+1,step+1);

```

```

function value = sumlog(x,temperature)
n=length(x);
y=x(1)*ones(length(temperature),1);
for i=2:1:n;
y=y+x(i).*(log10(temperature).^(i-1));
end;
value=10.^y;

```

APPENDIX C

SOLVING THE INVERSE HEAT CONDUCTION PROBLEM WITH LEAST SQUARE METHOD

The code used here is an example of the least square methods used to solve the IHTP. To be specific, this example is using the Levenberg-Marquardt iteration method. The reflective trust region method can be used by changing the solver option. The genetic algorithm (GA) needs to use a different solver sub-routine, though the general flow of the algorithm is the same.

The FDM model used is similar to the one shown in APPENDIX B. The fundamental algorithms are the same. The difference is that, instead of calculating only the temperature distribution of next time step, the *FDM_Global_NonConstant* function used here calculates the temperature distribution at all the time steps based on a pre-defined surface heat transfer coefficient curve.

The material properties of *AZ31B* magnesium alloy involved are discussed in Section 4.2.1 and fulfilled in the FDM model as shown in APPENDIX B.

```
close all;
clear;
clc;
global T n dx dt dimi size_effect x_SHC x_TC Tln2 Tair;
warning('off','all');
disp('Starting...select data file>>');
x_SHC=[-1.34947954934310;-382.537692081207;962.920075731903;-
997.725884688401;548.575442999494;-168.955851652423;27.6392175360364;-
1.87608749119116];
x_TC=[-194.526321179433;475.445772468405;-
481.347728186954;261.162318756297;-80.4458167450158;13.5008118152702;-
1.01326748410666;0.0114123543183431];
reduc=100;
size_effect=1;
dx=27e-6/size_effect;           %size of delta x
Tln2=-196;                       %coolant temperature
```

```

Tair=25; %air temperature
[filename, pathname]=uigetfile({'*.*','all files (*.*)'},'Pick the
input file');
tic;
disp('Reading data file>>');
File=fullfile(pathname,filename); %get the
input file
raw_data=importdata(File,'\t',1); %read
the data
dimi=size(raw_data.data);
time_ori=raw_data.data(:,1);
temperature_ori=raw_data.data(:,2:dimi(2));
length=2000;
[p,S]=polyfit(time_ori(1:length),temperature_ori(1:length),1);
err_line=S.normr/sqrt(length);
starting=-1;
for i=2001:1:dimi(1)-2
    if(starting==--1)
        if(min(abs(temperature_ori(i:i+2)-
polyval(p,time_ori(i:i+2))))>10*err_line)
            starting=i+reduc;
        end;
    else
        if(max(temperature_ori(i:i+2))<-190)
            ending=i-reduc;
            break;
        else
            ending=i-reduc;
        end;
    end;
end;
time=zeros(round((ending-starting)/reduc),1);
temperature=zeros(round((ending-starting)/reduc),1);
for i=1:1:round((ending-starting)/reduc)
    time(i)=mean(time_ori(starting+reduc*(i-1):starting+reduc*i-1));
    temperature(i)=mean(temperature_ori(starting+reduc*(i-
1):starting+reduc*i-1));
end;
dimi=size(time);
figure(1);
plot(time,temperature);
xlabel('Time (s)');
ylabel('Temperature (\circC)');
title('Calculated temperature data');
toc;
dt=time(2)-time(1);
n=1+round(12.7e-3/dx); %number of nodes
T=zeros(n,dimi(1)); %Whole temperature matrix, row for nodes,
column for steps
T(:,1)=temperature(1); %T: temperature of this step
order=5;
k=96.0; %thermal conductivity, in W/(m*C)
Cp=1.00e3; %heat capacity, in J/(kg*C)
rou=1.77e3; %density, in kg/m^3
h2=20; %surface heat transfer coefficient, air side,
in W/(C*m^2)
x=zeros(order+1,1);

```

```

x0=[0,0,0,0,0,1e4];
LB(1:order+1,1)=-Inf;
UB(1:order+1,1)=Inf;
options=optimoptions('lsqcurvefit');
options=optimoptions(options,'MaxFunEvals',2e5,'TolFun',1e-
6,'MaxIter',1e4);
options=optimoptions(options,'PlotFcns',@optimplotresnorm);
options=optimoptions(options,'Algorithm','levenberg-marquardt');
tic;
%err=FDM_Global(x0,time)-temperature;
[x,resnorm,residual,exitflag] =
lsqcurvefit(@FDM_Global_NonConstant,x0,time,temperature,LB,UB,options);
toc;
figure(1);
hold on;
plot(time,T(size_effect+1,:), 'r');
legend('Measurements', 'Calculated');
figure (3);
plot(T(1,2:dimi(1)),polyval(x,time(2:dimi(1))));
xlabel('Overheat Temperature (\circC)');
ylabel('Surface heat transfer coefficient (W/m^{2}\circC)');
title('Calculated surface heat transfer coefficient');
set(gca, 'YScale', 'log');
disp('Completed>>');

```


APPENDIX D

SOLVING THE INVERSE HEAT CONDUCTION PROBLEM WITH OVER-SAMPLING METHOD

The linear search algorithm used is based on over-sampling processing as described in the flow chart, Figure 4.17.

The FDM model for one dimensional heat transfer, which considers surface heat transfer on top and bottom sides, can be found in APPENDIX B.

The material properties of *AZ31B* magnesium alloy involved are discussed in Section 4.2.1 and fulfilled in the FDM model as shown in APPENDIX B.

```
close all;
clear;
clc;
global T step n dx dt dimi size_effect x_SHC x_TC Tln2 Tair;
reduc=100;           %Oversampling factor
size_effect=1;      %Spatial size factor
Tln2=-196;          %coolant temperature
Tair=24;            %air temperature
dx=27e-6/size_effect; %size of delta x
warning('off','all');
x_SHC=[-1.34947954934310;-382.537692081207;962.920075731903;-
997.725884688401;548.575442999494;-168.955851652423;27.6392175360364;-
1.87608749119116];
x_TC=[-194.526321179433;475.445772468405;-
481.347728186954;261.162318756297;-80.4458167450158;13.5008118152702;-
1.01326748410666;0.0114123543183431];
disp_cont=['Starting...size ratio = ',num2str(size_effect)];
disp(disp_cont);
disp_cont=['Oversampling factor = ', num2str(reduc)];
disp(disp_cont);
disp('Select data file>>');
[filename, pathname]=uigetfile({'*.*','all files (*.*)'},'Pick the
input file');
tic;
disp('Reading data file>>');
File=fullfile(pathname,filename);           %get the input file
raw_data=importdata(File,'\t',1);          %read the data
dimi=size(raw_data.data);
time_ori=raw_data.data(:,1);
temperature_ori=raw_data.data(:,2:dimi(2));
length=2000;
```

```

[p,S]=polyfit(time_ori(1:length),temperature_ori(1:length),1);
err_line=S.normr/sqrt(length);
starting=-1;
for i=2001:1:dimi(1)-2
    if(starting==-1)
        if(min(abs(temperature_ori(i:i+2)-
polyval(p,time_ori(i:i+2))))>10*err_line)
            starting=i+reduc;
        end;
    else
        if(max(temperature_ori(i:i+2))<-190)
            ending=i-reduc;
            break;
        else
            ending=i-reduc;
        end;
    end;
end;
time=zeros(round((ending-starting)/reduc),1);
temperature=zeros(round((ending-starting)/reduc),1);
for i=1:1:round((ending-starting)/reduc)
    time(i)=mean(time_ori(starting+reduc*(i-1):starting+reduc*i-1));
    temperature(i)=mean(temperature_ori(starting+reduc*(i-
1):starting+reduc*i-1));
end;
dimi=size(time);
figure(1);
plot(time,temperature);
xlabel('Time (s)');
ylabel('Temperature (\circC)');
title('Calculated temperature data');
toc;
dt=time(2)-time(1);
n=1+round(12.7e-3/dx); %number of nodes
h=zeros(dim(1)-1,1); %vector listing the surface heat transfer
coefficient
%surface heat transfer coefficient (test value), in W/(C*m^2)
T=zeros(n,dim(1)); %Whole temperature matrix, row for nodes,
column for steps
T(:,1)=temperature(1);%T: temperature of this step
tic
x=1e5;
%disp(dim(1));
dimi_disp=strcat('/',num2str(dim(1)));
for step=1:1:dim(1)-1
    LB = [-1e12]; % Lower bound: surface heat transfer
coefficient (test value), in W/(C*m^2)
    UB = [1e12]; % Upper bound: surface heat transfer
coefficient (test value), in W/(C*m^2)
%%%%%%%%%%%%%%%%%%%%%%%%%%%%%%%%%%%%%%%%%%%%%%%%%%%%%%%%%%%%%%%%%%%%%%%%
%%% Linear search Algorithm %%%
%%%%%%%%%%%%%%%%%%%%%%%%%%%%%%%%%%%%%%%%%%%%%%%%%%%%%%%%%%%%%%%%%%%%%%%%
    x=(UB+LB)/2;
    err=temperature(step+1)-FDM_Step_NonConstant(x);
%    err=temperature(step+1)-FDM_Step(x);
    while(abs(err)>=err_line*0.3)
        while((abs(err)>=err_line*3)&&(LB~=UB))

```

```

        if(err>0)
            UB=x;
        else
            LB=x;
        end;
        x=(UB+LB)/2;
        err=temperature(step+1)-FDM_Step_NonConstant(x);
%       err=temperature(step+1)-FDM_Step(x);
    end;
%     if(LB==UB)
%         disp('Y');
%     end;
%%%%%%%%%%%%%%%%%%%%%%%%%%%%%%%%%%%%%%%%%%%%%%%%%%%%%%%%%%%%%%%%%%%%%%%%
%%% Linear search Algorithm %%%
%%%%%%%%%%%%%%%%%%%%%%%%%%%%%%%%%%%%%%%%%%%%%%%%%%%%%%%%%%%%%%%%%%%%%%%%
    %note here the starting point of x is the answer of last step
    h(step)=x;
    disp_cont=['Step: ',num2str(step),dimi_disp,' @time:
',num2str(time(step))];
    disp(disp_cont);
end;
toc;
SHTC=[time(2:dimi(1)),T(1,2:dimi(1))'-Tln2,h];
%[ph,S2]=polyfit(SHTC(:,2),SHTC(:,3),9);
hold on;
figure(1);
plot(time,T(1+size_effect,:), 'r');
grid on;
legend('Measurements','Calculated data');
figure(2);
plot(SHTC(:,1),SHTC(:,3));
grid on;
set(gca, 'YScale', 'log');
figure(3);
grid on;
plot(SHTC(:,2),SHTC(:,3));
xlabel('Overheat Temperature (\circC)');
ylabel('Surface heat transfer coefficient (W/m^{2}\circC)');
title('Calculated surface heat transfer coefficient');
%hold on;
%plot(SHTC(:,2),polyval(ph,SHTC(:,2)), 'r');
set(gca, 'YScale', 'log');
fn1=textscan(filename, '%s%s', 'Delimiter', '.');
%filename2=strcat(char(fn1{1,1}), '_SHTC_S', num2str(size_effect), '.txt');
filename2=strcat(char(fn1{1,1}), '_SHTC.txt');
File2=fullfile(pathname,filename2); %generate the output file,file name
is 'INPUT FILE NAME_SHTC.txt'
output_file=fopen(File2, 'w'); %output to file
fprintf(output_file, 'Time (S)\tOverheat Temperature (C)\tSHTC
(W/(C*m2))\r\n');
fprintf(output_file, '%4.6f\t%4.3f\t%4.3f\r\n', SHTC');
fclose(output_file);
Rnorm=sumsqr(T(2,:)'-temperature);
disp('Completed>>');

```

APPENDIX E

DEFINING THE CUTTING EDGE RADIUS OF A CUTTING TOOL

The source data from the white light interferometer (Zygo® NewView™ 7300) are processed in the MetroPro® software, given in a matrix format. Each column contains the height values of the points on the cross Section surface.

Method I:

The algorithm is based on out-lying points' recognition and circular fitting to the curved Section.

```
close all;
clear;
clc;
disp('Starting...select data file>>');
[filename1, pathname1]=uigetfile({'*.*','all files (*.*)'}, 'Pick the
input file');
tic;
disp('Reading data file>>');
File1=fullfile(pathname1,filename1);           %get
the input file
raw_data=importdata(File1,' ',3);             %read
the data
toc;
lin_len=input('Please input the length of the straight part>>');
if isempty(lin_len)
    lin_len=250;
end;
tic;
dimi=size(raw_data.data);
dimi(1)=dimi(1)-1;
raw_dat=raw_data.data(1:dimi(1),:);
for i=1:2:dimi(2)
    raw_dat(:,i)=raw_dat(:,i)*1000;
end;
f_window=0;           %in case filtering is commented, set the window
size value to 0
%% Moving average filtering %%
ac=1;
f_window=5;
bc=ones(f_window,1)/f_window;           %averaging every
10 samples
raw_dat2=raw_dat;
for i=1:dimi(2)/2
```

```

    raw_dat(:,2*i)=filter(bc,ac,raw_dat(:,2*i));           %Filtering
end;
disp_str=['Moving average filtering every ',num2str(f_window),'
samples'];
disp(disp_str);
%%% Moving average filtering %%%
line1=zeros(2,1);
line2=zeros(2,1);
incl_ang=zeros(dimi(2)/2,1);
Cir=zeros(3,1);
RadCrv=zeros(1,dimi(2)/2);
n=5;    %number of points for seg check
n_sig=3;    %number of sigma for error range
for i=1:1:dimi(2)/2
    figure;
    hold on;
    plot(raw_dat(:,2*i-1),raw_dat(:,2*i),'-b');
    plot(raw_dat2(:,2*i-1),raw_dat2(:,2*i),'--g');
    xlabel('Location (um)');
    ylabel('Height (um)');
    title('Profile Map');
    [line1,s1]=polyfit(raw_dat(f_window:lin_len+f_window,2*i-
1),raw_dat(f_window:lin_len+f_window,2*i),1);
    [line2,s2]=polyfit(raw_dat(dimi(1)-lin_len+1:dimi(1),2*i-
1),raw_dat(dimi(1)-lin_len+1:dimi(1),2*i),1);
    incl_ang(i)=(pi-atan(line1(1))+atan(line2(1)))/pi*180;
    err_line1=s1.normr/sqrt(lin_len);
    err_line2=s2.normr/sqrt(lin_len);
    for j=lin_len+f_window:1:dimi(1)-n
        if(min(abs(raw_dat(j:j+n,2*i)-polyval(line1,raw_dat(j:j+n,2*i-
1))))>(n_sig*err_line1))
            break;
        end;
    end;
    Cir_start=j;

line([0,raw_dat(j,1)+10],[polyval(line1,0),polyval(line1,raw_dat(j,1)+
0)],'Color','r');
    for j=dimi(1)-lin_len+1:-1:n
        if(min(abs(raw_dat(j:j+n,2*i)-polyval(line2,raw_dat(j:j+n,2*i-
1))))>(n_sig*err_line2))
            break;
        end;
    end;
    Cir_end=j;
    line([raw_dat(j,1)-
10,raw_dat(dimi(1),1)],[polyval(line2,raw_dat(j,1)-
10),polyval(line2,raw_dat(dimi(1),1))],'Color','r');
    [Cir(1:2),Cir(3)]=fitcircle(raw_dat(Cir_start:Cir_end,2*i-1:2*i),
'linear');
    %Cir=CircleFitByTaubin(raw_dat(Cir_start:Cir_end,2*i-1:2*i));
    %Cir=CircleFitByPratt(raw_dat(Cir_start:Cir_end,2*i-1:2*i));
    RadCrv(i)=Cir(3);
    plot(raw_dat(Cir_start,2*i-
1),raw_dat(Cir_start,2*i),'+m','MarkerSize',12);
    plot(raw_dat(Cir_end,2*i-
1),raw_dat(Cir_end,2*i),'+m','MarkerSize',12);

```

```

    ang=0:0.01:2*pi;
    xp=Cir(3)*cos(ang);
    yp=Cir(3)*sin(ang);
    plot(Cir(1)+xp,Cir(2)+yp,':r');
end;
toc;

```

Method II:

The algorithm is based on curvature radius calculation to either the curved section only or the whole profile line. The example given here is the prior case. In the latter case, local oscillation could create noise to the generated curve, but could be distinguished easily.

```

close all;
clear;
clc;
disp('Starting...select data file>>');
[filename1, pathname1]=uigetfile({'*.*','all files (*.*)'},'Pick the
input file');
tic;
disp('Reading data file>>');
File1=fullfile(pathname1,filename1);           %get
the input file
raw_data=importdata(File1,'\t',9);           %read
the data
toc;
lin_len=input('Please input the length of the straight part>>');
if isempty(lin_len)
    lin_len=250;
end;
cir_len=50;
tic;
dimi=size(raw_data.data);
dimi(1)=dimi(1)-1;
raw_dat=raw_data.data(1:dimi(1),:);
f_window=0;           %in case filtering is comment, set the window size
value to 0
%%% Moving average filtering %%%
ac=1;
f_window=10;
bc=ones(f_window,1)/f_window;           %averaging every
10 samples
raw_dat2=raw_dat;
for i=1:dimi(2)/2
    raw_dat(:,2*i)=filter(bc,ac,raw_dat(:,2*i));           %Filtering
end;
disp_str=['Moving average filtering every ',num2str(f_window),'
samples'];
disp(disp_str);
%%% Moving average filtering %%%
line1=zeros(2,1);
line2=zeros(2,1);

```

```

incl_ang=zeros(dimi(2)/2,1);
Cir=zeros(3,1);
RadCrv=zeros(dimi(1),dimi(2)/2);
RadCrvAvg=zeros(dimi(2)/2,1);
n=5; %number of points for seg check
n_sig=3; %number of sigma for error range
for i=1:1:dimi(2)/2
    [line1,s1]=polyfit(raw_dat(f_window:lin_len+f_window,2*i-
1),raw_dat(f_window:lin_len+f_window,2*i),1);
    [line2,s2]=polyfit(raw_dat(dimi(1)-lin_len+1:dimi(1),2*i-
1),raw_dat(dimi(1)-lin_len+1:dimi(1),2*i),1);
    incl_ang(i)=(pi-atan(line1(1))+atan(line2(1)))/pi*180;
    % figure;
    % hold on;
    % plot(raw_dat(:,2*i-1),raw_dat(:,2*i),'-b');
    % plot(raw_dat2(:,2*i-1),raw_dat2(:,2*i),'--g');
    % line([0,110],[polyval(line1,0),polyval(line1,110)],'Color','r');
    % line([0,110],[polyval(line2,0),polyval(line2,110)],'Color','r');
    err_line1=s1.normr/sqrt(lin_len);
    err_line2=s2.normr/sqrt(lin_len);
    for j=lin_len+f_window:1:dimi(1)-
1)
        if(min(abs(raw_dat(j:j+n,2*i)-polyval(line1,raw_dat(j:j+n,2*i-
1))))>(n_sig*err_line1))
            break;
        end;
    end;
    Cir_start=j;
    for j=dimi(1)-lin_len+1:-1:n
        if(min(abs(raw_dat(j:j+n,2*i)-polyval(line2,raw_dat(j:j+n,2*i-
1))))>(n_sig*err_line2))
            break;
        end;
    end;
    Cir_end=j;
    for j=Cir_start+cir_len:1:Cir_end-cir_len
        [Cir(1:2),Cir(3)]=fitcircle(raw_dat(j-cir_len:j+cir_len,2*i-
1:2*i),'linear');
        RadCrv(j,i)=Cir(3);
    end;
    RadCrvAvg(i)=mean(RadCrv(Cir_start+cir_len:Cir_end-cir_len,i));
    RadCrv(RadCrv==0)=1e3;
    figure;
    hold on;
    plot(raw_dat(:,2*i-1),RadCrv(:,i));
    axis([0, 110, 0, 50]);
    xlabel('Location (um)');
    ylabel('Radius of Curvature (um)');
    title('Calculated Radius of Curvature');
end;
toc;

```

A similar algorithm was developed too, with generally same flow, but calculates the local curvature radius by polynomial fitting and polynomial curvature calculation instead of circular fitting. An example is given as follows.

```

close all;
clear;
clc;
disp('Starting...select data file>>');
[filename1, pathname1]=uigetfile({'*.*','all files (*.*)'}, 'Pick the
input file');
tic;
disp('Reading data file>>');
File1=fullfile(pathname1,filename1); %get
the input file
raw_data=importdata(File1,'\t',9); %read
the data
toc;
lin_len=input('Please input the side extension of the line>>');
if isempty(lin_len)
    lin_len=50;
end;
tic;
dimi=size(raw_data.data);
dimi(1)=dimi(1)-1;
raw_dat=raw_data.data(1:dimi(1),:);
%%% Moving average filtering %%%
ac=1;
f_window=10;
bc=ones(f_window,1)/f_window; %averaging every
10 samples
raw_dat2=raw_dat;
for i=1:dimi(2)/2
    raw_dat2(:,2*i)=filter(bc,ac,raw_dat(:,2*i)); %Filtering
end;
disp_str=['Moving average filtering every ',num2str(f_window),'
samples'];
disp(disp_str);
%%% Moving average filtering %%%
toc;
tic;
RadCrv=zeros(dimi(1)-2*lin_len,dimi(2)/2);
n=4; %nth order polynomial fit
pxy=zeros(n+1,1);
warning('off','all');
for i=1:1:dimi(2)/2
    for j=1:1:dimi(1)-2*lin_len
        pxy=polyfit(raw_dat(j:j+2*lin_len,2*i-
1),raw_dat(j:j+2*lin_len,2*i),n);
        RadCrv(j,i)=abs(((1+polyval(polyder(pxy),raw_dat(j+lin_len,2*i-
1))^2)^1.5)/polyval(polyder(polyder(pxy),raw_dat(j+lin_len,2*i-1))));
    end;
    figure;
    plot(raw_dat(1+lin_len:dimi(1)-lin_len,2*i-1),RadCrv(:,i));
    axis([0, 110, 0, 50]);
    xlabel('Location (um)');
    ylabel('Radius of Curvature (um)');
    title('Calculated Radius of Curvature');
end;
warning('on','all');
toc;

```


The sub-routine *fitcircle* for circular fitting on scattered points used in the above mentioned algorithms is an open-shared work by Richard Brown (<http://www.mathworks.com/matlabcentral/fileexchange/15060-fitcircle-m>) based on Gander et al.'s publication (1994).

APPENDIX F

MESHING FOR GLOBAL RESPONSE

The meshing is based on rectangular meshing and the *griddata* interpolation command in Matlab®. The interpolation requires the surface to always pass the data points, thus the noise of original data would be kept in the obtained map. The detailed code is attached as follows.

```
close all;
clear;
clc;
warning('off','all');
disp('Starting...>>');
i=0;
legend_names={};
inp=double.empty(0,0);
dimi=double.empty(0,0);
while isempty(inp)
    [filename, pathname]=uigetfile({'*.*','all files (*.*)'}, 'Pick the
input file');
    tic;
    disp('Reading data file>>');
    location=input('Please input distance from the joint, in mm>>');
    i=i+1;
    File=fullfile(pathname,filename); %get
the input file
raw_data=importdata(File,'\t',1); %read
the data
    if isempty(dimi)
        old_dimi=[0,0];
    else
        old_dimi=old_dimi+dimi;
    end;
    dimi=size(raw_data.data);
    SHTC(old_dimi(1)+1:old_dimi(1)+dimi(1),:)=raw_data.data;
    SHTC(old_dimi(1)+1:old_dimi(1)+dimi(1),1)=location;
    inp=input('Press Enter to continue, input anything else to end>>');
end;
dx=1;
dy=0.2;
x_edge=[floor(min(SHTC(:,2))):dx:ceil(max(SHTC(:,2)))];
y_edge=[floor(min(SHTC(:,1))):dy:ceil(max(SHTC(:,1)))];
[X,Y]=meshgrid(x_edge,y_edge);
Z=griddata(SHTC(:,2),SHTC(:,1),SHTC(:,3),X,Y);
% Generate log-scale texture
T = real2rgb(log(Z), 'jet');
```

```
surf(X,Y,Z,T);
colormap jet;
h=colorbar;
set(h, 'YScale', 'log')
hold on;
grid on;
set(gca, 'Zscale', 'log', 'Clim', [min(Z(:)) max(Z(:))]);
set(gca, 'XDir', 'reverse');
xlabel('Overheat Temperature (\circC)');
ylabel('Distance from separation point (mm)');
zlabel('Surface heat transfer coefficient (W/m2\circC)');
title('Calculated surface heat transfer coefficient');
```

The *real2rgb* function used is a color rendering function written by Oliver Woodford as an open-shared resource. The source of the code can be found at the following URL:

<http://www.mathworks.com/matlabcentral/fileexchange/23342-real2rgb---colormaps>

(accessed on April 6th, 2014).

APPENDIX G

OPTIMIZATION WITH GENETIC ALGORITHM

The optimization with Genetic Algorithm is carried out through Matlab® Genetic Algorithm solver. The main function is attached as follows, explaining the variables, constraints, solver settings and overall approach flow.

```
close all;
clear;
clc;
ObjectiveFunction = @Obj_ProcSI_GA;    %set the objective function
nvars = 2;        % Number of variables
n=1;             % number of test runs
LB=zeros(nvars,1);
UB=zeros(nvars,1);
LB(:) = [50 17.2];    % Lower bound: cutting speed, m/min; nose radius,
mm;
UB(:) = [500 68.9];    % Upper bound: cutting speed, m/min; nose
radius, mm;
ConstraintFunction = @simple_contr2;    %nonlinear constraint function
x=zeros(1,nvars);
X0=[100 17.2];
options=gaoptimset('InitialPopulation',X0);
%set the initial values
options=gaoptimset(options,'MutationFcn',@mutationadaptfeasible);
%mutation function:
@mutationgaussian,@mutationuniform,@mutationadaptfeasible
options=gaoptimset(options,'PlotFcns',{@gaplotshowpopulation2,@Obj_Pro
cSI_GA},@gaplotbestf),'Display','off');
%plot functions
options=gaoptimset(options,'PopulationSize',100);
%population size, default is 20
options=gaoptimset(options,'CrossoverFraction',0.8);
%crossover fraction, default is 0.8
options=gaoptimset(options,'Generations',1e5,'TimeLimit',600);
%limit for: number of generations; number of time consumed in seconds
%options=gaoptimset(options,'TolFun',1e-12);
%change of fitness value tolerance
options=gaoptimset(options,'SelectionFcn',@selectiontournament);
%selection function:
%@selectionstochunif,@selectionremainder,@selectionuniform,@selectionro
ulette,@selectiontournament
options=gaoptimset(options,'Vectorized','off','UseParallel','Always');
%vectorization and parallel computing
tic
y=zeros(n,nvars+1);
for i=1:1:n
```

```
    disp_str=['Iteration number ', num2str(i), '/', num2str(n), '
initializing...'];
    disp(disp_str);
    [x, fval]=ga(ObjectiveFunction, nvars, [], [], [], [], LB, UB, [], options);
    y(i, 1:nvars)=x(:);
    y(i, nvars+1)=Obj_ProcSI_GA(x);
    %record the results of multiple test runs
end;
toc
```

REFERENCES

- Adler, D.P., Hii, W.W.S., Michalek, D.J., Sutherland, J.W., 2006. Examining the role of cutting fluids in machining and efforts to address associated environmental/health concerns. *Machining Science and Technology*, 10: 23–58.
- Allen, D., Bauer, D., Bras., B., Gutowski, T., Murphy, C., Piwonka, T., Sheng, P., Sutherland, J., Thurston, D., Wolff, E., 2002. Environmentally benign manufacturing: Trends in Europe, Japan, and the USA. *Transaction of the ASME*. 124: 908–920.
- Ameta, G., Mani, M., Rachuri, S., Feng, S., Sriram, R., Lyons, K., 2009. Carbon weight analysis for machining operation and allocation for redesign. *International Journal of Sustainable Engineering*, 2(4): 241–251.
- Analog Devices, 2012, AD8421: 3 nV/ $\sqrt{\text{Hz}}$, Low power instrumentation amplifier data sheet. Available at: http://www.analog.com/static/imported-files/data_sheets/AD8421.pdf. Accessed on March 5, 2013.
- Astakhov, V.P., 2008. Ecological machining: near-dry machining. In J.P. Davim (eds.) *Machining*. Springer, London, 195–223.
- Auracher, H., 2003. Some remarks on the Nukiyama Curve. *JSME TED Newsletter*, 42. Available at: <http://www.jsme.or.jp/ted/NewsLetter42/Auracher.pdf>, accessed on February 18th, 2014.
- Badurdeen, F., Shuaib, M., Metta, H., Stovall, C., Jawahir, I.S., Goldsby, T.J., 2011. An ontology-based approach to develop sustainable manufacturing metrics for supply chain evaluation. *Proceedings of NAMRI/SME*, 39: 152–161.
- Bankoff, S.G., 1958. Entrapment of gas in the spreading of a liquid over a rough surface. *American Institute of Chemical Engineers Journal*, 4: 24–26
- Bare, J., Gloria, T., Norris, G., 2006. Development of the method and U.S. normalization database for life cycle impact assessment and sustainability metrics. *Environmental Science and Technology*, 40: 5108–5115.
- Bell, D., Chou, J., Nowag, L., Liang, S., 1999. Modeling of the environmental effect of cutting fluid. *Tribology Transactions*, 42(1): 168–173.
- Bierma, T.J., Waterstraat, F.L., 2004. Total cost of ownership for metalworking fluids. Research report from Waste Management and Research Center at Illinois State University. Available at: www.istc.illinois.edu/info/library_docs/rr/rr-105.pdf. Accessed on July 25th, 2011.
- Bureau of Economic Analysis, 2011. Industry economic accounts. Available at: <http://www.bea.gov/index.htm>. Accessed on December 14th 2013.
- Burns, G.W., Scroger, M.G., 1989. The calibration of thermocouples and thermocouple materials. NIST Special Publication 250-35. Available at: <http://www.nist.gov/calibrations/upload/sp250-35.pdf>. Accessed on May 4th, 2013.

- Byrne, G., Scholta, E., 1993, Environmentally clean machining processes - a strategic approach. *CIRP Annals Manufacturing Technology*, 42:471–474.
- Chen, S.J., Biswas, S.K., Han, F., Satyanarayana, A., 1990. Modeling and analysis of controlled cooling for hot moving metal strips. *Monitoring and Control for Manufacturing Processes*, 44: 465–473.
- Chen, S.J., Tseng, A., 1992, Spray and jet cooling in steel rolling. *International Journal of Heat and Fluid Flow*, 13(4): 358–369.
- Childs, T.H.C., Maekawa, K., Maulik, P., 1988. Effects of coolant on temperature distribution in metal machining. *Materials Science and Technology*, 4: 1006–1019.
- Choi, A., Kaebernick, H., Lai, W., 1997. Manufacturing process modeling for environmental impact assessment. *Journal of Materials Processing Technology*, 70: 231–238.
- Ciafalo, M., Piazza, I., Brucato, V., 1999. Investigation of the cooling of hot walls by liquid water spray. *International Journal of Heat and Mass Transfer*, 42: 1157–1175.
- Courbon, C., Pusavec, F., Dumont, F., Rich, J., Kopek, J., 2013. Tribological behavior of Ti6Al4V and Inconel718 under dry and cryogenic conditions — Application to the context of machining with carbide tools. *Tribology International*, 66: 72–82.
- Dahmus, A., Gutowski, T., 2007. What gets recycled: an information theory based model for product recycling. *Environmental Science and Technology*, 41: 7543–7550.
- Dahmus, J. B., Gutowski, T., 2004. An environmental analysis of machining. ASME International Mechanical Engineering Congress and RD&D Expo, IMECE 2004, Anaheim, CA, USA.
- Daniel, C.M., Rao, K.V.C., Olson, W.W., Sutherland, J.W., 1996. Effect of cutting fluid properties and application variables on heat transfer in turning and boring operations. *Japan/USA Symposium on Flexible Automation*, 2: 1119–1126.
- De Nevers, N., 2004. *Fluid mechanics for chemical engineers*, 3rd Edition, McGraw-Hill Science/Engineering/Math, New York.
- De Silva, N., 2005. A new comprehensive methodology for the evaluation of product sustainability at the design stage of consumer electronics products. M.S. Thesis, Department of Mechanical Engineering, University of Kentucky.
- De Silva, N., Jawahir, I.S., Dillon, O.W., Russell, M., 2009. A new comprehensive methodology for the evaluation of product sustainability at the design and development stage of consumer electronic products, *International Journal of Sustainable Manufacturing*, 1(3): 251–264.
- Deb, S., Yao, S.C., 1989. Analysis on film boiling heat transfer of impacting sprays. *International Journal of Heat and Mass Transfer*, 116: 167–172.
- Dhar, N.R., Kamruzzaman, M., 2007. Cutting temperature, tool wear, surface roughness and dimensional deviation in turning AISI-4037 steel under cryogenic condition. *International Journal of Machine Tools and Manufacture*, 47: 754–759.

- Dhar, N.R., Paul, S., Chattopadhyay, A.B., 2002a. Machining of AISI 4140 steel under cryogenic cooling — tool wear, surface roughness and dimensional deviation. *Journal of Materials Processing Technology*, 123(3): 483–489.
- Dhar, N.R., Paul, S., Chattopadhyay, A.B., 2002b. The influence of cryogenic cooling on tool wear, dimensional accuracy and surface finish in turning AISI 1040 and E4340C steels. *Wear*, 249: 932–942.
- Dillon, Jr., O.W., 1966. The heat generated during the torsional oscillation of copper tubes. *International Journal of Solids Structures*, 2: 181–204.
- Ding, Y., Hong, S.Y., 1995. A study of the cutting temperatures in machining processes cooled by liquid nitrogen. *Society of Manufacturing Engineers*, MR95-133.
- Diniz Da Costa, J., Pagan, R., 2006. Sustainability metrics for coal power generation in Australia. *Trans IChemE, Part B, Process Safety and Environmental Protection*, 84(B2), 143–149.
- Gladwin, T.N., Kennelly, J.J., Krause, T.S., 1995. Shifting paradigms for sustainable development: implications for management theory and research. *Academy of Management Review*, 20(4): 874–907.
- Dreher, J., Lawler, M., Stewart, J., Strasorier G., Thorne., M., 2009. General Motor's metrics for sustainable manufacturing. MIT Sloan School of Management Report, Cambridge, Massachusetts: MIT Sloan School of Management.
- Drossel, W.G., Neugebauer, R., Wertheim, R., 2012. High speed cutting and high-performance cutting for improving resource and energy efficiency. *Proceedings of the 10th Global Conference on Sustainable Manufacturing, Istanbul, Turkey*, 211–218.
- Elkington, J., 1998. Partnerships from the cannibals with forks: The Triple Bottom Line of the 21st century business. *Environmental Quality Management*, 8(1): 37–51.
- Feng, S. C., Joung, C.B., 2009. An overview of a proposed measurement infrastructure for sustainable manufacturing. *Proceedings of the 7th Global Conference on Sustainable Manufacturing, Chennai, India*, 355–360.
- Feng, S.C., Joung, C., Li, G., 2010. Development overview of sustainable manufacturing metrics. *Proceedings of the 17th CIRP International Conference on Life Cycle Engineering 2010, Hefei, China*, 6–12.
- Foley, J.D., van Dam, A., Feiner, S.K., Hughes, J.F., 1995. *Computer graphics: Principles and practice in C*, 2nd edition. Addison-Wesley Professional, New York.
- Gander, W., Golub, G.H., Strebel, R., 1994. Least-squares fitting of circles and ellipses. *BIT Numerical Mathematics*, 34: 558–578.
- Gangadharan, P., Zanwar, A., Zheng, K., Gossage, J., Lou, H., 2012. Sustainability assessment of polygeneration processes based on syngas derived from coal and natural gas. *Computers and Chemical Engineering*, 39: 105–117.
- Goedkoop, M., 1995. *The Eco-Indicator 95, Final Report*. National Reuse of Waste Research Programme (NOH) Report 9523. Available at: <http://www.pre->

- sustainability.com/download/EI95FinalReport.pdf. Accessed on October 18th, 2012.
- Graham, D., 2000, Going dry. *Manufacturing Engineering*, 123(1): 72–28.
- Granados, S., Jawahir, I.S., Fernandez, J., 2009. A comprehensive criterion for sustainability evaluation of machining processes. *Proceedings of the 7th Global Conference on Sustainable Manufacturing*, IIT Madras, Chennai, India, December 2-4, 385–391.
- Greeley, M., Rajagopalan, N., 2004. Impact of environmental contaminants on machining properties of metalworking fluids. *Tribology International*, 37: 327–332.
- Gressel, M.G., 2001. Comparison of mist generation of flood and mist application of metal working fluids during metal cutting. *Dissertation, Department of Mechanical, Industrial, and Nuclear Engineering, University of Cincinnati*.
- Griffith, P., Wallis, J.D., 1960. The role of surface conditions in nucleate boiling. *Chemical Engineering Progress Symposium Series*, 56(30): 49–63
- Gupta, A., Vangari, R., Jayal, A.D., Jawahir, I.S., 2010. Priority evaluation of product metrics for sustainable manufacturing. in Alain Bernard (Eds), *Global Product Development*, 631-641.
- Gutowski, T., Branham, M., Dahmus, J., Jones, A., Thiriez, A., Sekulic, D., 2009, thermodynamic analysis of resources used in manufacturing processes. *Environmental Science and Technology*, 43: 1584–1590.
- Gutowski, T., Dahmus, J., Thiriez, A., 2006. Electrical energy requirements for manufacturing processes. *Proceedings of the 13th CIRP International Conference on Lifecycle Engineering*, Leuven, Belgium, May 31-June 2.
- Gutowski, T., Dahmus, J., Thiriez, A., Branham, M., Jones, A., 2007. A thermodynamic characterization of manufacturing processes. *IEEE International Symposium on Electronics and the Environment*, Orlando, Florida, USA, May 7-10.
- Gutowski, T., Murphy, C., Allen, D., Bauer, D., Bras, B., Piwonka, T., Sheng, P., Sutherland, J., Thurston, D., Wolff, E., 2005, Environmentally benign manufacturing: Observations from Japan, Europe and the United States, *Journal of Cleaner Production*, 13: 1–17.
- Hands, D., Sheehan, M.J., Wong, B., Lick, H.B., 1996. Comparison of metalworking fluid mist exposures from machining with different levels of machine enclosure. *American Industrial Hygiene Association Journal*, 57: 1173–1178.
- Hollmann, S., Klimmer, F., Schmidt, K.H., Kylian, H., 1999. Validation of a questionnaire for assessing physical work load. *Scandinavian Journal of Work, Environment and Health*, 25(2): 105–114.
- Hong, S.Y., 2001. Economical and ecological cryogenic machining. *Journal of Manufacturing Science and Engineering*, 123: 331–338.
- Hong, S.Y., 2006. Lubrication mechanisms of LN2 in ecological cryogenic machining. *Machining Science and Technology*, 10: 133–155.

- Hong, S.Y., Ding, Y., 2001. Cooling approaches and cutting temperatures in cryogenic machining of Ti-6Al-4V. *International Journal of Machine Tools and Manufacture*, 41: 1417–1437.
- Hong, S.Y., Ding, Y., Jeong, J., 2001. Friction and cutting forces in cryogenic machining of Ti-6Al-4V. *International Journal of Machine Tools and Manufacture*, 41(15): 2271–2285.
- Hong, S.Y., Ding, Y., Jeong, J., 2002. Experimental evaluation of friction coefficient and liquid nitrogen lubrication effect in cryogenic machining. *Machining Science and Technology*, 6(2): 235–250.
- Hong, S.Y., Zhao, Z., 1999. Thermal aspects, material considerations and cooling strategies in cryogenic machining. *Clean Technologies and Environmental Policy* 1: 107–116.
- Hsu, Y.Y., 1962. On the size range of active nucleation cavities on a heating surface. *Journal of Heat Transfer*, 84: 207–212.
- Ikra, P., Tanaka, C., Ohtani, T., 2005. Energy balance of the orthogonal cutting process. *Holz als Roh- und Werkstoff*, 63: 358–364.
- Incropera, F.P., DeWitt, D.P., 2000. *Fundamentals of heat and mass transfer*, 4th edition. John Wiley and Sons, New York.
- Institute for Sustainable Manufacturing (ISM), 2013. Development of metrics, metrology and a framework for product-process ontology for interoperability in model-based sustainable manufacturing. Project report, University of Kentucky.
- International Organization for Standardization (ISO), 1999. ISO 14031 environmental management – Environmental performance evaluation – Standards and guidelines. ISO: Geneva.
- International Organization for Standardization (ISO), 2009. The ISO 14000 family of international standards. Available at : http://www.iso.org/iso/theiso14000family_2009.pdf. Accessed on December 6th, 2012.
- Jackson, T., Roberts, P., 2000. A review of indicators of sustainable development: Report of Scottish enterprise tayside. Available at: http://www.researchgate.net/publication/254457999_A_REVIEW_OF_INDICATORS_OF_SUSTAINABLE_DEVELOPMENT_A_REPORT_FOR_SCOTTISH_ENTERPRISE_TAYSIDE. Accessed on September 9th, 2012.
- Jawahir, I.S., Badurdeen, F., Rouch, K., 2013. Innovation in sustainable manufacturing education. Proceedings of the 11th Global Conference on Sustainable Manufacturing, Berlin, Germany, 9–16.
- Jawahir, I.S., Dillon, O.W., 2007. Sustainable manufacturing processes: New challenges for developing predictive models and optimization techniques. Proceedings of First International Conference on Sustainable Manufacturing, Montreal, Canada, 1–19.

- Jawahir, I.S., Jayal, A.D., 2011. Product and process innovation for modeling of sustainable manufacturing process. In Seliger, G.; Khraisheh, M.; Jawahir, I.S. (Eds.), *Advances in Sustainable Manufacturing*. Springer, Berlin, Heidelberg, 299–305.
- Jawahir, I.S., Rouch, K.E., Dillon, O.W., Jr., Joshi, K.J., Venkatachalam, A., Jaafar, I.H., 2006a. Total life-cycle considerations in product design for manufacture: a framework for comprehensive evaluation. Keynote Paper in 10th International Research/Expert Conference, Barcelona, Spain, September, 1–10.
- Jawahir, I.S., Rouch, K.E., Dillon, O.W., Holloway, L., Hall, A., 2007. Design for sustainability (DFS): New challenges in developing and implementing a curriculum for next generation design and manufacturing engineers. *International Journal of Engineering Education*, 23(6): 1053–1064.
- Jawahir, I.S., Wanigarathne, P.C., Wang, X., 2006b. Product design and manufacturing processes for sustainability. In Kutz, M. (Eds), *Mechanical Engineers' Handbook: Manufacturing and Management*, 3rd Edition. Wiley. 414–443.
- Jayal, A.D., Badurdeen, F., Dillon, Jr., O.W., Jawahir, I.S., 2010. Sustainable manufacturing: Modeling and optimization challenges at the product, process and system levels. *CIRP Journal of Manufacturing Science and Technology*, 2(3): 144–152.
- Joshi, K.; Venkatachalam, A.; Jawahir, I.S., 2006. A new methodology for transforming 3R concept into 6R concept for improved product sustainability. *Proceedings of the IV Global Conference of Sustainable Manufacturing*. Prod. Dev. & LCE, São Carlos, Brazil, October, 3–6.
- Jun, S.C., 2005. Lubrication effect of liquid nitrogen in cryogenic machining friction on the tool-chip interface. *Journal of Mechanical Science and Technology*, 19(4): 936–946.
- Kaynak, Y., Lu, T., Jawahir, I.S., 2014. Cryogenic machining-induced surface integrity: a review and comparison with dry, MQL, and flood-cooled machining. *Machining Science and Technology*, 18: 149–198.
- Khan, F., Sadiq, R., Veitch, B., 2004. Life cycle iNdeX (LInX): a new indexing procedure for process and product design and decision-making. *Journal of Cleaner Production*. 12: 59–76.
- Kim, J., Park, K., Hwang, Y., Park, I., 2010. Sustainable manufacturing: A case study of the forklift painting process. *International Journal of Production Research*, 48(10): 3061–3078.
- Kirk, R., 2007. *Statistics: An Introduction*, 5th Edition. Wadsworth Publishing, Independence, KY, USA.
- Kondo, T., 1997. Environmentally clean machining in Toyota. *International Journal of the Japan Society for Precision Engineering*, 31(4): 249–252.

- Kong, D., Choi, S., Yasui, Y., Pavanaskar, S., Dornfeld, D., 2011. Wright P. Software-based tool path evaluation for environmental sustainability. *Journal of Manufacturing Systems*, 30: 241–247.
- Koza, J.R., 1992. *Genetic programming: On the programming of computers by means of natural selection*. MIT Press, Cambridge, MA, USA.
- Lange, J., 2009. Sustainable chemical manufacturing: A matter of resources, wastes, hazards, and costs. *Sustainable Chemistry and Green Chemistry*, 2: 587–592.
- Lee, S., Ham, H.J., Kwon, S.Y., Kim, S.W., Suh, C.M., 2013. Thermal conductivity of magnesium alloys in the temperature range from –125 °C to 400 °C. *International Journal of Thermophysics*, 34(12): 2343–2350.
- Lepkowski, J., 2004. Temperature measurement circuits for embedded applications. Microchip Technology Inc, available at: www.t-es-t.hu/download/microchip/an929a.pdf. Accessed on January 16th, 2012.
- Liow, J., 2009. Mechanical micromachining: a sustainable micro-device manufacturing approach?. *Journal of Cleaner Production*, 17: 662–667.
- Lu, T., Gupta, A., Jayal, A.D., Badurdeen, F., Feng, S.C., Dillon, O.W., Jawahir, I.S., 2011. A framework of product and process metrics for sustainable manufacturing. In Seliger, G.; Khraisheh, M.; Jawahir, I.S. (Eds.), *Advances in Sustainable Manufacturing*. Springer, Berlin, Heidelberg, 331–336.
- T. Lu, Rotella, G., Feng, S.C., Badurdeen, F., Dillon, Jr., O.W., Rouch, K.E., Jawahir, I.S., 2012a. Metrics-based sustainability assessment of a drilling process. In G. Seliger (Eds), *Sustainable Manufacturing*. Springer, Berlin, Heidelberg, 59–64.
- Lu, T., Rotella, G., Badurdeen, F., Dillon, Jr., O.W., Rouch, K.E., Jawahir, I.S., 2012b. A metrics-based sustainability assessment for different coolant applications in a turning process. *The Proceedings of 10th Global Conference on Sustainable Manufacturing*, Istanbul, Turkey, Oct 31 - Nov 2, 564–569.
- Lu, T., Shuaib, M., Rotella, G., Badurdeen, F., Dillon, Jr., O.W., Rouch, K.E., Jawahir, I.S., 2014a. Sustainability evaluation of manufacturing processes using a metrics-based Process Sustainability Index (*ProcSI*), part I: Development of a comprehensive methodology. Manuscript submitted to *Journal of Cleaner Production*.
- Lu, T., Shuaib, M., Rotella, G., Badurdeen, F., Dillon, Jr., O.W., Rouch, K.E., Jawahir, I.S., 2014b. Sustainability evaluation of manufacturing processes using a metrics-based Process Sustainability Index (*ProcSI*), part II: Method applications and validation. Manuscript submitted to *Journal of Cleaner Production*.
- Mancini, R., 2013. *Op amps for everyone*, 4th Edition. Newnes, London.
- Marksberry, P.W., 2004. An assessment of tool-life performance in NDM (near dry machining) of automotive steel components for sustainable manufacturing. Dissertation, Department of Mechanical Engineering, University of Kentucky.
- Marquardt, E.D., Le, J.P., Radebaugh, R., 2000. Cryogenic material properties database. Keynote of the 11th Cryocooler Conference, Keystone, Colorado, USA, June 20 –

22. Available at: http://cryogenics.nist.gov/Papers/Cryo_Materials.pdf. Accessed on March 29, 2014.
- Martins, A., Mata, T., Costa, C., Sikdar, S., 2007. Framework for sustainability metrics. *Industrial and Engineering Chemistry Research*, 46: 2962–2973.
- Matweb, 2013a. Nitrogen, N₂. Available at: <http://www.matweb.com/search/DataSheet.aspx?MatGUID=a12c5c74a43c4ab393f6235b012e9aff>, accessed on February 27, 2013.
- Matweb, 2013b. Carbon dioxide, CO₂. Available at: <http://www.matweb.com/search/DataSheet.aspx?MatGUID=5d8d9e87288943928df12425308a822d>, accessed on February 27, 2013.
- Ministry of Housing, Spatial Planning and the Environment, 2000, Eco-Indicator 99 Manual for Designers. Available at: www.pre-sustainability.com/download/manuals/EI99_Manual.pdf. Accessed on December 8th, 2012.
- Monteiro, J., Araujo, O., Medeiros, J., 2009a. Sustainability metrics for eco-technologies assessment, part I: preliminary screening. *Clean Technologies and Environmental Policy*. 11: 209–214.
- Monteiro, J., O. Araujo, J. Medeiros, 2009b. Sustainability metrics for eco-technologies assessment, part II: Life cycle analysis. *Clean Technologies and Environmental Policy*. 11: 459–472.
- Naidu, S., Sawhney, R., Li, X., 2008. A methodology for evaluation and selection of nanoparticle manufacturing processes based on sustainability metrics. *Environmental Science and Technology*, 42: 6697–6702.
- National Council for Advanced Manufacturing (NACFAM), 2009. Sustainable manufacturing. available: <http://nacfam02.dev.web.sba.com/PolicyInitiatives/SustainableManufacturing/tabid/64/Default.aspx>. Accessed on November 11th, 2013.
- NIOSH (National Institute for Occupational Safety and Health), 1998a. Criteria for a recommended standard: occupational exposure to metalworking fluids, U.S. Department of Health and Human Services, Public Health Service, Centers for Disease Control and Prevention, National Institute for Occupational Safety and Health, Cincinnati, Ohio, DHHS (NIOSH) Publication No. 98-102.
- NIOSH (National Institute for Occupational Safety and Health), 1998b, Criteria for a recommended standard: occupational noise exposure, U.S. Department of Health and Human Services, Public Health Service, Centers for Disease Control and Prevention, National Institute for Occupational Safety and Health, Cincinnati, Ohio, DHHS (NIOSH) Publication No. 98-126.
- NIOSH (National Institute for Occupational Safety and Health). 2007. Health hazard evaluation and technical assistance report: HETA 005-0227-304. Available at: <http://www.cdc.gov/niosh/hhe/reports/pdfs/2005-0227-3049.pdf>. Accessed on January 18th, 2014.

- National Institute for Standards and Technology (NIST), 2011, Sustainable manufacturing indicators repository. Available at: <http://www.nist.gov/el/msid/smir.cfm>. Access on August 15th, 2012.
- National Institute of Standards and Technology (NIST), 2012. NIST ITS-90 Thermocouple Database. Available at: http://srdata.nist.gov/its90/main/its90_main_page.html. Accessed on November 11th, 2012.
- Ness, B., Urbel-Piirsalu, E., Anderberg, S., Olsson, L., 2007. Categorizing tools for sustainability assessment. *Ecological Economics*, 60(3): 498–508.
- Occupational Safety and Health Administration (OSHA), 1997. Occupational noise exposure. Code of Federal Regulations, 29 C.F.R. 1910.95.
- OECD (Organization for Economic Co-operation and Development), 2012. OECD sustainable manufacturing indicators. www.oecd.org/innovation/green/toolkit/oecd sustainable manufacturing indicators.htm. Accessed on December 6th, 2012.
- Ozisik, M.N., 1989. Boundary value problems of heat conduction, Dover, New York.
- Ozisik, M.N., 1993. Heat Conduction, 2nd Edition. Wiley-Interscience, New York.
- Ozisik, M.N., Orlande, H.R.B., 2000. Inverse heat transfer: Fundamentals and applications. CRC Press, New York.
- Pfefferkorn, F.E., Lei, S., Jeon, Y., Haddad, G., 2009. A metric for defining the energy efficiency of thermally assisted machining. *International Journal of Machine Tools and Manufacture*, 49: 357–365.
- Pitts, D., Sissom, L.E., 2011. Schaum's outline of heat transfer, 2nd Edition. McGraw-Hill, New York.
- Popke, H., Emmer, T.H., Steffenhagen, J., 1999. Environmentally clean metal cutting processes — machining on the way to dry cutting. *Proceedings of the Institution of Mechanical Engineers*, 213(B): 329–332.
- Pu, Z., 2012. Cryogenic machining and burnishing of *AZ31B* magnesium alloy for enhanced surface integrity and functional performance. Dissertation, Department of Mechanical Engineering, University of Kentucky.
- Pusavec, F., Krajnik, P., Kopac, J., 2010a. Transitioning to sustainable production – Part I: Application on machining technologies. *Journal of Cleaner Production*, 18: 174–184.
- Pusavec, F., Kramar, D., Krajnik, P., Kopac, J., 2010b. Transitioning to sustainable production – part II: Evaluation of sustainable machining technologies. *Journal of Cleaner Production*, 18: 1211–1221.
- Putnam, D., Eng, P., 2002. ISO 14031: Environmental performance evaluation. *Confederation of Indian Industry Journal*, 1–10.
- Rotella, G., Lu, T., Settineri, L., Jawahir, I.S., 2012. Machining of AA7075 aluminum alloy: A process optimization for sustainability. *Proceedings of the 10th Global*

- Conference on Sustainable Manufacturing, Istanbul, Turkey, Oct 30 – Nov 2, 501–506.
- Rotella, G., Priarone, P.C., Rizzuti, S., Settineri, L., 2011. Evaluation of the environmental impact of different lubrorefrigeration conditions in milling of γ -TiAl Alloy. Proceedings of 18th CIRP International Conference on Life Cycle Engineering, Braunschweig (DE), May 2nd - 4th, 365–370.
- Rotella, G., Umbrello, D., Dillon, Jr., O.W., Jawahir, I.S., 2012. Evaluation of process performance for sustainable hard machining. Journal of Advanced Mechanical Design, Systems, and Manufacturing, 6(6): 989-998.
- Saloni, D.E., Lemaster, R.L., Jackson, S.D., 2005. Abrasive machining process characterization on material removal rate, final surface texture, and power consumption for wood. Forest Products Journal, 55(12): 35–41.
- Sarkar, P., Joung, C., Carrell, J., Feng, S., 2011. Sustainable manufacturing indicator repository. Proceedings of the ASME 2011 International Design Engineering Technical Conferences & Computers and Information in Engineering Conference (IDETC/CIE), Washington, DC, USA, August 29-31.
- Schmidt, W.P., Taylor, A., 2006. Ford of Europe's Product Sustainability Index. Proceedings of 13th CIRP International Conference on Life Cycle Engineering, Leuven, Belgium, May 31–June 2, 5–10.
- Shen, G., Gandhi, A., Arici, O., Sutherland, J.W., 2001. A model for workpiece temperatures during peripheral milling including the effect of cutting fluids. Transactions of NAMRI/SME, 29: 265–272.
- Shiina, K., Nakamura, S., Narita, K., 2000. Investigation of the cooling of hot walls by liquid water spray. Journal of Heat Transfer – Asian Research, Scripta Technica, 29(4): 280–299.
- Shuaib, M., SeEVERS, D., Zhang, X., Badurdeen, F., Rouch, K., Jawahir, I.S., 2014. Product Sustainability Index (*ProdSI*) – A metrics based framework to evaluate the total life-cycle sustainability of manufactured products. Journal of Industrial Ecology, 18(4): 491–507.
- Sikdar, S., 2003. Sustainable development and sustainability metrics. AIChE Journal, 49(8): 1928–1932.
- Sikdar, S., 2009. On aggregating multiple indicators into a single metric for sustainability. Clean Technologies and Environmental Policy, 11: 157–161.
- Singh, R.K., Murty, H.R., Gupta, S.K., Dikshit, A.K., 2012. An overview of sustainability assessment methodologies. Ecological Indicators, 15(1): 281–299.
- Sokovic, M., Mijanovic, K., 2001. Ecological aspects of the cutting fluids and its influence on quantifiable parameters of the cutting processes. Journal of Materials Processing Technology 109: 181–189.
- Sozbir, N., Chang, Y.W., Yao, S.C., 2003. Heat transfer impacting water mist on high temperature metal surfaces. Transaction of ASME, 125: 70–74.

- Sreejith, P.S., Ngoi, B.K.A., 2000. Dry machining: machining of the future. *Journal of Materials Processing Technology*, 101: 287–291.
- Steinhilper, R., 1993. *Remanufacturing: The ultimate form of recycling*. Fraunhofer IRB Verlag, 1–24.
- Streeter, V.L., 1962. *Fluid mechanics*, 3rd Edition. McGraw-Hill, New York.
- Sun, J., Ju, C., Yue, Y., Gunter, K.L., Michalek, D.J., Sutherland, J.W., 2004. Character and behavior of mist generated by application of cutting fluid to a rotating cylindrical workpiece, part 2: Experimental validation, *Journal of Manufacturing Science and Engineering*, 126: 426–434.
- Sustainable measures, 2009. Characteristics of effective indicators. Available at: <http://www.sustainablemeasures.com/node/92>. Accessed on October 5th, 2011.
- Sutera, S.P., Skalak, R., 1993. The history of Poiseuille's Law. *Annual Review of Fluid Mechanics*, 25: 1–20.
- Sutherland, J.W., Kulur, V.N., King, N.C., Turkovich, B.F., 2000. An experimental investigation of air quality in wet and dry turning. *CIRP Annals Manufacturing Technology*, 49: 61–64.
- Tabone, M., Cregg, J., Beckman, E., Landis, A., 2010. Sustainability metrics: Life cycle assessment and green design in polymers. *Environmental Science and Technology*, 44: 8264–8269.
- The World Bank, 2013. Manufacturing, value added (% of GDP). <http://data.worldbank.org/indicator/NV.IND.MANF.ZS/countries/1W-US?display=graph>. Accessed on 12th December 2013
- Thorne, P.S., DeKoster, J.A., Subramanian, P., 1996. Environmental assessment of aerosols, bioaerosols, and airborne endotoxins in a machining plant. *American Industrial Hygiene Association Journal*, 57(12): 1163–1167.
- Tong, L.S., Tang, Y.S., 1997. *Boiling heat transfer and two phase flow*, 2nd Edition. Taylor & Francis, New York.
- Trinh, K.T., 2010. On the Blasius correlation for friction factors. arXiv.org open access, available at: <http://arxiv.org/ftp/arxiv/papers/1007/1007.2466.pdf>. Accessed on February, 11, 2014.
- United Nations World Commission on Environment and Development (UNWCED), 1987. *Report of the World Commission on Environment and Development*, United Nations.
- US. Department of Commerce website, 2009. Available at: http://trade.gov/competitiveness/sustainablemanufacturing/how_doc_defines_SM.asp. Accessed on October 5th, 2012.
- US. Environmental Protection Agency (EPA), 2012. *The Emissions & Generation Resource Integrated Database (eGRID) 2012 V1.0*. Available at: <http://www.epa.gov/cleanenergy/energy-resources/egrid/index.html>. Accessed on August 3rd, 2012.

- Veleva, V., Ellenbecker, M., 2001. Indicators of sustainable production: Framework and methodology. *Journal of Cleaner Production*, 9: 519–549.
- Walmart, 2009a. Walmart announces Sustainable Product Index. Available at: <http://news.walmart.com/news-archive/2009/07/16/walmart-announces-sustainable-product-index>. Accessed 10.08.2012.
- Walmart, 2009b. Supplier sustainability assessment: 15 Questions for suppliers. Available at: http://az204679.vo.msecnd.net/media/documents/r_3863.pdf. Accessed 10.08.2012.
- Walmart, 2012. Walmart Corporate Sustainability Index. Available at: www.walmartstores.com/sustainability/9292.aspx. Accessed 5 October 2012.
- Wanigarathne, P.C., Liew, J., Wang, X., Dillon, Jr., O.W., Jawahir, I.S., 2004. Assessment of process sustainability for product manufacture in machining operations. *Proceedings of Global Conference on Sustainable Product Development and Life Cycle Engineering*, Berlin, Germany, 305–312.
- Wanigarathne, P.C., 2006. Experimental and analytical modeling of near-dry turning operations with coated groove tools for improved sustainability. Dissertation, Department of Mechanical Engineering, University of Kentucky.
- Weinert, K., Inasaki, I., Sutherland, J.W., Wakabayashi, T., 2004. Dry machining and minimum quantity lubrication. *Annals of the CIRP*, 53(2): 511–537.
- Wyen, C.F., Knapp, W., Wegener, K., 2012. A new method for the characterization of rounded cutting edges. *The International Journal of Advanced Manufacturing Technology*, 59: 899–914.
- Yasa, E., Alpagan, U., Pilatin, S., Colak, O., 2012. A review on the improvements in machinability of Ti-6Al-4V. *Proceedings of the 10th Global Conference on Sustainable Manufacturing*, Istanbul, Turkey, Oct 30 - Nov 2, 790–795.
- Ye, J., Schoenung, J.M., 2004. Technical cost modeling for the mechanical milling at cryogenic temperature (Cryomilling). *Advanced engineering materials*, 6(8): 656–664.
- Yildiz, Y., Nalbant, M., 2008. A review of cryogenic cooling in machining processes. *International Journal of Machine Tools and Manufacture*, 48: 947–964.
- Yuan, C., Zhai, Q., Dornfeld, D., 2012. A three dimensional system approach for environmentally sustainable manufacturing. *CIRP Annals - Manufacturing Technology*. 61(1): 39–42.
- Yue, Y., Sun, J., Gunter, K.L., Michalek, D.J., Sutherland, J.W., 2004. Character and behavior of mist generated by application of cutting fluid to a rotating cylindrical workpiece, part 1: Model development. *Journal of Manufacturing Science and Engineering*, 126: 417–425.
- Zhang, X., Lu, T., Shuaib, M., Rotella, G., Huang, A., Feng, S.C., Rouch, K., Badurdeen, F., Jawahir, I.S., 2012a. A metrics-based methodology for establishing Product Sustainability Index (*ProdSI*) for manufactured products. *Leveraging Technology for a Sustainable World: Proceedings of the 19th CIRP Conference on Life Cycle*

Engineering, University of California at Berkeley, Berkeley, USA, May 23 - 25, 435–441.

Zheng, Y., Li, H., Olson, W.W., Sutherland, J.W., 2000. Evaluating cutting fluid effects on cylinder boring surface errors by inverse heat transfer and finite element methods. *Journal of Manufacturing Science and Engineering*, 122: 377–383.

VITA

Name

Tao Lu

Place of Birth

Nanjing, Jiangsu Province, China

Education

B.S. in Mechanical Engineering, Southeast University, Nanjing, China

May, 2007

Experience

Editorial Assistant (06/2011 ~ 10/2014), Machining Science and Technology, Taylor & Francis

Editorial Assistant (1/2014 ~ 10/2014), International Journal of Sustainable Manufacturing, Inderscience

Research Assistant (08/2008 ~ 10/2014), Institute for Sustainable Manufacturing, University of Kentucky, Lexington, KY

Teaching Assistant (08/2007 ~ 05/2008), Department of Mechanical Engineering, University of Kentucky, Lexington, KY

Publications:

Book Chapters:

T. Lu, A. Gupta, A.D. Jayal, F. Badurdeen, S.C. Feng, O.W. Dillon, Jr., I.S. Jawahir, 2011. A Framework of product and process metrics for sustainable manufacturing, in: G. Seliger; M. Khraisheh; I.S. Jawahir (Eds.), *Advances in Sustainable Manufacturing*. Springer, Berlin, Heidelberg, 331–336.

T. Lu, G. Rotella, S. C. Feng, F. Badurdeen, O. W. Dillon, Jr., K.E. Rouch, I.S. Jawahir, 2012. Metrics-based sustainability assessment of a drilling process, in: G. Seliger (Eds), Sustainable Manufacturing. Springer, Berlin, Heidelberg, 59–64.

G. Rotella, **T. Lu**, L. Settineri, O.W. Dillon Jr., I.S. Jawahir, 2012. Dry and cryogenic machining: comparison from the sustainability perspective, in: G. Seliger (Eds), Sustainable Manufacturing, Springer Berlin Heidelberg, 95–100.

Badurdeen, F., M. Shuaib, **T. Lu**, I.S. Jawahir, 2014. Sustainable value creation in manufacturing at product and process levels: a metrics-based evaluation. in: A.Y.C. Nee (Eds), Handbook of Manufacturing Engineering and Technology. Springer, 3343–3375.

Journal Papers:

T. Lu, S. Wang, J. Li, P. Lucas, M. Anderson, K. Ross, 2012. A simulation study to improve performance in the preparation and delivery of antineoplastic medications at a community hospital. *Journal of Medical Systems*, 36:3083–3089.

Y. Kaynak, **T. Lu**, I.S. Jawahir, 2014. Cryogenic Machining-Induced Surface Integrity: A Review and Comparison with Dry, MQL, and Flood-Cooled Machining. *Machining Science and Technology*, 18(2): 149–198.

T. Lu, M. Shuaib, G. Rotella, S.C. Feng, F. Badurdeen, O.W. Dillon, Jr., K.E. Rouch, I.S. Jawahir, 2014. Sustainability evaluation of manufacturing processes using a metrics-based Process Sustainability Index (*ProcSI*): Part I: development of a comprehensive methodology. *Journal of Cleaner Production*, submitted.

T. Lu, M. Shuaib, G. Rotella, S.C. Feng, F. Badurdeen, O.W. Dillon, Jr., K.E. Rouch, I.S. Jawahir, 2014. Sustainability evaluation of manufacturing processes using a metrics-based Process Sustainability Index (*ProcSI*): Part II: method applications and validation. *Journal of Cleaner Production*, submitted.

A.H. Kheireddine, A.H. Ammouri, **T. Lu**, I.S. Jawahir, R.F. Hamade, 2014. an experimental and numerical study of the effect of cryogenic cooling on the surface integrity of drilled holes in *AZ31B* Mg alloy. *Journal of Materials Processing Technology*, submitted.

Conference Papers:

T. Lu, G. Rotella, F. Badurdeen, O.W. Dillon, Jr., K.E. Rouch, I.S. Jawahir, 2012. A Metrics-based sustainability assessment for different coolant applications in a turning process. The Proceedings of 10th Global Conference on Sustainable Manufacturing, Istanbul, Turkey, Oct 31 - Nov 2, pp. 564–569.

I.S. Jawahir, Z. Pu, S. Yang, G. Rotella, Y. Kaynak, **T. Lu**, A. Deshpande, D. Umbrello, O.W. Dillon, Jr., 2012, Cryogenic Processing of Materials for Enhanced Product Life, Performance and Sustainability. Keynote paper, 15th International Conference on

Advances in Material & Processing Technologies, September 23-26, Wollongong, NSW Australia.

I.S. Jawahir, **T. Lu**, 2014. Metrics-based sustainability evaluation of manufacturing processes. Proceedings of ICMC 2014, Stadthalle Chemnitz, Germany, 83–104.

G. Rotella, **T. Lu**, L. Settineri, I.S. Jawahir, 2012. Machining of *AA7075* aluminum alloy: a process optimization for sustainability. Proceedings of the 10th Global Conference on Sustainable Manufacturing, Istanbul, Turkey, Oct 30 – Nov 2, 501–506.

X. Zhang, **T. Lu**, M. Shuaib, G. Rotella, A. Huang, S.C. Feng, K.E. Rouch, F. Badurdeen, I.S. Jawahir, 2012. A metrics-based methodology for establishing Product Sustainability Index (ProdSI) for Manufactured Products, Proceedings of the 19th CIRP International Conference on Life Cycle Engineering, Berkeley, USA, May 2012, 435–441.

A.H. Kheireddine, A.H. Ammouri, **T. Lu**, I.S. Jawahir, R.F. Hamade, 2013. An FEM analysis with experimental validation to study the hardness of in-process cryogenically cooled drilled holes in Mg *AZ31b*. Procedia CIRP, 8: 588–593.